Optimal design of aluminium extrusion dies using a novel geometry based approach.

Lin, Chao

School of Engineering
University of Wales, Swansea

Optimal Design of Aluminium Extrusion Dies using a Novel Geometry based Approach

Chao Lin
BSc.

Thesis submitted to the University of Wales in candidature for the degree of Doctor of Philosophy

2005

DECLARATION

This work has not previously been accepted in substance for any degree and is not being concurrently submitted in candidature for any degree.

Signed _____ (candidate)

Date 22/11/2005

STATEMENT 1

This dissertation is being submitted in partial fulfillment of the requirements for the degree of Doctor of Philosophy.

Signed _____ (candidate)

Date 22/11/2005

STATEMENT 2

This dissertation is the result of my own investigations, except where otherwise stated. Other sources are acknowledged by footnotes giving explicit references. A bibliography is appended.

Signed _____ (candidate)

Date 22/11/2005

STATEMENT 3

I hereby consent for my dissertation, if accepted, to be available for photocopying and for inter-library load, and for the title and summary to be make available to outside organizations.

Signed _____ (candidate)

Date 22/11/2005

谨以此文献给我的父母。

To my parents.

Summary

Aluminium extrusion is a forming process used for manufacturing straight and long aluminium products. Among all aspects of the process, extrusion die design is the key issue for producing high-quality extrudates. The approaches to design extrusion dies can be broadly classified into three groups; trial and error, empirical based approach and numerical simulation based approaches.

By using the first two methodologies, the quality of extrusion die designs are intrinsically and strongly linked with designers' experience and skill. As the required forms for extrusions become more complex, these two approaches becomes less useful. Besides, since the design knowledge is held by designers, it is more often a 'black art', and the personnel movement can influence the design work significantly. On the other hand, with the advent of computers and greatly enhanced computing capability, many new approaches have been introduced for designing extrusion dies in last few decades. However, even with the current computing power, the numerical simulation approach has its limitations, particular in time required and even accuracy. Extrusion process involves complex constitutive relationships and large deformation of material.

To overcome the limitations posed by current available design approaches, a new geometry based methodology has been proposed in this thesis. The new methodology combines empirical design formulae, geometry reasoning technique and optimization algorithm together. The work originates from the earlier work done by Miles *et al.* [1, 2, 3, 4], and Armstrong and his colleagues [5, 6, 7, 8, 9, 10, 11, 12],

In this research work, a new knowledge representation scheme is developed so that historical data can be easily gathered and reused. By using empirical bearing length design formulae with historical data, a new bearing length estimation approach is introduced so that new profiles can be designed based on past good designs. A novel die layout design approach has also been developed and validated. This new method uses bearing length estimation algorithms with maximum *bearing length difference* to give radial or flat layout for single/multi-hole dies. By using medial axis transform, a set of new geometry reasoning algorithms have been studied. These algorithms give a general and robust way to analyze two-dimensional geometry shapes. A brand-new die profile categories have been proposed to avoid the drawbacks held by current classification. A new algorithm

and a set of new classifying criteria have been introduced. Based on medial axis transform and geometry reasoning technique, extrusion die profiles can be classified into different category correctly and efficiently.

This research work shows that all the proposed approaches give several feedback paths in extrusion die design process. Therefore, not only historical data can be reused for new designs, but it is also possible to acquire and represent design knowledge and to optimize the whole design process.

Acknowledgements

I would like to express the utmost gratitude to both of my supervisors. Prof. Roland. W. Lewis for his invaluable support and special thanks to Dr. Rajesh S. Ransing for guiding and supporting my research work particularly on the geometric reasoning side. Dr. Ransing shared his wisdom and knowledge with me continuously and enthusiastically. Without his selfless support, this research work could never have been completed.

I would like to thanks Prof. David T. Gethin, Dr. William K. S. Pao and Dr. Maghana R. Ransing for their help. Your rich knowledge and experience showed me an constructive path for my research work. Thanks to Dr. Minkesh P. Sood for all help and discussion on the medial axis work and all the happy times that we shared together.

Thanks to Dr. Yafang Liu, Dr. Xinshe Yang and his wife, Dr. Min Liu, Dr. Yuanjian Tong and his wife Xiaoling Wang, Dr. Hai Deng and his wife, Dr. Huabin Ying, Dr. Jinglei Yu and her husband, Dr. Mingguo Tang and his family and so many other friends for all their brilliant ideas and sweet memories that we shared during my research study period at Swansea.

A very sincere thanks is due to my parents, sisters and brothers in law for their utmost selfless and endless support, help and love. Without them, my dreams and research work could never have reached this stage.

I also acknowledge my gratitude to EPSRC for their financial support for my research work. Thanks are also due to Transcendata Ltd. and Dr. Geoff Butlin in particular for supporting the work by providing their software — CADfix®. Thanks for Dr. Mark R. Jolly and Dr. Qang Li for useful discussion on FE simulation for extrusion die designs.

At last, I would like to thank to you all for everything you did for me.

Contents

List of Figures

List of Tables

Chapter 1

Introduction

1.1 Background

Extrusion is a deformation process which is one of the major industrial processes. By applying a heavy load to the material, this process squeezes the billet in a closed container through a die to give shaped products. Aluminum extrusion transforms the billet into a continuous length of uniform cross-section-shape products such as bars, solid and hollow sections, tubes, wires and strips.

For the extrusion process, the material flow inside the billet is very complicated and unpredictable, which leads to a non-uniform flow velocity at the die opening exits. Die designers use the frictional resistance between the billet and die to balance the flow velocity in order to obtain products of acceptable quality. At the moment, there are three design approaches; a trial and error design approach based on experiments, an empirical design approach and numerical simulation based design approaches.

To appreciate the difficulty of the task, Figure 1.1 shows some example extruded sections. Many feature geometric complexity and furthermore and extrusion die may be designed to include more than one section. Currently, extrudate quality, defined in terms of straightness, is achieved by designing the die to have different land length over which the extrudate flows. The design of this land is crucial to success. The process is further complicated by the positioning of the opening within the die face since upstream flow is influenced by the cylinder wall in the

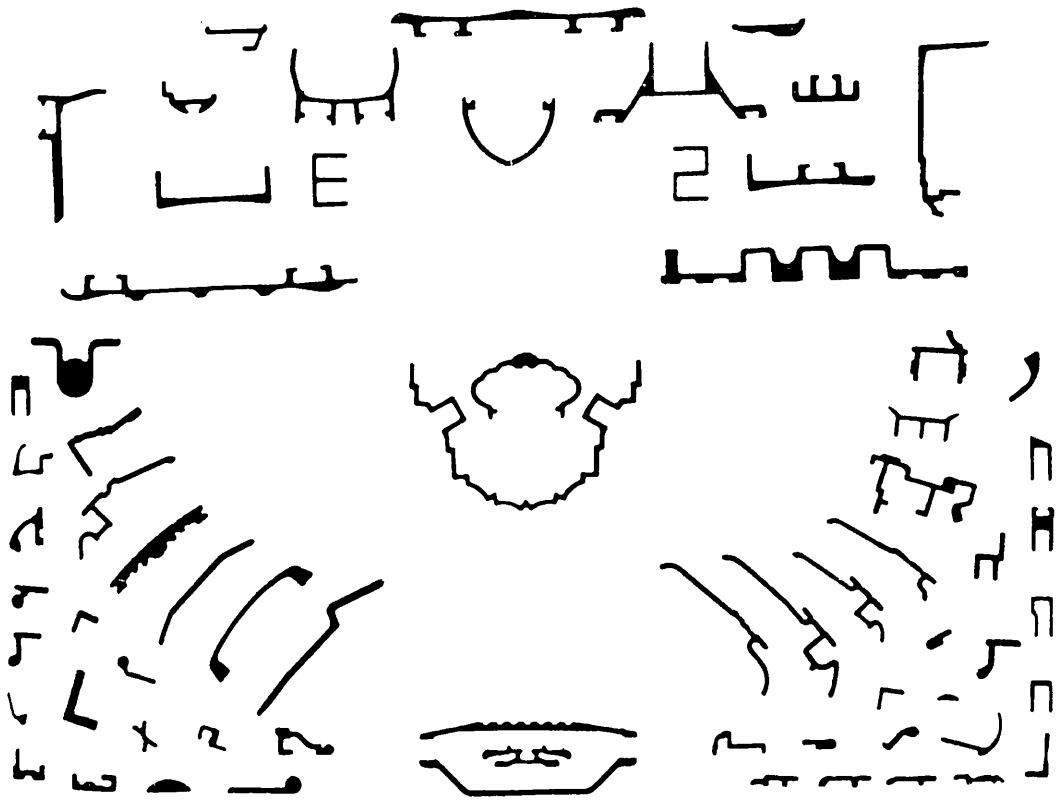

Figure 1.1: Examples of extrusion die opening profiles [13]

extrusion machine. This summarises the complexity of the task that is presented to the die designer.

Different design approaches have their own advantages and disadvantages. For example, for trial and error methods the whole design work remains in the designers' mind. Acquiring and representing this design knowledge becomes extremely difficult. The empirical design approach fails to reuse past good results thereby, losing out on the potential of learning from past successful practices. Numerical methods, such as the finite element method involve heavy costs in terms of time, money and expertise. This is due particularly to section complexity and the arrangement of apertures in the die. Extrusion simulation for these geometric sections are uncertain for a number of reasons and a computing run will require several days to perform, thus alternative schemes must be considered. Besides, all current methods fail to re-use historical data and to link the geometric information with the simulation process.

In an effort to overcome these limitations, a new design approach has been developed and is proposed in this thesis. Using this new approach, the most important

aspects of extrusion dies can be classified and quantified by using several new algorithms in a more scientific way. Past good designs can be reused by the new approach for suggesting new designs. Finally, an optimization algorithm is used based on all useful design information for various design rules to achieve optimal designs.

1.2 Scope of the Work

The research work was divided into five main tasks viz. recognition of the geometric feature, prediction of bearing length, developing an algorithm for extrusion die layout design, shape classification for extrusion dies and finally design optimization. The main research activities to accomplish these tasks were:

- Acquiring knowledge and understanding of the extrusion process, extrusion equipment, die design rules and design approaches.
- Obtaining an understanding of bearing length design approaches, bearing length design rules and empirical design formulae.
- Developing a bearing length prediction algorithm based on empirical design formulae. Deriving new bearing length design formulae wherever required.
- Understanding the layout design for extrusion dies and developing a method to optimize extrusion die layout based on geometric information of profiles and dies.
- Developing a new knowledge representation scheme so that the old design can be reused and further analysis can be undertaken.
- Seeking a full optimization solution for extrusion dies so that optimal design results can be obtained for new profiles.

The research contributions are summarised as follows:

- A novel design data representation approach for extrusion dies has been developed. This new approach makes it easier to gather and save design information and presents a 'novel data reusing method' by which design rules can be trained and the design knowledge can be represented.

- Based on empirical design formulae, a new method for predicting bearing length is introduced. Using this new data representation approach, empirical design formulae can be optimized based on historical design data.

- A new bearing length design formula has been derived which contains non-linear design factors and can fit historical data better than current linear bearing length design formulae.

- Several general purpose geometric reasoning algorithms, using the medial axis transform, have been developed and investigated. These algorithms can recognize and quantify shape features quickly and efficiently.

- A versatile extrusion die classification approach, based on geometric reasoning algorithms, has been developed. This new approach can classify and quantify different extrusion dies based on their shape features.

1.3 Publication List

Following are the publications produced during my research study period:

R. S. Ransing, W. K. S. Pao, C. Lin, M. P. Sood and R. W. Lewis, *An Enhanced Interpolation Algorithm using Medial Axis and its Application to Hotspot Prediction in a Mould-Casting Assembly*, International Journal of Cast Metals Research, February 2005, Vol. 18, No. 1, pp. 1-12.

W.K.S. Pao, R.S. Ransing, R.W. Lewis and C. Lin, *A medial-axis-based interpolation method for solidification simulation*, Finite Elements in Analysis and Design, 2004, Vol. 40, pp. 577-593

C. Lin, R.S. Ransing and R.W. Lewis, *Optimal Bearing Length Design for Extrusion Dies using Medial Axis Transform*, Proceedings 11^{th} Annual Conference of the Association for Computational Mechanics in Engineering, University of Strathclyde, UK, 24^{th}-25^{th} April, 2003, pp. 25-28

W. K. S. Pao, C. Lin, M. P. Sood, R. S. Ransing and R. W. Lewis, *Medial Axis Based Interpolation Tool-Kit for an Approximate Estimation Of Casting Temperature*, Proceedings 10^{th} Annual Conference of the Association for Computational

Mechanics in Engineering, University of Wales Swansea, UK, 14^{th}-17^{th} April, 2002, pp. 89-92.

R. S. Ransing and C. Lin, *Bearing Length Prediction using Historical Data*, submitted to Materials Processing Technology

C. Lin, R. S. Ransing, M. P. Sood and R. W. Lewis, *An Innovative Layout Design Approach Part I: Single-hole Extrusion Dies*, submitted to International Journal of Production Research

C. Lin, R. S. Ransing, R. W. Lewis and M. P. Sood *An Innovative Layout Design Approach Part II: Multi-hole Extrusion Dies*, submitted to International Journal of Production Research

Geometric based Extrusion Die Auto-classification using Medial Axis Transform, under preparation.

1.4 Thesis Layout

This thesis is subdivided into nine chapters. The following is a synopsis for each one.

Chapter 1 Introduction
Gives a brief introduction of the research work. The research objectives and tasks are defined and a summary of research contribution is given. The thesis structure and layout of each chapter is included.

Chapter 2 Aluminium Extrusion
This chapter first provides a brief description of the historical and current status of aluminium extrusion processes. The next section describes the different types of extrusion processes and the equipment used for extrusion. Different flow patterns obtained due to the friction are explained. Various types of extrusion dies designs and die design layouts are then explained. The bearing length design, pocket design and hollow section die design are introduced. This chapter provides the background and understanding of the extrusion process and sets the context for Chapter 3 which defines the objectives for this research study along with the review of relevant literature.

Chapter 3 Extrusion Die Design Approaches
This chapter defines the objectives of the research work. The first section describes the basic die design procedures used by die designers based on trial and error, experiments, intuitive skills and historical good designs and brings out the disadvantages of this inefficient approach. The second section views and presents extrusion die design as a type of optimisation process and describes how a die designer uses various types of design parameters and design rules to achieve the best possible results. However, the design loop is still encapsulated with the designer and is not fully explained. The section then goes on to describe how various empirical design formulae are used by die designers to demystify and explain the extrusion process and the limitations that still remain in this approach. The advantages and limitations of the numerical simulation (Finite Element Method) approach are then briefly discussed with regard to extrusion die design. The chapter then proposes an ideal optimisation process for extrusion die design that uses a feedback mechanism to use and build on design information provided by successful designs, FE simulations results and 'good' experiments. This section sets the context and structure for the rest of the thesis. The last section then provides a commentary based on a review of literature on existing trial and error approaches, empirical bearing length design formulae and FEM based approaches. The concluding section summarises the comparison of all these approaches and the limitations posed by them.

Chapter 4 Medial Axis Transform
The chapter introduces and provides an insight and understanding of the medial axis transform. The first section defines MAT, provides examples of MAT and describes the properties of MAT. The next section then describes various algorithms used to generate MAT which is followed by a section detailing its application in various industrial fields and finally summarises the understanding and learning gained from this review.

Chapter 5 Bearing Length Prediction using Historical Design Data
This chapter aims to achieve the objectives set out in Chapter 3, build on the knowledge gained and the potential offered by the medial axis transformation described in Chapter 4 and presents a novel knowledge representation scheme based on geometric reasoning techniques. The chapter describes a typical extrusion die designs process and the various methods that are used by die designers to achieve best results highlighting the widely used design rules based on bearing

length. The next section then describes the bearing length design process that uses empirical design formulae. In an effort to overcome the limitations posed by empirical design formulae and numerical simulation approaches, a new approach for die design representation is proposed in the next section which ensures that historical information from past successful designs is stored and re-used to optimise empirical design formulae. The approach is then validated using a case study.

Chapter 6 An Innovative Layout Design Approach for Extrusion Dies
This chapter further explores geometric reasoning techniques and proposes a new approach for an optimal design for orientation and locations of the die openings in multi-hole extrusion dies. After briefly providing a background on extrusion die layout design, the next section discusses current approaches for such designs and highlights their limitations. A new innovative approach, based on empirical bearing length design formulae, is then introduced for die layout design. The fourth section describes a general concave and convex shell boundary generating algorithms. These algorithm are used to calculate valid design zones for both single- and multi-hole die layout design work. Optimal layout designs for single- and multi-hole dies based on bearing length difference (BLD) distribution are proposed. The proposed approach is then validated using four case studies and finally conclusions are drawn from the work.

Chapter 7 Geometry Reasoning using Medial Axis Transform
The first section of this chapter shows two geometry model definitions and basic geometry information contained in MAT. The second section discusses the classification of MAT vertices and edges. The following sections introduce geometry reasoning algorithms using MAT one by one. Section three talks about a branch searching algorithm. The fourth section illustrates how to use topology shape of MAT to determine whether a geometry model has a hole and how to calculate the number of holes in the geometry. The next section introduces a new algorithm which can be used to separate tips and rough-boundary sections from normal sections. Section six introduces the topic of local aspect ratio which comes from a typical aspect ratio and how to use it to find out critical sections of a shape. The seventh section shows several shape factors and algorithms which can be used to evaluate the complexity of geometric shapes.

Chapter 8 Extrusion Die Classification based on Shape Features

This chapter introduces a new shape classification category and approach for extrusion dies. The first section of this chapter shows the shape groups widely used by die designers and a brand-new shape category based on different criteria. Several well-known design factors are introduced in the second section. Based on the geometric reasoning algorithms mentioned in Chapter 7, a new classification algorithm and several new criteria have been introduced in Section two as well. The last section shows three classification cases using the new algorithm and criteria.

Chapter 9 Conclusion and Future Work

This chapter brings out the conclusions from this research work, and recommendations are made for possible future research.

Chapter 2

Aluminum Extrusion

Chapter Layout

This chapter first provides a brief description of the historical and current status of the aluminium extrusion process. The next section describes the different types of extrusion processes and the equipment used for extrusion. Different flow patterns obtained due to the friction are explained. Various types of extrusion dies designs and die design layouts are then discussed. The bearing length design, pocket design and hollow section die designs are introduced. This chapter therefore, provides the background and understanding of the extrusion process and sets the context for Chapter 3 which defines the objectives for this research study along with the review of relevant literature.

2.1 Aluminium Extrusion

Extrusion can be described as a plastic deformation process in which a block of metal (billet) is forced to flow through a die for obtaining desired objects. A schematic example of an extrusion press is shown in Fig. 2.1.

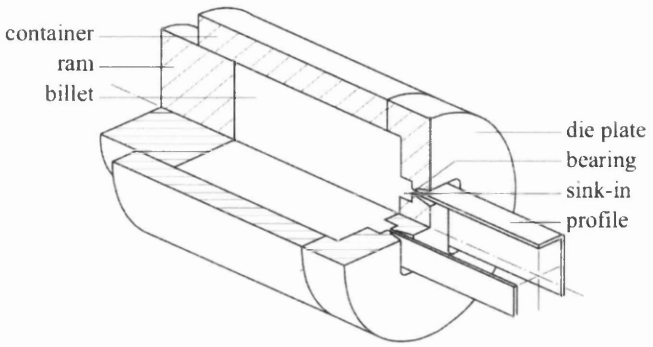

Figure 2.1: Extrusion press (schematic) [18].

The extrusion process is capable of producing long and straight metal or polymer products such as bars, solid and hollow sections, tubes, wires and strips. Some common aluminum extrusion products are shown in Fig. 2.2.

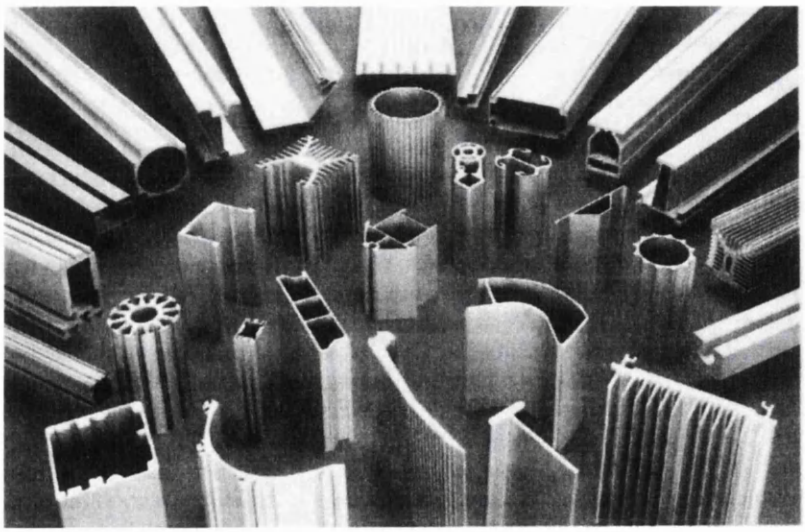

Figure 2.2: Common extrusion products [19].

2.1.1 The History of Extrusion

Our understanding and earlier perception of the principles of extrusion is based on the pioneering work of Bramah that resulted in a patent in 1797 [20]. He developed a press in which molten lead from an iron pot was pumped into a long projecting tube, which served as a die Fig. 2.3(a). A tapered mandrel was supported concentrically with the tube by a bridge in its enlarged end. This was the first recorded claim of the development of a machine which clearly contains the ideas of extrusion, whilst also suggesting the idea of die-casting.

In 1820, Thomas Burr constructed a press operated by hydraulic power for manufacturing lead pipes by extrusion [20]. In this press, a container was sealed with a close-fitting plunger, a steel die and a screwed mandrel was attached to the hydraulic ram (Fig. 2.3(b)). After the lead which was poured into the container through the die-orifice has solidified, the hydraulic ram is operated to force the lead flow through the die to form the pipe.

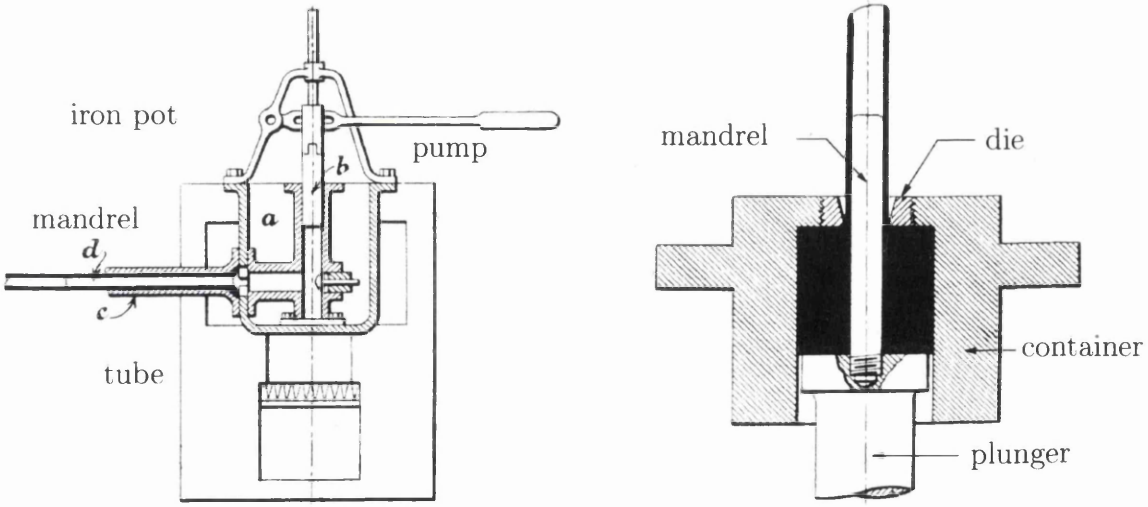

(a) Bramah's lead-pipe machine

(b) First press for hydraulic extrusion of lead pipes

Figure 2.3: Extrusion press in history [20].

In 1863, Shaw used a press in which pre-cast hollow billets of lead, with an internally cast sleeve of tin were charged cold into the container. His experiments showed that it was difficult to get a correct shape of the sleeve for providing a uniform lining of tin in the pipe.

A remarkable press with advanced features was invented in France by Hamon in 1867 [20]. The principal points of interest were

- The use of a fixed mandrel bar over which the extrusion ram travelled.
- The container was made with ducts in its outer jacket through which steam or hot gases could be circulated to raise its temperature to 210 °C
- An auxiliary hydraulic ram was used to bring the die and die-holder into position against the container, where it was locked.
- An accumulator was introduced into the hydraulic system. Although the hydraulic accumulator had been invented by Sir William Armstrong in 1840, it is not known to have been used before this in connection with extrusion.

2.1.2 Extrusion presses for sheathing electric cables

In 1879, Borel in France and Wesslau in Germany developed the first methods by which a lead sheath could be directly extruded into cables. In both cases vertical extrusion presses were used [20].

2.1.3 Extrusion to copper alloys

The advances in the field of extrusion in the lead industry and the advantages that it offered attracted interest and research for its possible utilisation for other metals, such as brass alloys. However, brass alloys are not sufficiently plastic to undergo the heavy deformations involved in extrusion until they are heated to a temperature of at least 600 °C.

Alexander Dick overcame the problems being faced in higher melting point alloy extrusion processes [20]. One of Dick's early designs is shown in Fig. 2.4. The horizontal frame was tied together by four rods. A heavy crosshead formed one end of the press and supported the die, which was held in position against the container by a pair of jaws, pivoted at the base of the crosshead. The container, held and centred by the set-screws, was surrounded by a furnace jacket heated by coke or gas. The billet, heated to a plastic state, was fed into the container

from the front. For preventing the ram from becoming wedged by escaping metal past its sides, a disked or corrugated disc (the modern dummy block) was placed between it and the billet. At the end of the extrusion, the jaws were opened to allow the die and discard to be pushed out.

Dick is credited with many firsts for the progress he engineered in the field of extrusion such as an electrically heated container, experiments with different copper alloys, various types of fixed and floating mandrels. It is observed that although radical changes in design and accessory equipments have taken place during the last century, the extrusion presses even now are essentially constructed on the principles laid down by Dick [20].

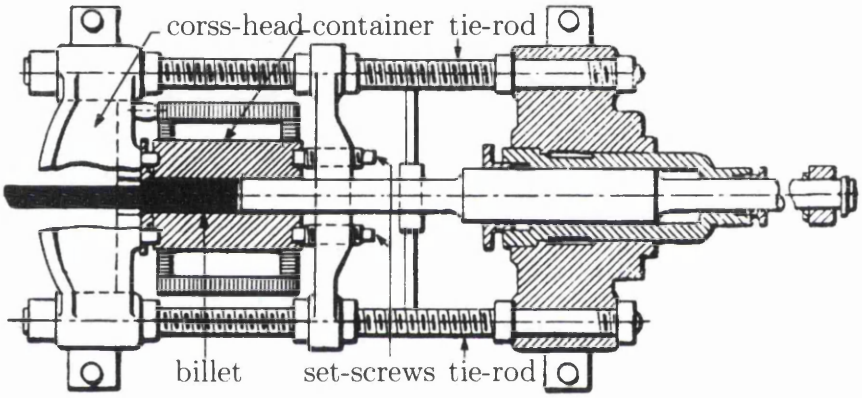

Figure 2.4: Horizontal extrusion press designed by Alexander Dick in 1894. [20]

2.1.4 Extrusion at Present

As one of the most important manufacturing processes, extrusion has assumed a very significant role in present day industry.

According to the Aluminum Association the United States' aluminum industry is producing about $39.1 billion annually in products and exports [21]. The U.S. Aluminum industry employs over 145,000 people with an annual payroll of about $5 billion. Top markets for the Aluminum industry are in the field of transportation, beverage cans and other packaging and building construction.

In 2000, aluminum overtook plastic with an average content of 257 lbs per vehicle becoming the third most-used material in automobiles. Automakers are increas-

ingly choosing aluminum to improve fuel economy, reduce emissions and enhance vehicle performance.

As mentioned by the European Aluminium Association [22], Extruded products constitute more than 50% of the market for aluminium products in Europe of which the building industry is the biggest consumer. Extruded products increased steadily with an average annual growth rate of 3.3% in last 20 years.

2.2 Extrusion Process and Equipments

The extrusion process can be carried out by means of two basic modes - direct and indirect extrusion.

2.2.1 Direct and Indirect Extrusion

Direct extrusion is the simpler of the two modes. It can be carried out with or without a lubricant, with or without a shell in the latter case. Almost all metals tend to shear at the container interface, thus adding to the force required to extrude the metal and depositing a layer at that interface. (Fig. 2.5(a)).

In indirect extrusion, the die at the front end of the hollow stem moves relative to the container but there is no relative displacement between the billet and the container. Therefore,, there is no friction between the billet and container wall and also there is no displacement of the billet centre relative to the peripheral regions. Therefore, the load decreases. (Fig. 2.5(b)).

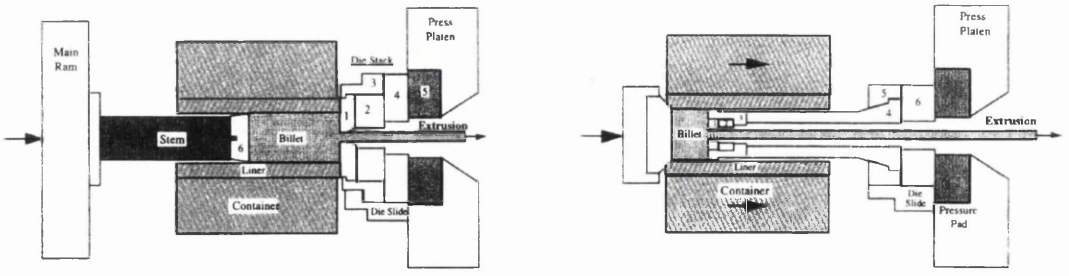

(a) Direct extrusion press

(b) Indirect extrusion press

Figure 2.5: Direct and indirect extrusion press[23].

The major difference between these two modes is that there is no friction between the billet and container for the case of the indirect mode, whereas, in the direct mode the outer shell of the billet moves relative to the container as extrusion proceeds thus causing friction, often resulting in shearing of the billet. The ease with which the process is carried out depends on the selection and application of the lubricant.

Figure 2.6 shows the loads in direct and indirect extrusion. As shown by the curve which indicates the load/displacement of direct extrusion, the load increases very rapidly at the beginning as the billet fills the container. A further increase in pressure results in a cone-shaped deformation zone in front of the die. The pressure falls as the billet length decreases. By avoiding friction between the billet and the friction between the centre and peripheral parts inside the billet, the indirect extrusion mode needs much less pressure in the beginning. Therefore a less varying pressure load can be achieved as the smoother curve indicates in Figure 2.6.

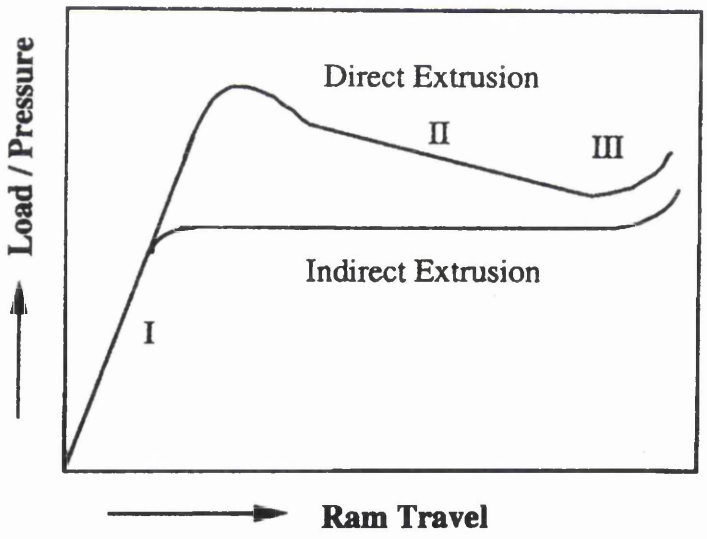

Figure 2.6: load/displacement curves for direct and indirect extrusion [23].

The main advantages of indirect extrusion are that, there is a $25-50\%$ reduction in peak load compared to direct extrusion and also a higher permissible extrusion speed. Since the extrusion pressure is not related to billet length, there is no limit as to the load required and is only limited by the length of the hollow stem. A lower temperature increase, service time of inner liner and other tools increased, and more uniform deformation of the complete billet cross section are some of

the other advantages.

The disadvantage of indirect extrusion arises because of the modified flow in this mode, as a result impurities or defects on the billet surface affect the surface of the extrusion and are not automatically retained as a shell or discard in the container. Therefore, machined billets have to be of the size of the hollow stem. Another disadvantage which is not easily overcome is that the product must travel the length of the stem before it is possible to quench. Because of these limitations indirect extrusion has not been as popular as the direct process.

2.2.2 The Extrusion Press

Figure 2.7(a) shows a modern direct extrusion press. In fact the basic design remains unchanged from Dick's earlier press. Figure 2.7(b) shows a modern indirect press for rod and tube extrusion.

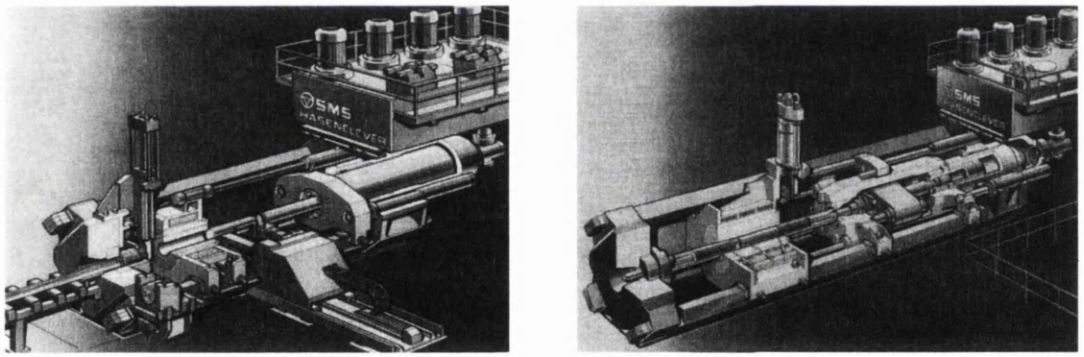

(a) Direct extrusion press (b) Indirect extrusion press

Figure 2.7: Modern extrusion press (schematic) [19].

2.3 Material Flow in Extrusion

2.3.1 Typical Flow Patterns in Extrusion

The extrusion process is quite complicated and unpredictable. It is well known that in almost all cases, the flow rate inside the extrusion billet is uneven. There

are many reasons which lead to a non-uniform flow rate. For example, friction is one of the major flow rate changing factors.

During the extrusion process, the billet is sliding inside the container such that the friction between billet and container wall, the friction between billet and extrusion dies and the friction between centre and peripheral part of billet are generated. Besides temperature distribution, material properties, extrusion speed and etc. can also influence the flow rate.

By using grid method, numerous flow patterns in extrusion have been detected by many investigators. All those flow are classified into four types and are marked as S, A, B and C in Figure 2.8.

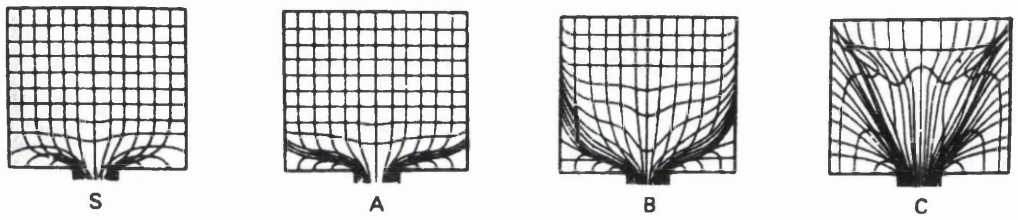

Figure 2.8: Typical flow patterns in extrusion [20, 13].

Flow Pattern S

Effective lubrication reduces friction at the liner wall or at the surface of the die and die holder; as a result, the rear part of the billet moves as a rigid body through the die. Only the front part of the billet, which enter the deformation zone, deforms evenly. The behaviour of the metal flow is indicated in the figure as a uniform grid in the whole billet and only a very small area close to the die orifice shows distortion.

Flow Pattern A

If there is no friction between the billet and container wall it is still not possible to avoid the friction between the billet and die surface - flow pattern A would be detected. This pattern shows a bigger dead zone compared to pattern S. This type of flow occurs during the lubricated extrusion of soft alloys such as lead, tin,

α-brasses, tin bronzes and copper with an oxide cover.

Flow Pattern B

This pattern occurs if there is friction at both the container wall and at the surfaces of the die and die holder. The peripheral zones are retarded at the billet/container interface, whereas the lower resistance causes the material in the centre to be accelerated toward the die. The dead metal zone is large. This flow type can be seen in copper without oxide skin and in most aluminium alloy extrusion processes.

Flow Pattern C

This flow type occurs in hot extrusion when the friction is high, and the flow stress of the material in the cooler peripheral regions of the billet is considerably higher than that in the centre. The dead metal zone is now much larger as compared to type B.

2.4 Extrusion Dies

2.4.1 Basic Structure of Solid Dies

Extrusion dies can be divided into solid and open shape dies. Solid dies are used for simple solid shape extrudates. Open shape dies, which have welding chambers, are used for semi-hollow and hollow shapes.

A two piece solid die is shown Figure 2.9. As illustrated, the thickness of the die opening side wall is called the bearing length. There may be a recess (pocket) in front of the extrusion die opening (face to the billet). An additional plate, called a die backer, could be placed after the die with a wider recess to provide extra strength. The structure of hollow dies are more complicated and may include other structure types such as bridges, portholes etc.

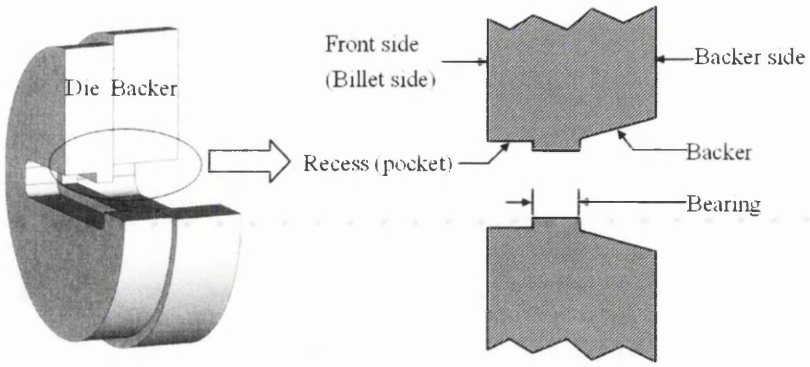

Figure 2.9: Basic structure of a solid die.

2.4.2 Dies for Solid Sections

Flat dies are used for solid section extrudates. A flat die is a piece of metal plate with an orifice through which metal flows. A turned ring is used to position the die with the die holder. Some flat dies have a recess around the die orifice for adjusting metal flow. A die backer and/or feeder plate is also used with the flat die during the extrusion process (Figure 2.10).

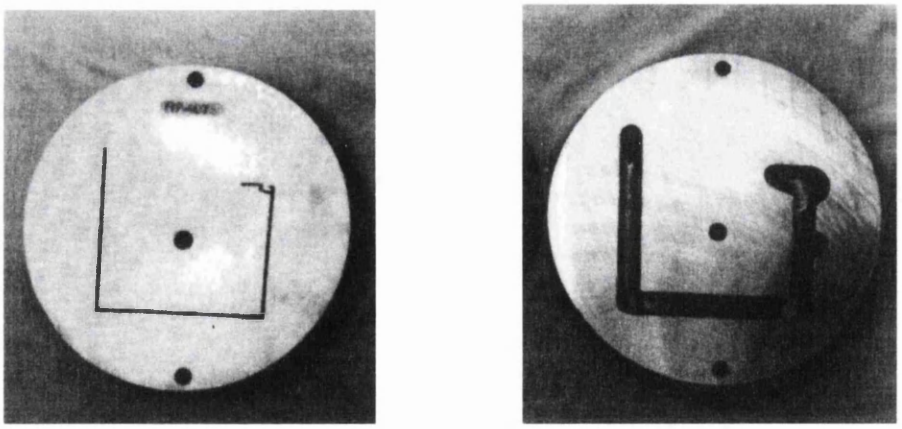

(a) Flat die (b) Die backer

Figure 2.10: Flat die and die backer [23].

2.4.3 Dies for Hollow Sections

Dies used for hollow sections are bridge dies, spider dies and porthole dies. Due to the advancements made in the field of extrusion technology, these dies are being

produced today and would not have been thought possible a few years ago.

Bridge Dies

The bridge die is principally used when the surface finish is of paramount importance. The die operates at low temperatures, because the discard is removed at the end of each extrusion. The large discard is a disadvantage. Bridge dies are the most expensive of the hollow section dies, because of the very high machining costs involved to obtain the finished products (Figure 2.11).

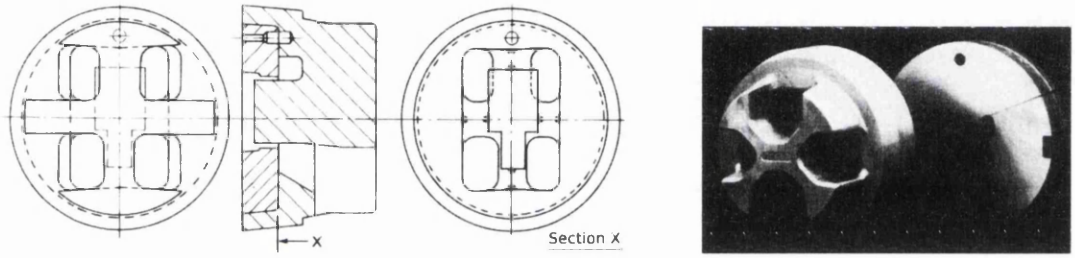

Figure 2.11: Bridge die [13].

Spider Dies

The spider die (Figure 2.12) originated in America and is mainly used for large hollow sections with low extrusion ratios [13]. The major advantages are increased stability of the die, the large welding chamber around the section that ensures a favourable material flow, and the die can be replaced frequently at a low cost because the quality of the internal surfaces of the section need not be as high as the external surfaces. The disadvantage is that it has to be cleaned by pickling for a long time before any checks or alterations can be made. The residue in the conical section can be only partly removed in the press.

Porthole Dies

This type of die can almost always be used and represents the best and most suitable development for meeting modern requirements. Porthole dies are also

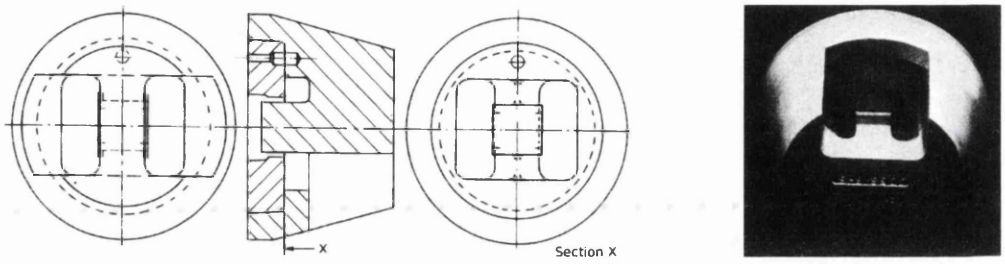

Figure 2.12: Spider die [13].

suitable for multi-hole dies and the enclosed type of construction gives a high degree of stability (Figure 2.13).

Porthole dies have many advantages e.g. the extrusion ratio can be selected by using the optimum material flow; the discard can be partly removed; it can be used with the maximum section circumscribing circle diameter relative to the container diameter; sections with large variation in shape can be produced only with porthole dies. The major disadvantage is that porthole dies are very difficult to correct because of the poor accessibility to the sliding region of the die.

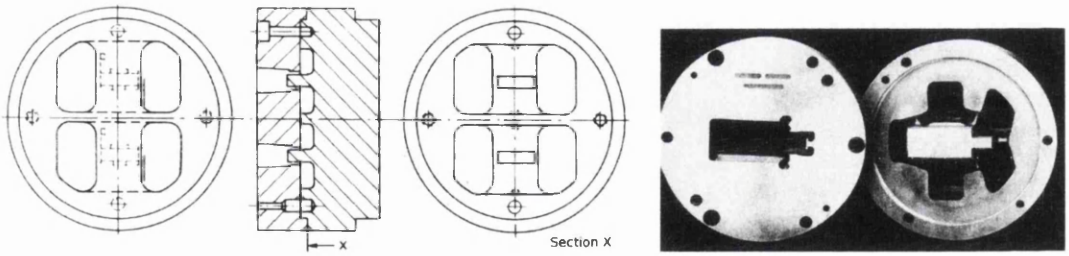

Figure 2.13: Porthole die [13].

2.5 Extrusion Die Design

Extrusion die design is the most important aspect of the entire extrusion process. Many design factors can influence extrusion die design, such as press procedure and maintenance, pressure, temperature etc. The skill and experiments of individual die designers are vital to the production and quality of extrusion dies. Due to the complexity and flexibility of the design work, there are no two truly identical designs. Though the design work for the extrusion dies might be looked

upon as some kind of "black-art", the goal remains the same i.e. to get high quality extrudates and maintain high productivity. The basic considerations of die design are:

- The number of die openings
- Location and orientation of die openings
- Optimization of bearing length design
- Other feature design
- Other design factors related with temperature, load, material, etc.

2.5.1 Die Layout Design

The first step for the extrusion die design is the layout design. For any die and die opening profile, a proper layout has to be chosen before other design work can be initiated. The basic layout design factors are ([23]).

- Proper clearance between the die opening and the container wall
- Proper clearance between different die openings for multi-hole dies
- Balanced metal flow to avoid distortion of the shape
- Ease in die design and manufacture
- To avoid overlapping and scratching a particular part of the extrusion on the run-out table.

A proper clearance between die openings and the container wall is required to avoid the oxide skin of the billet being flown into the extrudates. The clearance between different die openings can also provide strength to avoid cracking and deflection in the die.

For multi-hole dies, there are two kinds of layout design–flat layout and radial layout. In a flat layout design, all the major axes of the die openings are either parallel or perpendicular to the radius of the die whereas, in a radial layout design,

all the die openings' major axes lie along the radius of the die. Two examples for flat and radial layout design are shown in Figure 2.14(a) and 2.14(b) respectively.

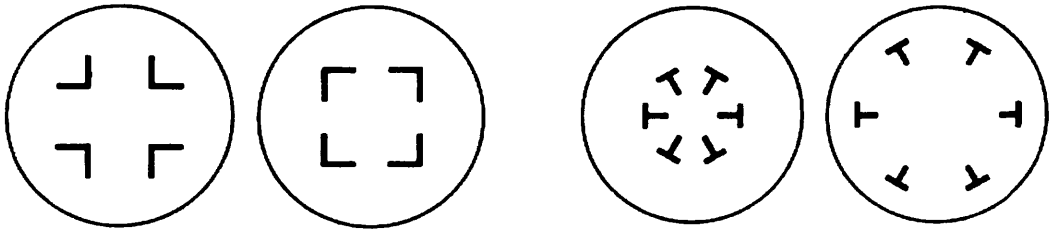

(a) Flat layout design (b) Radial layout design

Figure 2.14: Spider die [13].

Though the flow behaviour inside an extrusion billet is very complicated, designers still use some simple rules to get an even flow. For example, instead of using the geometrical centre of the die opening profiles, the centres of gravity (CG) of these profiles are used as the reference point for design work. For a single-hole die, the die opening is placed on the central part of the die in such a manner that the die opening's CG is located at the die centre. For a multi-hole die, the CG of each die opening coincides with the CG of the sub-region of the die.

2.5.2 Bearing Length Design

Extrusion dies are very important for the extrusion process. They not only decide the shape of extrudates, but also influence the quality, cost and productivity. Of all the kind of configuration methods of a die, the bearing length design is the most important. The material flow velocity of an extrusion billet is non-uniform due to the friction between the billet-container and billet-die frictions as mentioned before. Though the behaviour of the flow is very complicated and difficult to estimate, there are two major factors which are in charge of the flow pattern. The first factor is the section width of the die opening profile and the length of bearing. It is obvious that the wider section will allow the material to flow through easily and the thick bearing will generate greater friction and retard the flow. In the direct extrusion process, the frictional resistance at the billet container interface slows down the flow near the billet surface. The centre of the billet moves faster than the periphery of the billet. This leads to the second

factor which is related to the radial distance from the die centre. According to these two factors, the primary bearing length design depends on:

- The distance of the opening from the centre of the billet
- The section thickness (width)

Figure 2.15 shows a schematic solid die. It clearly shows that even for a very simple rectangle bar shape die opening profile, a parabola-shaped bearing length design is required to get rid of the effect caused by different radial distances of each part of the die.

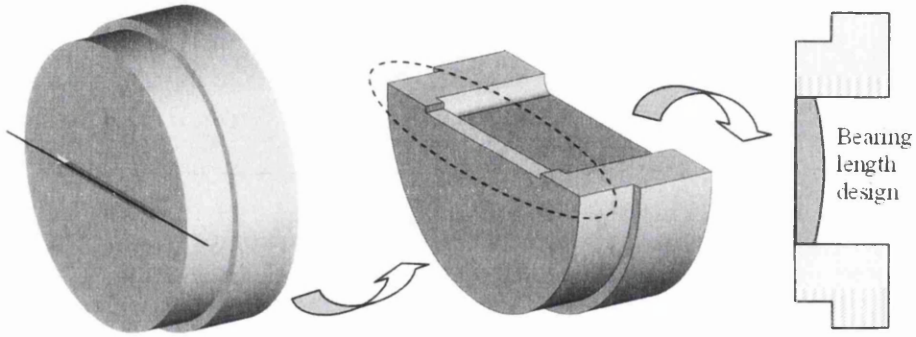

Figure 2.15: Bearing length design of a solid die.

Besides the major design factors, there are several minor design factors. For example, the bearing length should be reduced around the corner or tip areas. The reason is that the friction in these areas is larger than for a normal section. Sharp changes of bearing length have to be avoided. Otherwise, extra flow discontinuity might be introduced which could cause failure.

2.5.3 Pocket (Recess) Design

Besides the bearing length, pocket, sometimes also called a recess, is another used design method. A recess die has a single-stage recess around the die opening at the front side of a die (the surface faces the billet). An example of a recess die is shown in Figure 2.16.

A single-bearing die is some kind of modification of a single-stage recess die. The

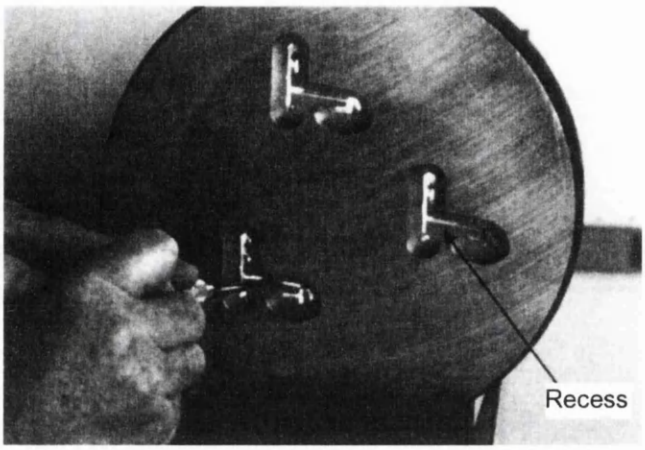

Figure 2.16: Recess die. [23]

single-bearing die has multiple stages of cavities and allow aluminium to be easily pushed through the die at higher production rates [24] (Figure 2.17).

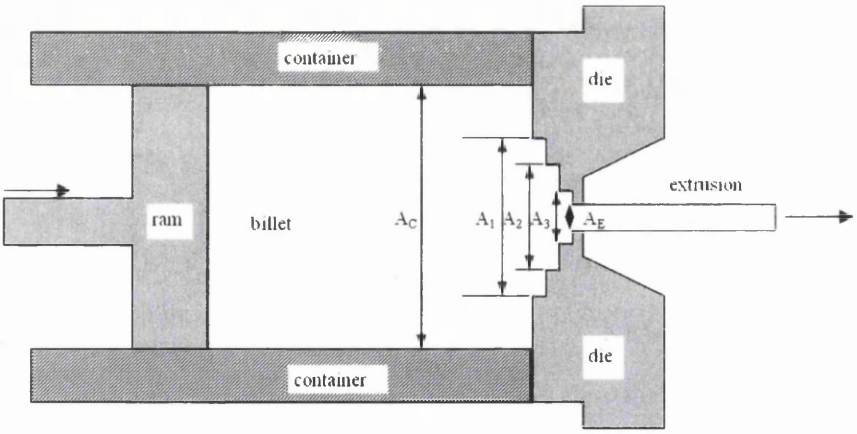

Figure 2.17: Three-stage single-bearing die.

The increase in extrusion speed in single-bearing dies can be explained by using the volume constancy relation that is given by [23]:

$$A_C V_R = A_{C_m} V_{C_m} = A_E V_E \tag{2.1}$$

where A_C is the area of container bore, and V_R is the speed of the ram. A_E and V_E are the area and velocity of the extrudate respectively. A_{C_m} is the mean area of the stepped cavity ($A_{C_m} = (A_1 + A_2 + A + 3)/3$). The speed of extrusion is given by:

$$V_E = \frac{A_{C_m} V_{C_m}}{A_E} \tag{2.2}$$

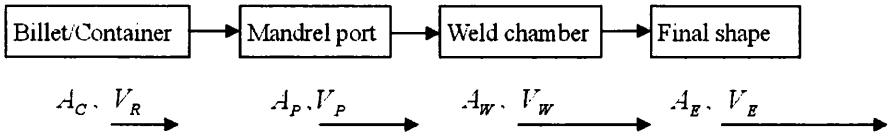

Figure 2.18: Control volume of porthole hollow die [23].

For a fixed area of extrusion, V_E is proportional to the area of the cavity and the speed of the metal flowing through the cavity.

2.5.4 Hollow Section Die Design

For a hollow die, the metal flow through the whole die is in three steps. In the first step, the metal flows from the billet to the mandrel port. In stage two, the metal flows into the weld chamber. In the last stage, the metal flows through the gap between the mandrel and cap (die) to get the final shape.

The volume constancy relationship, as shown in Figure 2.18 for a hollow die, is given by:

$$A_C V_R = A_P V_P = A_W V_W = A_E V_E \tag{2.3}$$

where A_P is the area of the port in the mandrel, V_P is the material speed through the mandrel port, A_W is the area of the weld chamber and V_W is the material speed through the weld chamber [23].

2.6 Summary

A short introduction on aluminium extrusion has been given in this chapter. A basic knowledge about the extrusion process, equipment and dies are mentioned. For extrusion dies, different type of dies are shown and the primary design aspects for extrusion dies are covered as well. It is clear that the flow pattern inside a billet is complicated and unpredictable. Bearing length design and layout design are two major design facts by which an uniform exit velocity can be achieved and for which reasonable extrudates can be made.

Chapter 3

Extrusion Die Design Approaches

Chapter Layout

This chapter defines the objectives of this research work. The first section describes basic die design procedures used by die designers based on trial and error, experiments, intuitive skills and historical good designs. It will also bring out the disadvantages of this inefficient approach. The second section views and presents extrusion die design as a type of optimisation process and describes how a die designer uses various types of design parameters and design rules to achieve the best possible results. But the design loop is still captive with the designer and is not fully explained. The section then goes on to describe how various empirical design formulae are used by die designers to demystify the design task and explain the limitations that still remain in this approach. The advantages and limitations of numerical simulation (Finite Element Method) approach are then briefly discussed with regard to the extrusion die design. The chapter then proposes an ideal optimisation process for extrusion die design that uses a feedback mechanism to use and build on design information provided by successful designs, FE simulations results and 'good' experiments. This section sets the context and structure for the rest of the thesis. The last section then provides a commentary based on review of literature on existing trial and error approaches, empirical bearing length design formulae and FEM based approaches. The concluding section summarises the comparison of all these approaches and the limitations posed by them.

3.1 Extrusion Die Design Objects

3.1.1 Typical Extrusion Die Designer Design Process

Extrusion die design and die making are the most important aspects of the entire extrusion process. Extrusion die design work is a difficult, expensive and time-consuming procedure. For example, trail-and-error design procedures introduce additional costs for the extrusion works as much as $45 \sim 50\%$ on average. For a flat die, this number can go up to $90 \sim 100\%$. Each trial extrusion on average delays the die design about three days [25].

For any new die, a designer would start his work by inspecting the shape of the die profile. This step gives the geometrical information such as width, length, shape etc. The designer then estimates design parameters, such as bearing length, choke, relief, pocket, etc., based on the geometrical information and produces an initial extrusion die design. The die with the initial design is then put into the extrusion process for further testing. If poor quality extrudates are produced, a correction in the design is undertaken. If the design is very bad, all design parameters might have to be checked again by the designer and a new design would be given for another trial extrusion. A flow chart of a typical extrusion die design procedure is shown in Figure 3.1.

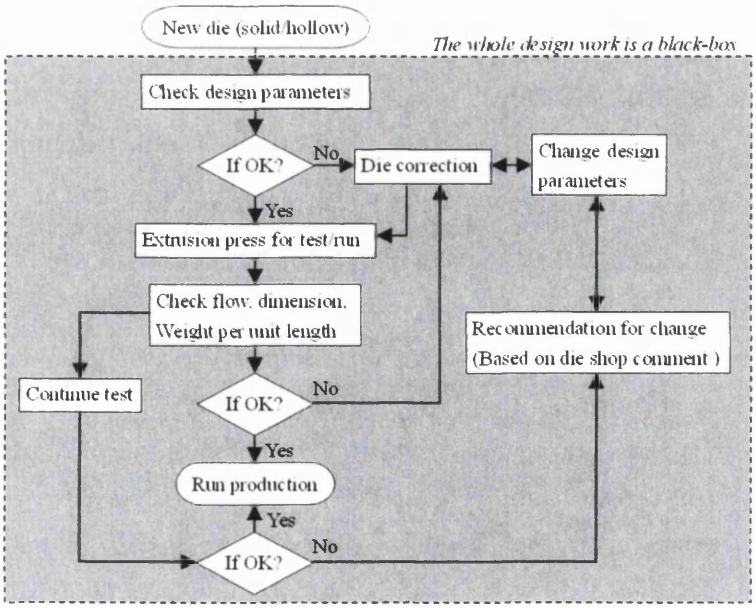

Figure 3.1: Typical design procedures and die variables.

3.1.2 Research Objects

As mentioned in the previous sub-section, during the whole design-correction-redesign circle, the designer does his job based on experiments, skill and historical good designs. The whole design knowledge therefore is kept in the designers' mind and works as a 'black box' for other people. The objective target of this research work is to investigate a better way to reveal and capture the design knowledge and store this in such a way that a computer can re-use it properly. Since the die profile shape is an important design parameter for die designers, a new extrusion die classification scheme is also introduced in this research work. The following chapters will cover the topics given below:

- Extrusion die design knowledge representation and bearing length design using historical data
- Extrusion die layout design based on bearing length estimation result
- Extrusion die classification using a set of new geometrical analysis criteria

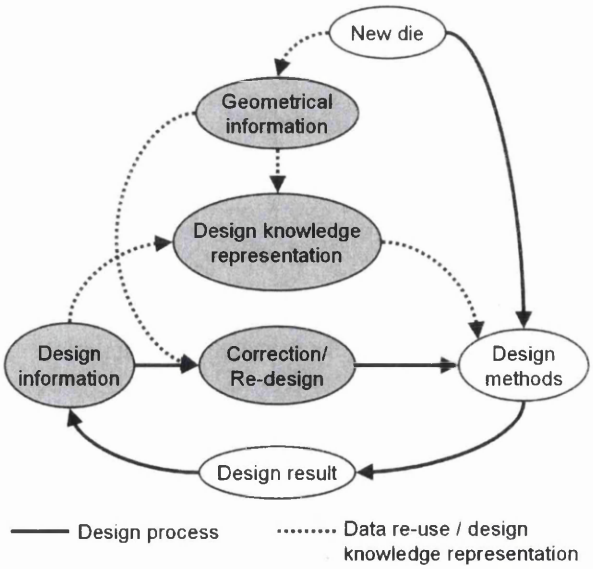

Figure 3.2: A brief layout of the research objects

A brief chart for showing the relationship between the research objects is shown in Figure 3.2. All solid lines indicate the typical die design process. As shown in the figure, design methods and die correction/re-design are the major parts

in the process. Grey ellipses and doted lines in the figure show the research objects. The basic idea of the research work is using die classification result to choose properly optimised design rules for an extrusion die and to re-use previous successful designs to retrieve and optimise extrusion die design rules.

Due to the sensitivity of the design data and the similarity of the optimization approaches, only channel shape die opening profiles and widely used Miles96/97 formulae are chosen for demonstrating the approach. However, other profile shapes and bearing length design methods should work properly as well. More detailed layouts of each part of the work are introduced in the following sub-section.

3.2 Optimization for Extrusion Die Design

3.2.1 The Concept of Optimization

Actually, extrusion die design work can be seen as some kind of optimization process. In general, optimization is the process by which optimal results can be achieved under given constrains. For any given problem, the target of the optimization is to get the maximum or minimum value of one or several object functions. For some very simple cases, the maximum and minimum value of an object function can be deduced directly. But in the common case, the object functions are either too complex to solve or may not capture the true physics. Hence, if an optimization algorithm is employed, several loop steps might be needed to get an optimal answer. A schematic flow chart of the optimization process is shown in Figure 3.3. Please note that the loop (feedback) in the figure is essential for the approach.

3.2.2 Optimization Process for Extrusion Die Design

For extrusion die design, the simplified optimization process (the design process) is shown in Figure 3.4. As shown in the figure, the whole design process can be divided into a few steps. The first step is to check design parameters such as die profile section widths, lengths, radial distances and shapes and give an initial design based on this information. The design rules are indicated by a function

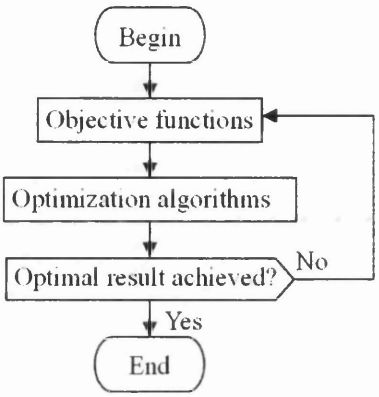

Figure 3.3: Flow chart of general optimization process

f with several input variables. The input variables of the function are design parameters used by the die designer. The second step is to check the design. Step 3 is to justify the extrusion quality of testing dies. If the quality is not good, the die correction, or a re-design step, is needed. This is marked as step 4 in the figure. If the checked result is good enough, the design work is complete and the die is ready for use, marked as Step 5 in the figure.

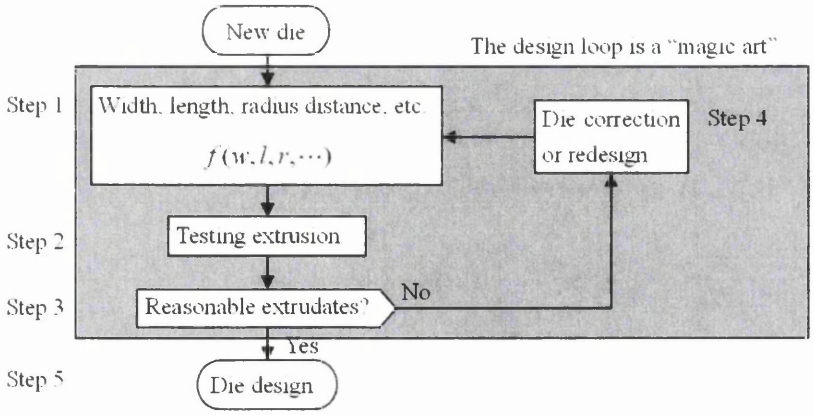

Figure 3.4: Flow chart of general optimization process

It is clear that all the design processes, whether the parameter-assignment step or die correction step, are finished by the die designer. The design loop is however hidden in the designer's mind during the whole process. To reveal the magic steps of extrusion die design work, researchers have tried different ways and one of them is to use an empirical design formulae. The basic idea of this approach is to simplify the designers' knowledge and skill into several design rules and use modelling techniques to quantify and integrate them.

3.2.3 Empirical design formulae and Extrusion Die Design Process

The schematic figure(Figure 3.5) shows the basic idea and the status of empirical design formulae in the extrusion die design process. As shown in the figure, empirical design formulae can partly assist the designer to produce an initial die design. It is also clear that this approach has two major limitations. It marginally reduces the design effort. However, most of the part still remains in the black box. The other problem is that there is no feedback to improve the design formulae. It means that there is no way to modify or optimize extrusion die design formulae based on correction and modification results given by expertises. So the historical data can not be re-used.

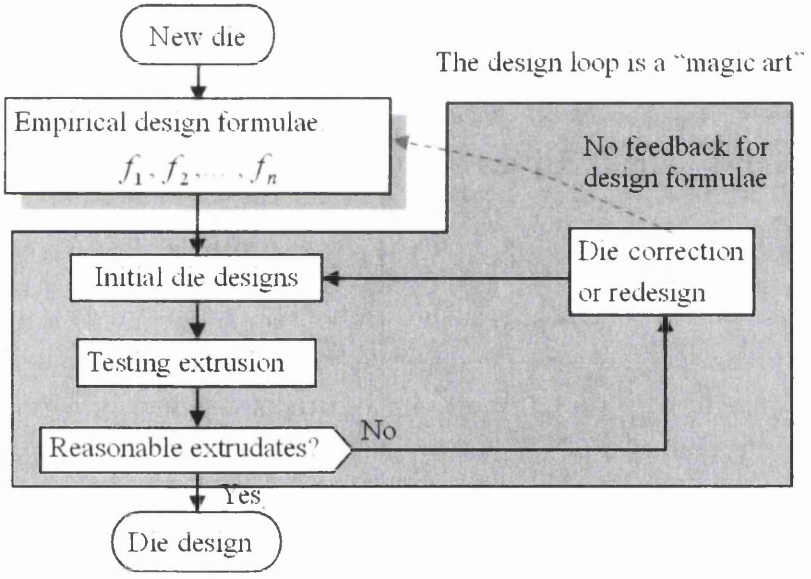

Figure 3.5: The position of empirical design formulae in the extrusion die design process

3.2.4 FE simulation and Extrusion Die Design Process

As a powerful and versatile approach, the finite element method (FEM) is widely used to solve extrusion problems. FE simulation is used to simulate material flow, temperature, pressure etc. The characteristics of extrusion design work decides that numerical simulation can not be used for the design work alone as it can not

account for heuristic and geometric information in the form of rules. However, it can be coupled with some other approaches to get better results.

In most cases, numerical simulation can be used to conduct 'virtual experiments' to assess the design work as shown in Figure 3.6. As high-lighted in the figure, FE simulation can be used to model the extrusion process so that die design quality can be estimated without experiments. Also, all simulation result can be kept in the computer for further analysis. Similar to empirical design formulae approach, traditional numerical methods have limitations too. The first is that numerical simulation results can not be used for die correction or modification. The other problem is that simulation result data can not be reused automatically for design work. Again, the whole design loop is a black box like other approaches discussed before.

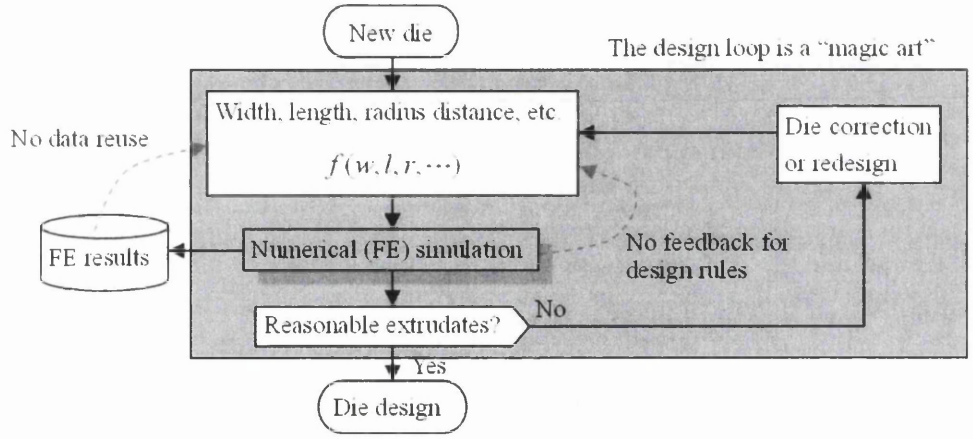

Figure 3.6: The position of numerical simulation in extrusion die design

3.2.5 Ideal Optimization Process for Extrusion Die Design

The previous discussion illustrates that the traditional design process, empirical design formulae and numerical simulation methods have their own benefits and limitations. Among these limitations, a lack of support for data reusing and design knowledge representation are the major ones. To overcome these disadvantages, a new design process is developed (Figure 3.7). The most obvious differences in this process, as compared to the previous approaches, are the three

new feedback steps where design information comes from all successful past designs, FE simulation results and good experiments. As each feedback step creates a loop in the design process, all past successful design information can be reused for new extrusion dies. The ability to reuse these data actually is the key issue for design knowledge acquirement and representation. If any method can be used to reuse the historical data properly, it may be considered as a tool to mimic the skill of an experienced designer.

Among the four design loops shown in the figure, the die correction loop still needs the designer's effort. The other three loops can be done automatically so that the black box can be avoided. Because not all historical data contains explicit design/correction information a new procedure, which can link ed to historical data with design rules, is needed. In another words, a proper method has to be used to convert the design output results into design parameters.

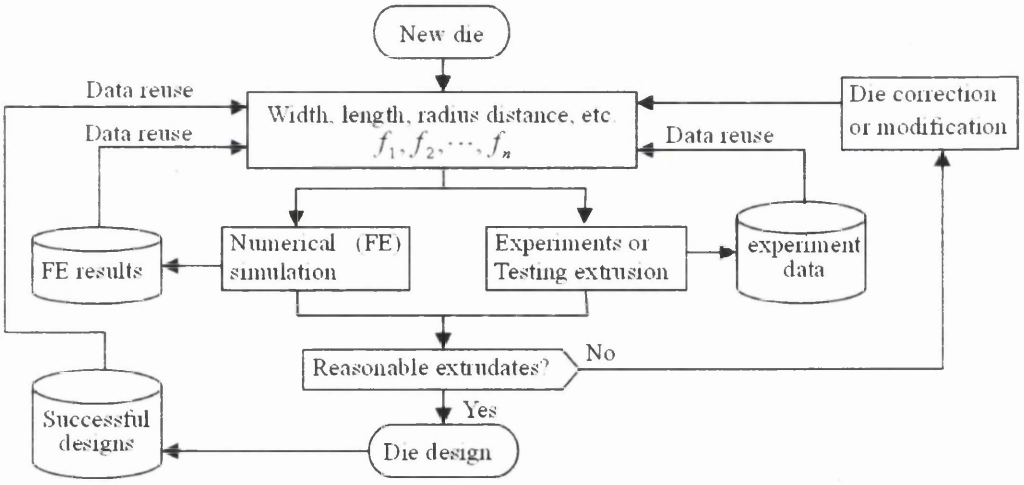

Figure 3.7: Ideal design process for extrusion dies

A modified design process flow chart of this research work is shown in Figure 3.8. Since successful designs, extrusion die experimental data and FE simulation do not give specific design information, all design/correction knowledge and skills are kept in the designers' mind. For the same reason, it extremely difficult to obtain reusable data on historical designs and FE simulation results using existing design approaches. It is clear that for knowledge representation and data reusing, the development of a versatile and robust method is necessary.

In this research work, a new design approach, based on geometry reasoning tech-

niques, is introduced from which the limitation of current design approaches can be avoided. At the same time, the new approach shows the possibility of design knowledge representation and data reusing. Since the approach is a general method for linking design information with extrusion dies, most design results, such as FE simulation results, can be linked with the die opening profiles.

For doing this, several historical data reuse rules are introduced by this new approach (illustrated as $g_1, g_2, \cdots, g_n$ in the figure). By using geometric reasoning technique, geometric information for any given die can be calculated automatically. Furthermore, design information can be captured and separated from die designs, can be analyzed and stored independently as well.

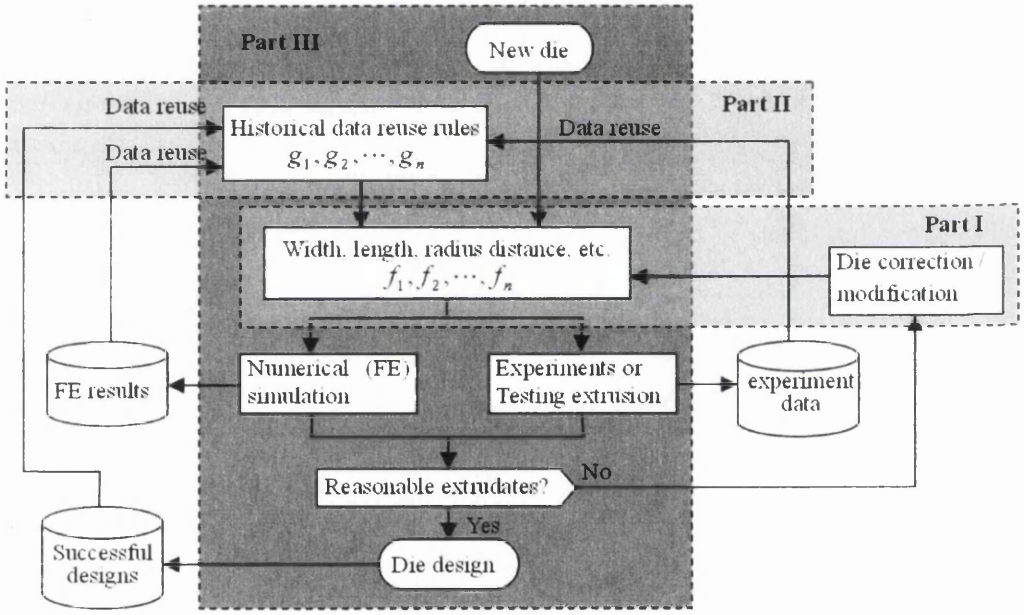

Figure 3.8: Design process used in this research work for extrusion dies

Outline of the Research Work

Based on the current understanding of the design procedure, a new design knowledge representation method is introduced. By combining empirical bearing length design formulae with historical data and geometric information, the new approach shows how to reuse the data to get bearing length design for new dies (Chapter 5). Since the layout design is another key issue for extrusion dies, a novel approach is established so that fast single/multi-hole die layout designs can be achieved.

The details of the approach is discussed in Chapter 6. The procedure covered by Chapter 5 and 6 are marked as **Part I** in Figure 3.8.

For extrusion die design, the die classification is important as different dies have different shape features and design requirements. Although the classification topic was covered by quite a few researchers during previous years, most of them only classify and not quantify extrusion dies. Besides, the current classification method is very approximate. By using the medial axis transformation process (will be introduced in Chapter 4), a set of general purpose geometry reasoning algorithms are developed and validated in Chapter 7. Based on these algorithms, extrusion die classification and quantification algorithms and results are illustrated in Chapter 8. The position of these two chapters are indicated as **Part II** in Figure 3.8.

At last, all-aspect optimization approach for extrusion dies can be implemented (marked as **Part III** in the Figure 3.8).

3.3 Extrusion Die Design Approaches

3.3.1 Trial-and-error Approach

The first design approach used by an extrusion die designer is a trial-and-error approach. By doing experiments and running tests, extrusion die designers accumulate their design knowledge and skill.

During the extrusion process, the distortion of the metal flow causes problems. The original investigation of flow in metals during extrusion was studied by Tresca in 1860s [20]. Since then, several approaches were introduced for flow investigation. Among these approaches, the Disc method and longitudinal grid method (also called as grid pattern or coordinate method) are widely used.

The first step for a designer to design a new die is to check the die opening profile and give an initial design. Then, the die is tested in an actual operation which is followed by metal flow and/or extrudates quality investigation. If the quality is not good enough, the designer corrects or re-designs the die. The whole process is shown in Figure 3.9.

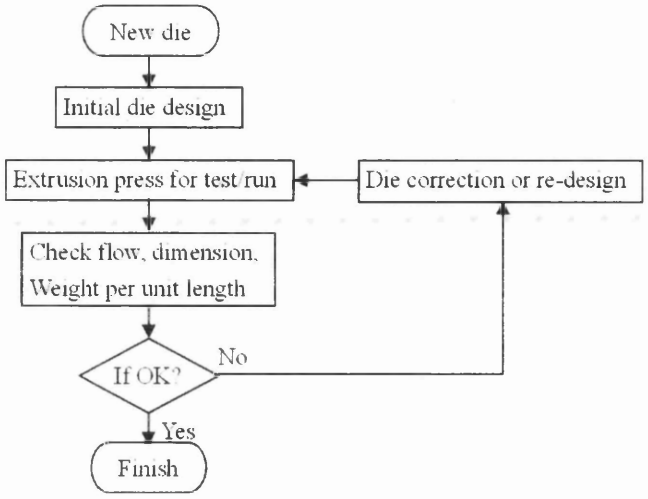

Figure 3.9: Trial-and-error design process for extrusion dies

3.3.2 Empirical Bearing Length Design Formulae

Three schematic solid dies are shown in Figure 3.10. Bearing length is the major controlling factor for retarding the metal flow. It also determines the products quality, speed of extrusion and life time of the die. The most common and widely-used bearing is parallel bearing (Figure 3.10(a)). The friction between billet surface and die can be adjusted by changing the length of bearing. A longer bearing causes larger friction and slows down the flow velocity. Similarly, smaller bearing lengths lower friction thereby allowing the material to retain its velocity at higher speeds. A properly chosen bearing length profile can balance the flow rate inside a die opening quite well and produce reasonable extrudates.

Besides the parallel bearing design, there are two more ways to change the flow rate–choke and relief (Figure 3.10(b) and 3.10(c)). Choke is an incline bearing located at the front face of a die (as shown in Figure 3.10(b)). Relief is a similar feature at the back side of the die (Figure 3.10(c)). The angle of a choke can be as high as 3°. Relief angle can be as high as 7° ([23]). Choke can slow down the flow and relief speeds up it. Both of these measures can adjust the velocity locally.

Though it is very difficult to describe the behaviour of the flow, there are a few design parameters which are widely used by all die designers [23]:

- The distance of the opening from the centre of the billet

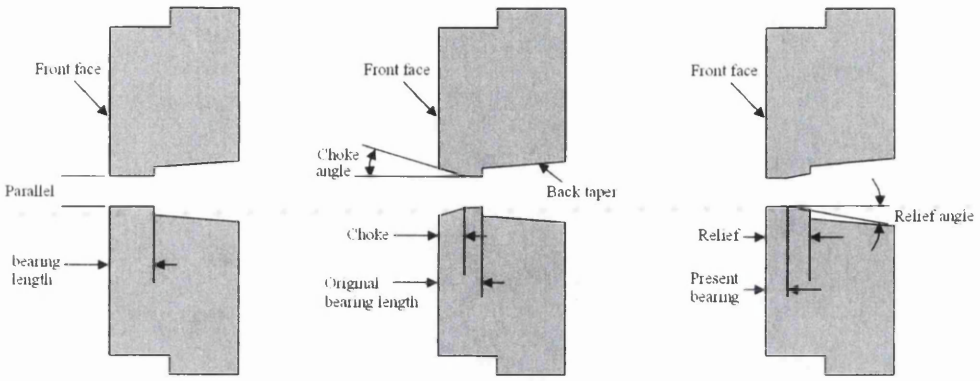

(a) Parallel bearing (b) Choke at front of bearing (c) Relief at back of bearing

Figure 3.10: Different type of solid extrusion dies

- The section thickness at that location
- The pocket shape and size.

By understanding the factors affecting and using the experience and skills of a die designers bearing length design, researchers have introduced several bearing length design formulae. The widely used formulae are listed below:

Lotzenhiser 77 formula

In 1977, Lotzenhiser described basic bearing length design rules [26]. These rules are :

1. A minimum bearing length ($3/32in. \approx 2.4mm$) should be maintained.
2. For small sections, bearing length should equal to about 4 times the section width (in European) or just equals to the section width (in USA).
3. Minimum bearing lengths are often established at the farthest ends of legs or tips to the centre of die
4. Bearing length is increased $1/32inch$ ($0.8mm$) per $1/2in.$ ($12.7mm$) toward the centre of the die for any die with section thickness less than $3/16in.$ ($4.8mm$).

5. Tips and legs use 4/5 of normal bearing length.
6. Bearing length design should be smoothed if abruption exists.

The bearing length design rules described by Lotzenhiser indicate following bearing length design formula (Eq. 3.1).

$$\begin{aligned} b &= 2.4mm \leq 4.0w\frac{0.8(R-r)}{12.7} \leq 4.8mm \\ b_{tips} &= \frac{4}{5}\, b_{normal} \end{aligned} \tag{3.1}$$

Castle 88 formula

In 1988, Castle *et al.* gave a set of similar design rules [27]:

1. Increase bearing length 0.25mm for every 20mm reduction in radius
2. The minimum bearing length for a wall thickness of 1mm should be 2 mm
3. Bearing length should be 1.5-2 times of the wall thickness
4. Assign minimum bearing length to slowest part (the farthest and thinnest part)
5. Tips of legs usually use 1.5mm bearing length

Following the design rules, a bearing length design formula was also given (Eq. 3.2).

$$\begin{aligned} b &= C_1 w\frac{0.25(R-r)}{20} \\ b_{tips} &= 1.5mm \end{aligned} \tag{3.2}$$

where $1.5 \leq C_1 \leq 2.0(mm)$.

Stockdale 92 formula

Stockdale gave a rough design rules in 1992 [28]

1. Find the thinnest wall that is closest to the liner. Assign a bearing length value that equals the wall thickness for that point

2. Other bearing length is based on this reference bearing length

3. Bearing length should take count of the leg and tip effect

4. Walls bearing blends must be provided

The design rules given by Stockdale can be described by the following formulae (Eq. 3.3).

$$b = C_2 \left[C_1 \frac{w}{w_{min}} \right] b_{min} \tag{3.3}$$

where C_1 is a proportional factor for the reference bearing length, C_2 is a constant for the leg and tip effects.

Miles 96 formula

In 1996, Miles *et al.* gave specific bearing length design rules for extrusion dies and a corresponding design formula (Eq. 3.4). A sloping hat function was given by Miles *et al.* (Eq. 3.5) for smoothing the design results. In the paper, medial axis transform (MAT) was introduced for the design work. Due to the power of MAT, most geometric related information of any given extrusion die profile can be automatically calculated. Therefore, the bearing length design can be calculated easily by the formula. In the paper, some primary auto-processes were looked at [1].

$$b = w\,(2 + C(R - r)) \tag{3.4}$$

where b is the bearing length at boundary point p in mm, w is the width of the section at p in mm, r is the distance of the section at p from die centre in mm, R is the distance of the furthest part of the orifice from the die centre in mm and C is a constant, which typically equals 1/80.

$$y = \begin{cases} 0 & x < -L \\ \frac{1}{L}\left(1 + \frac{x}{L}\right) & -L \leq x < 0 \\ \frac{1}{L}\left(1 - \frac{x}{L}\right) & 0 \leq x \leq 0 \\ 0 & L < x \end{cases} \tag{3.5}$$

where $L = 5mm$ is used in the paper for acceptable smoothing effect of bearing length design.

Thomma 96 formula

In 1996, Thomma and Reissner also provided a bearing length design formula (Eq. 3.6).

$$l_B = \left[a.w - \frac{r}{20}.\frac{d_u}{d_B.f}\right] \frac{k_1}{k_2 + s} \geq 2.5mm \tag{3.6}$$

where l_B is the bearing length, w is the section width, a is a constant and $1 \leq a \leq 2$, d_u is diameter of profile circumscribing circle, d_B is diameter of billet and s is extrusion speed.

Though the formula gives an explicit representation for bearing length calculation, how to fix the constants of the formula, such as a, k_1, k_2 and so on,is not covered in the paper.

Miles 97 formula

Miles *et al.* modified their bearing length design formula again in 1997 [4]. Two set of bearing length design rules used by European countries and USA were mentioned in the paper.

The design rules used by North American die designers are:

1. A minimum bearing, dependent on the orifice width, is assigned to a point nearest the container wall
2. Bearing length is increased by $0.8mm$ per $13mm$ toward the die centre
3. Bearing length is increased in direct proportion to the orifice width, after the allowance given in (2)
4. Ends of legs have the bearing of the leg

The design rules used by European die designers are:

1. A bearing length of $1.5 - 2.0$ times the orifice width is allocated to the "slowest" part of the section away from the centre of the die
2. The ratio of bearing length divided by wall thickness is increased by 0.25 for every $20mm$ reduction in radius from the die centre

3. The minimum bearing length for a wall thickness of 1mm is $2mm$. Ends of legs are usually allocated a bearing length of $1.5mm$

According to the bearing length design rules, Miles *et al.* introduced a new bearing length design formula:

$$\frac{b}{w} = \frac{B}{W}(1 + C(R - r)) \tag{3.7}$$

where C is a constant, W is a reference die opening section width, R is the radius of the circle which just can hold the whole die opening, r is the distance from die opening section the die centre and w is the section width.

Advantage and Disadvantage of Empirical Design Formulae

Table 3.1 shows major the advantages and disadvantages of all six mentioned bearing length design formulae. From the table we can find that each design formulae has its own limitations. The common limitation is that none of them take die classification and data reuse philosophy into account. There is only one formula that can handle local effects of bearing length design work and unfortunately, the formula can not be implemented automatically. Another problem is that none of them can take into account the non-linear flow that occurs along the die radius.

The advantages of empirical bearing length design formulae are:

- Fast design result capability.
- Easy to learn.
- Easy to use.
- Easy to make appropriate computer programs with fixed constants.

3.3.3 Finite Element Method

Due to the fast growing technology, today's computer hardware and software are much more powerful than before. Therefore, more complicated and higher

Table 3.1: Bearing length design formulae characteristics

Formulae	Lotzenhiser	Castle	Stockdale	Thomma	Miles96	Miles97
Constants knowability	o	o	-	-	•	o
Auto-calculate possibility	-	-	-	-	•	•
Non-linear effects	-	-	-	-	-	-
Local effects	o	o	o	-	-	-
Data reusability	-	-	-	-	-	-
Die classification	-	-	-	-	-	-

(• fully supported, o partly supported, – does not support)

precision numerical simulations can be achieved. As one of the most successful numerical simulation methods, the finite element method (FEM) has been widely used for extrusion process simulation.

Although people started FE simulation work for the extrusion process in the 1970s, the related research work has increased in the late-1980s. From the 1990s till now, more and more useful and realistic simulation works have been done.

Herberg *et al.* [34] used FEM to simulate ram forces, pressures and temperatures of the extrusion process.

In 1996 Mooi *et al.* [35] illustrated their simulation works based on an Arbitrary Lagrangian Eulerian FE simulation. The results showed pressure, temperature and stress distribution of the extrusion billet.

Lof *et al.* [36, 37, 38] did FE simulation for aluminium extrusion based on an elasto-viscoplastic material model. The work shows the pressure, Von Mises stress and other physical properties' distribution in a three-dimensional extrusion model. Two formulae are also given for linking FE simulation results with die design work (Eq. 3.8).

$$\begin{aligned} P(t,s,o) &= C_1 t^{n_1} + C_2 s t^{n_2} o^{C_3 t^{n_3}} \\ P(t,s,o,r) &= C_1 t^{n_1} + C_2 s t^{n_2} o^{C_3 t^{n_3}} + C_4 r^{n_4} \end{aligned} \tag{3.8}$$

where t is the profile section thickness, o is the pocket offset (half of the pocket width) and s is the depth of pocket, r is the distance from the calculating point to the die centre.

Zhang *et al.* [39] demonstrated a finite element method based flat-face die bearing length determination approach. By using FE method with 3D mesh results, the research work showed the approach which can simulate potential flow rate for extrusion process and give bearing length designs based on the simulation results.

Lee *et al.* [40, 41] did three-dimensional FE analysis for the flat-die hot extrusion process. By using FE simulation, the displacement and deformation of work pieces can be simulated. For FE simulation, a constant bearing length is used as the initial design of a flat-die and the corresponding exit velocity are checked for die correction. By coupling a modified Miles'96 bearing length design formula with FE simulation procedures, Lee *et al.* showed a way to link FEM with extrusion die design formulae.

Li *et al.* [42, 43, 44] in Birmingham University used DEFORM^{TM}-3D®, a commercial simulation package, to simulate extrusion process. Their work reveals that the metal flow behaviour in aluminium extrusion and the influence die pocket design.

As mentioned previously, FEM simulation is a physics-oriented approach. The simulation results contains physical parameters rather than heuristic design information. For extrusion work, the results are displacements, temperature distributions, pressure and/or stress distributions and so on. Very few researchers have discussed the interpretation of FE results in terms of extrusion design parameters, heuristics and past successful designs. The major properties of these approaches are listed in Table 3.2.

3.4 Conclusion

3.4.1 Comparison of Die Design Approaches

All extrusion die design approaches have their own advantages and disadvantages. The most interesting part of them are shown in Table 3.3.

It is clear that for trial-and-error design approach, the advantages are the design quality and flexibility. However, this approach is time-consuming and expensive. It is also difficult for a new designer to understand and use all the design rules. As

Table 3.2: Properties of numerical simulation approaches

Research work	Herberg *et al.*	Mooi *et al.*	Lof *et al.*	Lee *et al.*	Li *et al.*
Method	FE	FE	FE	FE	FE
Simulation area (billet)	•	•	•	•	•
Simulation area (bearing)	-	-	-	•	-
Simulation area (pocket)	-	-	-	-	•
Coupled with empirical formulae	-	-	•	•	-
Linked with geometric features	-	-	-	-	-
Data reusability	-	-	-	-	-

(• fully supported, o partly supported, – does not support)

Table 3.3: Advantage and disadvantage of die design approaches

Design approach	Trial-and-error	Empirical design formulae	FE simulation
Speed	-	•	-
Design quality	•	-	o
Cost	-	•	•
Learnability	-	•	-
Easy-to-use	-	•	-
Flexibility	•	o	-
Design knowledge accumulation	-	-	-
Data reusability	o	-	-

(• good, o medium, – bad)

for an empirical design formulae based approach, the benefits are its high-speed, low-cost and easy to learn and use. The main limitation of this method is that the design quality is low. On the other hand, FE simulation provides high quality design. But it is a slow and difficult to learn and use.

It is clear that all these three design approaches are away from the ideal design process. Besides the main limitations, none of them support design knowledge acquisition and data reusing.

3.4.2 Summary

In this chapter, the objectives of this research work have been presented and typical Extrusion die design process were introduced. In Section 3, three widely used design approaches and their advantages and limitations were mentioned. It is clear that all currently available design approaches are very limited and therefore, a flexible, automatic and robust design approach is needed for extrusion die design. In the following chapters, a geometric reasoning based new extrusion die design approach will be presented. Since medial axis transform is a powerful tool for geometry reasoning work, the definition and primary properties of the medial axis transform will be introduced in the next chapter.

Chapter 4

Medial Axis Transform

Chapter Layout

The chapter introduces the medial axis transformation process and provides an insight in its use as a geometric reasoning tool. The first section defines MAT, provides examples of MAT and describes properties of MAT. The next section then describes various algorithms used to generate MAT which is followed by a section detailing its application in various industrial fields and finally summarises the understanding and learning gained from this review.

4.1 Medial Axis Transform (MAT)

4.1.1 Introduction

Medial Axis (MA) and Medial Axis Transform (MAT) was first proposed by Blum in 1967. He used it for extracting and representing planar shapes [45, 46, 47]. Blum proposed the medial axis transform as a representation that embodies the skeleton of an object as well as the width of the object at every point on the skeleton

The definition of MAT

The concept and construction of the medial axis can be visualised by an example in which each point on the boundary of the geometry is set alight and the fire is allowed to propagate inward at a uniform rate until it is quenched by meeting the fire from the opposite side. The locus of the points at which the fire meets and gets quenched is the medial axis (as illustrated in Figure 4.1(a)). The medial axis also can be defined as the locus of the centre of an inscribed circle (for 2D geometry) or a sphere (for 3D geometry) of maximal diameter as it rolls within the domain while maintaining contact with the domain boundary on at least two points (Figure 4.1(b)).

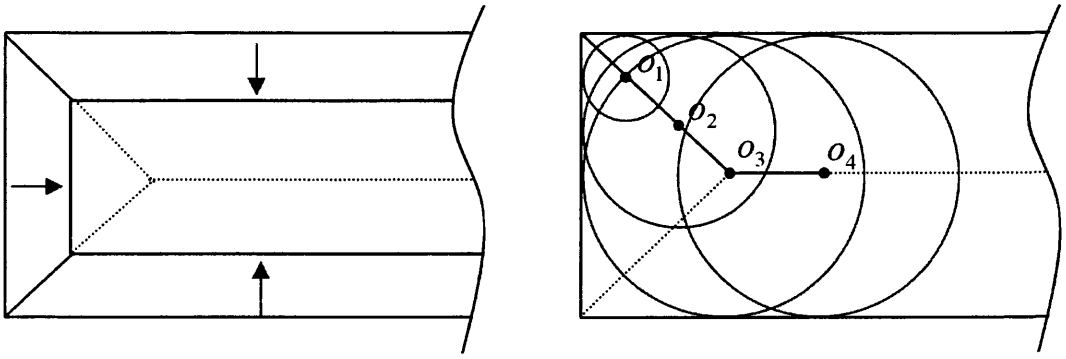

(a) Wild fire definition (b) Inscribed circle definition

Figure 4.1: The definition of medial axis transform

MAT and Radius Function

If the medial axis is combined with the radius function which defines the distance between the geometry boundaries and the locus where the fire fronts meet, it is referred to as the medial axis. For each segment of the medial axis, the radius of an inscribed circle at each point on the axis is unique and is equal to the distance between that point to the geometry boundary.

For example, consider a geometry shape and its medial axis transform which are shown in Figure 4.2(a). For segment l_1, chose point A as the start point and B as the end point. Since each point on the segment between A and B has a corresponding radius (such as r_1, r_2 and r_3 in the figure) the mapping result can be defined as a function, which is called the radius function of the medial axis. The radius function of l_1 and l_2 are shown in Figure 4.2(b) as f_1 and f_2 respectively.

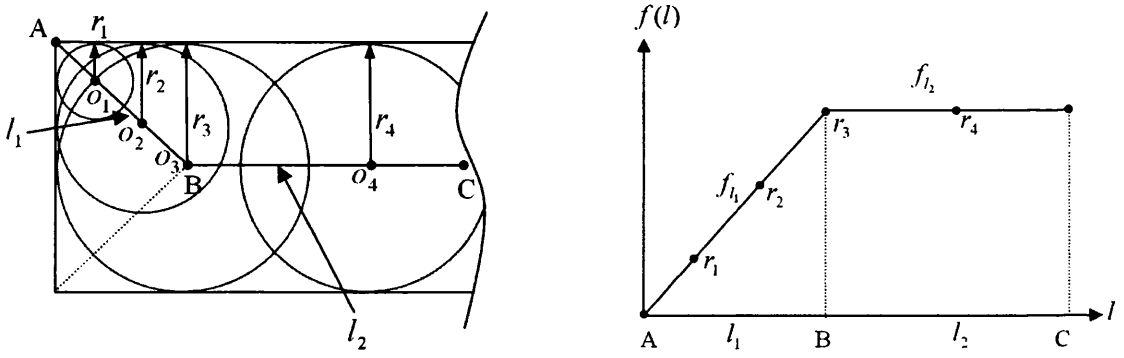

(a) Radii of inscribed circles

(b) Radius function of MAT

Figure 4.2: Radius function of medial axis transform

Since a medial axis transform representation embodies both the substance of each part of an object and the connections between adjacent parts, it is a very powerful tool and is widely used for different applications.

4.1.2 MAT Examples

Some examples of medial axis transform are shown in Figure 4.3.

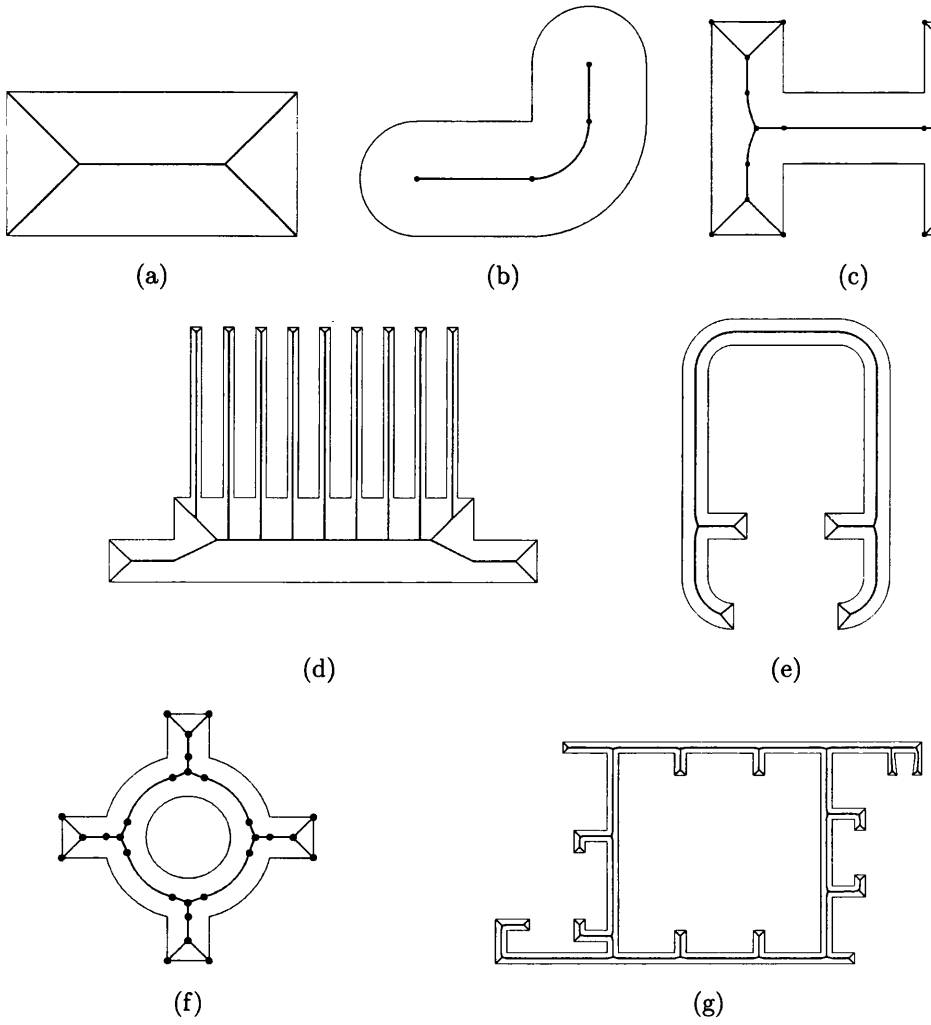

Figure 4.3: Medial axis transform examples

4.1.3 The Properties of MAT

The most important feature of MAT is that it is another kind of representation using which, the original shapes can be simplified with useful geometric information. For example, a MAT result with its radius function contains the size, regional width and length of the original shapes. Therefore, MAT is also referred to as *the skeleton* or *symmetric axis transform* of a shape.

Another interesting property of MAT is that the MAT results are very sensitive to the definition of the shape boundaries. If the radius function is ignored, MAT results can be similar for different original shapes and can be very different for similar original shapes.

For example, Figure 4.4 shows MAT results for two different shapes. It is clear that though both MAT results are exactly the same (single straight lines in each case), but the original shapes are different. Another example is given in Figure 4.5. This example shows the MAT results for two different geometry shapes. It is obvious that the shape of MAT is nearly the same, but the shape of the original geometry object is remarkably different.

(a) MAT of a round-corner bar shape

(b) MAT of a dumbbell shape

Figure 4.4: Similar medial axes of different shapes

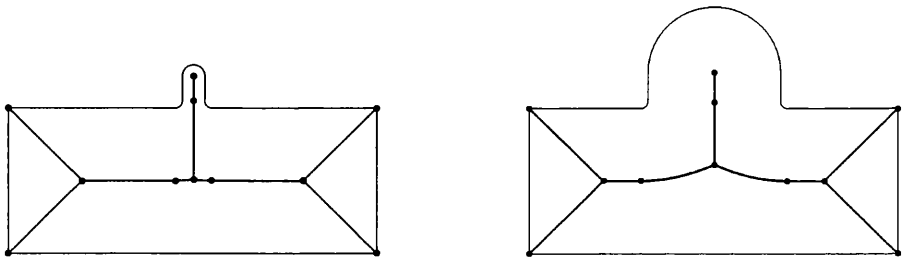

(a) (b)

Figure 4.5: Similar medial axes of different shapes (example 2)

On the other hand, similar shapes might give different MAT results. An example is shown in Figure 4.6. It is clear that the geometry shapes in Figure 4.6(a), 4.6(b) and 4.6(c) are quite similar with each other except for some tiny recesses or lumps on the boundaries, but the MAT results are very different.

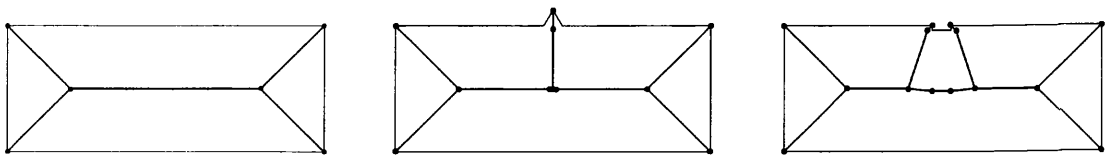

(a) (b) (c)

Figure 4.6: Similar shapes lead to different MAT results

Some other properties of MAT mentioned by Ramanathan and Gurumoorthy are [48]:

- *Uniqueness.* There is an unique MAT for a given object.
- *Invertibility.* By combining the medial axes and its radius function, the original geometry shapes can be re-constructed.
- *Dimensional reduction.* The dimensionality of a MAT is lower than the original geometry objects.
- *Topological equivalence.* A MAT is topologically equivalent to the original shape.

4.2 Algorithms for Generating MAT

A review of the literature reveals that generating a medial axis transform is a difficult task and a lot of research has have been undertaken in recent years.

Sheehy *et al.* illustrated a MAT generating algorithm using domain Delaunay triangulation [49, 7]. The research work shows that the medial axes (for two-dimensional shapes) or the medial surface (for three-dimensional volumes) can be generated using *Delaunay* triangulation.

The Delaunay triangulation is the geometric dual of the Voronoi diagram. The Voronoi diagram was first formally introduced by mathematicians *Dirichlet* and *Voronoi* [50, 51, 52]. A Voronoi diagram is a partitioning result for a set of points in a 2D plane or 3D space. The partitioning divided the plane or the space using convex polygons such that each polygon contains exactly one generating point and every point in a given polygon is closer to its generating point than to any other. A Voronoi diagram is sometimes also known as a Dirichlet tessellation. The cells are called Dirichlet regions or Voronoi polygons [53]. A Voronoi diagram can be generated by using the *divide and conquer* algorithm [54], *Sweep* algorithm [55, 56] or other algorithms.

Figure 4.7(a) shows a Delaunay triangulation result for some arbitrary points. The Corresponding Voronoi diagram of the same point set is shown in Figure 4.7(b).

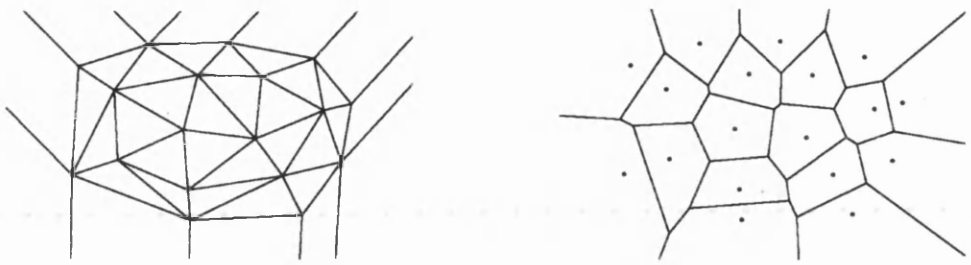

(a) Delaunay triangulation example (b) Corresponding Voronoi diagram

Figure 4.7: Delaunay triangulation and corresponding Voronoi diagram

Figure 4.8 shows how a medial axis transform can be obtained based on Delaunay triangulation mesh results. By controlling the density of these points, a high quality MAT result can be achieved. The algorithm comprises the following steps:

1. Generate a set of points which lie on the boundaries of the target shape.
2. Generate a Delaunay triangular mesh based on these points (Figure 4.8(a))
3. For each triangle of the mesh result, find out the circumcenter (Figure 4.8(b))
4. Connect all circumcenters properly and the result is a very good approximation of the medial axis transform (Figure 4.8(c))

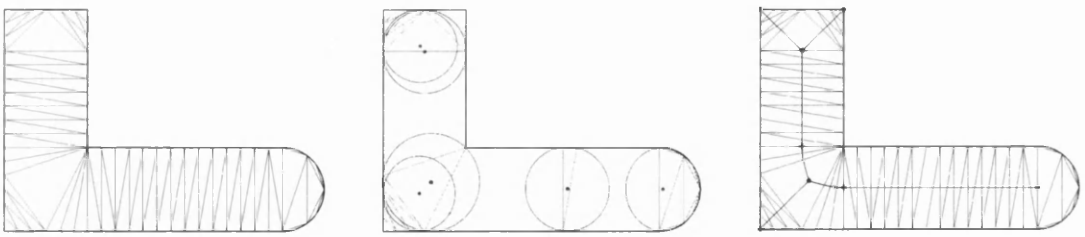

(a) Delaunay triangulation mesh result (b) The circumcenter of a Delaunay triangle approximates an inscribed circle (c) The media axis transform

Figure 4.8: Delaunay triangulation and medial axis transform

Vaneker discussed several formulae for MAT generation in his thesis [57]. These formulae give a theoretical solution for simple straight or arc boundaries. For example, Eq. 4.1 gives the medial axis transform between two arcs.

$$\begin{aligned} x^2 + y^2 &= (R_1 + i \times R)^2 \\ x^2 + l \times (y + j \times E)^2 &= (R_2 + k \times R)^2 \end{aligned} \tag{4.1}$$

where for convex-convex boundaries, $i = 1$, $j = -1$, $k = 1$, $l = 1$; for convex-concave boundaries, $i = 1$, $j = -1$, $k = -1$, $l = 1$ and for concave-concave boundaries, $i = -1$, $j = -1$, $k = -1$, $l = -1$.

Ramanathan and Gurumoorthy gave an algorithm for constructing the medial axis transform of curvilinear boundary shapes [48]. Their research work illustrates that by finding *foot points*, *branch point* and handling *reflex corners*, the MAT of curvilinear boundary domains can be generated.

Dey *et al.* showed a MAT generation approach for 3D volumes based on Voronoi diagram (2004). Their research work showed that though the Voronoi diagram based MAT generation approaches are quite successful, due to the complexity of 3D geometry objects MAT can not be obtained by trimming Voronoi diagram based on simple algorithms. For example, some vertices of the Voronoi diagram, which are called *poles*, will still be retained after the trimming process. Dey *et al.* introduced a new algorithm by which the poles can be avoided and the MAT results are generated from a sub-complex Voronoi diagram directly [58].

Culver *et al.* provided another accurate algorithm to compute the internal Voronoi diagram and medial axis for three-dimensional polyhedrons. By recursively finding neighbouring junctions along the seam curves, the algorithm gives exact representation of the MAT [59].

4.3 Applications of MAT

Being an accurate and powerful representation of geometry shapes, the medial axis transform is useful for a lot of applications. For example, MAT can be used to re-construct the original object [61, 12]. This technique is very useful when geometry models have been re-constructed from a set of sample points.

Since MAT gives a simple way to calculate the regional aspect ratio and/or surface to volume ratio, it can be used to identify thin sheets and slender bar structures in a solid model. Casement *et al.* [10] illustrated how thin parts of a 2D or 3D geometry model can be found automatically by using MAT .

Armstrong and his colleagues did a great deal of work on geometry reasoning based on MAT, e.g. for numerical simulation methods, such as finite element

method Good mesh generation algorithms are quite important for generating high quality mesh results.

Armstrong *et al.* [8] showed that by using MAT, the regional aspect ratio of a given geometry object can be easily calculated and therefore, the geometry object can be partitioned automatically.

Since MAT shows the skeleton of the original geometry object and contains abundant geometric information, Armstrong *et al.* [9, 62] also studied how the dimension of a geometry object can be reduced or added. Their research work shows that three-dimensional geometry objects can be converted into their 1D/2D equivalents for the purpose of analysis. On the other hand, since the original objects can be reconstructed based on its medial axis transform result, three-dimensional objects can be re-constructed from their 1D/2D MAT results .

Since MAT is a *skeleton* with thickness information (radius functions) of each skeleton segments of the original objects, it is a very good replacement of the original shape definition for geometric reasoning work. For example, Lockett *et al.* introduced an algorithm for feature recognition based on medial surfaces [63]. By using a pixel-based medial axis transform, Cecilia Di Ruberto illustrated how general two-dimensional shapes can be recognized using shape features of the MAT results [64]. Mortara *et al.* showed a solution for polygon blending based on an approximate skeleton which is MAT [65].

Most approaches which use geometry models need geometric information. For example, almost all engineering research work nowadays uses geometry objects to model the real world. Therefore, MAT can be used for these works to reduce the complexity of the problems.

For instance, Pao *et al.* [66, 67, 68] demonstrated a few algorithms to couple FE method with MAT to estimate the temperature distribution or to predict the hot-spots for castings.

As for extrusion die design, Lin *et al.* [69] show a bearing length design method using MAT.

4.4 Conclusion

In this chapter, *Medial Axis Transform* (MAT) has been introduced. As mentioned, MAT is an effective replacement of the original geometry objects for geometry-feature-related works. A lot of research works and algorithms which are linked with MAT have been introduced in the past. Due to its properties, MAT is a very powerful tool for shape recognition, geometric reasoning and other related problems.

Chapter 5

Bearing Length Prediction using Historical Design Data

Chapter Layout

This chapter sets out to achieve the objectives set out in Chapter 3, builds on the knowledge gained and potential offered by the medial axis transformation described in Chapter 4 and presents a novel knowledge representation scheme based on geometric reasoning techniques. The chapter describes a typical extrusion die designs process and the various methods that are used by die designers to achieve best results highlighting the widely used design rules based on bearing length. The next section then describes the bearing length design process that uses empirical design formulae. In an effort to overcome the limitations posed by an empirical design formulae and numerical simulation approaches, a new approach for die design representation is proposed in the next section which ensures that historical information from past successful designs is stored and re-used to optimise empirical design formulae. The approach is then validated using a case study.

5.1 Introduction

A well-designed extrusion die is one of the most important stages during the Aluminium extrusion process. This task is generally undertaken by an experienced die designer. The experience is gained using a trial-and-error method by analysing past successful designs and on a few occasions, using the results given by advanced numerical modelling techniques. Representing past designs and knowledge on computers is a challenging task and is still an active area of research.

A novel knowledge representation scheme based on geometric reasoning has been presented in this chapter. Design attributes, such as cross sectional thickness, die openings' orientation and distance to the die centre, end or tip effects have been characterised into special normalised design variables. The aim of this new approach is to store useful information from previously successful die designs so that this information can be used as an aid to design new dies. The bearing length information associated with a past design is stored as a hyper-surface in a multi-dimensional design space defined by the special normalised design variables. The new successful designs are then obtained by altering the shape of the hyper-surface in such a way that the error is minimised on all past successful examples. An example is provided to illustrate how this methodology can be used to design a new industrially relevant die.

The process of extrusion was explained in detail in Chapter 2 and 3. An extrusion die is a piece of metal which is placed in the front of the container during the extrusion process. Shaped holes, known as die openings, are created to allow the material to flow through to obtain wanted extrudates. A schematic of an extrusion die is shown in Figure 5.1. For an extrusion die, the die opening profile has the same shape as the extrudate which would be built-up. The side wall of the die opening is called the bearing. During the extrusion process, the friction between the billet and bearing retards the flow. Longer bearing lengths generate greater friction and reduce the flow rate. A "recess", also called a pocket, is often made in the front side of the die to allow easy entry of the material. Wider recesses lower the friction and boost the flow rate. A "backer" might be put at the other side of a die to lend extra support to the die. The holes in a backer do not touch the material and do not influence the flow rate at all. In addition to the bearing length and pocket size, radial effects lead to another design factor,

location and orientation, or say layout of the die openings. Since the flow rate varies along the radial direction, different locations and orientations can influence the flow rate as it varies along the radial direction.

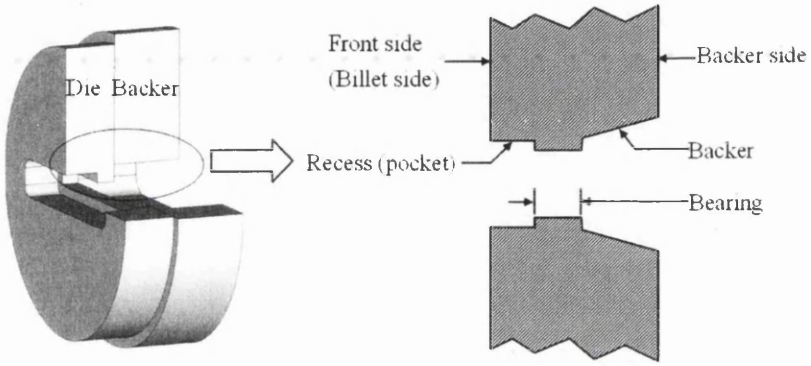

Figure 5.1: Extrusion solid die (Schematic)

5.2 Extrusion Die Design

5.2.1 Typical Extrusion Die Design Process

The design scheme frequently used by most die designers is a trial-and-error approach. For any new extrusion die opening profile, the first step taken by a designer is to check the design requirements and constraints, such as the number of die openings, the layout of the die, the size of die and so on. Then, the shape of the new profile is studied and basic geometric information, such as the size, section width, legs, tips and tongues are checked and calculated by the designer. Using his experience and skills, an initial die design is given by the designer based on this pre-calculated/checked information.

This first design can be checked by test runs. If the design gives unsatisfactory extrudates, a die correction process is undertaken. If, however, the testing result is unsatisfactory, then the die has to be re-designed.

A brief flow chart of design procedures is shown in Figure 5.2. Most design decisions are taken by designers based on their intuitive knowledge and skills and there is no explicit way to know how the die is designed or what kind of criteria are used. The whole design process is a 'black-box' and the design work

is some kind of "magic art". Since the design knowledge and skills are saved in an individual designers' mind, then maintaining and transferring the design knowledge and experience becomes an extremely difficult job.

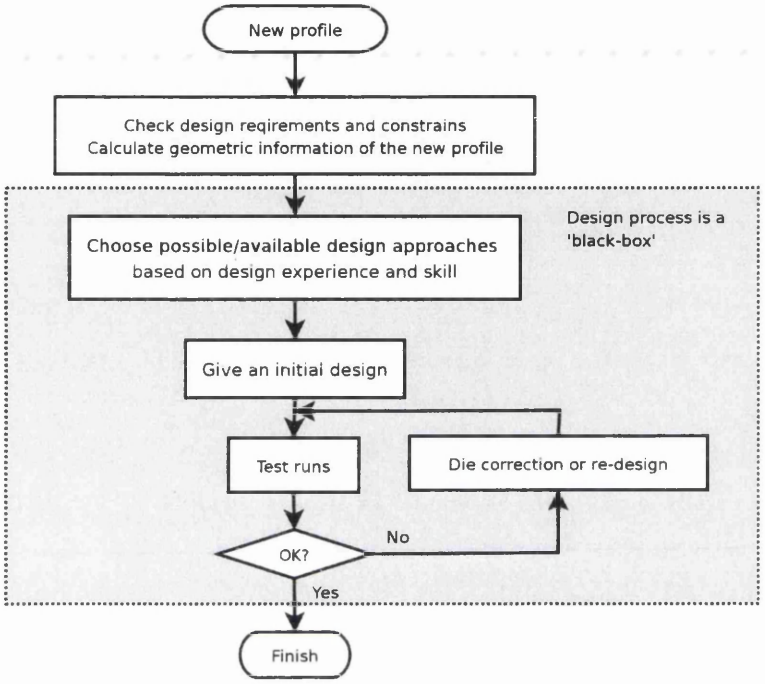

Figure 5.2: Extrusion die design process

Some widely used design methods are discussed in the following sub-sections.

5.2.2 Extrusion Die Design Methods

As mentioned in Chapter 2, one of the problems faced during the extrusion process is that the flow of an extrusion billet is nonuniform at the exit. The design work for extrusion dies, therefore, attempts to find a way to achieve uniform exit velocity at each die opening.

Uneven flow inside the extrusion billet can be caused by many factors. For example, when the billet moves in the container, the friction between the billet and the container wall causes the material near the wall to move slower than the material near the billet centre. As the material moves, the friction between the billet and die plate also retards the flow. Different material properties, friction ratios, ram loads and lubricants also influence the flow of material from among

these, the billet-die friction and distortion of billet material around the die are the most important factors which causing nonuniform flow.

Several methods have been used to understand the behaviour of the flow. The grid method is a widely used approach by which a grooved billet is used to check the flow inside it [20, 13]. With the advancements made in numerical methods, such as the finite element method (FEM), and fast developing computer technology, numerical simulation is playing an important role in extrusion flow investigation [70, 71, 29, 36, 37, 38, 40, 41, 42, 43, 44].

In the literature the following design methods have been suggested to achieve a uniform flow rate [13, 23, 19]:

- Layout design
- Bearing length design
- Pocket design
- Bridge etc. design

The bearing length design, is however, the most extensively used method for production dies [23, 70].

5.2.3 The Design and Representation of Extrusion Dies

Nowadays, designers use computer and CAD software to create, modify and store their designs. Though each CAD system uses different geometry definition methods and data format, all CAD systems perform their jobs in a similar way, that is to define geometry models by using primer shapes such as points, lines, arcs, surfaces etc. These save the geometry model either in a vector based data format or pixel based data format.

For any extrusion die opening profile, designers usually mark their designs by numbers on the figures either on a piece of paper or on the computer screen. The numbers indicate the lengths of bearing (in most cases in millimetres). Bearing length varying steps are marked as several short line segments on the chart.

Two bearing length designs given by designers for channel shape die openings are shown in Figure 5.3(a) and 5.3(b) respectively. For extrusion die design, the

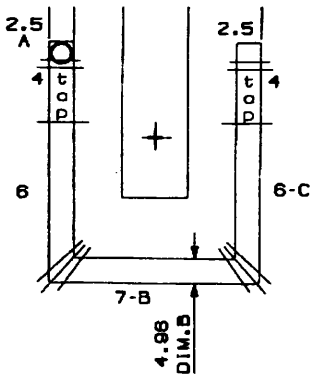

(a) Bearing length design for channel shape die opening, example 1 [42]

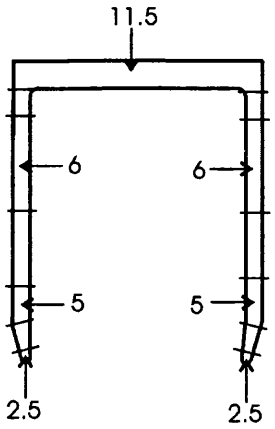

(b) Bearing length design for channel shape die opening, example 2 [57]

Figure 5.3: Bearing length designs did by die designers.

following geometric information is important:

- Die opening geometry definition
- Die openings location and orientation
- Bearing length
- Other design information such as pockets, bridges etc.

It should be noticed that the design approaches used by designers tightly bind the design processes and results with the geometric information.

5.2.4 Bearing Length Design Rules

Although the flow behaviour during the extrusion process is very complicated and often unpredictable, die designers are still able to summarise a few bearing length design rules based on their knowledge and experience as mentioned in Chapter 3. The basic idea about the design rules is to increase the bearing length in the area where higher flow speed is maintained and reduce the bearing length for such area where the speed of the flow is low.

Extrusion die designers and researchers have tried and developed a series of rules. Some of these design rules have been successfully adapted world-wide. The rules given by Castle *et al.* in 1988 are [27]:

1. Increase bearing length $0.25mm$ for every $20mm$ reduction in radius
2. The minimum bearing length for a wall thickness of $1mm$ should be $2mm$
3. Bearing length should be 1.5-2 times the wall thickness
4. Assign minimum bearing length to the slowest part (the farthest and thinnest part)
5. Tips of legs usually use $1.5mm$ bearing length

Miles *et al.* proposed some similar design rules in 1997. The design rules illustrated by them and used by European designers are [4]:

1. A bearing length of $1.5 - 2.0$ times the orifice width is allocated to the "slowest" part of the section away from the centre of the die
2. The ratio of bearing length divided by wall thickness is increased by 0.25 for every $20mm$ reduction in radius from the die centre
3. The minimum bearing length for a wall thickness of 1mm is $2mm$. Ends of legs are usually allocated a bearing length of $1.5mm$

Though different designers uses different design rules and some design rules may contradict each other, designers keep trying to use and implement these design rules in one way or another. Empirical bearing length design formulae is one such successful approach that has been widely adopted by die designers.

5.2.5 Empirical Bearing Length Design Formulae

Following the design rules, some empirical bearing length design formulae have been proposed. The six most popular design formulae have been discussed in Chapter 3 and two of them are reproduced here again:

$$b = w\,(2 + C(R - r)) \tag{5.1}$$

where b is the bearing length at boundary point p in mm, w is the width of section at p in mm, r is the distance of section at p from die centre in mm, R is the distance of the furthest part of the orifice from the die centre in mm and C is a constant, typically equal to 1/80 [1].

$$\frac{b}{w} = \frac{B}{W}(1 + C(R - r)) \tag{5.2}$$

where W is a reference die opening section width, R is the radius of the circle which can just hold the whole die opening, r is the distance from die opening section the die centre and w is the section width [4].

These two formulae have been used in following sections of this chapter.

5.2.6 FE Simulation for Bearing Length Design

Owing to the fast progress of computer hardware, software and numerical simulation methods, especially the Finite Element Method, the numerical simulation process has become increasingly faster in the last two decades. These simulation processes also give better and more accurate results.

Numerical methods generally in form more on explaining physical properties rather than other things. For example, FE simulation for extrusion process normally uses visco-elasto-plasticity or viscosity flow models to simulate the extrusion processes. It can give a distribution of the results of temperature, pressure, stress and flow velocity or the displacement of materials [18, 72].

Though FE simulation can not give any extrusion die design information directly, it can be used for extrusion die optimization work if linked appropriately as a procedure for some processes. For instance, Lee *et al.* introduced an approach by which FE simulation can be used to optimize empirical bearing length design formulae [40, 41].

Despite its many advantages FE also has some disadvantages at the same time. One such disadvantage of the FE method is that it still remains a time-consuming process even with the advent of very powerful computing power. Problems associated with mesh distortion and large deformation ADD to the complexity. Besides, it is also not easy to link FE simulation results with extrusion die design work.

To overcome these limitations posed by empirical design formulae, numerical methods and experiments, a novel approach based on empirical design formulae with data reuse capability is introduced in the following sections.

5.3 Bearing Length Design Process

5.3.1 Design Process using Empirical Design Formulae

The bearing length design approaches were explained in previous sections and this section will now investigate how MAT can be used for extrusion die design work. Miles 96 formula was used (Eq. 5.1) to illustrate it. The formula can be re-written as a function with a more general format:

$$b = f(w, r, R, C) \tag{5.3}$$

where r is the radial distance from an interested point of the die opening to the die center, w is the regional section width of die opening, R is the radius of the minimal circle by which the whole die opening can be included and C is a constant. Actually, R is the maximum value among all values of r. So, it can be written as r_{max}. Thus, the formula could take the following form:

$$b = f(w, r, r_{max}, C) \tag{5.4}$$

Eq. 5.4 shows that there are only four parameters and two of them are correlated. Therefore in essence, only three parameters are used by the formula. Further more, the parameter C is a constant during the calculation so there are only two independent input parameters.

If we assume the design rules as a set of functions, the whole design work undertaken by extrusion die designers takes three steps:

- The first step of the design work is to analyze a die opening profile to get related geometric information and to check other design parameters such as die diameter, ram load, temperature, etc.
- The second step is to use all the information which has been gathered in step 1 as input parameters for these functions and get the design results.

- The last step is to check the design results.

For instance, suppose a channel shape profile is required to be designed (the left-side shape in Figure 5.4). For each segment of the profile, the regional section widths, radial distances and other design parameters would be calculated by designers. A bearing length design can then be carried out by using the value of these parameters and appropriate design rules. The whole design process is shown in Figure 5.4.

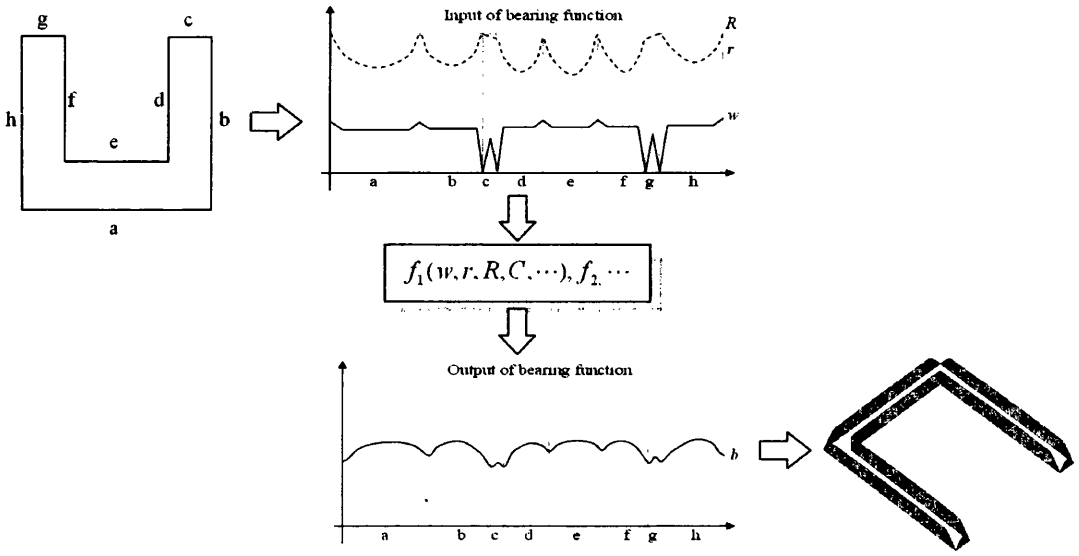

Figure 5.4: Abstract bearing length design process

The whole design work comprises using design variables and design functions to get the bearing length designs. For this channel shape case, parameters such as w, r, R, $f_1(w, r, R, C, \cdots), f_2, \cdots$ are used to get the bearing length design–b (Figure 5.4).

The whole process can be divided into three stages:

1. Data preparation for design variables such as section width, radial distance and so on

2. Design rules/formulae selection

3. Bearing length calculation

In order to reveal the "black art" for extrusion designs, any new method to implement the design process needs to have robust and automatic algorithms. The rest part of this chapter introduces a novel approach for bearing length prediction using historical design data.

5.4 New Approach to Die Design Representation

5.4.1 Extrusion Die Design Variables and Design Spaces

As mentioned earlier, the bearing length design rules used by designers are strongly linked with the geometric information of the die opening profile. Therefore, geometric parameters are used by bearing length design formulae (Eq. 5.1 and 5.2). Since bearing length design formulae can be converted into a general format as given in Eq. 5.4, a more general description would be:

$$b = f(x_1, x_2, \cdots, C_1, C_2, \cdots) \tag{5.5}$$

where $x_1, x_2, \cdots$ are design variables, $C_1, C_2, \cdots$ are constants.

The function is defined as a relation that uniquely associates members of one set with members of another set. Therefore, a function is a *many-to-one* relation. According to the definition, all values of $x_1, x_2, \cdots$ and $C_1, C_2, \cdots$ can be chosen as one set and all possible bearing length designs, i.e. all values of b, as another set. The design formulae can be described as mapping rules which show the relationship between the geometric information of die opening profiles and the correct bearing length designs.

For a function, $y = f(x_1, x_2, \cdots, x_n)$ if its domain and range are represented by real numbers (i.e. $x_1, x_2, \cdots, x_n$ and y), the function can then be described by a hyper-surface in $n+1$ dimensional real space. As a simple case, function $y = x^2$ has one parameter and can be described as a parabola in a two-dimensional real space.

As for extrusion design rules, a similar scheme has been proposed. If only the *width effect* is taken into account for bearing length design process, the design

formula can be described as:

$$b = C_1 w + C_2 \tag{5.6}$$

where C_1 and C_2 are constants.

It is clear that Eq. 5.6 indicates a straight line in two-dimensional space (a schematic example is shown in Figure 5.5).

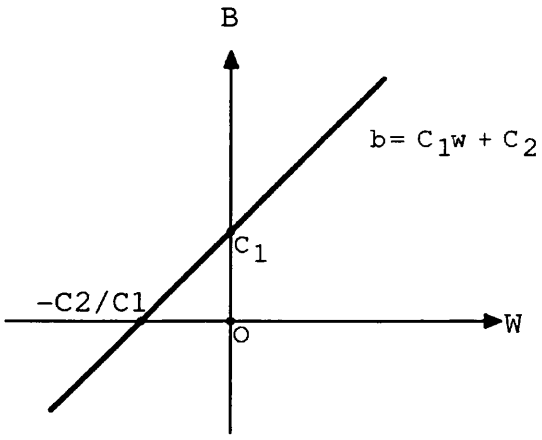

Figure 5.5: Function $b = C_1 w + C_2$ in two-dimensional space

For extrusion dies, both section widths (wall thicknesses) and bearing lengths of extrusion dies are limited. For example, minimum bearing is normally thicker than $1mm$ and for parallel bearings, the maximum value should be less than $25mm$. On the other hand, for empirical bearing length design formulae, the rules break down for very wide ($> 15mm$) and very narrow ($< 1mm$) sections [4]. Therefore, the design formulae is only valid for a range of possible values. For this reason, the input and output value of Eq. 5.6 are limited. It is clear that the input range of the function is: $w \in [1mm, 15mm]$ and the output value should take the range: $b \in [1mm, 25mm]$.

Since functions are mapping rules which map input sets to output sets, the illustrated design formula just maps possible section widths, w, to corresponding bearing length, b. Combining w with b, a duplex $< w, b >$ is formed. It is clear that a duplex, say $< w_1, b_1 >$, can be defined as a point in a two-dimensional Euclidean space with the coordinates: (w_1, b_1). All possible values of these duplexes define a sub-space in the two-dimensional space. A design space for Eq. 5.6 is shown in Figure 5.6.

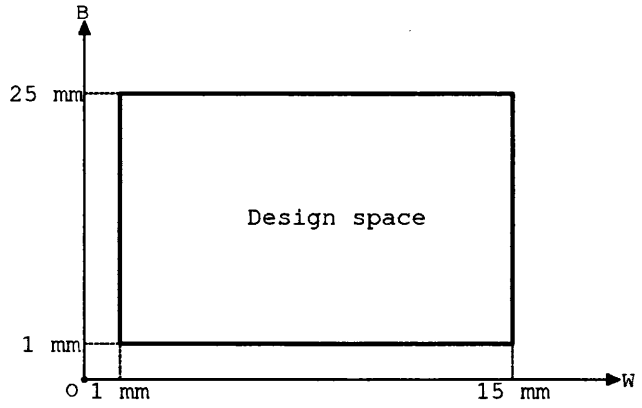

Figure 5.6: Design space defined by $b = C_1 w + C_2$

Though the example uses a linear equation to demonstrate the idea about design variables and design space, the non-linear equations can also be used for the design work as long as these new equations are located in the design space.

Similarly, if one more design factor, say the radial distance r, is used for bearing length design, the design formula will have two input variables, one output variables and several constants. The formula then becomes:

$$b = C_1 w + C_2 r + C_3 wr + C_4 \tag{5.7}$$

Therefore, the design space is defined by a triplex ($< w, r, b >$) and the design space is a sub-space of a three-dimensional Euclidean space. In this case, Eq. 5.7, or other design formulae, can be described by planes or curvilinear surfaces in design spaces.

If more than two design factors are used for bearing length design work, the design space is a high-dimensional space and the design formulae have to be defined by hyper-surfaces, which can not be clearly displayed in the three-dimensional space.

Since different die design criteria and rules are used by different die designers and industries as mentioned in Chapter 3, the lower and upper boundaries of the design space do not fit each other perfectly. Besides, different design empirical formulae and the value of constants in these formulae can expand, or shrink, the design space. Therefore, a more uniform design space have to be achieved for designing work. The details about uniforming the space are now discussed in the following sub-section.

5.4.2 Normalized Design Variables and Spaces

As extrusion die designers choose design rules and parameters based on their experience and the requirements, the details about each design process vary a great deal. For example, a bearing length equals $1mm$, $1.5mm$ or $1 \sim 2mm$ can be chosen as the minimum bearing length by different designers. The valid die opening section widths also varies from $6mm$ to $15mm$ in different rules sets [27, 1, 4]. In addition, die design can scale the design results to fit some requirements [27]. All these lead to different design space sizes.

To fix this problem, a normalization technique has been proposed before further analysis take place. The algorithm first sets the minimum value of each design variables as 0 and the maximum value as 1, then normalize the whole design formula such that it fits in this normalized design space. Therefore, the design formulae now becomes:

$$b = f(w', r', R', \cdots, C_1', C_2', \cdots) \tag{5.8}$$

where $w' \in [0, 1]$, $r' \in [0, 1]$, $R' \in [0, 1]$ etc.

The design factors and how possible design values can be described as design variables and design spaces are discussed in this section. The next question is how to determine and optimize the design formulae using past successful designs. This is explained in the next section.

5.5 Die Design Rules Determination and Optimization

As mentioned in Chapter 3, although die designers used empirical design formulae for years, there is no explicit approach to optimize these design formulae and to determinate the value of design parameters. A new approach is now illustrated in this section which ensures that historical design information can be reused to optimize empirical design formulae.

5.5.1 Design Variables and Design Rules

As illustrated in the previous section, all possible values of a design formula define a corresponding design space. By contrast, each design value with corresponding design variables' values define a point in the space. For one, or several, well-designed dies, the design information of these dies can be represented as a set of points in the design space. For instance, if only section width is taken into account, section widths with relative bearing lengths define a set of points in a two-dimensional design space (Figure 5.7(a)).

If the design rules are known, a least-square fitting algorithm can be used to optimize the design rules based on these points. For example, Figure 5.7(b) shows a schematic fitting result for the historical design data. It is noticed that since the value of both section widths and bearing lengths are limited, the optimized formulae are only effected in the allowable data ranges. In the figure, a dashed line indicates the optimized design formula and a solid line segment shows the validated range of the formula. The minimum and maximum section widths are w_{min} and w_{max}.

Since the optimized design formula is continuous, for any given new section width, the corresponding bearing length design can be calculated easily (the width and length are marked as w_{new} and b_{new} in Figure 5.7(c)).

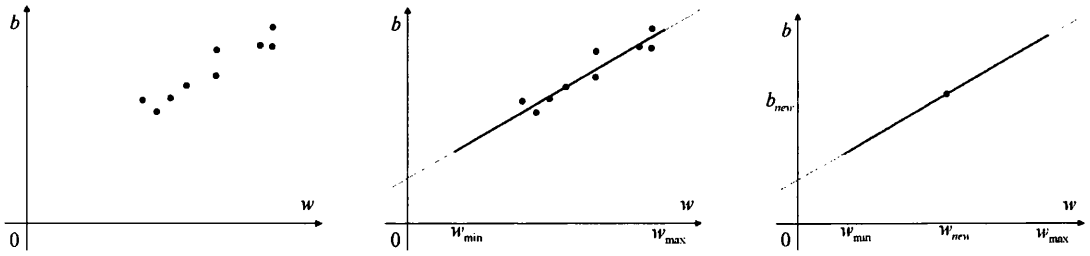

(a) Successful design data in the design space

(b) Least-square fitting result for historical data

(c) New designs based on optimized design formulae

Figure 5.7: Design formulae optimization and determination in 2D space

If two design variables, say section width w and radial distance r, are used for the design work, the design variables are located in a three-dimensional space as mentioned earlier. Similar to the two-dimensional case, each possible design data define a point in the three-dimensional space (Figure 5.8(a)). A plane can be

used to fit these design data and therefore, a linear design formula is optimized (Figure 5.8(b)). It is clear that for any new section widths and radial distances, bearing length design can be calculated by the optimized formula. This is illustrated in Figure 5.8(c) where w_{new} is the new section width, r_{new} is the new radial distance and b_{new} is the corresponding bearing length.

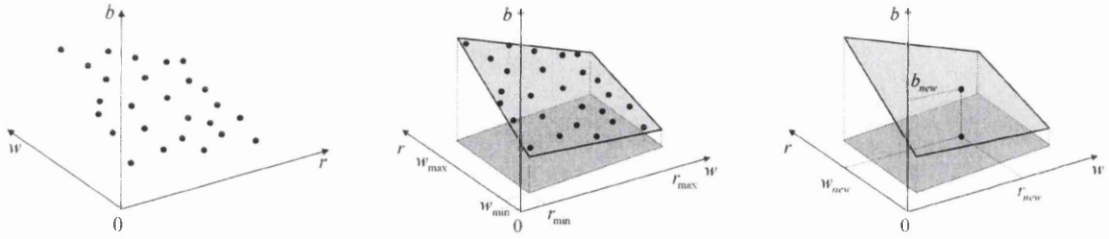

(a) Successful design data in the design space

(b) Least-square fitting result for historical data

(c) New designs based on optimized design formulae

Figure 5.8: Design formulae optimization and determination in 3D space

5.5.2 Design Information Representation in Design Space

A schematic example for representing design information in design space is illustrated in Figure 5.9. Figure 5.9(a) shows a bearing length design for a channel shape die opening. Bearing length and profile section width are marked by numbers on the design sheet. The table in Figure 5.9(b) shows section widths and bearing length design information for the channel shape. The positions of each sampling point are numbered from 1 to 7 individually as shown in 5.9(a). In Figure 5.9(c), section widths and bearing lengths are described as individual points in the design space.

For any given die design profile, the radial distance of each section can be calculated easily if the location and orientation of the die opening is known. For the channel shape die, the die opening is located at the centre of the die as the die center is marked as a small cross in Figure 5.10(a). Therefore, the radial distances and bearing lengths of the die are known (Figure 5.10(b)). For each radial distance and bearing length duplexes, the corresponding points are shown in Figure 5.10(c).

For the same die design (Figure 5.11(a), both section widths and radial distances are used as input design variables for the bearing length function. As mentioned

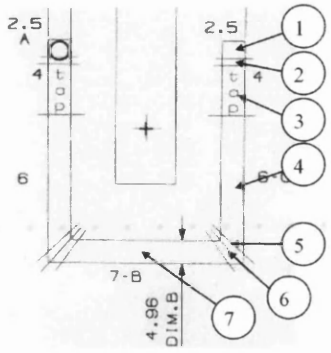

(a) Bearing length design for a channel shape

No.	w	b
1	4.81	2.5
2	4.81	3.25
3	4.81	4.0
4	4.81	6.0
5	5.5	6.25
6	5.80	6.5
7	4.96	7.0

(b) Design information

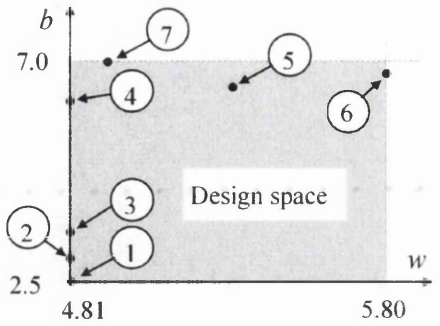

(c) Bearing length design information in design space

Figure 5.9: Representation of section width and corresponding bearing length in a 2D design space

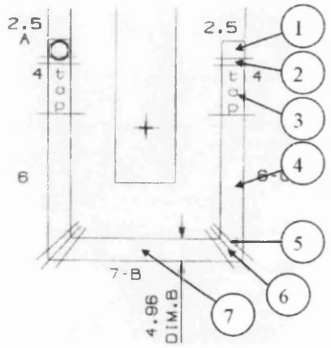

(a) Bearing length design for a channel shape

No.	r	b
1	26.0	2.5
2	22.5	3.25
3	19.5	4.0
4	21.5	6.0
5	31.0	6.25
6	31.5	6.5
7	26.0	7.0

(b) Design information

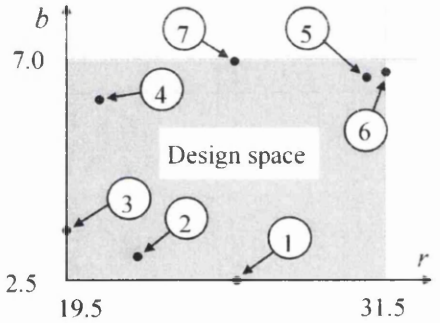

(c) Bearing length design information in design space

Figure 5.10: Representation of section radial and corresponding bearing length in a 2D design space

earlier, all possible triplexes $< w, r, b >$ define a three-dimensional design space as shown in Figure 5.11(c). In this case, each point in the space is defined by a given section width, a radial distance and a bearing length. For example, point 5 in the Figure 5.11(c) has coordinates (5.5, 31.0, 6.25) and indicates the design result at the fifth testing point as shown in Figure 5.11(a).

Using this approach, the design information of past successful designs can be gathered and stored on a computer. Different die designers may use different design parameters and/or constants based on their experience. However, all die designers agree that bearings can be scaled within limits [4]. This may cause problem when more than one design results are put into the same design space

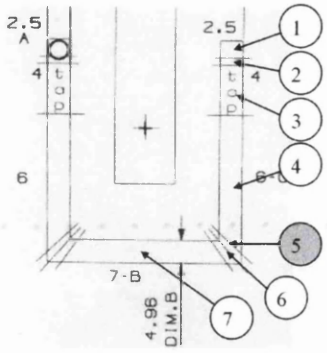

(a) Bearing length design for a channel shape

No	w	r	b
1	4.81	26.0	2.5
2	4.81	22.5	3.25
3	4.81	19.5	4.0
4	4.81	21.5	6.0
5	5.5	31.0	6.25
6	5.80	31.5	6.5
7	4.96	26.0	7.0

(b) Design information

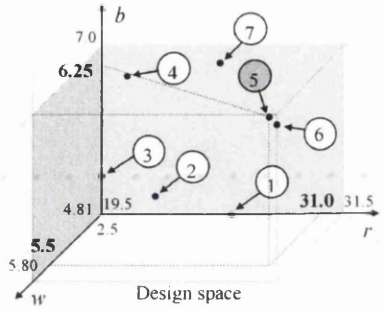

(c) Bearing length design information in design space

Figure 5.11: Representation of both section widths and radial distances and corresponding bearing lengths in a 3D design space

and therefore, to avoid this problem, normalized design variables and design spaces are needed.

5.5.3 Data in Normalized Design Space

To illustrate the difference between the original and the normalized design space, bearing length designs for two channel die openings shown in Figure 5.3 are used. The design results for the die, which is shown in Figure 5.3(a), are denoted by black circles in Figure 5.12. The design information for die in Figure 5.3(b) is marked by black triangles in the figure. Figure 5.12(a) shows that all circles and triangles roughly lie on a straight band. But each set of points belong to different bands with a wide gap between these bands. Figure 5.12(b) and 5.12(c) show similar representation for different set of design data.

To fix the problem, normalized design spaces are used to make different data bands overlap with each other. As can be seen in Figure 5.13 that specific input and output data ranges are normalized in such a way that all results are located between 0 and 1. It is clear that in the normalized design spaces, design data for different die openings are quite similar and the gaps between different design data bands are scaled.

This approach shows a new and effective way to capture and store extrusion die design informations using design spaces. As the data representation of this

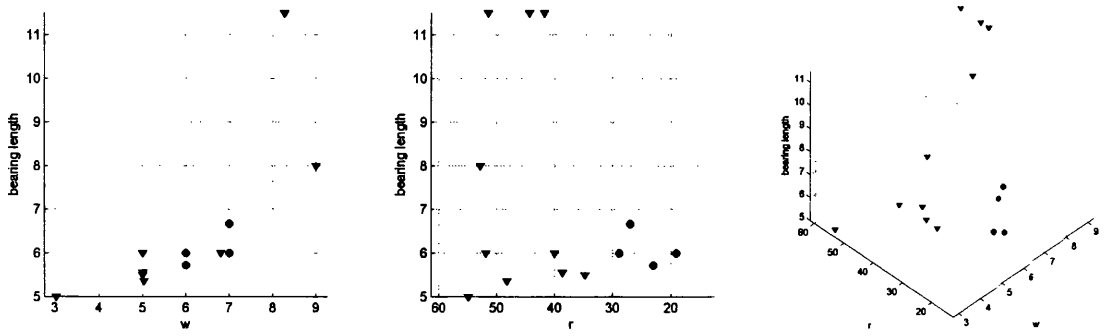

(a) Section width – bearing length in 2D design space

(b) Radial distance – bearing length in 2D design space

(c) widths and distance – bearing length in design space

Figure 5.12: Bearing length design results in original design spaces

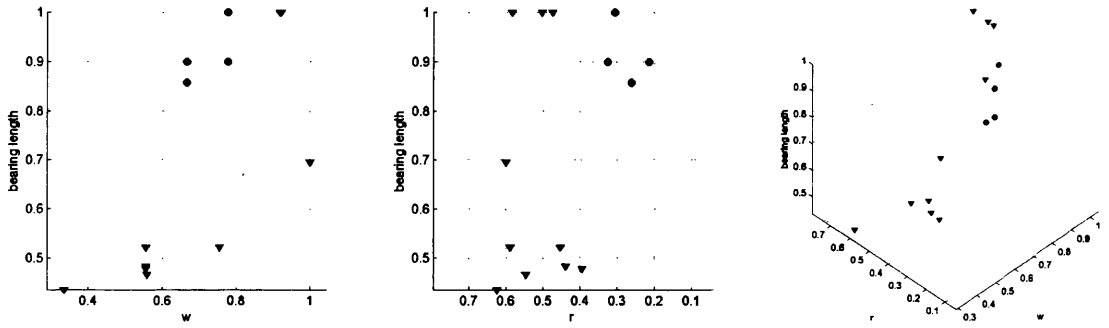

(a) Section width – bearing length in normalized 2D design space

(b) Radial distance – bearing length in normalized 2D design space

(c) widths and distance – bearing length in normalized 3D design space

Figure 5.13: Bearing length design results in normalized design spaces

approach is quite straightforward, it shows the capability of reusing the data which will be discussed now in the next sub-section.

5.5.4 Design Knowledge Representation for Extrusion Dies

As mentioned earlier, extrusion die design rules can be defined by a single or a combination of formulae. These formulae can be described as curvilinear curves, surfaces or hyper-surfaces in the corresponding design spaces. Each design formula represents some kind of design knowledge by describing a specific relationship between the design factors and the design objects. Therefore, an appropriate

choice of design formulae is required to store the knowledge on computer and its subsequent use for designing new die profiles.

The design knowledge representation mainly comprises of two sub-tasks:

1. finding out the proper expression of each design formulae for the required design rules and
2. finding out the optimal design parameters of each design formulae so that optimal designs for new die opening profiles can be achieved

For solving the first sub-task, empirical bearing length design formulae are used to represent the design knowledge (rules); For the second task, the new design information representation scheme which was mentioned in the previous sub-section and an optimization approach, such as a least-square fit algorithm, are used to get the optimized design formulae. This is illustrated step-wise in the following paragraphs.

Design Knowledge Representation Scheme for Linear Design Formulae

To validate our design knowledge representation scheme the widely used bearing length design formula, Miles 97 formula (Eq. 5.2), is used. The details about the design formula have already been discussed in Chapter 3. More details can be found in Miles *et al.* paper [4].

The formula can be re-written as:

$$b = C_1 w + C_2 w(R - r) \tag{5.9}$$

where $C_1 = \frac{B}{W}$, $C_2 = C\frac{B}{W}$. Since B and W are reference bearing lengths and section widths respectively, a typical value for $\frac{B}{W} = 2.0mm$ is used during the testing process.

Using a general least-square fitting algorithm with the design data which is shown in Figure 5.13, two constants, C_1 and C_2, of the Eq. 5.9 can be fixed. The optimization result shows a three-dimensional surface in the design space. The w-b side view, r-b side view and 3D view of the surface are shown in Figure 5.14(a), 5.14(b) and 5.14(c) respectively.

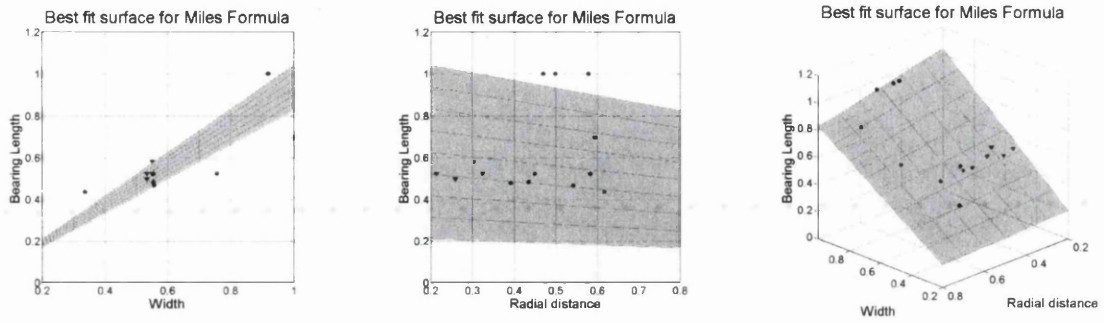

(a) w-b side view of fitting result

(b) r-b side view of fitting result

(c) 3D view of fitting result

Figure 5.14: Optimization result for Miles97 formula

Though the result shows that this knowledge representation approach can potentially work, the distances between each data point and the three-dimensional surface are considerably large. One of the reasons which can explain this gap is that during the extrusion process, the central part of the billet flows faster than the peripheral area due to the friction between the billet and the container wall [20, 13, 26]. The research by Li *et al.* shows a parabolic flow velocity profile in the axial direction [73]. The FE simulation result is shown in Figure 5.15

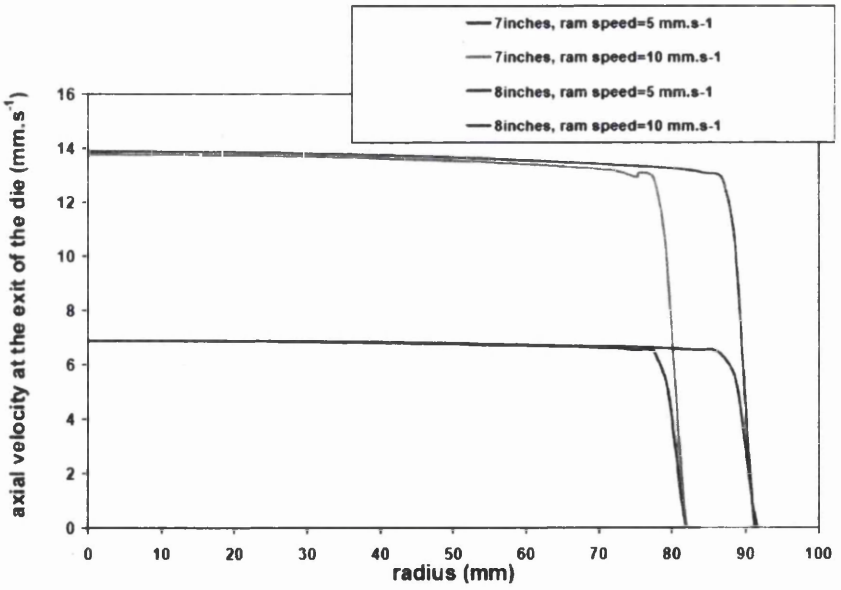

Figure 5.15: FE simulation for axial exit flow rate at die openings [73]

To reduce this deviation, a new bearing length design formula has been introduced in this research.

Design Knowledge Representation for Non-linear Design Formulae

As shown in Chapter 3, designers normally consider the radial effect by which an uneven flow rate in the radial direction can be reduced. However, all of them use linear design rules for achieving this [27, 1, 4]. In Eq. 5.2, the radial effect is represented by the term $(R - r)$.

On the other hand, our new design formula takes the radial distance ratio as one of the primary design factors. The equation is:

$$b = C_1 w \left[1 + C_2 \left(\frac{r}{R}\right)^2\right] \tag{5.10}$$

where w is section width, r is radial distance, R is the radius of extrusion dies, C_1 and C_2 are constants.

Similar to the previous case, a non-linear least-square fitting algorithm is used for the new bearing length design formula. The optimization result is shown in Figure 5.16. It is clear that the optimization result is a non-linear three-dimensional surface in the design space.

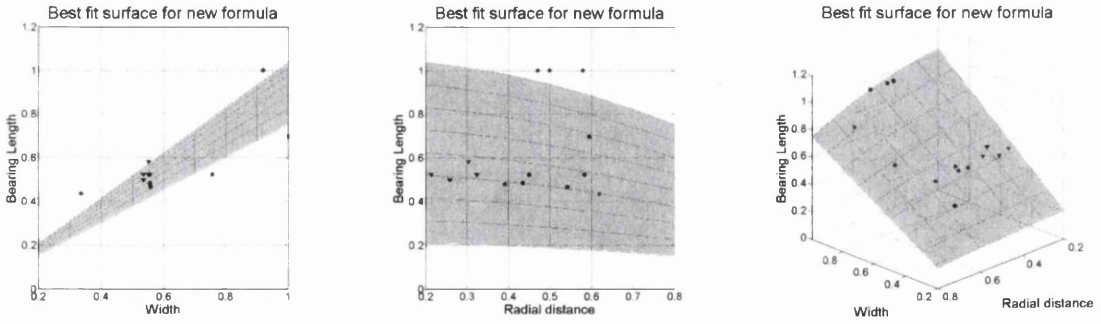

(a) w-b side view of fitting result

(b) r-b side view of fitting result

(c) 3D view of the fitting result

Figure 5.16: Optimization result for new bearing length design formula

In this section, a novel design information capturing and keeping approach for extrusion dies is introduced. By using normalized design spaces, historical design data can be described and reused easily. Furthermore, these design spaces can be used to represent and optimize the design knowledge for extrusion die designs.

5.6 Overview of the New Approach

The flow chart for the whole approach is shown in Figure 5.17. Compared with Figure 5.2, this new flow chart indicates that the new design approach separates design knowledge gathering and storing procedures from the main design process. Therefore, by using this approach, extrusion die design knowledge can be gathered, optimized and stored in computers and will no longer remain captive with individual designers. This capability allows demystifying of the "black art".

Besides, good new designs can be put into a design database for optimization purposes. On the other hand, optimized design formulae can be saved in a design formulae database so that optimization procedures are not required to be repeated for each new design process. Such feedbacks mechanisms introduce data reusing capability.

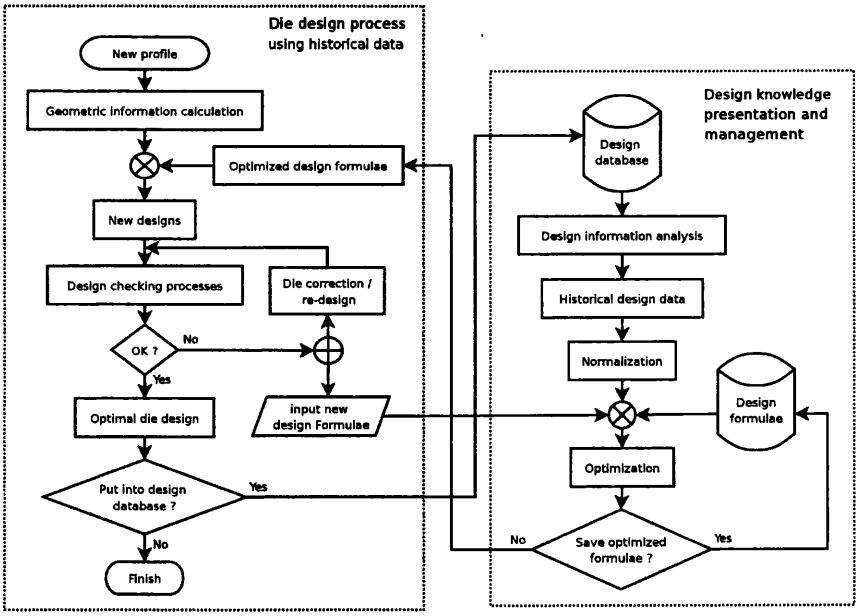

Figure 5.17: Flow chart of bearing length prediction process

Table 5.1 shows the primary properties of the new approach. Compared with general empirical design formulae (Table 3.1), this approach provides a much better solution for extrusion die design. However, it is also clear that due to the limits of the bearing length design formulae used by the approach, local effects and die shape classification information can not be handled by the approach at this moment.

Table 5.1: Properties of the bearing length prediction approach

Properties	New approach
Constants knowability	•
Auto-calculate possibility	•
Non-linear	•
Local effects	-
Data reuse	•
Die classification	-

(• fully supported, o partly supported, – does not support)

5.7 Approach Validation

To validate the new approach, an extrusion die profile which was used by Miles *et al.* is chosen (Figure 5.18(a)). Figure 5.18(b) shows the MAT result of the profile.

(a) Perimeter of a die orifice [1] (b) MAT

Figure 5.18: Die profile and its medial axis transform result

For testing their bearing length design formula, Miles *et al.* marked the segments of the profile as *a*, *b*, ..., *h*. Figure 5.19(a) shows a designer's design for the die opening orifice. The bearing length design result shown in Figure 5.19(b) was given by Miles *et al.* based on their design formula (Eq. 5.1). Figure 5.19 shows the design result based on the optimized Miles97 bearing length design formula.

It is clear that the result given by the optimized design formula fits both designer's and empirical design formulae designs quite well. Therefore, as a new design knowledge acquiring and representing method, the new approach can quickly and accurately predict bearing length based on historical designs.

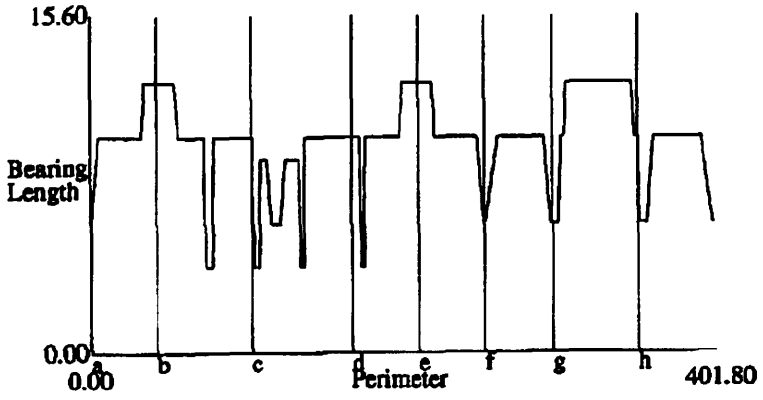

(a) Bearing length design given by die designer [1]

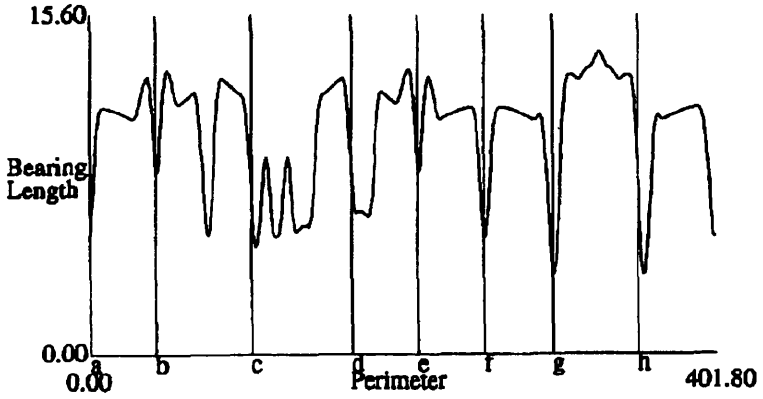

(b) Bearing length design given by Miles *et al.* [1]

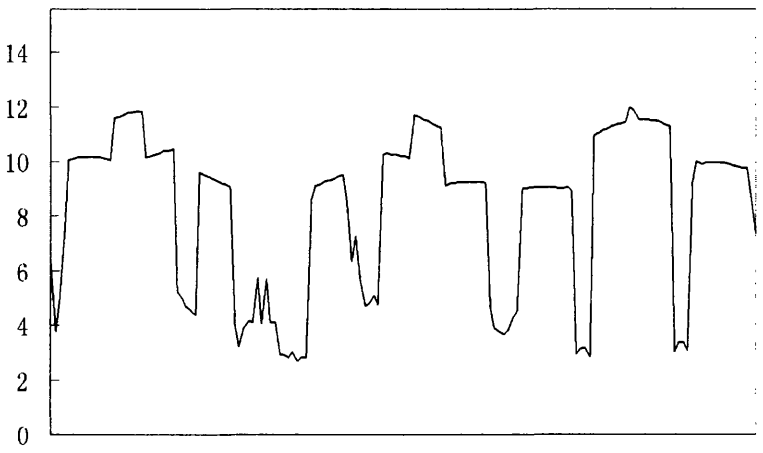

(c) Design calculated by optimized design formula

Figure 5.19: Optimization result for new bearing length design formula

5.8 Conclusion

A novel approach for extrusion die bearing length design has been discussed in this chapter. This new approach uses historically successful designs to train the proposed design algorithm. A well trained design algorithm then efficiently predicts the bearing lengths. The approach is more concerned with the relationship between geometrical information of die opening profiles and the corresponding design rules and results. It does not engage with the details on how to simulate the design process or any particular design formulae. This lends a novelty to the proposed approach as it has the capability to reuse design information from successful old designs. In addition, the new results can also be introduced as a feedback for the training loop so that the design algorithm can be updated and trained to provide more accurate design results over time.

In this chapter, both the past design and the new design belong to one shape group. Therefore, challenges remain to develop a technique to classify and quantify shape groups and to choose a proper shape group for bearing length prediction. Only the width and radial effects have been covered in this chapter and further work is therefore required to incorporate more design features, such as tip effect. Besides, not all design procedures are taken out from the designer-held knowledge at the moment. The following chapters will now reveal more design work from the "black box".

Chapter 6

An Innovative Layout Design Approach for Extrusion Dies

Chapter Layout

This chapter further explores geometric reasoning techniques and proposes a new approach for an optimal design for orientation and locations of the die openings in multi-hole extrusion dies. After briefly providing a background on extrusion die layout design, the next section discusses current approaches for such designs and brings out their limitations. A new innovative approach based on empirical bearing length design formulae is then introduced for die layout design. The fourth section describes general concave and convex shell boundary generating algorithms. These algorithms are used to calculate valid design zones for both single- and multi-hole die layout design work. Optimal layout designs for single- and multi-hole dies based on bearing length difference (BLD) distribution are proposed. The proposed approach is then validated using four case studies and finally conclusions are drawn from the chapter.

6.1 Introduction

The complexity of aluminium extrudate profiles used in every day life has increased in recent years; the pressure on reducing manufacturing costs has increased many fold. A single cavity die with a die opening located at the centre of the die offers an easiest route to manufacture the extrudate. However, the productivity can be quadrupled if four die openings are designed in the same die.

To avoid the distortion of extrudate shapes, the die openings must be designed in such a way that the exit velocity of the extrudate remains uniform. The location and orientation of die openings alter the parabolic input velocity profile in a complex way. The design of a multi-hole die is a challenging task requiring experience and expertise.

The current methods to design orientation and number of die openings in a multi-hole die are based on a trial and error method. The die designer makes a guess for the initial specification of the location and orientation of die openings and then assesses his/her choice either by conducting pre-production trials experiments or computer simulation.

This chapter illustrates a methodology-perhaps for the first time-where a user can specify the extrudate geometry and number of die openings required and the proposed methodology will provide an optimal specification of location and orientation of die openings. The bearing length calculations are based on the widely used Miles formulae (Eq. 3.4 [1, 4]) and the results are shown for many industrially relevant extrudates.

6.2 Background

6.2.1 Extrusion Die Layout Design

As described earlier in Chapter 2, extrusion is a deformation process by which aluminium alloy material is forced to flow through a die to get shaped extrudates. The shape of holes (die openings) in an extrusion die follows the profile of the extrudate. During the process, a ram pushes a cylindrical billet in the container and forces the material of the billet to flow through the die openings.

Owing to the temperature variations in the billet, limited billet length and friction between billet, container walls and ram, the flow of material is non-uniform [13]. This leads to various defects. A uniform exit flow velocity at the die openings has to be achieved to get good extrudates. This necessitates the development of appropriate die design. Extrusion die designs therefore strive to adjust the friction so as to achieve a more or less uniform flow rate.

During the extrusion process, friction is the most important factor that causes defects. Proper adjustment of friction resistance so as to to achieve a more uniform flow rate is one of the main objectives during the extrusion die design process. For a given extrudate profile, material and container, the extrudate section thickness, material properties and friction between the billet and container are fixed and therefore, the only possible way to change the flow rate is the adjustment of frictional resistance in the extrusion die.

The following methods have been used for extrusion die design.

- Die layout design
- Bearing length design
- Pocket design
- Other methods such as choke and relief of bearing, bridge and porthole design

The Bearing retards the flow due to the friction generated between the material and itself whereas a pocket reduces the friction between the billet and die surface and allows the material to enter die opening more easily thereby speeding up the flow rate.

During the extrusion process, the flow rate is non-uniform inside the billet. Due to the interior friction of the billet and the friction between the billet and container wall, the fluid flows faster in the central part of the billet as compared to the peripheral parts. Therefor, the die layouts are taken into account during the design procedures. Besides these major methods, choke, relief, bridge, porthole and other design factors are also used to control the flow rate inside a die.

6.2.2 Current Approach for Extrusion Die Layout Designs and Their Limitations

For die layout design, the approaches discussed in Chapter 3 still hold. In brief, the typical way is a trial-and-error approach which is slow, expensive and highly dependent on the designers' experience and skill. Since the whole optimization process is undertaken by the designer, it is extremely difficult to transfer the design knowledge from one person to another and to quantify or maintain the design quality.

Because the bearing length and pocket design play a vital role during extrusion process, most of the research work is focused on bearing length and pocket design problems. There is almost no reference to research on the extrusion die layout design issue. This is true for empirical design formulae as shown in Chapter 3.

Numerical simulation approaches are severely limited for layout optimization problems. The layout design cares more about the shape, location and orientation of die openings rather than the material, temperature and such physical properties. A numerical simulation tool is either too difficult to implement, or is too slow.

Since the traditional approaches can not resolve the layout design problem satisfactorily, a new layout design approach is introduced during this research that gives fast and reasonable results. The details of the approach are explained in the next section.

6.2.3 New Approach for Extrusion Die Layout Design

Figure 6.1 shows a simplified extrusion layout design flow chart of the current design approach and a proposed new approach. As can be seen in the figure, during normal extrusion die design process, the designer suggests a number of die openings' location and orientation and size of the die. Then the designer gives the bearing length and/or pocket design for the die. Finally, experimental or numerical simulations are used to check the designs. If the result is unsatisfactory, then the designer corrects the design and runs the simulation again. This is repeated till a satisfactory design is obtained (Figure 6.1(a)).

On the other hand, the proposed new approach only requires designer input for number of die openings and the profile and the rest of the process is accomplished by the computer. An optimization methodology is applied to obtain the optimal designs. During this optimization process, calculation procedures are used to get criteria information which is required by the optimization algorithm. For example, bearing length design along a die opening perimeter is used by the optimization algorithm to demonstrate the approach in this chapter. The flow chart of this new approach is shown in (Figure 6.1(b)).

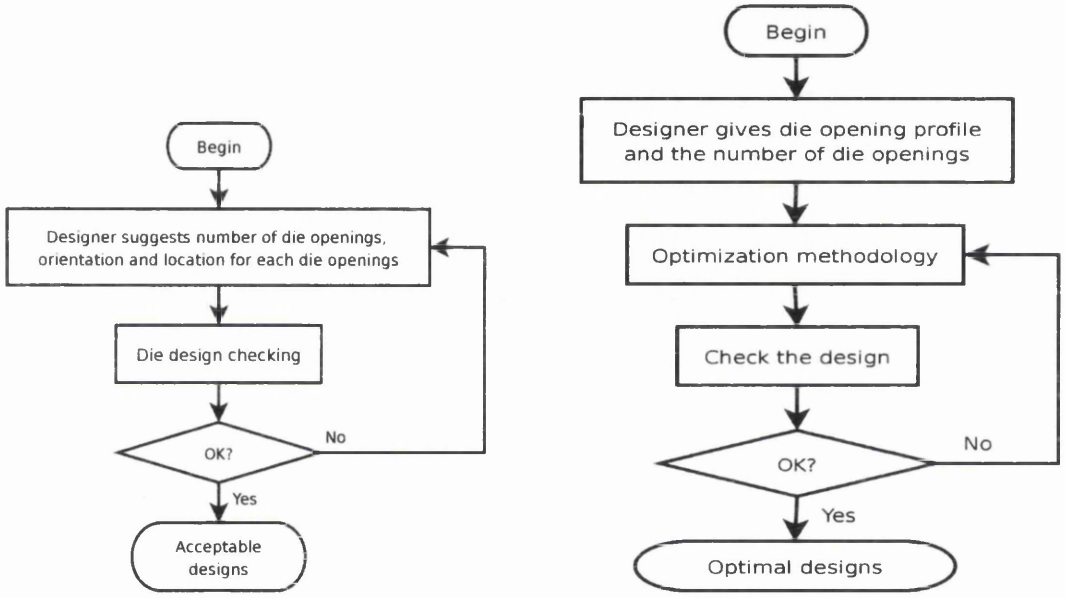

(a) Current layout design approach

(b) Proposed layout design approach

Figure 6.1: Current and proposed design approaches for extrusion dies.

Figure 6.1 illustrates the advantages of the proposed approach over the traditional method which are

1. Due to the difference of design checking procedure, the normal approach only checks a small range of possible design choices and provides an acceptable design. But the new approach explores all possible choices and checks essential designs as many times as is necessary to arrive at an optimal design

2. The feedback loop in a normal approach is quite long and incorporates manual inputs. This leads to a longer designing cycle, more errors and difficulties in knowledge transfer. By contrast, the new approach limits the

feedback loop within computer. No manual inputs are required after the first step. This results in a faster design speed, robustness and facilitates easy collection of knowledge and its accumulation for future use.

6.2.4 Bearing Length Design

The bearing length is one of the most important design factors for extrusion dies. Different lengths of bearing directly influence the friction between billets and dies. Although the flow behaviour is complex, even for a simple die, die designers use the design rules to guide the process [26, 27, 1, 4]. The most important ones to consider are that the bearing length should be proportional to the width of the die openings and the fact that the material flow rate at the centre of the extrusion billet is faster than that in peripheral areas should always be considered. Further more, the bearing length should be correct for a particular geometry structure as it can influence the flow of material inside the billet. For example, the end of legs of die openings should have a lower bearing length as compared to normal shape parts. Finally, a minimum value of about 2 to $3mm$ should be maintained in the design for keeping proper die strength.

As mentioned in Chapter 3, Miles *et al.* gave two bearing length design formulae in 1996 and 1997 respectively (Eq. 3.4 and Eq.3.7). The values of constants in the design formulae, e.g. constant C can be determined using experiments or numerical simulation results. The methodology is to choose a proper design criteria by which the objective function, average bearing length deviation in this case, can be quantified. Then an optimization method is applied for the objective function repeatedly until the optimal design is achieved. Several experiments or numerical simulations are carried out during the optimization process. Lee *et al.* have successfully illustrated how numerical simulation results are used to determinate the design factors of Miles formulae [40, 41].

6.2.5 Extrusion Die Layout Design

The different material flow rate due to friction is also known as a radial effect. In addition the different die opening layout also poses difficulty in controlling twisting and handling on a run-out table. In a multi-hole die, the die opening

locations and orientations also influence the flow rate. The presence of these known and unknown factors that influence the flow rate points to a need to develop a more robust die layout design. The ideal layout design should provide

- Proper clearance between die openings and the container wall and proper clearance between die openings
- Balanced metal flow
- Ease in die design and manufacture

For single-hole dies, the design issue is the location and orientation of the die opening. For multi-hole dies, the design needs to take care of the layout between different die openings. There are two basic die layout types for multi-hole dies – flat layout and radial layout (Figure 6.2). In a flat layout, all major axis of the die openings are either parallel or vertical to one direction, as illustrated in Figure 6.2(a). In a radial layout, the major axis of each die openings lies along a radius, as illustrated in Figure 6.2(b). Though academic researchers have spent

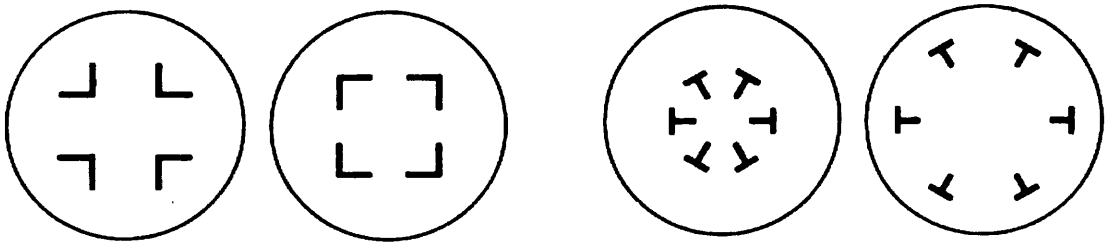

(a) Flat layout (b) Radial layout

Figure 6.2: Multi-hole die layout types [13].

more time studying the effects of bearing length than the die layout, there is still a need for fresh research work to be carried out. Some of the design rules are:

- For a single-hole die, put the gravity centre of the die opening at the centre of die.
- Put the thinnest parts of the die opening at the centre of the die for single-hole die.
- Keep at least a $\frac{1}{4}in.$ up to $1\frac{1}{2}in.$ clearance between side wall and openings.

6.3 New Approach for Die Layout Design

A new approach for die layout designing has been presented here. Instead of calculating only few specific reference locations of the die centre, this approach calculates the objective function value on a grid of all possible reference locations of the die centre and the optimal layout design.

The object of this approach is to get a minimum bearing length variation. For this purpose, the Bearing Length Difference (BLD) was used as a design criteria to quantify the design quality. The well known bearing length design formula, Miles96 formula (Eq. 3.4) was used to implement the proposed approach. The formula uses section width, radial distance to die centre and maximum radial distance, i.e. w, r and R as design variables. The constant C was set to 1/80 as mentioned in Miles *et al.* work [1].

In Miles work, the design variable w is related to the shape of the die opening and not with the layout design. Design variable r and R are related to die opening location and orientation. The die opening locations and orientations can be described in two ways. The first uses a global coordinate system, that uses the die centre as the original point. Three variables, x, y, and rotation angle α are needed for describing the location and orientation (Figure 6.3(a)). The second method is based on a local coordinate system that uses a reference point of die opening as the original point (as shown in Figure 6.3(b)) and the centre of a die is then defined by local coordinates, such as x' and y' in the figure. As a result, die opening locations and orientations can be described by two design variables that use local coordinates of the die centre. The problem is thus simplified to find out the optimal values of x' and y' so achieve the minimum bearing length difference.

The process of choosing proper local coordinate system is simplified by opting for the geometric centre of the die profile. Or, alternatively it could be a corner of the die profile as shown in Figure 6.4(a). The left-bottom corner of a 'L' shape profile was chosen as the original point of the local coordinate. The direction of the axis is fixed parallel to the major axis of the die opening. After this, a grid of points was chosen for calculating the bearing length difference. Each point in the grid corresponds to a possible position of the die centre e.g. the corresponding die layouts for selected reference points P_1 and P_2 are shown in Figure 6.4(b) and

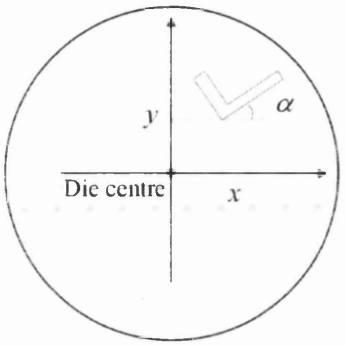

(a) Layout design representation in global coordinate system

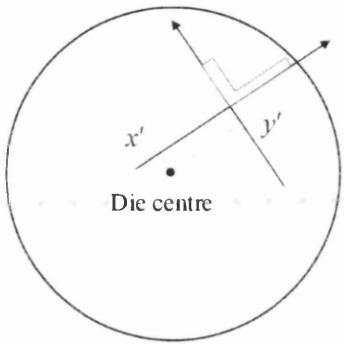

(b) Layout design representation in local coordinate system

Figure 6.3: Extrusion die layout design representation are different in different coordinate systems.

6.4(c) respectively.

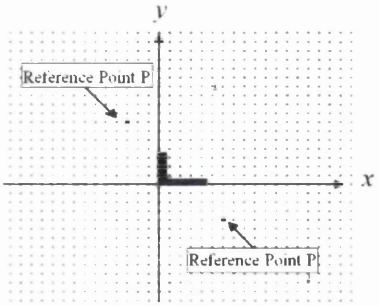

(a) Grid of reference points

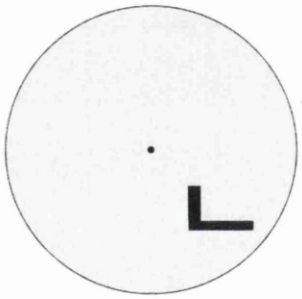

(b) Die opening layout corresponding to P_1

(c) Die opening layout corresponding to P_2

Figure 6.4: Reference points grid and its corresponding die layout.

6.3.1 The Bearing Length Difference Distribution

For an extrusion die design, all geometrical information is known if the die opening profiles and die layout are fixed. Therefore, by using a bearing length estimate approach, which was discussed in a previous chapter, it is easy to calculate the bearing length for each part of the die opening.

In the following sections, the widely used Miles96 formula (3.4) is chosen for bearing length estimation. Geometrical information of the die opening profile, such as section width w, section radial distance r and maximum radial distance

R are essential for the calculation. It is trivial that all this information is available if the die layout is known. For example, for a 'L' shape profile w, r and R can be easily owned by using MAT (as shown in Figure 6.5(a)). Figure 6.5(b) shows a bearing length estimation result for the 'L' shape profile. After this step, bearing length difference can be calculated using Eq. 6.1.

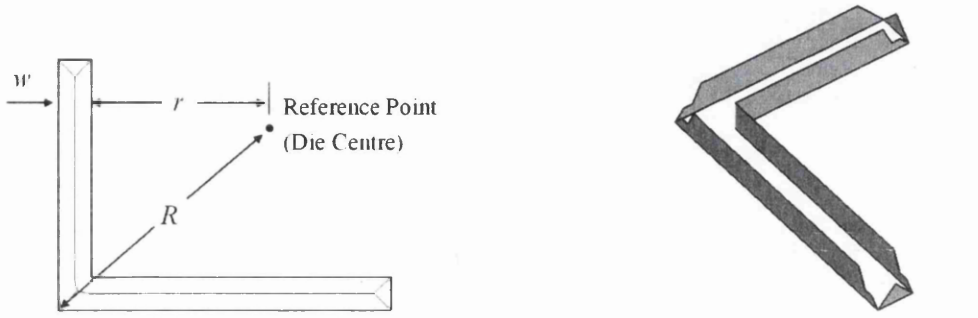

(a) 'L' shape profile with its medial axes (b) Bearing length distribution

Figure 6.5: Bearing length calculation.

Since the object of a die layout design is to find out the optimal location and orientation where low bearing length variation is achieved. For this reason, the bearing length difference distribution result is used for the optimization work. The procedures for calculating the bearing length difference (BLD) distribution are described as follows:

1. Generate a medial axis transform for the given die opening profile
2. Choose a reference points grid. The size of the grid should be larger than the extrusion die. The density of points in the grid should high enough so that a reasonable precision is maintained.
3. Choose a reference point in the grid
4. Calculate the bearing length distribution
5. Calculate the bearing length difference (BLD) using Eq. 6.1. Save the result with the corresponding reference point.
6. If not all of the available reference points are used, repeat step 3

$$BLD = b_{max} - b_{min} \tag{6.1}$$

As an example, the BLD distribution of the 'L' shape die opening profile is shown in Figure 6.6. The flow chart of the whole calculation process is shown in Figure 6.7.

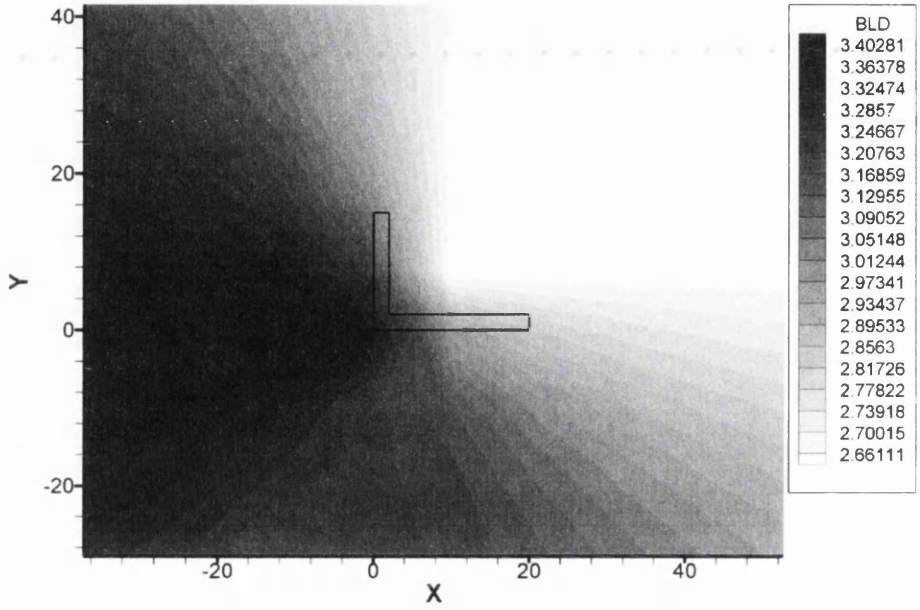

Figure 6.6: Bearing length difference (BLD) distribution of 'L'-shape die opening.

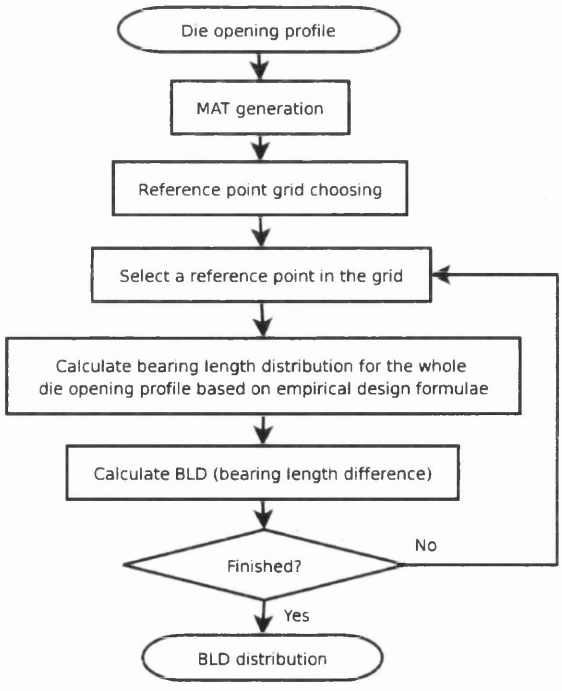

Figure 6.7: Flow chart of bearing length difference (BLD) distribution calculation.

6.4 Concave and Convex Shell Boundary Generation

6.4.1 The Definition of Concave and Convex Hulls

Convex Hull

Quite often the "natural boundary" of a set of points is required. The mathematical name for the natural boundary of a point set is the so called "convex hull". The definition is that the *convex hull* of a set of points in the plane is defined to be the smallest convex polygon containing them all [74]. The definition of a convex polygon is: a *convex polygon* is a 2D polygon with the property that any line connecting any two points inside the polygon must itself lie entirely inside the polygon [74].

Figure 6.8 shows three examples of convex polygon shape. By contrary, three concave shapes are shown in Figure 6.9.

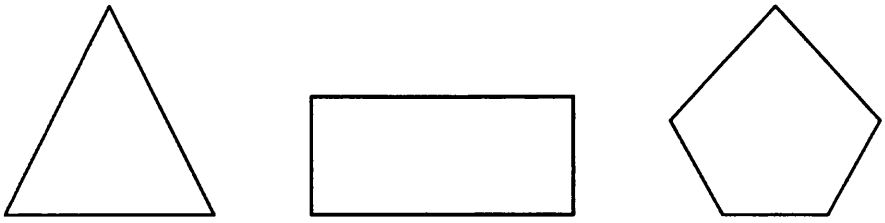

(a) Example 1 (b) Example 2 (c) Example 3

Figure 6.8: Convex polygons

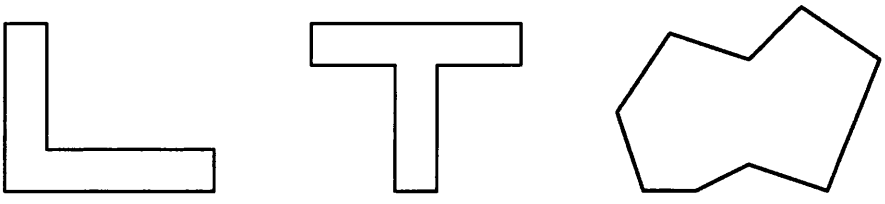

(a) Example 1 (b) Example 2 (c) Example 3

Figure 6.9: Concave polygons

An example is illustrated for the definition in Figure 6.10. In this case, there are

30 points. As can be seen in the figure, 10 of them are on the natural boundary (numbered as $P_1, P_2, \cdot, P_{10}$ in the figure). It is clear that the natural boundary is a convex polygon with all 30 points inside it.

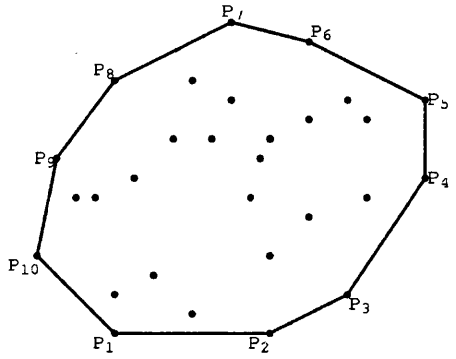

Figure 6.10: The convex hull for a point set

For any given die opening profile, the calculation of the valid design zones is based on the size and shape of the profile and the size of the die. This calculation is essential for the optimization method. The following sections will illustrate the calculation procedure for determining the valid design zones based on convex and concave hull generation algorithms.

6.4.2 Concave and Convex Shells

Shell of Geometry Models

In real life, a cover of a liner of something can be find everywhere. For example, a pair of gloves are covers for our hands. The cap of a pen is a cover for the nib. A bearing is some kind of liner for the axis so that it can rotate smoothly. If the objects are modeled in a computer based on geometric definition, the cover and/or liner is the outer and/or inner shell of the geometry model respectively. Figure 6.11(a) shows a 'L' shape geometry model with straight boundaries. The vertices of the boundary segments are named as P_0, P_1, P_2, P_3, P_4 and P_5. Figure 6.11(b) shows the outer shell of the model. The shell boundary segments are made by straight lines and arcs alternatively. The vertices of the segments are $CP_1, CP_2, \cdots, CP_{11}$.

Now, let us see how to generate the shell boundary for a geometry model. As the

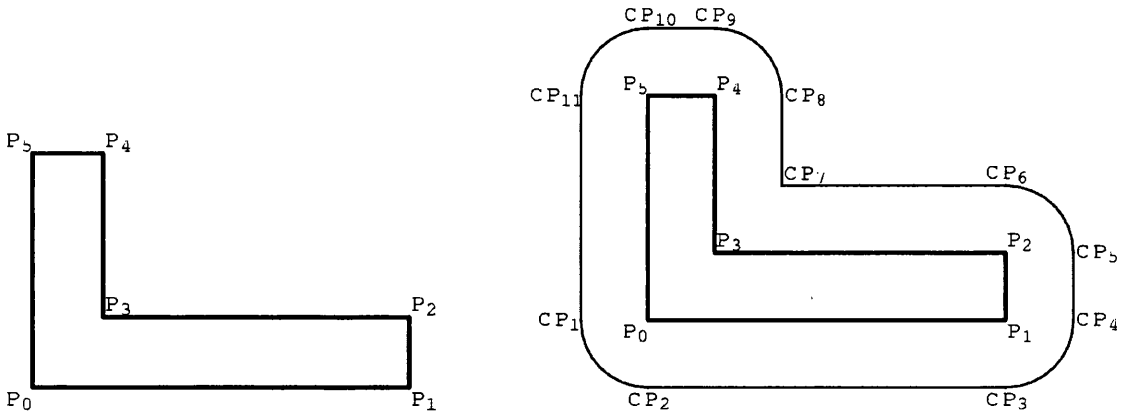

(a) 'L' shape geometry model (b) A shell of the model

Figure 6.11: Geometry model and its shell

simplest 2D geometry models are polygons, only straight boundaries are taken into account in this case. Actually, the boundary of a common polygon are straight lines and there are only three possible relationship between any two adjacent segments. That is, the two segments touch each other smoothly, in other words, they look like a simple line, or the point of constancy marks a corner. In the last case, the corner shape could be concave or convex. All three possible cases are shown in Figure 6.12 (Please notice that the boundary of geometry are marked as P_1, P_2 and P_3. And the area bellow the boundary are inner side of the geometry models). Figure 6.12(a) shows the first case with smooth connection. Figure 6.12(b) and 6.12(c) show concave and convex corner respectively.

Primary Algorithm for the Shell Generation

It is clear that a concave shell for a two-dimensional geometry can be described as the result of the *Minkowski sum*. The definition of the sum is [75]: Let A and B be two sets of points in the plane. the points in a established coordinate system can be viewed as vectors. Define the *sum* of A and B as $A+B = x+y|x \in A, y \in B$, where $x+y$ is vector sum of the two points. The following paragraphs illustrate an algorithm by which the Minkowski sum can be calculated easily.

The basic idea for a polygon shape shell generation is to expand each boundary segment towards the outer side of the geometry and then re-construct the whole new boundary based on the expanded results. Figure 6.12(a) undertaken the

simplest case. To achieve this, two boundary segments, P_1P_2 and P_2P_3, have been moved to a new position by uniform thickness with reference to the original position. The new boundary segments S_1S_2 and S_2S_3 are the shell boundary for the original shape. If a vector is used for the generation work, the algorithm can be described as to move a vector with length w along each boundary segments and maintain the vector's direction as the normal direction of each segments, the trace of the vector end-points give the shell boundary. In this simple case, v_1, v_2 and v_3 are three positions when the vector is moved to point P_1, P_2 and P_3. The trace of the vectors' end-points are S_1,S_2 and S_3, which define the key-points of the shell boundary.

The expanded algorithm becomes a little bit more complex when corners are formed at the joining point of two boundary segments. It is clear that the vector direction changes at the corner point.

The Overlapping and Gaping of Expended Boundary

If we define the geometry boundary exploring direction as the positive direction for the angles (e.g. the direction of $P_1 \rightarrow P_2 \rightarrow P_3$ for $\angle P_1P_2P_3$ in Figure 6.12). For a concave corner, the angle of the vector decreases. At the other side, for a convex corner, the angle increases. This feature causes overlapping or gaping between expanded line segments (as shown in Figure 6.12(c) and 6.12(b)). Therefore, for a concave corner, the intersection has to be calculated and an intersection point should be used for the final result of the shell boundary (P_i in Figure 6.12(b)). For a convex corner, a piece of arc should be used to fix the gap between two segments (arc $S_{2a}S_{2b}$ in Figure 6.12(c)).

6.4.3 Shell Generation for Curvilinear Boundaries

The majority of shapes not only contain straight lines but also curves. Now, let us check how a shell can be created for a curvilinear boundary. Figure 6.13 shows the simplest curvilinear boundaries, that is arcs. Just as for straight boundaries, curvilinear boundaries can be classified into two groups–convex and concave. For example, the thick lines in Figure 6.13(a) and Figure 6.13(b) show a convex and concave individually. The thin lines in these figures are corresponding shells.

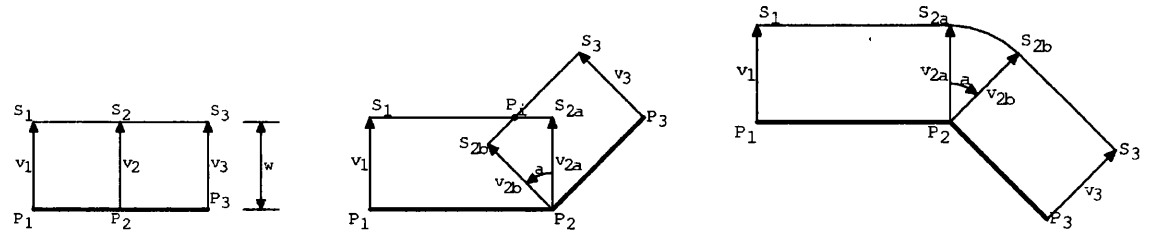

(a) Shell generation for straight Boundaries

(b) Shell generation at concave vertex

(c) Shell generation for convex vertex

Figure 6.12: Three possible corner shapes and corresponding 'expanded' boundary segments

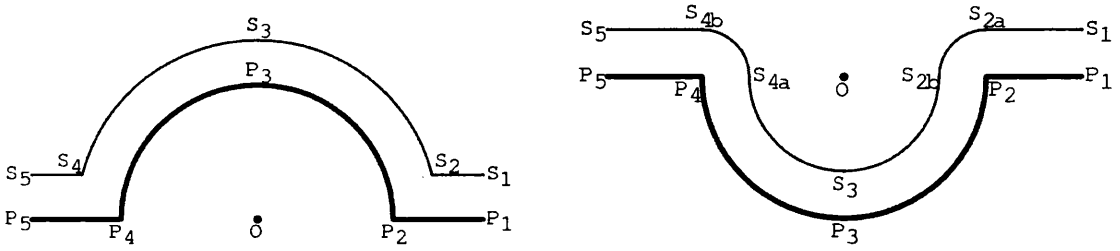

(a) Shell of convex boundary

(b) Shell boundary generation for convex vertex

Figure 6.13: Shell of convex and concave boundaries

Similar to the shell for straight-boundary shapes, the shell for curvilinear-boundary shapes keeps the distance between the shell and the shape boundary, say it is w. That is for any point, say point p, on the shell, the minimum distance between the point and the shape boundary is w. Suppose the corresponding point by which the minimum distance can be achieved is q. This implies that the direction of $\overrightarrow{qp}$ is the normal direction of point q.

An arbitrary shape is used to illustrate this argument. The shape boundary and corresponding shell are partly shown in Figure 6.14. Consider point P on the shell. There must exist at least one point on the shape boundary where the minimum distance (shell thickness w) is achieved. Say the corresponding point is q. Suppose O is the centre of curvature at point q. Choose point p as the center of a circle with radius w. It is trivial that the circle will touch the shape boundary at point q as shown in the figure. Line l is the tangent line at point q for the boundary. Because qp is a radius of the circle and l is a tangent line for the circle at point q, qp is perpendicular to l. At the other side, since l is the tangent line at q, it perpendicular to the normal direction of the boundary

at point q. So, qp is the normal direction of the boundary at point q.

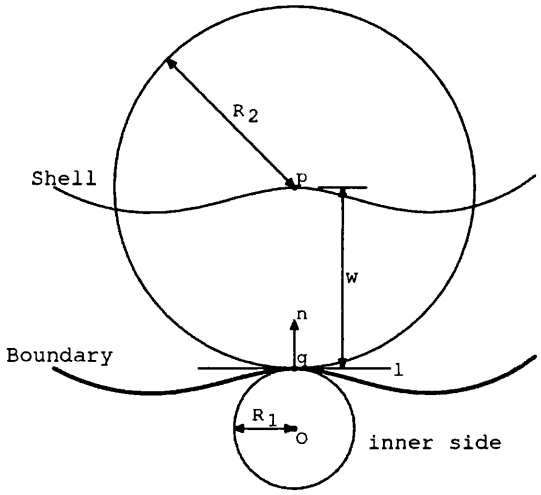

Figure 6.14: Boundary normal direction and Shell thickness

The procedure for generating a shell for curvilinear boundaries is as follows:

1. Move a vector, which length equal to the thickness of the shell, along the shape boundaries, the trace of the vector's end-point is the shell boundaries except:

2. If a convex corner is found, the vector changes its direction without moving. The start and end direction are defined by the left-side and right-side boundaries' normal direction.

3. If a concave corner is found, the vector changes its direction by using the same rules as for a convex corner. If the trace interlaces with itself, the interlacing part should be removed.

The three possible shell results that can be generated are shown in Figure 6.15. It is clear that all sharp convex corners cause a round corner in the shell (Figure 6.15(a)). For concave corners, the following three possible situations need to be considered:

1. The shell thickness is less than the curvature radius of the corner. The shell follows the shape of the boundary in this case (Figure 6.15(a)).

2. The shell thickness just equals the curvature radius. A sharp corner will be generated in this case (Figure 6.15(b)) .

3. The thickness of the shell is greater than the curvature radius. The boundary of the shell interlaces itself under this condition (Figure 6.15(c)).

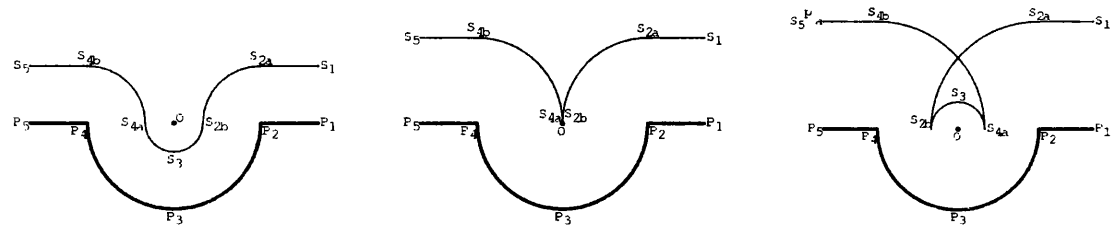

(a) Shell thickness is less than radius of curvature

(b) Shell thickness equals to radius of curvature

(c) Shell thickness is larger than radius of curvature

Figure 6.15: Interlacing of curvilinear shell boundaries

A computer program is designed for shell generation by following the rules and special circumstances described herein. To simplify the implementation, discrete shape boundaries are used. i.e., all curvilinear shape boundaries are meshed into small straight segments before the generating process begins. For each node, the left-side and right-side normal direction is calculated. The node is a corner or on a curvilinear boundary if the two directions are different. For such condition, a loop is implemented to generate several new points so that the shell boundary is continuous and smooth. If interlacing boundaries are generated, an extra procedure is used to remove the interlacing parts.

The flow chart of the whole algorithm is shown in Figure 6.16.

6.4.4 Convex Shell Generation

A fundamental property of the convex hull is that when any line is moved from outside of the hull hits the boundary points first. Under some circumstances, this property is extremely useful. As an instance, for extrusion die layout design, to keep the clearance distance between the container wall and die opening or the clearance between different die openings can use the property. The following paragraphs illustrate a very simple algorithm and its implementation.

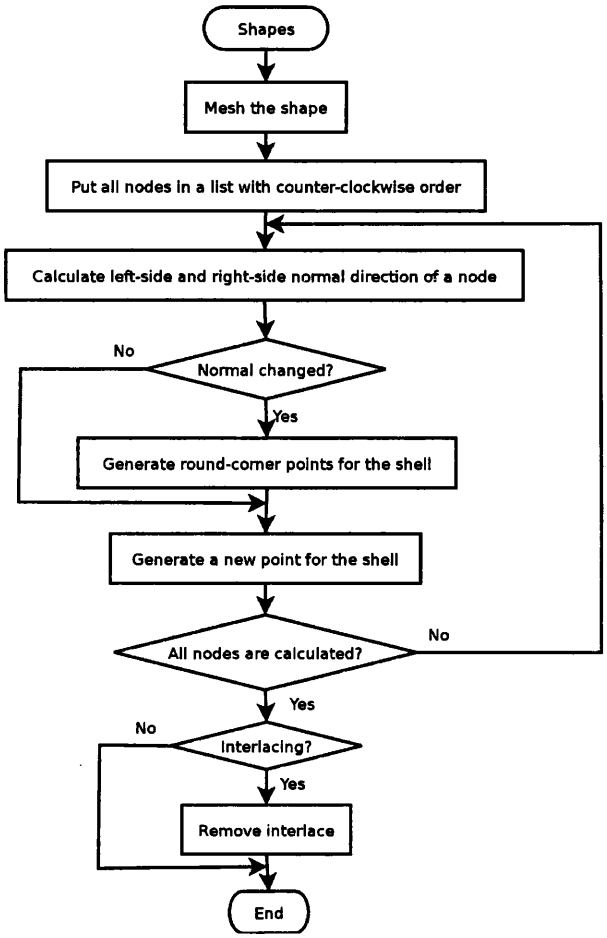

Figure 6.16: The flow chart for concave shell generation

To illustrate the algorithm, an arbitrary points set is used (Figure 6.17)). The algorithm is (More details about the algorithm can be found in [74]):

1. The first step is to find a start point which belongs to the convex hull. The property of convex hull that is outside lines hit the boundary points first leads to a simple searching algorithm – the point with minimum y coordinates must be a boundary point. If there are more than one points with the same y_{min}, choose the most left one (which has minimum x coordinates among them). This is true because it is the result as given by a horizontal line hits from the bottom. (P_1 in Figure 6.17(b)). Mark the counting angle as 0.

2. Find out the point in the set so that the angle between the horizontal and the line segment from start point to this new point is minimal but

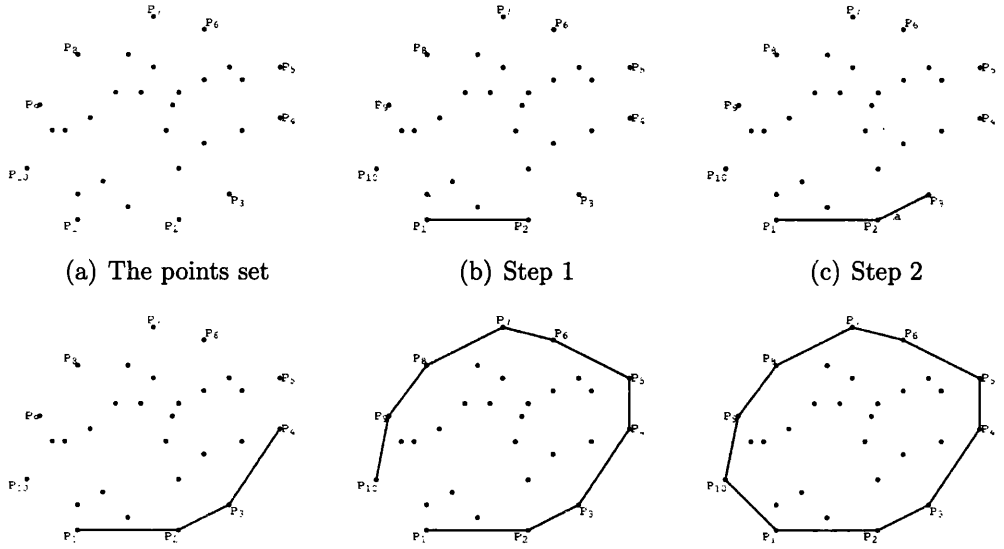

(a) The points set (b) Step 1 (c) Step 2

(d) Step 3 (e) Step 9 (f) Step 10

Figure 6.17: Package-wrapping for convex hull generation

greater than or equal to the counting angle. Put this point in the result list and reset the counting angle by the new angle. For example, point P_2 in Figure 6.17(b) is the right one since the angle between horizontal and P_1P_2 is 0 and the counting angle is 0 at the moment. Figure 6.17(c) illustrates the implementation issue in this algorithm even clearer. In this step, point P_2 already in the result list. So, we find out the next point based on P_2. As shown in the figure, the angle of P_2P_3 to horizontal is the minimal in all left points and the angle is greater than the counting angle. So, P_3 is the next point of the convex hull.

3. Repeat step 2 until the boundary of the hull returns to the start point (Figure 6.17(b) ... Figure 6.17(f)).

The final result is shown in Figure 6.17(f). It is clear that the final result is a convex polygon and it is the convex hull for the points.

The whole process of convex hull generation is shown in Figure 6.18.

On combining a concave shell boundary construction algorithm with a convex hull generation algorithm then a convex shell boundary can be constructed. The flow chart for convex shell construction is shown in Figure 6.19.

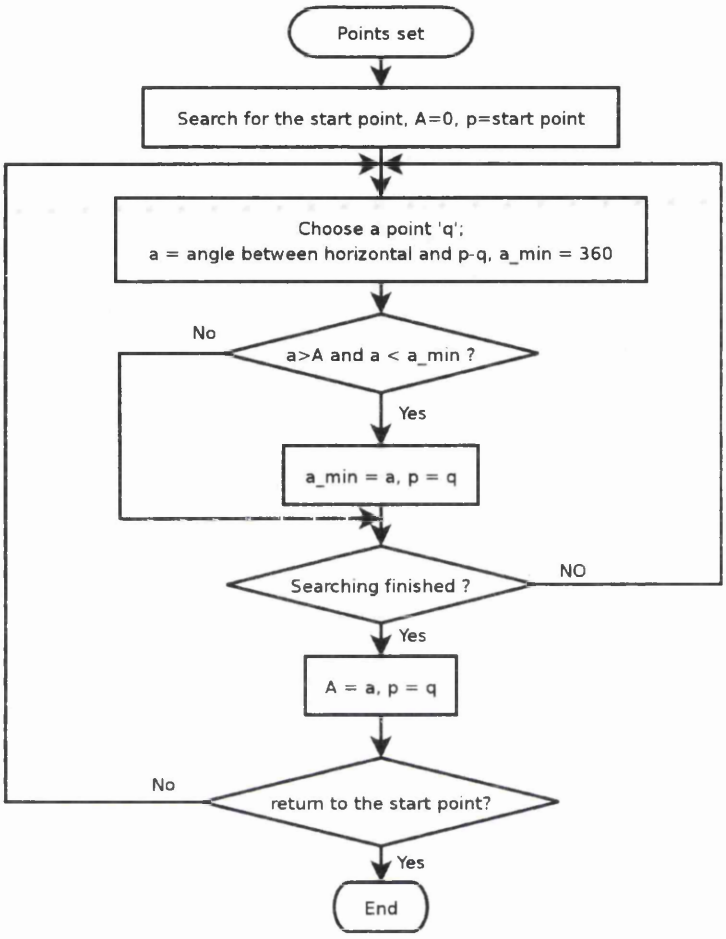

Figure 6.18: Flow chart for convex hull generation

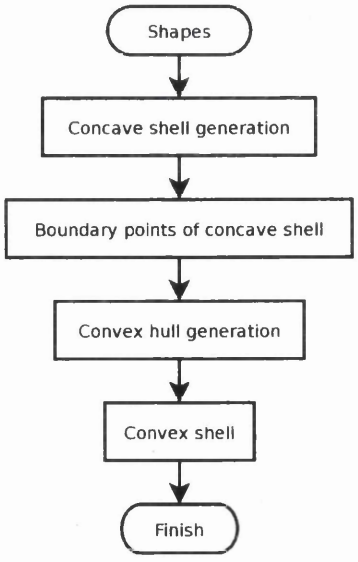

Figure 6.19: Convex shell construction

6.4.5 Concave and Convex Shell Generation Examples

Case 1

Figure 6.20 shows the shell generation results for a 'L' shape.

Figure 6.20(b) shows the expanded shape boundary segments. An interlacing loop of the shell boundary is clearly shown in the figure. In Figure 6.20(c), the loop is removed and the concave shell is constructed for the shape. Figure 6.20(d) shows a convex shell for the shape.

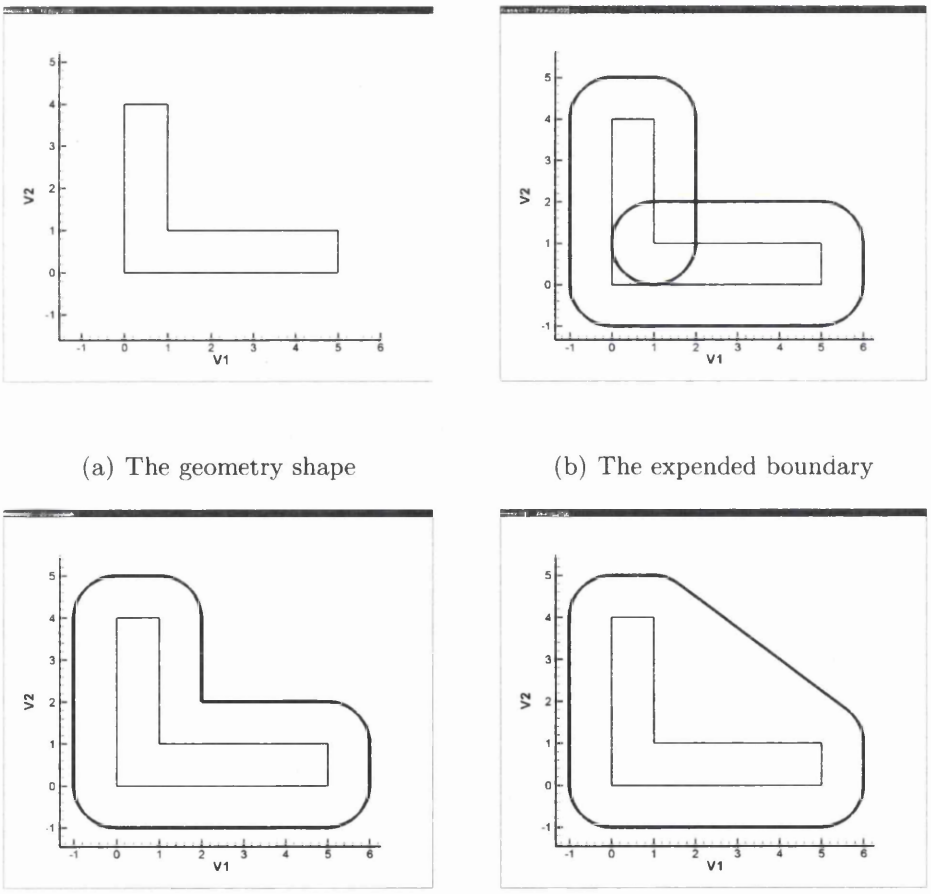

(a) The geometry shape

(b) The expended boundary

(c) Concave shell

(d) Convex shell

Figure 6.20: Shell generation for 'L' shape

Case 2

A 'T' shape geometry object is used for checking the algorithms in this case. Its shape, expanded boundaries, concave and convex shells are shown in Figure 6.21(a), 6.21(b), 6.21(c) and 6.21(d) respectively.

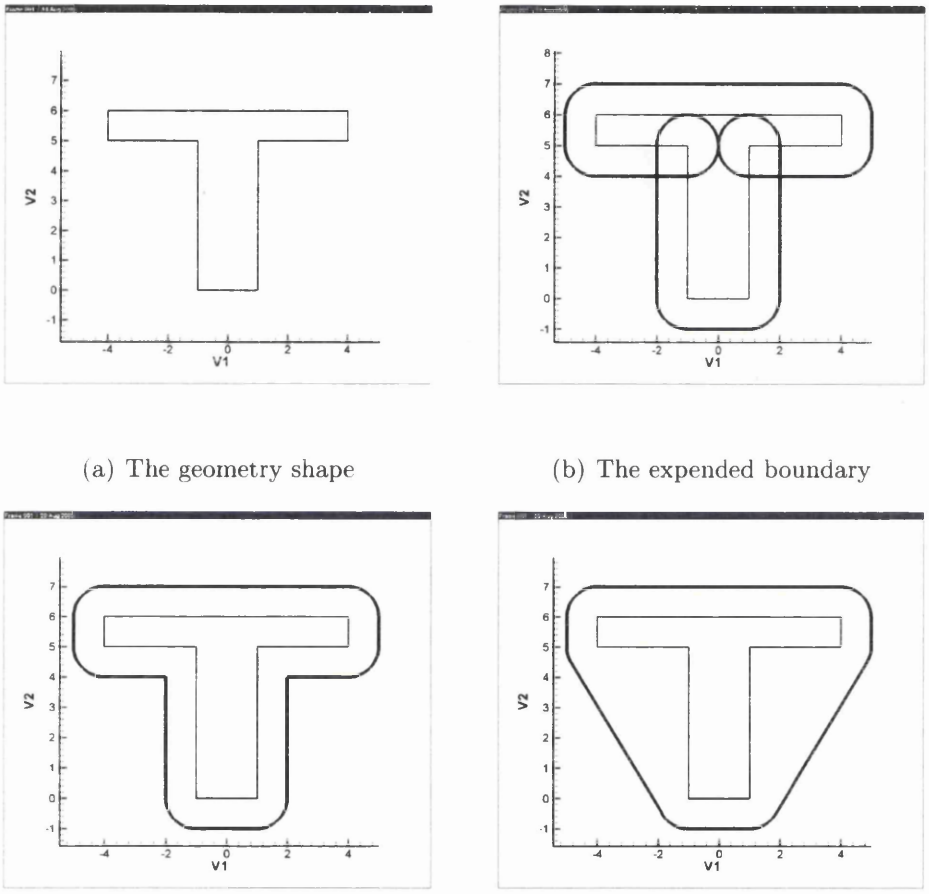

(a) The geometry shape

(b) The expended boundary

(c) Concave shell

(d) Convex shell

Figure 6.21: Shell generation for 'T' shape

Case 3

In this case, a more realistic geometry shape has been tested. This shape contains convex and concave corners and curvilinear boundaries. The shape, expanded boundaries, concave and convex shell of the shape are shown in Figure 6.22(a), 6.22(b), 6.22(c) and 6.22(d) respectively.

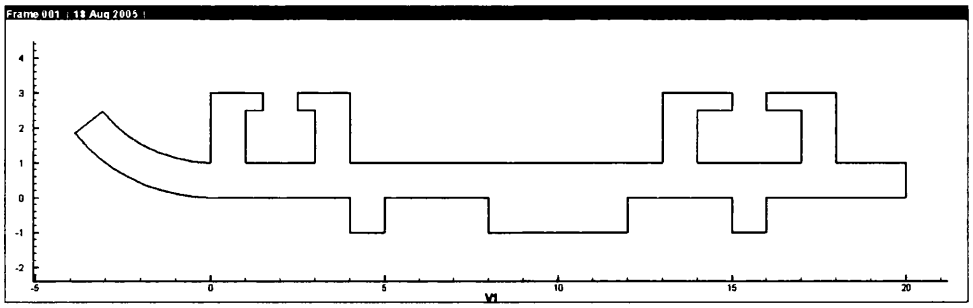

(a) The geometry shape

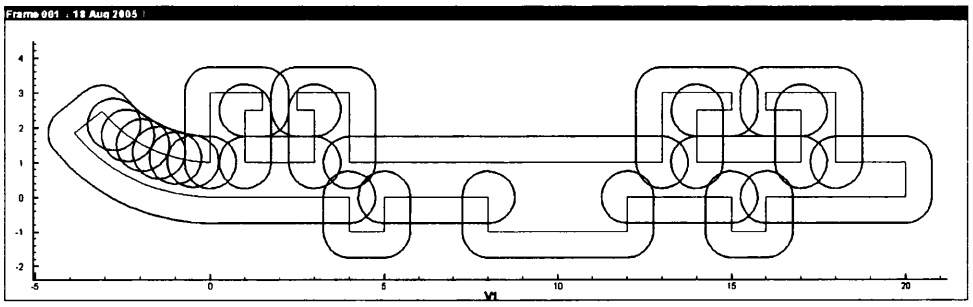

(b) The expended boundary

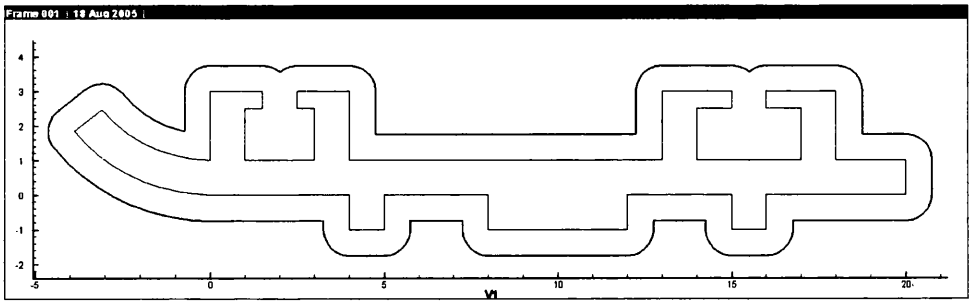

(c) Concave shell

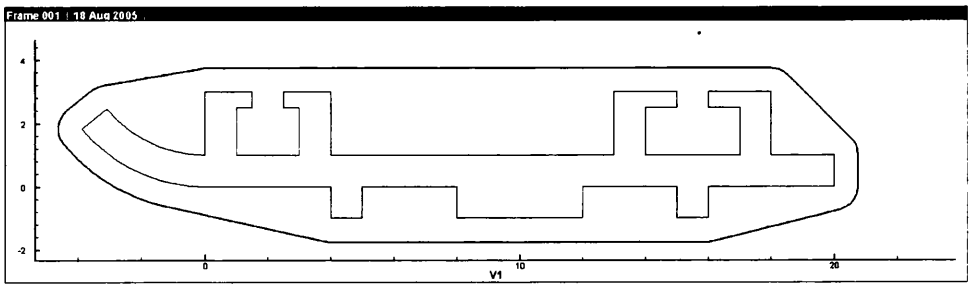

(d) Convex shell

Figure 6.22: Shell generation for a complex shape

6.4.6 Conclusion

This section explained the procedure for generating concave and convex shells for geometry shapes. Concave and convex shells with arbitrary thickness were constructed easily and efficiently. In the previous sub-section, three geometry shapes were used to validate the algorithms.

6.5 Optimal layout design for single-hole die based on BLD distribution

For a single-hole die layout design, a proper clearance between the die opening and the side wall has to be maintained. For a given profile of die opening, this clearance means the minimum distance between any container wall and the die opening boundary points. The clearance can be described as a ring-shape zone close to the inner side of the die, with a thickness equalling the minimum allowed clearance value. An example is shown in Figure 6.23(a). The hatched 'ring' shape area is the clearance zone for the 'L' shape die opening profiles. The remaining part of a die forms a design space where the die opening can be located. The white circular area in Figure 6.23(b) is a design space and the die opening marked as 1, 2, 3, 4 and 5 are five possible layout designs.

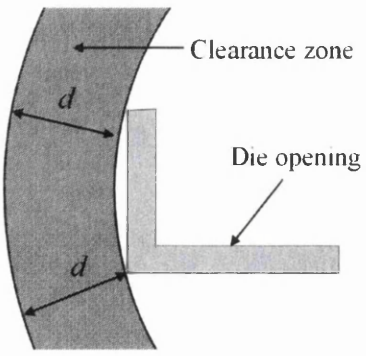

(a) Clearance zone between die opening and container wall

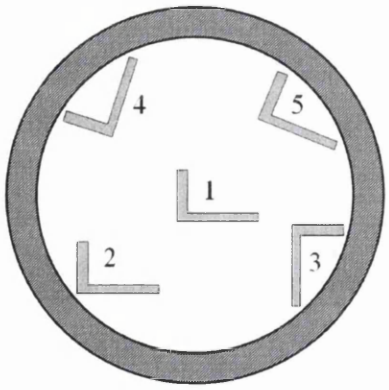

(b) Possible location and orientation of die openings

Figure 6.23: Clearance between container wall and die opening and corresponding possible location and orientation.

Although the original definition of clearance distance is very simple and clear, it is not easy to optimize the die layout using it. In order to overcome this difficulty, the clearance zone around the die opening and its corresponding valid design zone are introduced.

Two procedures are developed to get the clearance zone of a given die profile. The first step is to create an enlarged polygon (it is a concave polygon in most cases) which is similar to the shape of the die opening profile and has a uniform thickness (Figure 6.24(a)). Since the shape of the die is always a circle, all concave parts of the clearance zone can not remain in contact with the die. For example, when the edge of the die touches the zone edge at point P_1 and P_2 (Figure 6.24(a)), the hatched area between the clearance zone and the die edge is not in contact with the die. The correct clearance zone is the corresponding curvilinear convex zone shown as the hatched area in Figure 6.24(b). Due to the complexity of the calculations, a simple convex polygon is used in this research work instead of the curvilinear shape to describe the clearance zone. An example of simplified clearance zone is shown in Figure 6.24(c).

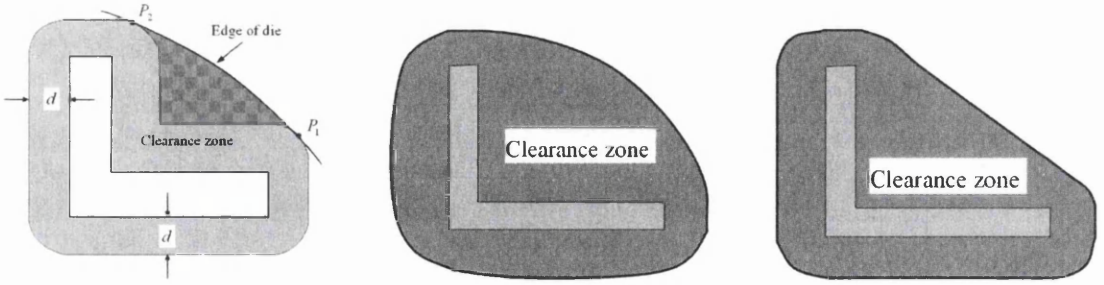

(a) Clearance zone (concave) (b) Clearance zone (convex) (c) Simplified clearance zone

Figure 6.24: 'L' shape die opening profile and related concave and convex hulls as clearance zones

6.5.1 Calculation of the Valid design Space

If a proper clearance zone is available, the possible location and orientation of the die opening can be easily chosen. This is accomplished by moving or rotating along the die opening with its clearance zone making sure that both of them are within the die plate. The clearance zone around the die opening works like a bumper and keeps the right clearance for the layout design. An example of an

'L' shape die opening is shown in Figure 6.25. The figure clearly shows that the clearance zone works correctly and the results are similar to the previous method.

Although the convex clearance zone method is used by designers, it is not suitable for computer programming. Similar to the bearing length calculations in a global coordinate system, the movement of the die opening causes increased complexity in the algorithm and its implementation. This is the reason to introduce the concept of a valid design space which is related with the local coordinate system.

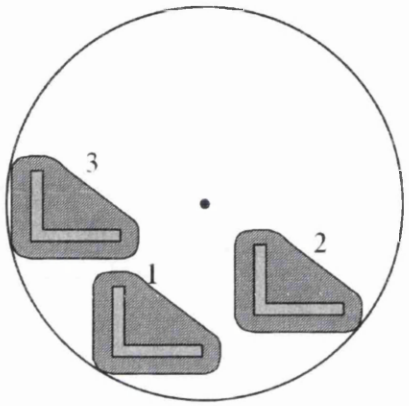

Figure 6.25: Die opening location and orientation relative to die plate.

The different location and orientation of the die opening can be linked to the movement of a die opening within the die plate. It can also be described as moving a die plate around the die opening and keeping it enclosed. For three possible die opening locations and orientations that are marked as 1, 2 and 3 in Figure 6.25, the die centre positions relative to the corresponding die opening are shown in Figure 6.26. For the first position, the left-bottom corner of the clearance zone touches the die plate. The contact point and die centre are indicated as P_1 and O_1 in Figure 6.26. Please note that the vector n_1 which starts from P_1 and ends at O_1 is a radius of the circle (die plate) and it is perpendicular to the curvilinear boundary line of clearance zone at point P_1. Relative positions of the die centre for the second and third cases are also shown in this figure. This property induces the following algorithm which can give the valid design space. In Figure 6.27 , the most inner white 'L' shape area indicates the die opening. The grey area is the simplified convex-hull as the clearance zone of the profile as mentioned before. For all points on the boundary of the clearance zone (such as $P_1, P_2, \cdots, P_{13}$ in

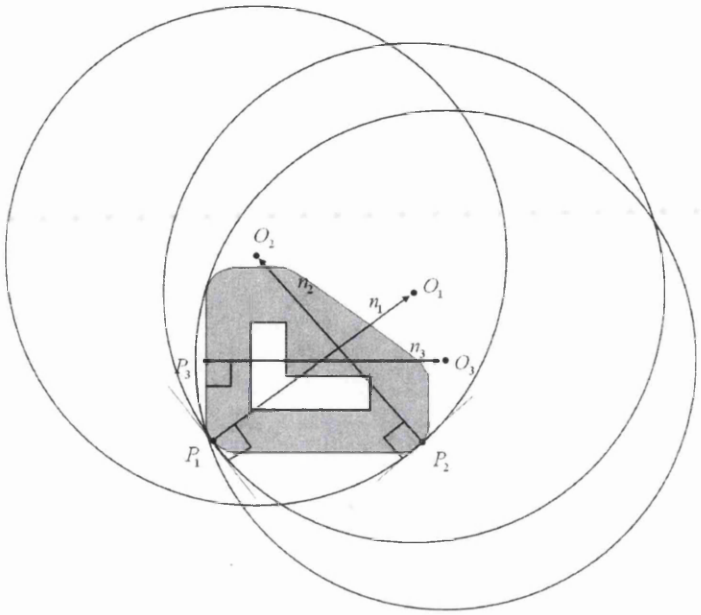

Figure 6.26: Die plate position in relation to location and orientation of die opening.

the figure), a corresponding vector with the same length as the die radius is put on the point. The direction of the vector is perpendicular to the tangent line at that point and it points to the 'inner' part of the profile. The end of the vector gives a a relative position of the die centre ($O_1, O_2, \cdots, O_{13}$ in Figure 6.27). The locus of those vector ends defines a closed curvilinear boundary as indicated by the dashed line in the figure. The curve interlaces at some position such as the cross-point between n_2 and n_3. Each segment of the curve means the die plate touches a segment on the clearance zone boundary. It is clear that if the clearance between the container wall and the die opening is maintained, none of the die opening segments would be located in the clearance zone. This indicates that for the interlace part of the valid design zone boundary, the most inner curve should be chosen as the final result. For example, v_1 is the cross point of curve n_1, n_2 and n_3, n_4. If the die center is located at the outside of curve n_1, v_1, n_2, some part of the extrusion die container must cross boundary P_1, P_2. This means that the proper clearance zone can not be obtained in the area close to the left-bottom corner of the profile. Similarly, if the die center is located at the outsize of curve n_3, v_1, n_4, the distance between the profile right-bottom corner and container wall is less than the requirement. So, curve $n_1, v1$ and v_1, n_4 should be the right boundary of the valid design zone. The final boundary of

valid design space is obtained by removing the overlapping parts of the original results (Figure 6.28).

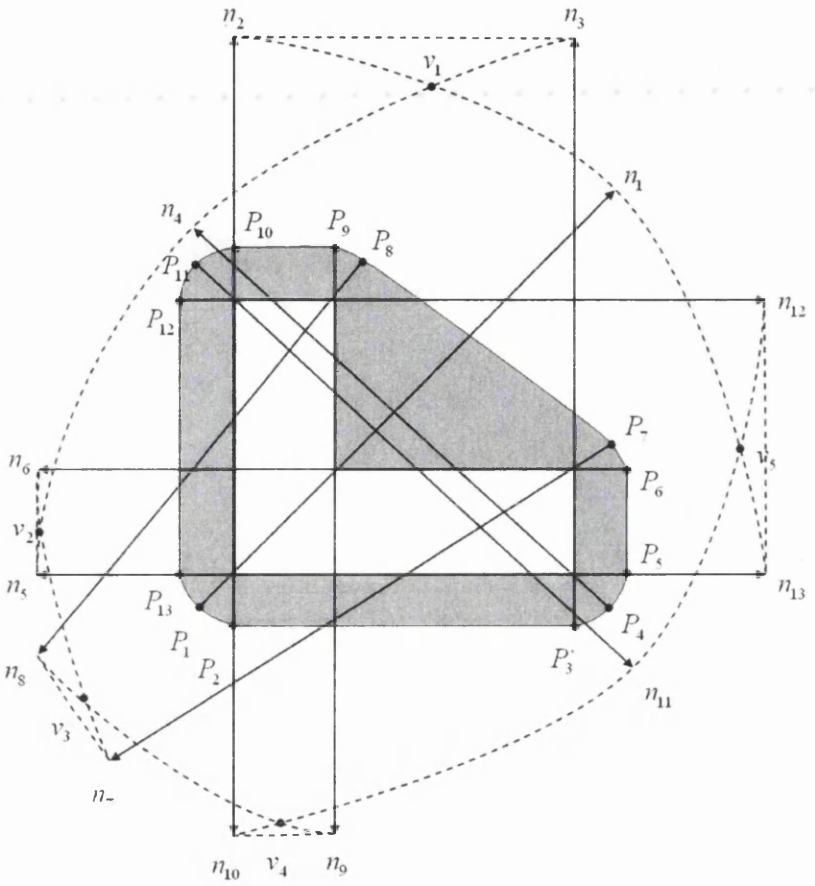

Figure 6.27: Valid design zone calculation.

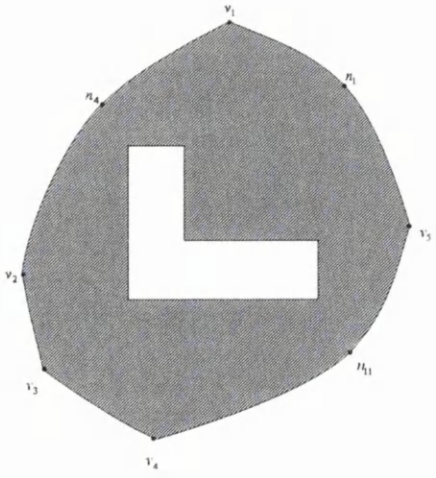

Figure 6.28: Valid design zone for L-shape die opening profile.

The final step for a single-hole die layout design is to find the optimal position for the die centre. Since the design objective is to achieve a minimum bearing length difference, this step is implemented by combining BLD distribution along the valid design space. For example, by using the combination of BLD distribution result of the 'L' shape die opening (Figure 6.6) on its valid design space (Figure 6.28), the BLD distribution for all possible layout design was calculated and is shown in Figure 6.29(a). Based on this, the optimal position for the die centre is found and is marked as point O in Figure 6.29(a). Its corresponding layout design is shown in Figure 6.29(b).

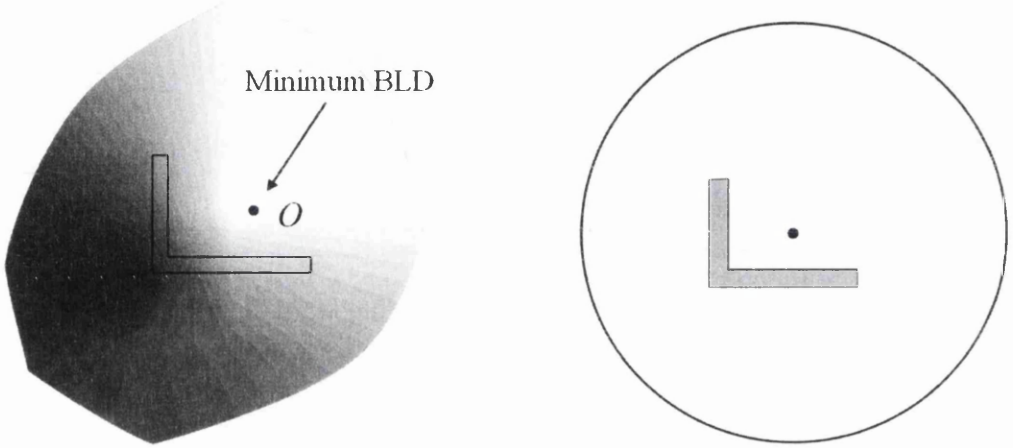

(a) BLD distribution in valid design zone

(b) Optimal layout design

Figure 6.29: BLD distribution in the valid design zone of a 'L' shape die opening profile and its optimal layout design

6.6 Multi-hole Die Layout Design

A single-hole die layout design has only one constraint, that is the clearance between the die opening and the container wall. A single-hole die must keep the clearance between the die opening and the container wall. The multi-hole die layout design has however, more than one constraint, a few of these are:

- Maintain proper clearance between die openings and container wall
- Maintain proper clearance between openings

- Number of die openings
- Rotation limits that are restricted by layout style (e.g. radial or flat layout)

6.6.1 Design Space for Multi-hole Die Layout Design

The first constraint has already been discussed in the previous section. The second constraint indicates that a proper distance has to be maintained between different die openings [23]. A similar method can be implemented for dealing with the second constraint i.e. the clearance between die openings (also called bridge width). Figure 6.30(a) shows a clearance zone for a 'L' shape die opening and the thickness of the zone is $w/2$. Since the die opening could be of any shape, a concave, but not convex, clearance zone should be used for the layout design. For example, Figure 6.30(b) shows a possible layout for two 'L' shape die openings. The distance between them is w. Another two examples with flat and radial layouts are shown in Figure 6.30(c) and 6.30(d) respectively. It is now clear that if we move the die with its clearance zone during the design process and make sure there are no interlaces between any zones, the proper clearance distance between each die openings can be achieved and maintained.

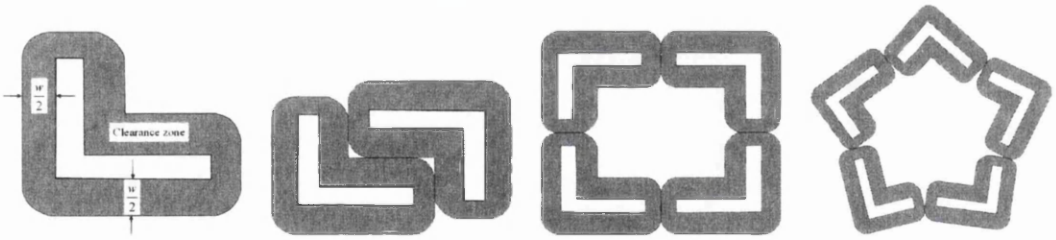

(a) Clearance zone (b) Layout example 1 (c) Layout example 2 (d) Layout example 3

Figure 6.30: Clearance zone for keeping proper gap between die openings.

A Boolean subtraction was applied to combine two clearance restrictions. The valid design zone for a multi-hole die layout design can be obtained by subtracting the clearance zone (bridge width zone) from a valid design zone that was described in the previous section. A valid design zone example for multi-hole die layout is in Figure 6.31 as a hatched region in the most right figure.

Once the valid design space is established, the corresponding BLD distribution is calculated. An example of the 'L' shape is shown in Figure 6.32 (the most right)

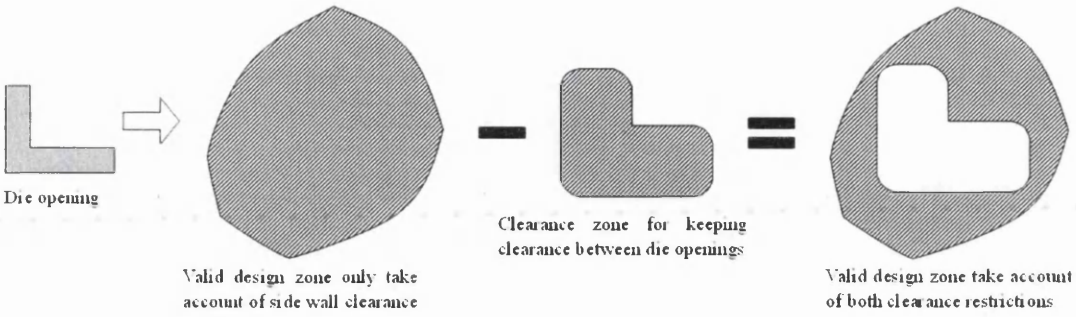

Figure 6.31: Final shape of valid design zone for multi-hole dies.

obtained by using Boolean operation with the valid design space as the mask.

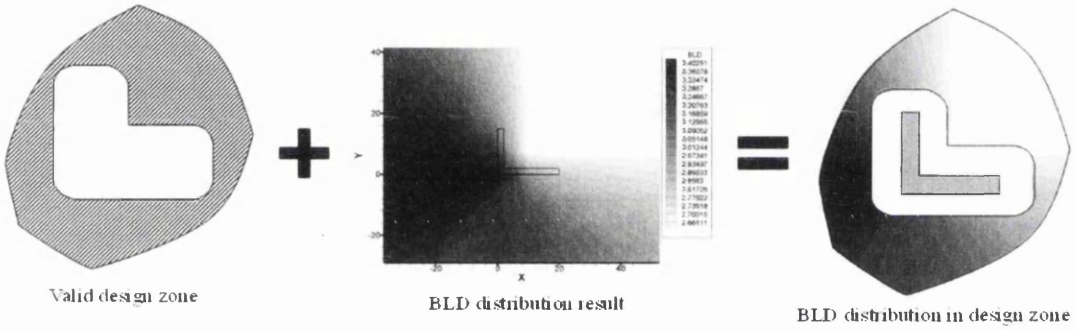

Figure 6.32: BLD distribution in valid design zone of multi-hole dies.

6.6.2 Radial Layout Design

In the case of a radial layout, the major axis of each die openings lies along a radius. All die openings lie around the die centre evenly (Figure 6.2(b)). The final task can now be accomplished in two steps:

1. Finding out the major axis of the die opening
2. Determining how many die openings the die will have and arranging them

The Choice of Major Axis

The following two criteria should to be considered for designing axis selection. First, the major axis should located where a low BLD value can be obtained.

Secondly, the design properties should be stable and easy to manufacture. E.g. for a good layout design, BLD should change slowly and smoothly while moving the die opening along the major axis. Or else the design becomes difficult to understand and correct.

Figure 6.33 illustrates an example for choosing the major axis. As shown in the figure, line 1, 2, and 3 are good choices for the major axes. All these three lines pass through a low BLD area. The variation of BLD values along these lines is acceptably low. By contrast, line 4 and 5 are considered as poor choices. Though the BLD value in the area in which the line 4 passes is not very high, the variation of BLD along the line is large. In the case of line 5, the the BLD variation is comparatively small, but BLD value in that area is very high.

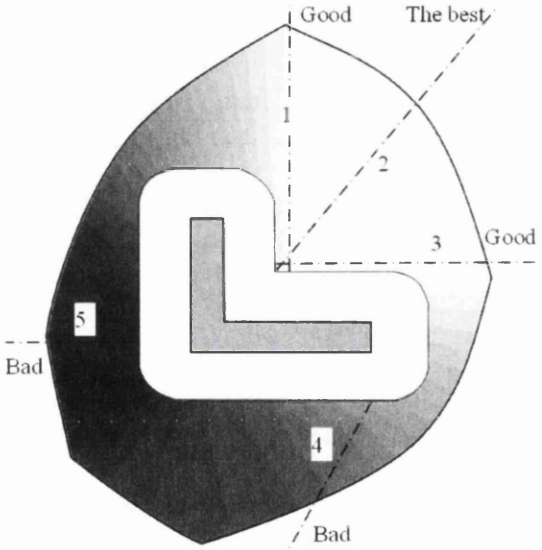

Figure 6.33: Major axis selection for radial layout design.

Radial Distance Selection and the Number of Die Openings

The next task in the multi-hole layout optimization problem is to choose an optimal value for the radial distance. First, a decision is required on the number of die openings that can be in the die plate and second, the best radial distance value must be determined.

Consider a common radial layout for a multi-hole die as shown in Figure 6.34(a). Three die openings were put in a die at equal distances. It is clear that the span

angle (angle α in the figure) of each die opening is $360°/N$, where N is the number of die openings. In most cases, the radial distance of the die openings and the corresponding span angles are not fixed. The possible selection range is shown in Figure 6.34(b). The range is determined by three constraints viz:

- The span angle must be less than the maximum angle given by $360°/N$. Where N is the number of die openings.
- The die centre must be put in the valid design space
- The clearance between openings should be maintained.

The span angle of a die is obtained by selecting a point on the major axis within the design space and from this point, two tangent lines to the boundary of the clearance zone are used. The angle between these two tangent lines is the span angle of the die opening. For example, in Figure 6.34(b), for point P_1, the two tangent lines are l_1 and l_2. Angle α is the span angle. This point lying on the outer boundary of valid design zone (P_1 in the figure) gives the minimum angle. Now move P_1 from the outer boundary toward the inner boundary and P_2 is obtained where the span angle equal to $360°/N$(Figure 6.34(b)). All the positions between P_1 and P_2 are within the valid design space. The last step is to find a position in this range where the minimum value of BLD can be obtained. (P_1 in this case as shown in Figure 6.34(b))

After calculation, all three design variables are known:

1. The number of die openings (N, which is decided by the designer)
2. The radial distance (distance between the die centre location P_1 and reference point P_0 (Figure 6.34(b)).
3. The die opening rotation angle (angle between major axis and design axis, marked as θ in Figure 6.34(b))

The value of these variables gives the final layout design as shown in Figure 6.34(a).

If the number of die openings is not fixed, this method can also be used to determine the maximum die openings number possible in a radial layout die. As mentioned earlier, the intersection point of the outer design zone boundary and

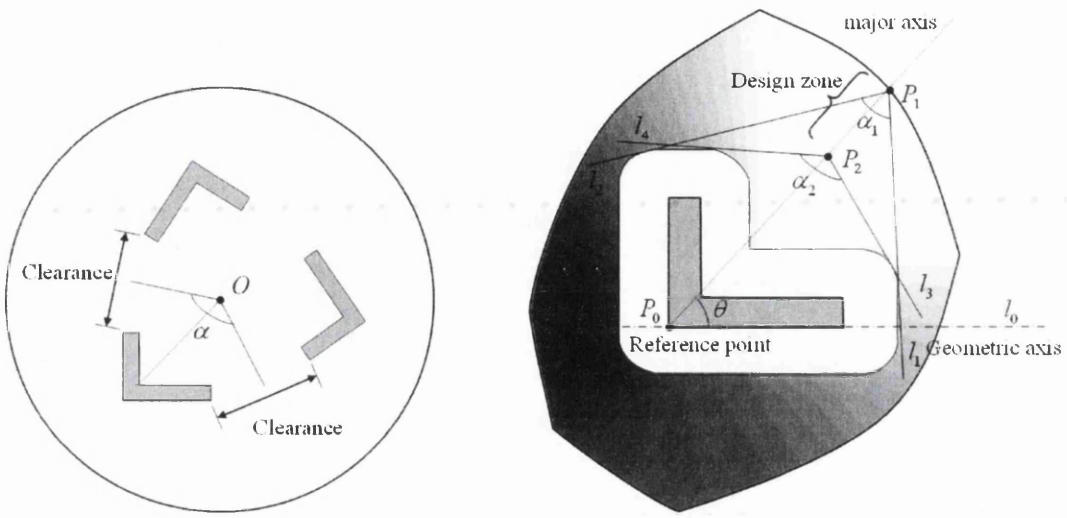

(a) Span angle of die openings (b) Angle selection range and radial distance

Figure 6.34: Radial distance and corresponding span angle.

design axis gives a minimum span angle of the die opening. The maximum die openings number can be calculated as:

$$N_{max} = \left\lfloor \frac{360°}{\alpha_{min}} \right\rfloor \tag{6.2}$$

Flat Layout Design

Compared with a radial layout design, the flat layout has even more constraint. One of the major limiting factors is that the major axes of all die openings should either be parallel or perpendicular to a single die radius. Another limiting factor is whether a symmetric layout is permissible. The first constraint indicates that the rotation angle of the die opening (the angle between design axes and major axis) should either equal 0° or 90°. However, symmetric opportunities such as 180° and 270° are other possible values.

Combining these two constraints, a scan line technique is used to find out the valid design space. This calculation is based on the design space calculation procedure used in the previous section. Figure 6.35(a) shows how to find out the valid design space by using a scan line which is parallel to the major axis. As shown in the figure, the process starts with a line that touches the top-outer boundary of the original design zone (l_{start}). The line continuously scans down until it leaves the bottom of the outer boundary. The lowest position of the scan

line is marked as l_{end} in the figure. When the scan line just touches the inner boundary of the design space the scan line position is marked as l_1. It is marked as l_2 when it leaves the inner boundary of the design space. The region of design zone between l_1 and l_2 is the invalid design space (darken areas in Figure 6.35(a)). The remain parts of design space are valid design spaces (vertical layout). Please note that the inner boundary of the original design space forms the region of the inter-die-openings clearance zone. If the scan line moves vertically, a horizontal layout of the valid design space is obtained (Figure 6.35(b)).

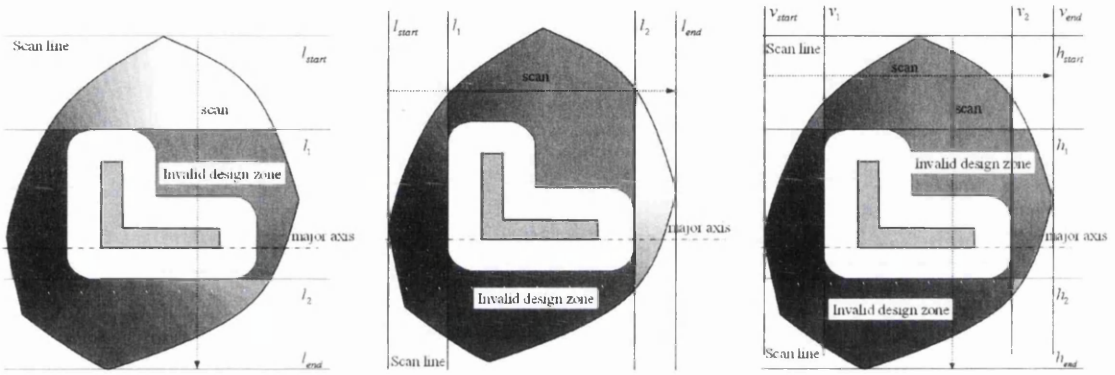

(a) Horizontal scan (b) Vertical scan (c) Horizontal and vertical scan

Figure 6.35: Valid design space and corresponding scan lines for symmetric flat die design.

Once the valid design space is determined, the next task is to determine a reference position of the die center within the design space such that the minimum BLD value is achieved. The task now is to find out a position in the valid design space. It is useful to note here that each design axis is used as a line of symmetry during the design process. If only one direction design axis is used, only two die openings can be placed in the die. In another case, if both horizontal and vertical design axes are used then up to four die openings can be placed in a die.

For example, for a two-hole horizontal layout only a vertical scan line can be used to get the proper valid design zones. The optimal die centre relative to the die openings is the point where the minimum BLD value is achieved within the valid design space. If the optimal position is found, the location and orientation of the other die openings can be easily fixed. A schematic optimal layout design result for a two-hole 'L' shape profile die is shown in Figure 6.36(a).

Similar design algorithm can be used for a two-hole vertical layout or a four-hole flat layout die. Two schematic design examples for 'L' shape die opening profile are shown in Figure 6.36(b) and 6.36(c) respectively.

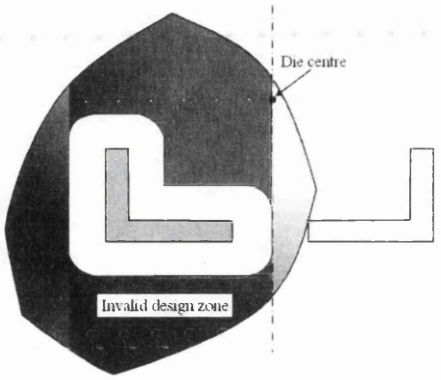

(a) Vertical scan line and horizontal layout design for two-hole die

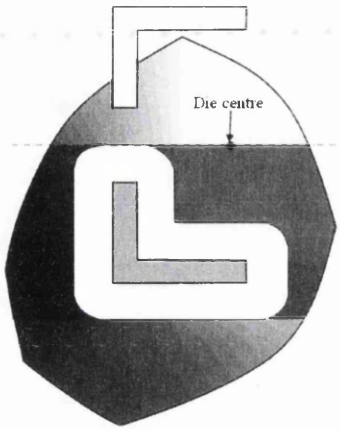

(b) Horizontal scan line and vertical layout design for two-hole die

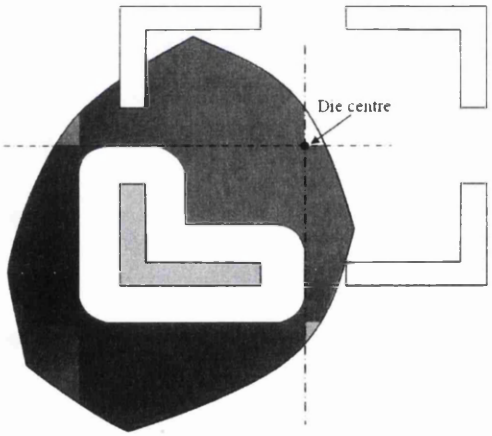

(c) Both horizontal and vertical scan line and corresponding flat layout design for four-hole die

Figure 6.36: Scan lines and corresponding flat die layout design for multi-hole dies.

6.7 The Whole Optimization Process of the Approach

The whole extrusion die layout optimization process is shown in Figure 6.37.

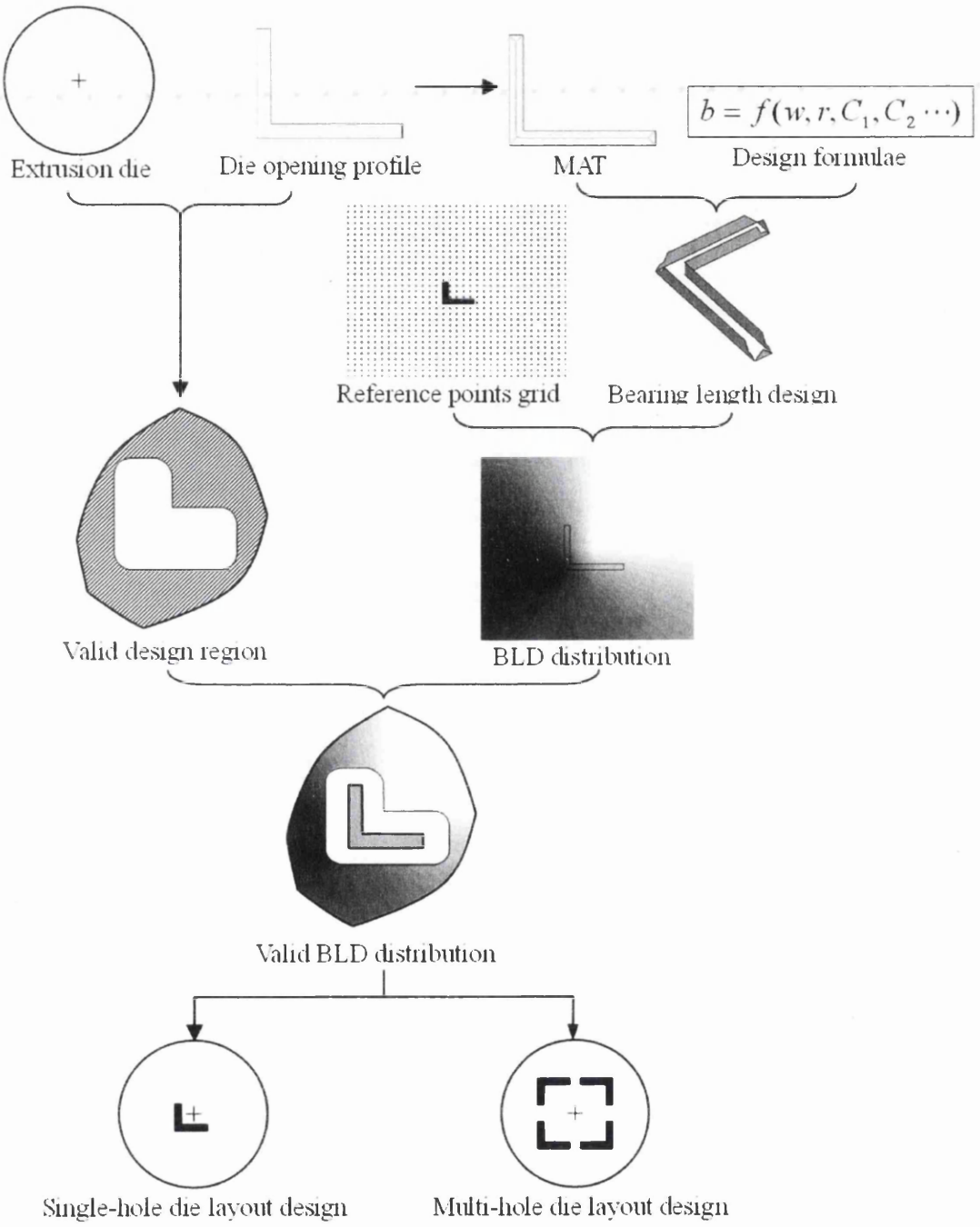

Figure 6.37: Main procedures of proposed approach for extrusion die layout design.

6.8 Validation of the New Approach

6.8.1 Single-hole Die Layout Design

Case Study 1

To test the proposed layout design methodology for single-hole dies, a simple channel-shape profile was used (Figure 6.38(a)). The BLD distribution result is shown in Figure 6.38(b). It is obvious that the centre of the channel is the best candidate location for the extrusion die centre. A schematic optimization result is shown in Figure 6.38(c). This optimization result agrees with one of the well-known layout design rules. The design rule recommend to arrange a die opening such that the die centre coincident to the center of gravity of the die opening profile [23].

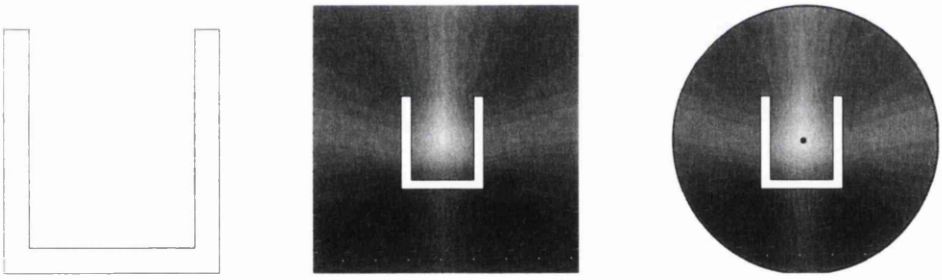

(a) Die opening profile with MAT (b) BLD distribution (c) Layout design

Figure 6.38: Extrusion die layout design (case study 1)

Case Study 2

A general polygon shape die opening profile mentioned by Lotzenhiser is chosen [26] to test the proposed methodology. Figure 6.39(a) shows the profile shape and its medial axis transform result. Figure 6.39(b) shows the BLD distribution result of the profile. It is obvious that the best position is very close to the thinnest part of the profile. This result compares favourably with the common practice for the single-hole die design rule of a single-hole die where the designer put the thinnest part of the die opening at the centre of the die. A designer's design of

the die is shown in Figure 6.40(a) [23, 26]. The corresponding optimization result done by the new approach is shown in Figure 6.40(b). The optimization result agrees well with the preferred designer's design.

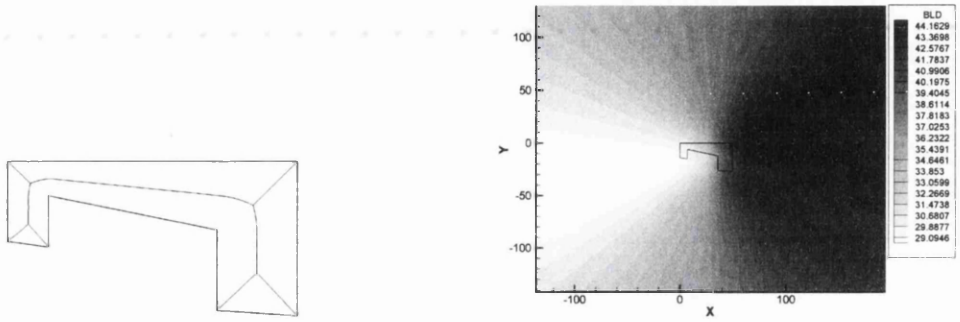

(a) Die opening profile with MAT (b) BLD distribution

Figure 6.39: Extrusion die layout design (case study 2)

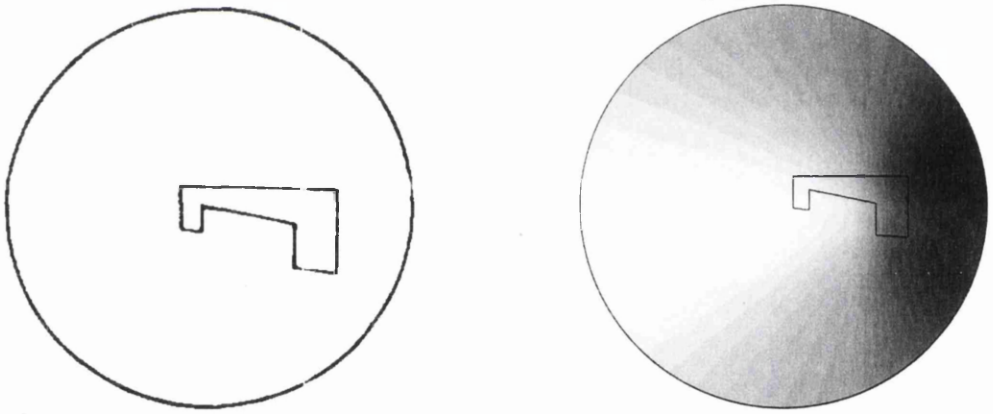

(a) Die layout design by die designer (b) Optimization result of die layout design

Figure 6.40: Extrusion die layout design (case study 2)

6.8.2 Radial Layout Design of Multi-hole Dies

Case Study 3

A radial layout has been validated in this example. A 'T' shape profile is chosen (Figure 6.41(a)). The BLD distribution and the details of central part of BLD distribution are shown in Figure 6.41(b) and 6.41(c) respectively.

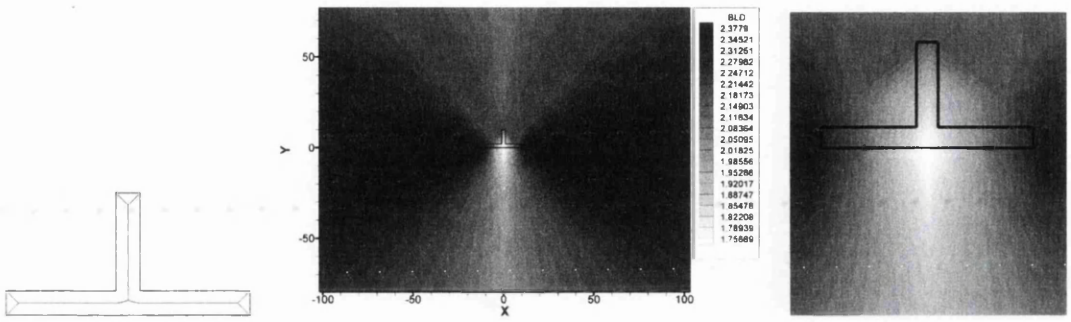

(a) Die opening profile with MAT

(b) BLD distribution

(c) Details of BLD distribution

Figure 6.41: Extrusion die layout design (case study 3)

The layout optimization results for 2-hole, 4-hole, 5-hole and 6-hole dies are shown in Figure 6.42, 6.43, 6.44 and 6.45 respectively.

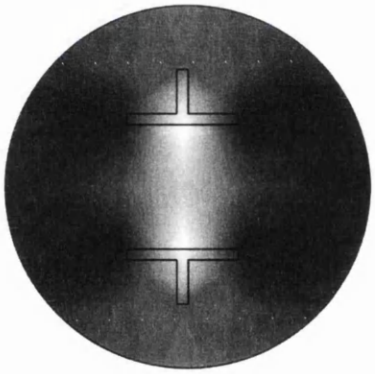

Figure 6.42: 2-hole die layout design

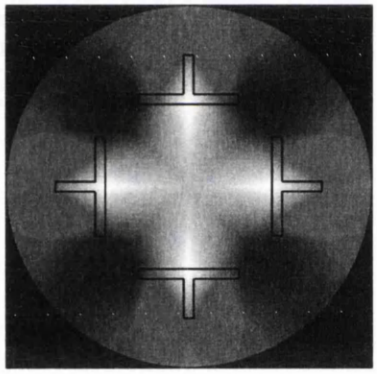

Figure 6.43: 4-hole die layout design

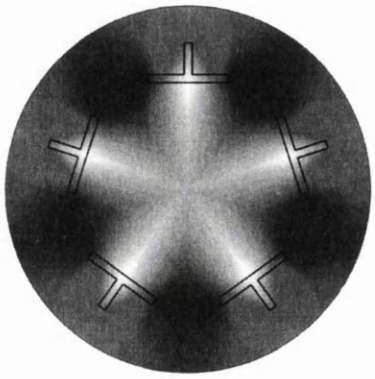

Figure 6.44: 5-hole die layout design

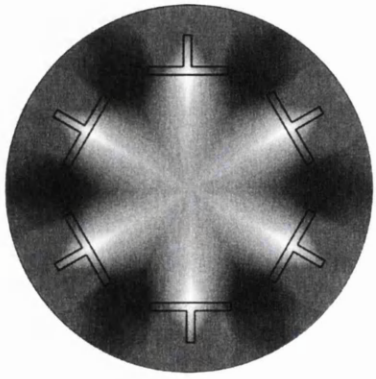

Figure 6.45: 6-hole die layout design

6.8.3 Flat Layout Design of Multi-hole Dies

Case Study 4

A 'L' shaped die profile is used in this example to validate the proposed methodology on the multi-hole flat layout designs (Figure 6.46(a)). Figure 6.46(b) shows BLD distribution of the profile. Figure 6.47(a) illustrates suggested good design for 4-hole dies [13, 23]. Design results given by the approach is put in Figure 6.47(b). The figures illustrates that the results compare well with layout design rules.

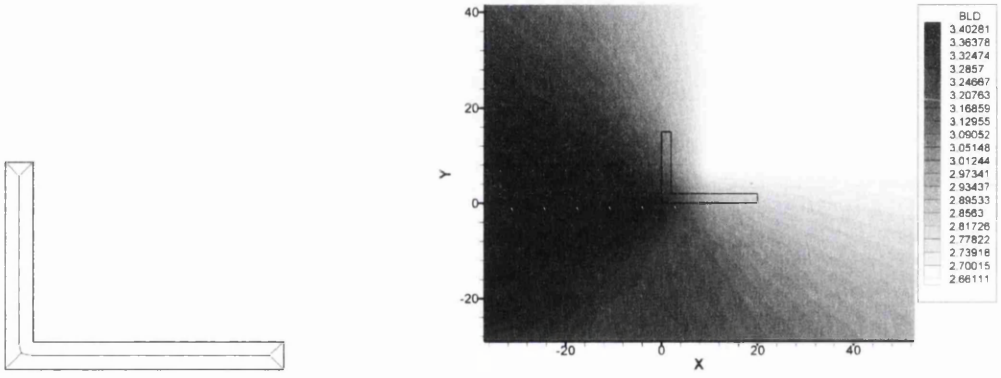

(a) 'L' shape profile with MAT (b) BLD distribution

Figure 6.46: Extrusion die layout design (case study 4)

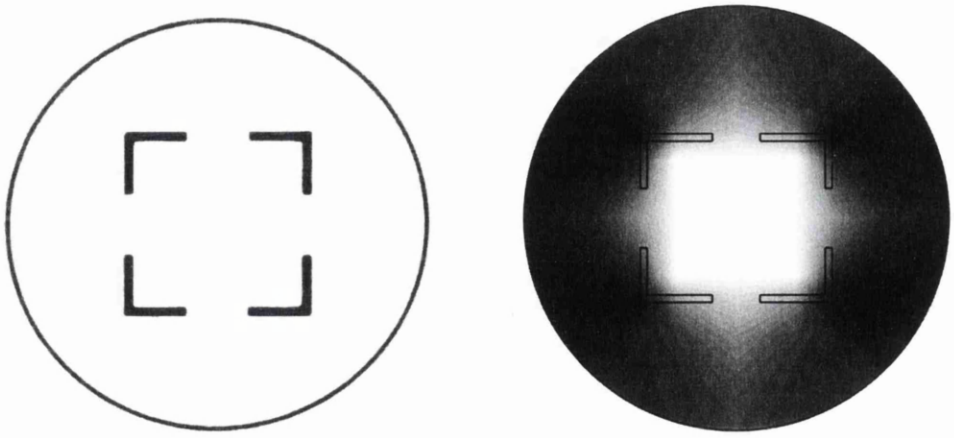

(a) 'L' shape profile with MAT (b) BLD distribution

Figure 6.47: Extrusion die layout design (case study 4)

6.9 Conclusion

As one of the most important design issues, extrusion die layout design is very important for the industry. A novel approach was studied and illustrated in this chapter. By using a medial axis transform (MAT) and empirical bearing length design formulae, this new approach can quantify the extrusion die layout design quality quickly and efficiently. It not only estimates the design quality of any die opening profile but also gives the optimal layout for both single-hole and multi-hole dies.

Since the optimization algorithms used by the approach is quite flexible and only geometrical information and bearing length designs of profiles are needed, the whole optimization process can be used based on other bearing length design approaches rather than empirical design formulae. Though the objective function of the process is quite simple, it does fit layout guiding rules pretty well.

Due to the disadvantage of the empirical bearing length design formulae, this approach lacks the capability for getting high-accurate multi-hole die layout designs. But it does show a reasonable way which leads to the right answer. By using better bearing length prediction algorithms and geometry reasoning technique (in the next chapter), more details about extrusion die layout designs can be included and better results should be given.

Chapter 7

Geometry Reasoning using Medial Axis Transform

Chapter Layout

Geometric information and shape features are important for extrusion die design work. Therefore, several geometry reasoning algorithms using MAT have been studied. This chapter shows these algorithms in each section.

The first section of this chapter describes formats used for geometric definitions and illustrate the way geometry information is stored in MAT. The second section discusses the classification of MAT vertices and edges into different categories. The following sections introduce geometry reasoning algorithms using MAT one by one. Section three talks about branch searching algorithm. The fourth section illustrates how to use topology shape of MAT to determine whether a geometry model has a hole and how to calculate the number of holes in the geometry. The next section introduces a new algorithm which can be used to separate tips and rough-boundary sections from normal sections. Section six introduces local aspect ratio which comes from typical aspect ratio and how to use it to find out critical sections of a shape. The seventh section shows several shape factors and algorithms which can be used to evaluate the complexity of geometry shapes.

7.1 Introduction

A lot of extrusion die design works, such as die classification and bearing length calculation, are based on geometric information results. For such reason, a set of geometry reasoning algorithms have been studied. The properties of these algorithms will be discussed in each section individually and the application of these algorithms for extrusion die design will be introduced in the next chapter.

7.2 Primary Geometrical Information and MAT

7.2.1 Regional Width and Length of Geometry Models

Geometry Definition Formats

Before a geometry can be analyzed or manipulated, a proper definition approach has to be given. There are two basic ways to define a geometry object – vector based or pixel based. The pixel based storage approach uses pixels to mark the boundary or inner area of the geometry and normally stores the object as an image. On the other hand, a vector based geometry definition is close to a mathematical approach. It defines a set of subordinate objects by which the geometry could be described as the definition of geometry. These subordinate objects could be points, lines, arcs, curves and surfaces etc. Most computer aided design (CAD) software use the second approach to define and store geometry models in some specific file format, such as IGES, STL and so on.

Let's assume an example where a rectangle needs to be defined. The size of the rectangle is $w = 2$ and $h = 1$ with its left-bottom corner located at $(0, 0)$. Using the pixel based approach, a resolution has to be fixed before following steps can be implemented. Say 1 pixel equals 0.2 unit length. It is obvious that the definition need $\frac{1}{0.2} \times \frac{2}{0.2} = 5 \times 10 = 50$ pixels. A schematic figure is shown in Figure 7.1(a). If all the black pixels (boundary pixels) are marked as number '1' and all white pixels as '0', the image can be save in a data file which might take the format as shown in Figure 7.1(b).

Figure 7.2 shows a vector based definition for the same rectangle. The figure

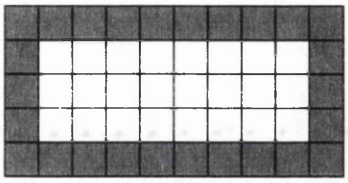

1,	1,	1,	1,	1,	1,	1,	1,	1,	1
1,	0,	0,	0,	0,	0,	0,	0,	0,	1
1,	0,	0,	0,	0,	0,	0,	0,	0,	1
1,	0,	0,	0,	0,	0,	0,	0,	0,	1
1,	1,	1,	1,	1,	1,	1,	1,	1,	1

(a) Pixel based geometry definition (b) Possible definition format of the geometry

Figure 7.1: Pixel based geometry definition format

shows that four points (p_1,p_2,p_3,p_4) and four lines (l_1,l_2,l_3,l_4,) are needed. A possible definition format for the geometry is shown in Figure 7.2(b).

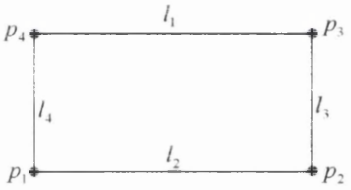

P1:	(0,0)
P2:	(2,0)
P3:	(2,1)
P4:	(0,1)
L1:	P3,P4
L2:	P1,P2
L3:	P2,P3
L4:	P4,P1

(a) Vector based geometry definition (b) Possible definition format of the geometry

Figure 7.2: Pixel based geometry definition format

Acquiring Size Information using MAT

The basic geometrical information needs to be obtained for any geometry defined for implementing any approach based on geometric reasoning. For two-dimensional geometry objects, the basic geometrical information includes width, height, location, rotation, section width and length etc. It is easy to find out all this information by using the original geometry definition. For example, the original definition does not contain any information about the width of the geometry, therefore, to obtain the width information, several searching and calculating processes are needed. One possible algorithm is to find out the points with minimum and maximum abscissa (p_1 and p_2 in this case) first. Then calculate the distance between these two points by $d = \sqrt{(x_2 - x_1)^2 + (y_2 - y_1)^2}$. It is clear that the

whole process is not so simple for some information, such as section local width. It is extremely difficult, or nearly impossible, to get the right answer by using the original definition.

Medial Axis Transform (MAT) is a very good substitute to achieve the above mentioned objective. For a rectangular shape object as shown in Figure 7.3(a), the medial axis transform result has 5 line segments and 6 vertices as shown in Figure 7.3(b). The medial axes indicates the main frame of the object and the radius function contains the local width information. It is thus clear that all the basic geometrical information can be obtained using MAT.

For example, geometry section width at point p is:

$$w_p = R(p) \tag{7.1}$$

where w_p is the regional section width at point p, R is the radius functions of the medial axes.

The length of the main medial axes roughly gives the length of the geometry. For this rectangular geometry, axis p_2p_3 is the main medial axis and it gives the approximate length of the geometry. That is:

$$L_s = L_{mainMAT} \tag{7.2}$$

where L_s is the length of section s and $L_{mainMAT}$ is the length of main medial axis of the section.

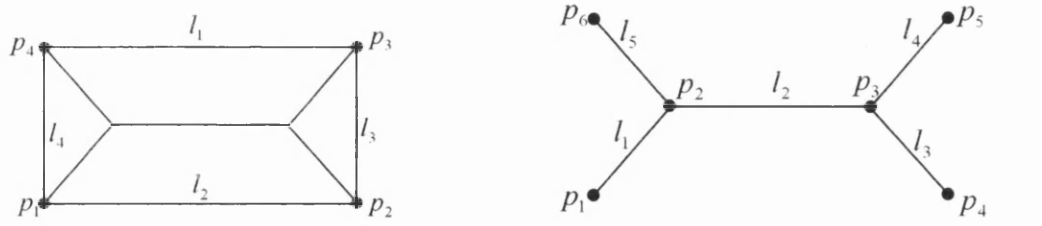

(a) Vector based geometry definition

(b) Possible definition format of the geometry

Figure 7.3: Rectangular shape and its medial axis transform

7.2.2 MAT Result and Corresponding Shape

It is proposed that the MAT can be considered as a type of geometry definition format. It contains the full geometrical information of a model. A MAT can

be used to re-construct the original geometry. For some application, this feature is extremely useful. For example, Donaghy *et al.* [9] show how to reduce the dimension of geometry models by using MAT. Amenta *et al.* [61] demonstrated a power crust construction approach based on MAT.

Since MAT is another representation format for geometries, a lot of classical geometry reasoning algorithms can be implemented using MAT directly. While some others can be implemented with a few simple modifications. For instance, Pao *et al.* [67, 68] demonstrated how MAT helps hot-spot prediction for the casting industry by coupling interpolation methods with FE simulation. Ruberto's [64] research work shows a shape recognition approach using medial axis transform. Li *et al.* [8] illustrated geometry auto-partitioning algorithms using MAT.

MAT results not only provide a more efficient and powerful tool to implement the existing algorithms but also leads to some new algorithms which can not be implemented using normal geometry definition methods.

7.3 MAT Vertices and Edges Classification

7.3.1 Geometry Models and Corresponding MAT Results

As discussed, a medial axis transform represents the skeleton of the original geometry object. It describes the main frame and the basic shape of the geometry even without radius functions. Figure 7.4(a) shows an 'L' shape geometry model. The corresponding medial axis transform result is shown in 7.4(b).

It is clear that the MAT result contains 9 segments and 10 vertices (crucial points) which are marked as $l_1, \cdots, l_9$ and $p_1, \cdots, p_{10}$ in Figure 7.5(a) respectively. For each vertex point, the number of connected medial axis segments is defined as the connection factor, or degree of connection, following Graph theory. In the following paragraphs, the concept of the degree of vertices is also used. For example, there is only one line segment, l_1, that connects with vertex P_1. So the degree of p_1 is 1. And for point p_2, it is clear that there are three segments (l_1, l_2 and l_3) connected with it. So, the degree of point p_2 is 3. The degrees for all individual MAT segments vertices are shown in Figure 7.5(b).

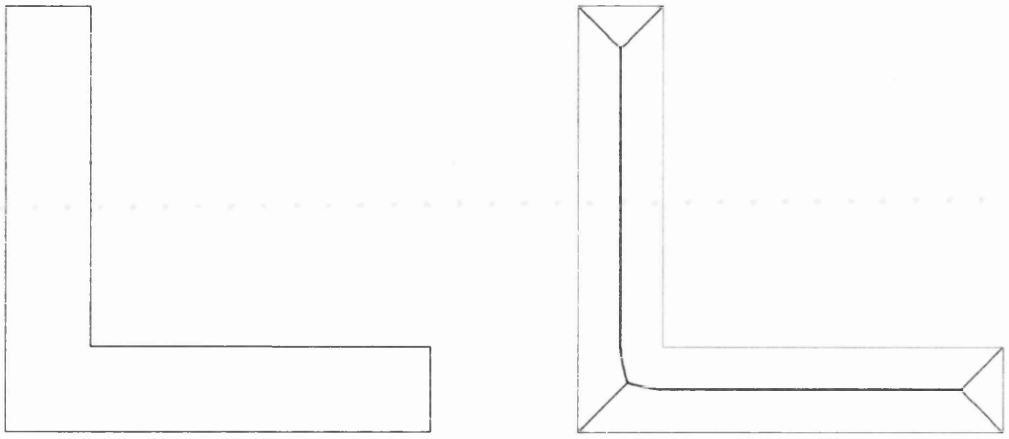

(a) 'L' shape geometry model (b) MAT result

Figure 7.4: 'L' shape geometry and its corresponding MAT result

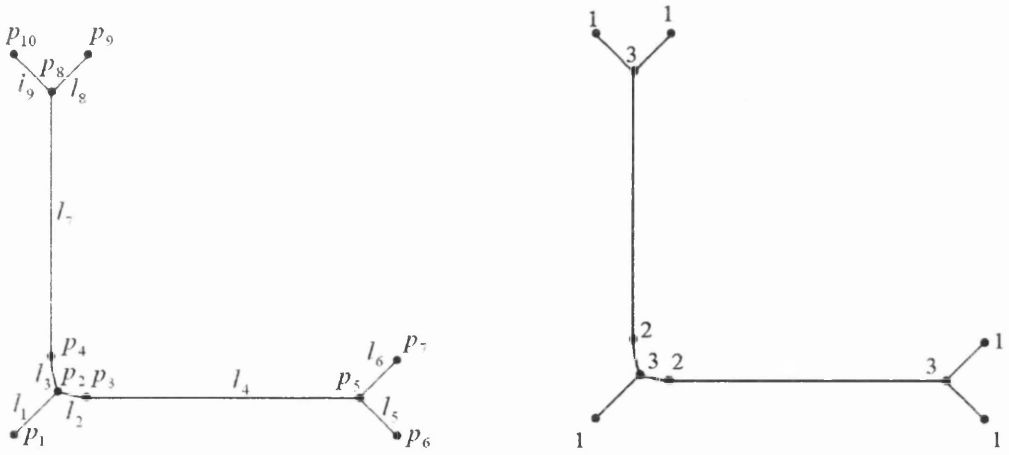

(a) 'L' shape geometry model (b) MAT result

Figure 7.5: 'L' shape geometry and its corresponding MAT result

According to the degree of connectivity for all possible cases, MAT vertices can be classified into 3 groups (Figure 7.6). In the first case, only one segment is connected with the vertex, that is the degree of connectivity equaling 1. This indicates that the vertex is an end point of a branch (Figure 7.6(a)). The second case shows two connected segments. It is normally caused by the discontinuity of boundary definition. In this case, either the boundary shape changed and a corner is built at the position, or the section width changed.(Figure 7.6(b)). The last case groups all vertices with the degree number more than 2. These types of vertices imply a junction of several sections of the geometry. Therefore, the degree of connectivity represents the number of connected sections. (Figure 7.6(c)

and Figure 7.6(d))

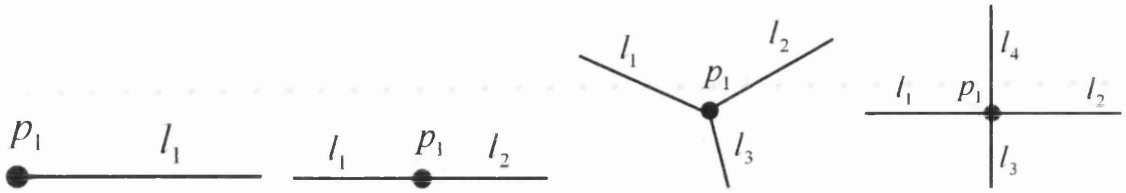

(a) $n = 1$ (b) $n = 2$ (c) $n = 3$ (> 2) (d) $n = 4$ (> 2)

Figure 7.6: Classification of MAT vertices based on degree of connectivity

Table 7.1: The classification of vertex

Types	Connectivity degree of vertex
1	$n = 1$
2	$n = 2$
3	$n > 2$

According to this classification of vertices, a MAT segment can be classified into six types. If the start point is marked as p_1 and the end point as p_2, and their degrees are n_1 and n_2 respectively, then the possible types are:

Table 7.2: The classification of edges

Types	Vertices connectivity degree of the edge
1	$n_1 = 1$ and $n_2 = 1$
2	$n_1 = 1$ and $n_2 = 2$
3	$n_1 = 1$ and $n_2 > 2$ or $n_1 > 2$ and $n_2 = 1$
4	$n_1 = 2$ and $n_2 = 2$
5	$n_1 = 2$ and $n_2 > 2$ or $n_1 > 2$ and $n_2 = 2$
6	$n_1 > 2$ and $n_2 > 2$

Figure 7.7 shows all six classification types for medial axis segments individually.

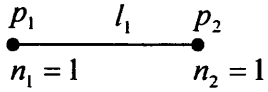

(a) Segment type 1

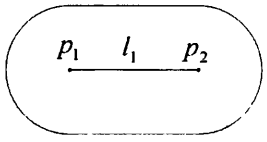

(b) Type 1 example

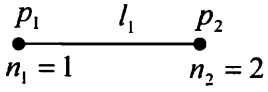

(c) Segment type 2

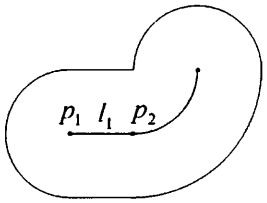

(d) Type 2 example

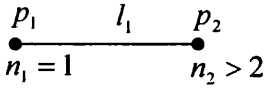

(e) Segment type 3

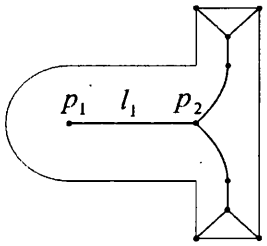

(f) Type 3 example

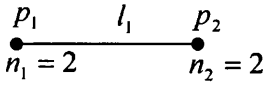

(g) Segment type 4

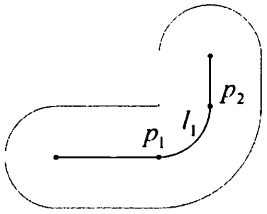

(h) Type 4 example

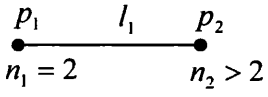

(i) Segment type 5

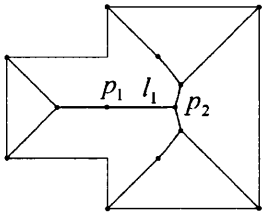

(j) Type 5 example

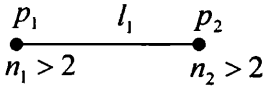

(k) Segment type 6

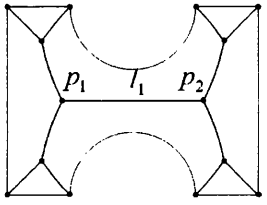

(l) Type 6 example

Figure 7.7: MAT segment classification examples

7.4 Geometry Auto-partitioning and Branch Searching

7.4.1 Branch Trimming and Main Medial Axes

For most geometry reasoning analyses, the main frame of a MAT result provides an interesting and promising option. A proper pre-process which can remove minor branches is quite essential for the analysis. In other words, an algorithm is needed to get the main medial axes. The following paragraphs introduce an algorithm where less-important tip branches can be removed from the main body of MAT which then is used for the analysis.

Due to the definition and construction properties, any sharp corner on the geometry boundary leads to a small branch with which one of the vertices touches the boundary. Some geometries have many blunt corners which are normally defined as a quarter of arc. This kind of round corner also generate a dangling segment in MAT result. It is clear that one of the vertices of these segments has 1 connectivity degree and non-zero radius. Therefore for any medial axes, if one of the vertex degree equals 1 and radius equals 0, it is tip branch of MAT. If the degree is 1 but the radius is non-zero, a radius limit can be given so that all segments with radii less than the prescribed limit would be deleted.

For example, Figure 7.8(a) and 7.8(b) show a 'T'-shape geometry and its medial axis transform. The degrees of connectivity of all MAT vertices are marked in the figure as well. The result shows that 6 vertices in the result have degree 1 and 0 radii (Marked as $p_1, p_2, \cdots, p_6$ in the figures). The main medial axes is shown in Figure 7.8(c).

Therefore, all tip branches can be removed from MAT results by the algorithm automatically and main medial axes are remained.

7.4.2 Branches Number Counting

For any given geometry, the number of branches and size of each branch are important geometric information. Main medial axes and junction points are used to get this information. In most case, any sharp tips or rectangular ends produce

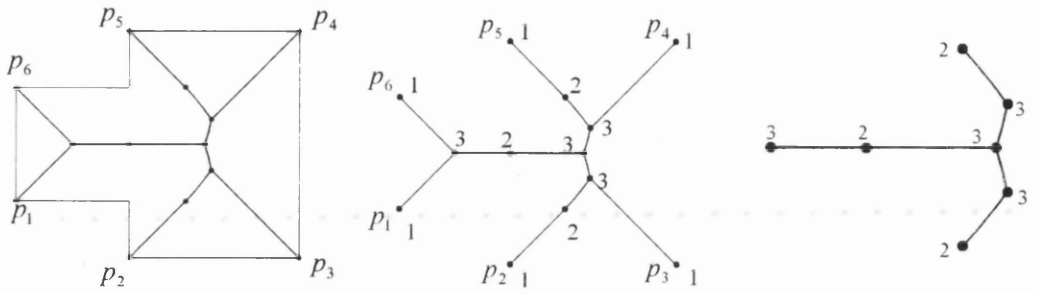

(a) The geometry (b) MAT result (c) Main medial axes

Figure 7.8: Medial axis transform and main medial axes

tip segments in MAT result as mentioned before. To get the correct branch number, the main medial axes result is used and the degree of connectivities on the main medial axes have to be re-calculated before the counting process take place.

Figure 7.9(a) shows the original connectivity degrees of the each vertices of the main medial axes. Using the same calculation rules, new degrees are re-calculated according to the new connection relationship using only the main medial axes (Figure 7.9(b)). As concluded earlier that vertex with degree greater than 2 (point p in the figure) indicates a junction point in the original geometry. If the main MAT is plotted into several sub-graph based on these junction points such as shown in Figure 7.9(c), the number of sub-graph is the number of geometry segments. In the example, the result shows that the original geometry has one junction point (p) and three segments (marked as S_1, S_2 and S_3 in the figure).

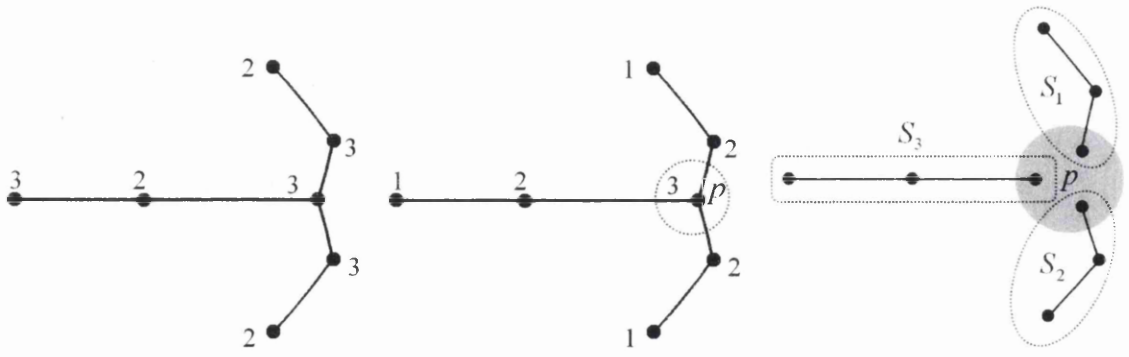

(a) The main medial axes and original degree of connectivities (b) New degree of connectivities (c) Junction vertex and geometry segments

Figure 7.9: Medial axis transform and main medial axes

It is clear that by partitioning the main medial axes at junction points, the number of medial axes' sections can be counted. So that the number of shape segments is also known.

7.4.3 Segments and Branches

Figure 7.10 and 7.11 illustrate another case of branch counting. An 'H' shape geometry model is used in this case (Figure 7.10(a)). The MAT result and connectivity degrees of all vertices are listed in Figure 7.10(b). The main medial axes and re-calculated degrees are shown in Figure 7.11(a). The result shows two junction points (p_1 and p_2 in the figure). It is trivial that five sub-graphs can be obtained if the original graph is split at these two points (marked as S_1, S_2, S_3, S_4 and S_5 in Figure 7.11(b)).

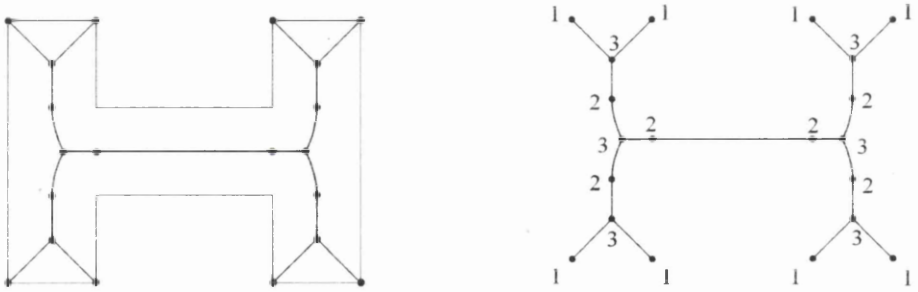

(a) 'H' shape geometry (b) MAT result and connectivity degrees

Figure 7.10: 'H' shape geometry and its MAT

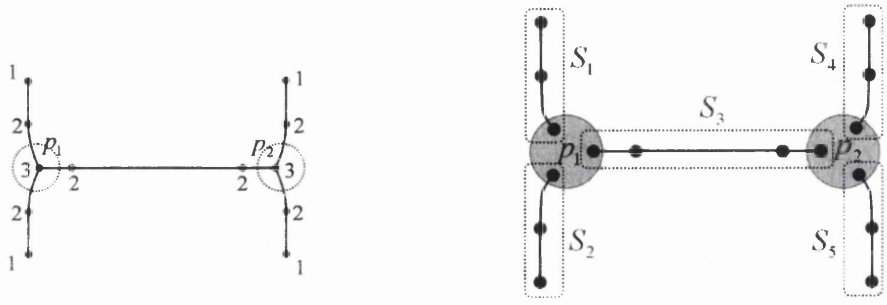

(a) Main medial axes and junction points (b) Internal and end segments

Figure 7.11: Branches and normal section classification for 'H' shape geometry

The counting result also shows that there are two kinds of segments. According

to the result of the MAT edge classification, the first segment type is $n_1 > 2$ and $n_2 > 2$. That is the edge type 6 (Table 7.2). For example, degree of one end vertex of segment S_1 is 1. And the others is 3. So, segment S_1 is an edge type 3 ($n_1 = 1$ and $n_2 > 2$). But for segment S_3, the connectivity degrees are 3 for both end vertices. So, segment S_3 is type 6 ($n_1 > 2$ and $n_2 > 2$). This indicates that segment S_1 is an end-section, or call it a branch and S_3 is a internal segment, or just call it a segment.

Therefore, segments can be classified into two groups, branches and segments (Table 7.3).

Table 7.3: The classification of MAT segments

Type	Geometry feature	Properties
1	Normal section	$n_1 > 2$ and $n_2 > 2$
2	Branches (legs)	$n_1 = 1, n_2 \geq 2$ or $n_1 \geq 2, n_2 = 1$

7.4.4 Flow Chart of the Algorithm

This sections shows that by trimming tip segments of MAT and by using auto-partitioning algorithm for main medial axes, the number of branching segments and inner segments of a shape can be counted. The whole algorithm for branch counting is shown in Figure 7.12

7.5 Hole Recognition using MAT

7.5.1 MAT and Corresponding Graph

A great many problems, such as geometry reasoning algorithms, are naturally focused on the relationship between different objects. For this purpose, a two-dimensional MAT result can be handled as a two-dimensional connected graph. For instance, Figure 7.13(a) shows an arbitrary geometry shape. It's MAT result is shown in Figure 7.13(b). If the medial axis vertices are changed into nodes and axes into edges, MAT results can be converted into a two-dimensional connected

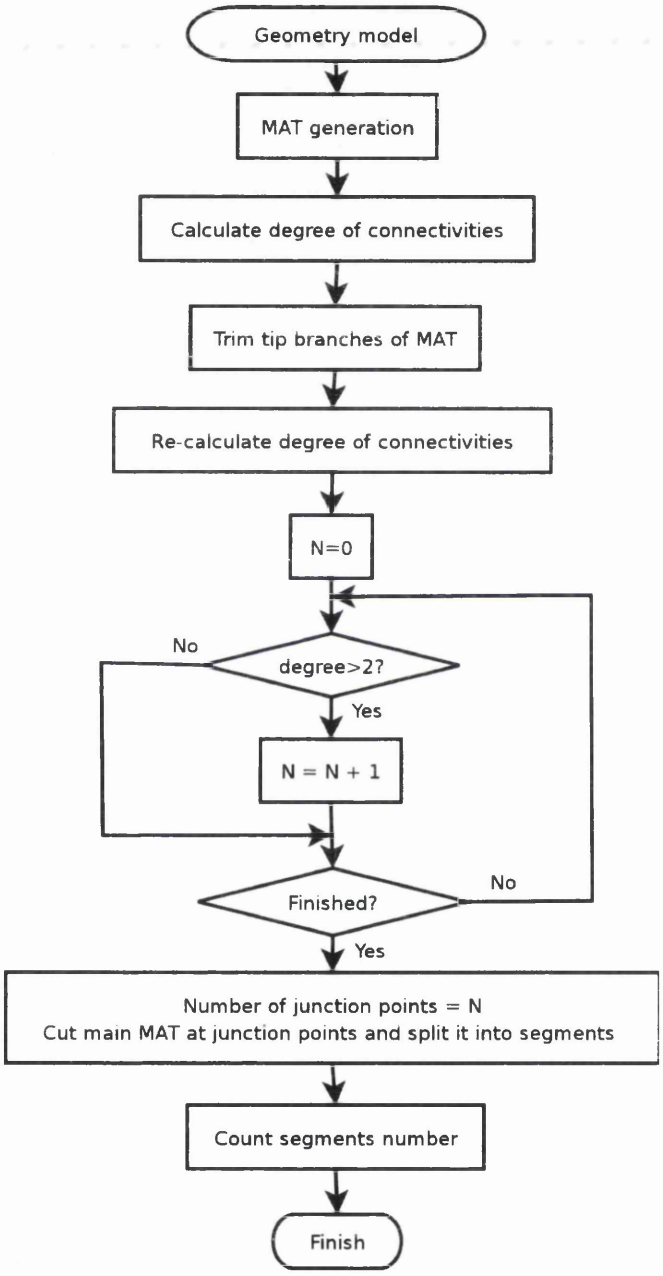

Figure 7.12: The procedures of branch searching algorithm

graph. A corresponding graph to the geometry is shown in Figure 7.13(c). By comparing figure 7.13(c) with 7.13(a) and 7.13(b), it is clear that for topological shape analysis, to handle a graph is much easier than handling a MAT result or the geometry itself.

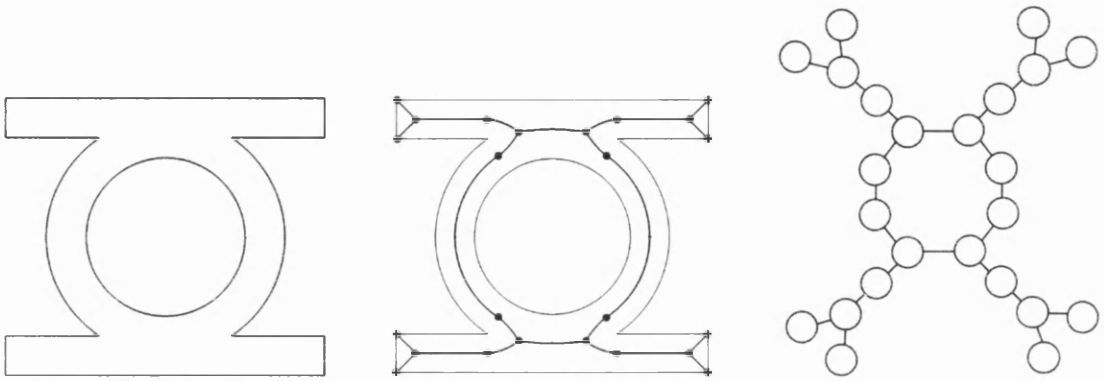

(a) Geometry model (b) MAT (c) Corresponding graph

Figure 7.13: Medial axis transform result and corresponding graph

7.5.2 Graph Simplification

For a graph, the topological shape and connection relationship are two of the most important aspects apart from the details of each vertices or edges. Therefore, a graph of a MAT result should be simplified before further analysis can take place.

According to the classification of edges, edge of type 4 has two (Table 7.2) type-2 vertices. A type-2 vertex has two connected edges ($n = 2$ as mentioned in Table 7.1). Therefore, both type-4 edges and type-2 vertices are an internal structure of a graph. Their existence would not influence the topological shape of a graph and thus, a graph can be simplified by removing all of type-4 edges and type-2 vertices. It is clear that important information, such as junctions and sections is still captured in the new graph.

Figure 7.14(a) shows a common graph with 10 vertices and 11 edges (marked as $A, B, \cdots, J$ and $e_1, e_2, \cdots, e_{11}$ respectively in the figure). In this example, that there are three type-2 vertices, which are C, D and F. A simplified graph can be constructed by removing C, D and F and re-link $A - G$ and $E - I$ with edge e_{247} and e_{68} (highlighted vertices and bold edges in Figure 7.14(b)). If loops in

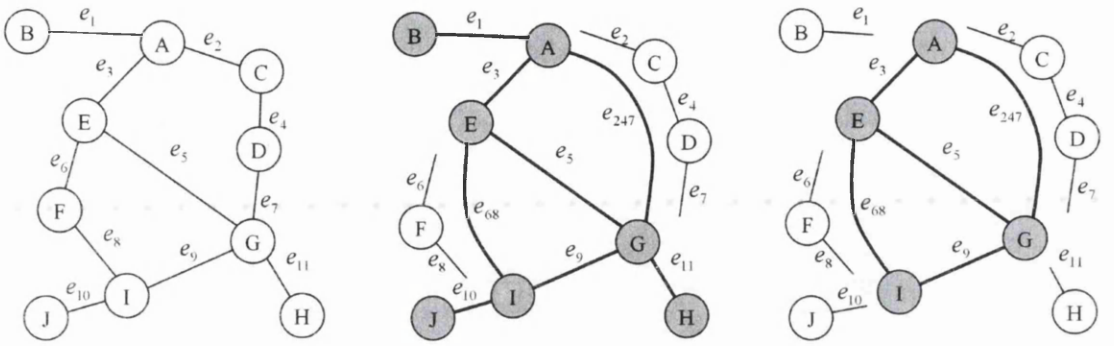

(a) A general 2D graph

(b) Simplified graph without vertices of degree 2

(c) Simplified graph without dangling segments

Figure 7.14: Simplification for 2-dimensional connected graph

the graph is a target, all type-1 vertices ($n = 1$) and type-2 and type-3 edges are also irrelevant and the graph can be further simplified. The process is simple and involves removing all type-1 vertices recursively and re-link the graph after each elimination operation. A simplified result for the graph is shown in Figure 7.14(c) (highlighted vertices and bold edges).

A few simplification procedures were discussed in the previous section. It was demonstrated by removing the tip branches and type-2 vertices, that the complexity of graphs can be reduced without changing the topological shapes. The following sub-section will discuss procedures for checking whether a graph contains any circle, and a calculation of the number of circles.

7.5.3 Graph Topology Shape and Circles

For a given two-dimensional connected graph, an often asked question is whether the graph contains loops or not. Two methods are introduced and explained in the following paragraphs to propose a solution for this query.

Method 1

In an effort to find out whether a connected two-dimension graph contains any loops, an efficient and simple method is to check the number of vertices and edges. The rule is: A graph contains no loop if the number of vertices is one more than

the number of edges. That is:

$$N_v = N_e + 1 \tag{7.3}$$

If the graph contains one or more loops, than Eq. 7.3 can not be held. Thus:

$$N_v \neq N_e + 1 \tag{7.4}$$

This is illustrated by considering a tree first with only a single node, n_{root} (Figure 7.15(a)). Thus, we have $N_v = 1$ and $N_e = 0$. It is clear that Eq. 7.3 holds true in this case. If a new node is inserted into the tree, then $N_v = 2$ and $N_e = 1$ and the equation still hold true (Figure 7.15(b)). Please note that on entering a new node to the tree, a new edge is inserted simultaneously. Therefore, it is be proved that for any given tree, if a new node is inserted without an edge, the new node is isolated in the tree. This does not follow the definition of *connected tree.* On the other hand, for any two nodes of the tree, say n_p and n_q which are in a connected tree, there must be two paths connecting each node to the root of the tree. Say the paths are $n_p \rightarrow n_{p-1} \rightarrow \cdots \rightarrow n_{root}$ and $n_q \rightarrow n_{q-1} \rightarrow \cdots \rightarrow n_{root}$. If a new edge which connects n_p and n_q is inserted, a loop is created ($n_p \rightarrow \cdots \rightarrow n_{root} \rightarrow \cdots \rightarrow n_q \rightarrow n_p$). According to the assumption that the graph contains only tree structures, this is not allowed. So, a new edge is inserted in the tree when inserting a new node. Thus for any tree, the number of vertices always equals the number of edges plus 1. Therefore Eq. 7.3 alway holds true. Figure 7.15(c) and 7.15(d) shows the cases when $N_v = 3$ and $N_v = 11$ respectively.

Hereby, by using the number of vertices and edges with a very simple calculation, whether any circles (holes) is contained by a two-dimension connected graph can be checked. Another algorithm is illustrated in the following paragraphs for the same thing.

Method 2

Another method to check whether a graph contains loop or not is to recursively remove dangling vertices and edges. Any edges in the result indicate that the graph has a loop structure. Otherwise, the graph is a *tree* or a *forest.* The specific steps of this method are:

1. Remove all type-2 nodes in the graph and re-link related vertices together

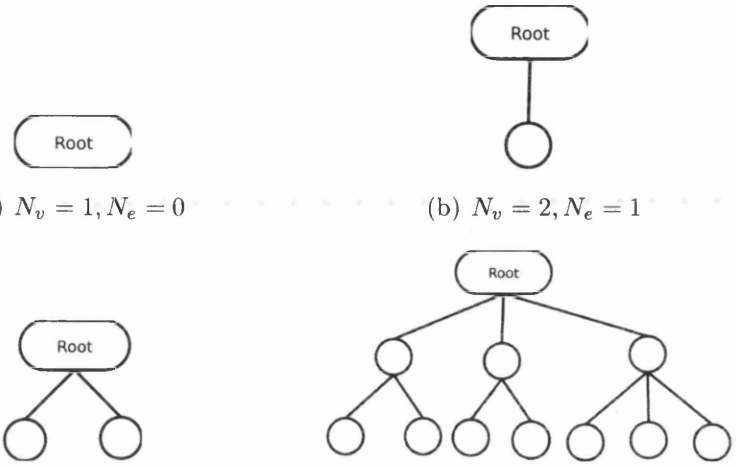

(a) $N_v = 1, N_e = 0$ (b) $N_v = 2, N_e = 1$

(c) $N_v = 3, N_e = 2$ (d) $N_v = 11, N_e = 10$

Figure 7.15: The relationship between the number of vertices and the edges of a connected tree

2. Remove all type-1 nodes in the graph
3. Re-calculate connectivity degree for all nodes
4. Repeat step (2) and (3) until no type-1 nodes can be found

If the graph does not contain any loop structure, we call it *tree* or *forest*. It is clear that in this case the simplification will lead to some stand-alone nodes without any edges. Two simplification examples for a tree and a forest are shown in Figure 7.16 and Figure 7.17 respectively. After the simplification, all graphs

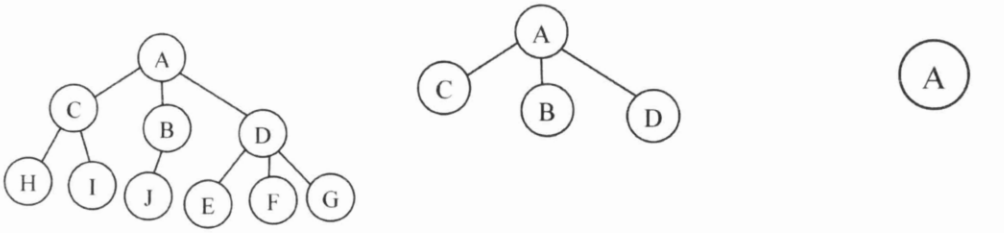

(a) Step 1 (b) Step 2 (c) Step 3

Figure 7.16: Loops searching result for a tree

can be classified into two groups:

1. Graph comprising only vertices

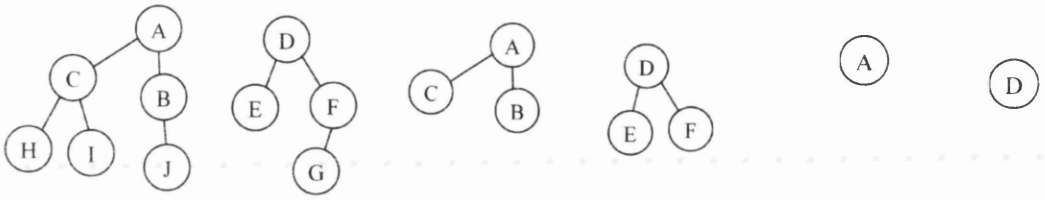

(a) Step 1 (b) Step 2 (c) Step 3

Figure 7.17: Loops searching result for a forest

2. Graph with vertices and edges

As has been discussed, the first case indicates a tree or forest structure while the second case implies there is at least one loop in the graph. This leads to the next question on how to find out the number of loops in a graph.

7.5.4 Number of Circles in a Graph

If a graph has circles, an important and useful information for it is the number of circles. As mentioned, dangling edges and vertices with degree 2 would not influence the counting result of a graph. They could be removed before the counting process to simplify the algorithm. Since there are so many ways to define a circle in a graph, a proper definition is needed before the counting process.

For any two-dimension connected graph with circles (an example is shown in Figure 7.18(a)), an outer circle is defined by the most outer edges and vertices. The outer circle and the closed area for this example are shown by bold lines and grey area in Figure 7.18(b). The inner circles of the graph are marked as C_1, C_2, $C_3$and C_4 in Figure 7.18(c) individually. As one kind of partitioning of the outer circle, the number of inner circles is what we are looking for. The inner circles do not overlap with each other and do not have any internal edges. These features lead to a simple formula which can be used to calculate the number of circles in a graph:

$$N_c = N_e - N_n + 1 \tag{7.5}$$

where N_c is the number of circles in a graph, N_e is the number of edges in the graph, N_n is the number of nodes.

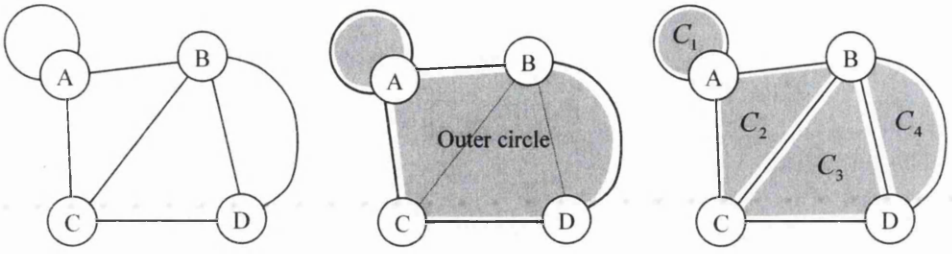

(a) A common graph (b) The outer circle (c) The inner circles

Figure 7.18: Loops searching result for a forest

To prove it, let us start with the simplest graph with only one vertex and no edge. It is clear that $N_n = 1$ and $N_e = 0$ in this case. There is only one circle in the graph. Eq. 7.5 is true for this status (Figure 7.19(a)). Following paragraphs check all possible ways by which the graph can be modified one by one:

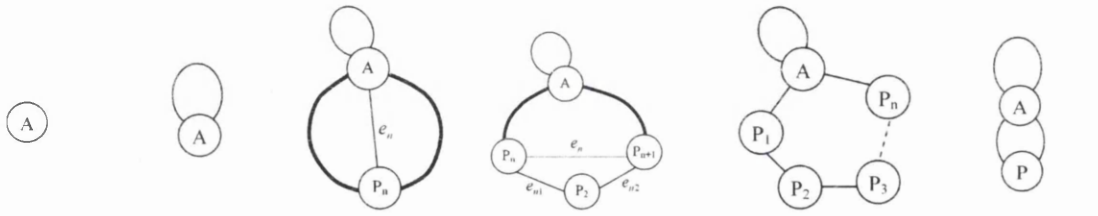

(a) Status 1 (b) Status 2 (c) Status 3 (d) Status 4 (e) Status 5 (f) Status 6

Figure 7.19: Loops searching result for a forest

1. Add only edges into the graph. Both ends of each edge connect with the same vertex (Figure 7.19(b)). In this case, each edge creates a new loop. If no two loops intersect each other (it is true, otherwise, the intersection points have to be inserted into the graph as new vertices), each loop create a new circle. That is for each new edge number of circles add one and number of edge add one. Suppose n new edges will be inserted into the graph. Since $N'_c = N_c + n$, $N'_e = N_e + n$ and $N'_n = N_n$, Thus:

$$\begin{aligned} N'_c &= N_c + n \\ &= N_e - N_n + 1 + n \\ &= (N_e + n) - N_n + 1 \\ &= N'_n + N'_e + 1 \end{aligned} \tag{7.6}$$

2. A new edge is put in the graph which connects with two vertices (Figure 7.19(c)). Since the new edge bisects the old circle and creates two new circles, the number of circles and number of edges are increased by one.

   In this case $N'_c = N_c + 1$, $N'_e = N_e + 1$, and $N'_n = N_n$. Thus:

$$\begin{aligned} N'_c &= N_c + 1 \\ &= N_e - N_n + 1 + 1 \\ &= (N_e + 1) - N_n + 1 \\ &= N'_n + N'_e + 1 \end{aligned} \tag{7.7}$$

3. Now new vertices are introduced into the graph. Each new vertex in this case splits one existing edge into two and insert itself into the graph. It is clear that the inserting vertex would not change the number of circles in the graph (Figure 7.19(d)) and it only increases the number of vertex by 1 and the number of edges by one.

   So, for each new vertex we have: $N'_c = N_c$, $N'_n = N_n + 1$ and $N'_e = N_e + 1$:

$$\begin{aligned} N'_c &= N_c \\ &= N_e - N_n + 1 + 1 - 1 \\ &= (N_e + 1) - (N_n + 1) + 1 \\ &= N'_e - N'_n + 1 \end{aligned} \tag{7.8}$$

4. Several vertices can be inserted into the graph one by one as discussed in (3). The result of insertion would not change the topological shape of the graph (Figure 7.19(e)). Actually, this case just repeat step 3 several times. Thereby the equation (Eq. 7.5) still hold true in this case.

5. Add n new circles in the graph. If each circle is formed by one vertex and two edges, there will be n new vertices and $n \times 2$ new edges in the graph. Figure 7.19(f) shows the case with $n = 1$.

   In this case, $N'_c = N_c + n$, $N'_e = N_e + n \times 2$ and $N'_n = N_n + n$.

$$\begin{aligned} N'_c &= N_c + n \\ &= (N_e - N_n + 1) + n + n - n \\ &= (N_e + 2n) - (N_n + n) + 1 \\ &= N'_e - N'_n + 1 \end{aligned} \tag{7.9}$$

If each circles contains more than one vertex and two edges, insert one vertex and two edges into the graph first for each circle (this is just proved). Then step 4 algorithm can be used so that the number of vertices and edges fit the requirement. The equation is still true.

Therefore, from the discussion in preceding section that in all five possible modifications, the number of circles in a graph can be calculation by Eq. 7.5.

7.5.5 An Overview of the Algorithm

The proposed algorithm is illustrated using a flow diagram in Figure 7.20. It can be seen that for any given geometry model, the output of the algorithm is the number of circles. This number indicates how many loops are there in the MAT results which represents the number of holes in the original geometry models.

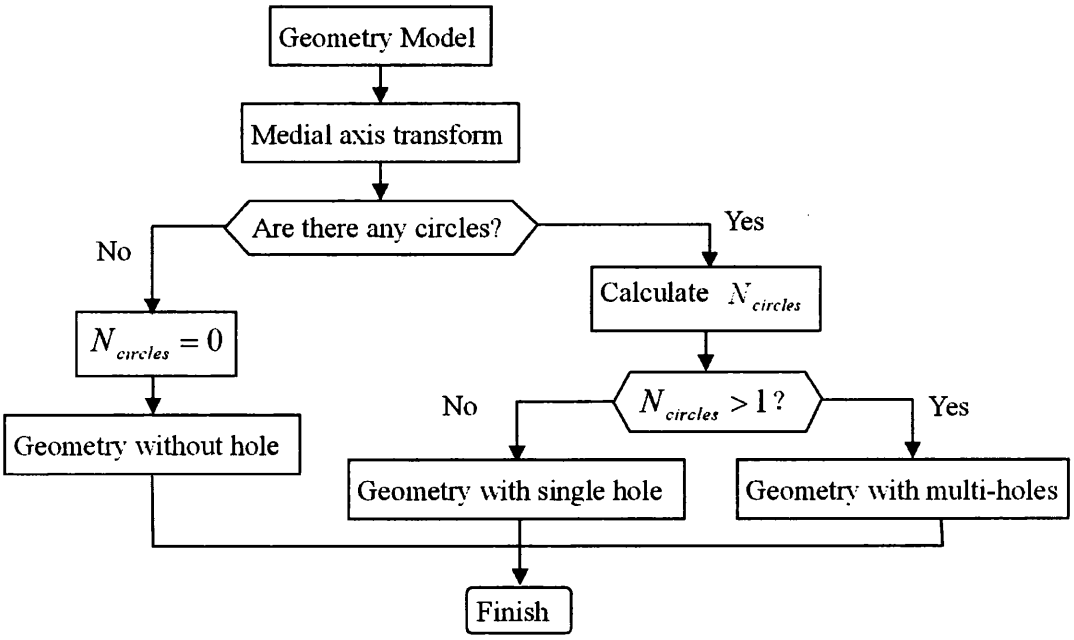

Figure 7.20: Procedures for calculating the number of holes

By using the number of circles as a criteria, geometry shapes can be classified into three groups (Table 7.4).

To validate the algorithms, some more realistic geometry shapes are checked. Following sub-section will illustrate the checking results one by one.

Table 7.4: Geometry classification based on the number of holes

Types	Geometry features	Hole number
1	Geometry does not have any hole	$N_c = 0$
2	Geometry has one hole (single-hole geometry)	$N_c = 1$
3	Geometry has more than one holes (multi-hole geometry).	$N_c \geq 2$

7.5.6 Case Study

Example 1

To test the algorithm, a more realistic geometry which has one hole is used (Figure 7.21(a)). Figure 7.21(b) shows the MAT result. The dots in the figure indicate medial axes vertices. The connectivity degree of each vertex is shown in Figure 7.21(c).

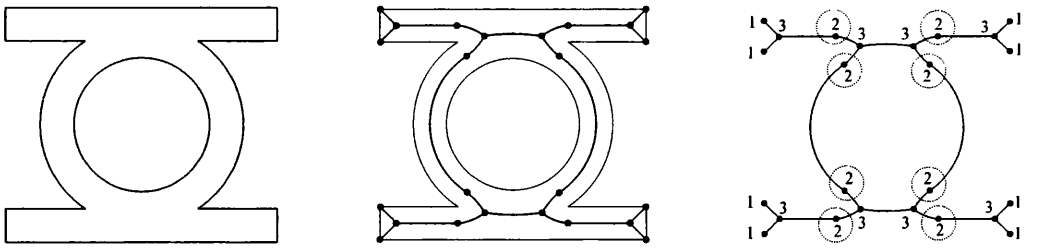

(a) Geometry shape (b) Mat result (c) The initial degree values

Figure 7.21: A common shape with its MAT and initial degrees

For implementing the algorithm, the first step for counting holes is to simplify the graph. All degree-2 vertices are removed first (Figure 7.21(c). Then all degree-1 vertices as shown in Figure 7.22(a) are removed. Step 3 comprises removal of type-2 and type-3 segments (Figure 7.22(b). Lastly, re-calculate the degree of connectivities and repeat last two steps until there is no type-1 vertex in the MAT result. The simplification resulting for this case is shown in Figure 7.22(c).

The MAT simplification result implies a graph which is shown in Figure 7.23. As can be seen, the graph has 4 vertices and 4 edges. According to Eq. 7.5, the number of circles of this graph should be: $N_c = 4 - 4 + 1 = 1$. The result from the algorithm matches accurately with the original geometry.

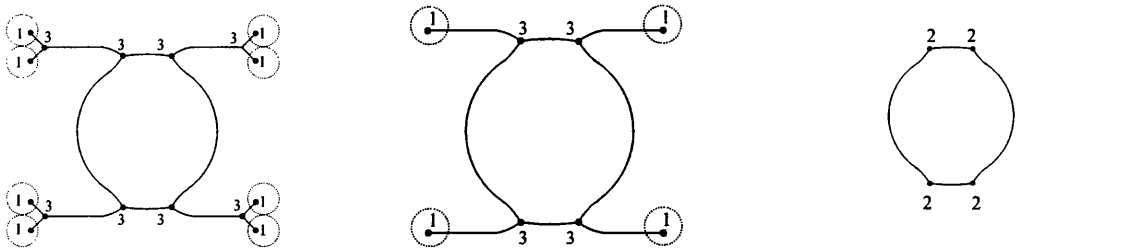

(a) Medial axes after removing of degree-2 vertices

(b) Medial axes after removing of degree-1 vertices

(c) Removing of 'tip' segments

Figure 7.22: Simplification Process

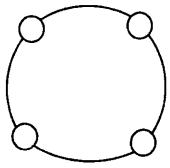

Figure 7.23: The graph according to simplified MAT

Example 2

Figure 7.24(a) shows a shape with two holes. The original and simplified MAT results for this shape are shown in Figure 7.24(b) and 7.24(c) respectively. It is clear from the graph, shown in Figure 7.25, that the graph has 2 vertices and 3 edges. Thus, the number of circles for this graph is: $N_c = 3 - 2 + 1 = 2$. Th prediction matches accurately with the original shape.

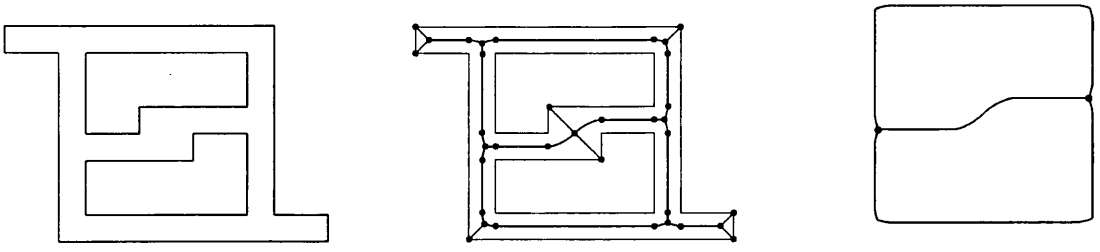

(a) Geometry shape

(b) Mat result

(c) Simplified MAT

Figure 7.24: The original and simplified MAT of a 2-hole shape

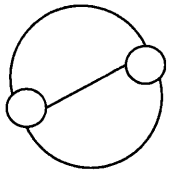

Figure 7.25: The graph according to simplified MAT

Example 3

This example shows a geometry shape with 5 holes in it (Figure 7.26). Figure 7.27 is the graph corresponding to the simplified MAT result.

As the graph has 8 vertices and 12 edges, the number of circles in the shape is: $N_c = 12 - 8 + 1 = 5$.

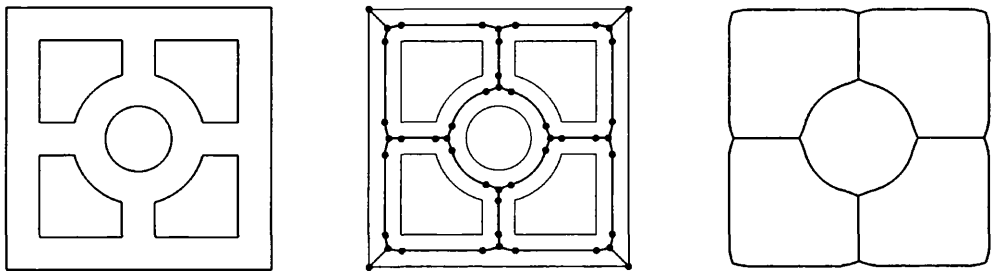

(a) Geometry shape (b) Mat result (c) Simplified MAT

Figure 7.26: The original and simplified MAT of a 2-hole shape

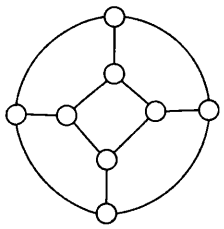

Figure 7.27: The graph according to simplified MAT

Summary

The accuracy of the algorithm is validated by these three examples. Using this MAT based algorithm, it is now possible to find out whether a given geometry shape has holes in it and the number of holes can also be found out simultaneously.

7.6 Recognition of Geometry Boundary Perturbations

7.6.1 The Sensitivity of MAT

Due to the very nature of MAT generation approaches, MAT results are very sensitive to the definition of geometry boundaries. Any perturbation on the boundary can result in dramatic changes to the MAT result.

Similar Geometry Shapes with Different MAT

The above mentioned sensitivity of MAT is illustrated by a very simple example as shown in Figure 7.28. Figure 7.28(a) shows a rectangular geometry with its medial axes. Since a rectangle has four corners, the MAT result contains four tip segments and one main axis. Figure 7.28(b) shows a similar geometry shape with three small lumps on one boundary segment. As can be seen in the figure, though the three bulges are quite small, the MAT result changes significantly. The result has three new tip segment with slightly changed main medial axis. Figure 7.28(c) shows another case which has a small recess on the boundary. Again, the MAT result is changed and two more new tip segments are generated. Figure 7.29 gives another example to explain this sensitivity of MAT to boundary perturbations.

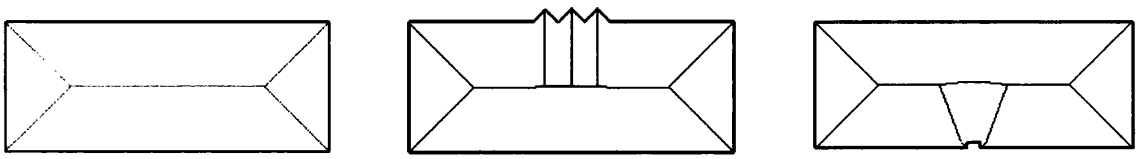

(a) A rectangle shape

(b) Rectangle with three tiny lumps on the boundary

(c) Rectangle with a small recess on the boundary

Figure 7.28: Sensitivity of MAT result to geometry boundary shapes (example 1)

Different Shapes with Similar MAT Results

In some cases, the medial axes of two different geometry shapes may look alike. Two geometries in Figure 7.30 provides an example of such a case. The geometry

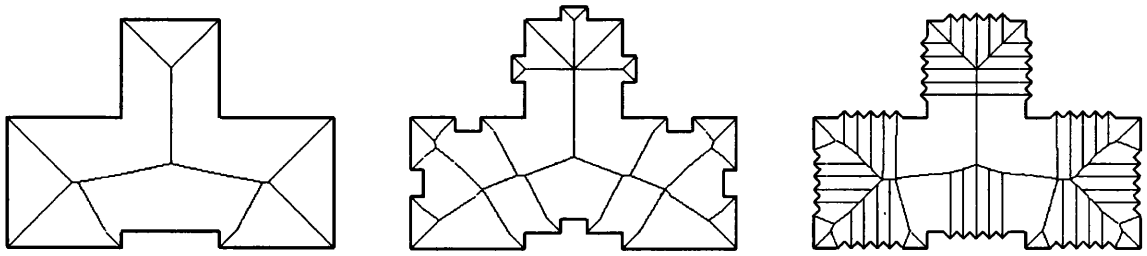

(a) Geometry shape 1 (b) Geometry shape 2 (c) Geometry shape 3

Figure 7.29: Sensitivity of MAT result to geometry boundary shapes (example 2)

at the left has a quite big dome-shape section (Figure 7.30(a)). The right side geometry only has a tiny sharp lump on the upper boundary (Figure 7.30(b)). Please note that the extra part of each geometry create similar medial axis segments (marked as l_1 in each figure). Except for a light difference on the main medial axis, the whole MAT results for each geometry are similar. This implies that the medial axes is not sufficient to distinguish different geometry shapes in some cases and further information is needed.

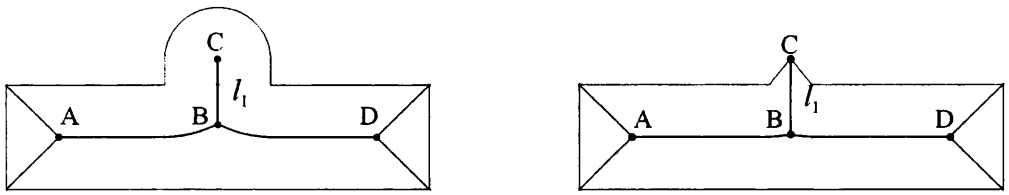

(a) A geometry with a dome

(b) A geometry with a sharp tip in the middle of the upper boundary

Figure 7.30: Sensitivity of MAT result to geometry boundary shapes (example 3)

7.6.2 Radius Function and its Differentiation

As mentioned in Chapter 4, the medial axis transform result contains not only the medial axes of geometries, but also the radius functions of these axes. This subsection will check if the radius function can be used for developing a perturbation recognition algorithm.

The geometries shown in Figure 7.30 are used to implement this idea. For each segments of main medial axes of each geometry ($A \rightarrow B \rightarrow C$ and $C \rightarrow B \rightarrow D$) the corresponding radii are listed in Table 7.5 and 7.6 individually.

Table 7.5: Radii of segment $A \rightarrow B \rightarrow C$

radius function of7.30(a)			radius function of 7.30(b)		
segment: $A \rightarrow B$			segment: $A \rightarrow B$		
distance	radius	ΔD	distance	radius	ΔD
-	0.5	0	-	0.5	0
0.10	0.5	0	0.10	0.5	0
0.20	0.5	0	0.20	0.5	0
0.30	0.5	0	0.30	0.5	0
0.40	0.5	0	0.40	0.5	0
0.50	0.5	0	0.50	0.5	0
0.60	0.5	0	0.60	0.5	0
0.70	0.5	0	0.70	0.5	0
0.80	0.5	0	0.80	0.5	0
0.90	0.5	0	0.90	0.5	0
1.00	0.5	0	1.00	0.5	0
1.10	0.505	0.005	1.10	0.5	0
1.21	0.521	0.016	1.20	0.5	0
1.31	0.546	0.025	1.30	0.5	0
1.42	0.581	0.035	1.40	0.504	0.004
1.52	0.625	0.044	1.50	0.521	0.017
segment: $B \rightarrow C$			segment: $B \rightarrow C$		
distance	radius	ΔD	distance	radius	ΔD
1.62	0.573	-0.052	1.61	0.422	-0.099
1.71	0.533	-0.04	1.72	0.331	-0.091
1.80	0.508	-0.025	1.83	0.253	-0.078
1.90	0.5	-0.008	1.93	0.19	-0.063
2.02	0.5	0	2.03	0.126	-0.064
2.15	0.5	0	2.13	0.063	-0.063
1.62	0.573	-0.052	2.23	0	-0.063

Figure 7.31 shows the plotting result of the radius functions. An important segments of MAT ($B \rightarrow C$ and $C \rightarrow B$) have been plotted twice, the curve for these data are symmetric as shown in Figure 7.31(a) and 7.31(b).

For normal section, the regional width is close to main frame width of the ge-

Table 7.6: Radii of segment $C \rightarrow B \rightarrow D$

radius function of7.30(a)			radius function of 7.30(b)		
segment: $C \rightarrow B$			segment: $C \rightarrow B$		
distance	radius	ΔD	distance	radius	ΔD
1.62	0.573	-0.052	2.23	0	-0.063
2.15	0.5	0	2.13	0.063	-0.063
2.02	0.5	0	2.03	0.126	-0.064
1.90	0.5	-0.008	1.93	0.19	-0.063
1.80	0.508	-0.025	1.83	0.253	-0.078
1.71	0.533	-0.04	1.72	0.331	-0.091
1.62	0.573	-0.052	1.61	0.422	-0.099
radius function of7.30(a)			radius function of 7.30(b)		
segment: $B \rightarrow D$			segment: $B \rightarrow D$		
distance	radius	ΔD	distance	radius	ΔD
2.86	0.581	-0.044	3.07	0.503	-0.018
2.96	0.546	-0.035	3.17	0.5	-0.003
3.06	0.521	-0.025	3.27	0.5	0
3.17	0.505	-0.016	3.37	0.5	0
3.27	0.5	-0.005	3.47	0.5	0
3.37	0.5	0	3.57	0.5	0
3.47	0.5	0	3.67	0.5	0
3.57	0.5	0	3.77	0.5	0
3.67	0.5	0	3.87	0.5	0
3.77	0.5	0	3.97	0.5	0
3.87	0.5	0	4.07	0.5	0
3.97	0.5	0	4.17	0.5	0
4.07	0.5	0	4.27	0.5	0
4.17	0.5	0	4.37	0.5	0
4.27	0.5	0	4.47	0.5	0

Table 7.7: Medial axes radius function data

ometry and the length is significantly greater compared to tiny sections. These characteristics cause smooth curves in the plotting figures with quite long distance between two peaks of the radius function, which indicates the doubled rough length of important segment (that is the distance of B-B in the figure).

The range of changes in widths and/or lengths of a normal section may be similar to smaller/perturbed section, but changing rate for the normal section will be much slower compared to small/perturbed section. For this, a derivative of radius function, R', is used for the analysis.

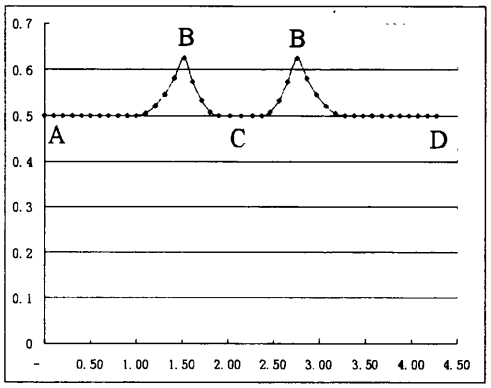

(a) Radius function of left-side geometry

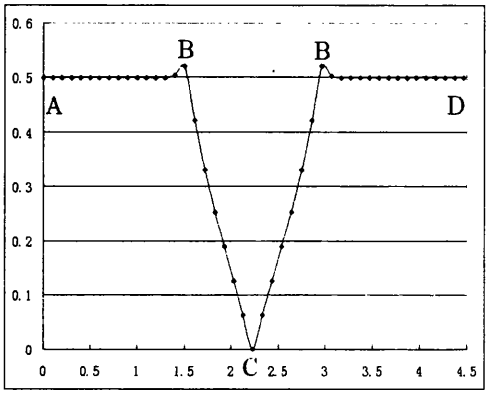

(b) Radius function of right-side geometry

Figure 7.31: The radius functions of the geometries which shown in Figure 7.30

Due to the limits of the software, a theoretical radius function can not be given, therefore discrete models are used for the analysis. For any geometry, the first step is to generate the medial axes and this can be done by the software automatically. The following step is to generate a two-dimension mesh for the medial axes. Then the radius of each node are calculated. By choosing a proper mesh density, the result provides a reasonable substitution of radius functions.

For a perturbation analysis, the derivative value at the junction points are more useful and important than tip points. The algorithm always starts the calculation from tip points. A backward derivative method is used so that the value is valid at the junction points. For point p_n, the derivative value can be calculated by:

$$R'_n = \frac{\Delta R_n}{\Delta l_n} = \frac{R(l_n) - R(l_{n-1})}{l_n - l_{n-1}} \tag{7.10}$$

Figure 7.32 shows the differentiations of the radius functions of the geometries. The figures illustrate that the regional section width of both models changed in the closing area of point B. But it is clear that the length and value of the changing area are different. For the left-side model, the maximum difference is 0.052. The length of the changed area is about 2.27. The value of the maximum difference for the right-side model is 0.099 and the length is about 1.87.

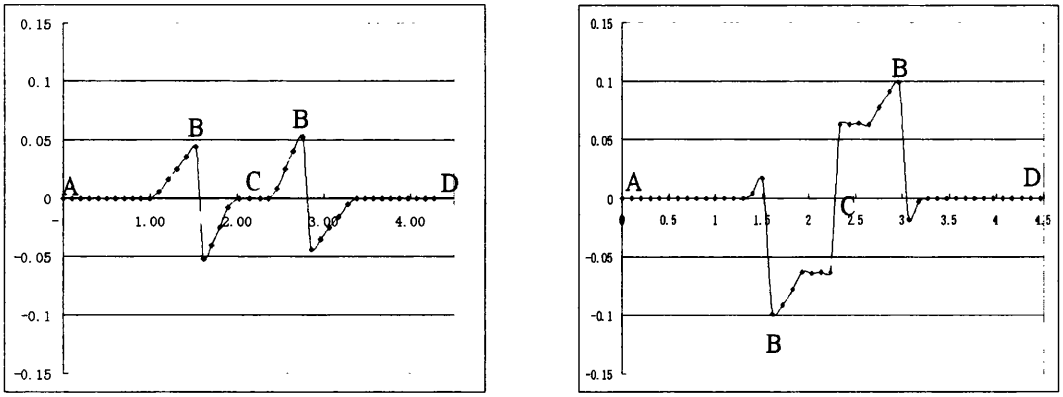

(a) differentiation for left-side geometry (b) differentiation for right-side geometry

Figure 7.32: The differentiation of radius functions

The results show how extra information provided by radius functions separate perturbations from normal sections of MAT. Although the algorithm predicted the result correctly and proved that the idea can be implemented, a more versatile and robust algorithm needs be introduced so that general shape geometry models can be handled easily and automatically. Note that for resolving this problem, the main frame and the holes are not taken into-consideration. The target are the leg and tip shape structures. In another words, the radius functions and their differentiation on the legs and tips need to be investigated. The following paragraphs proposes an algorithm to solve this problem.

7.6.3 Initial Searching Area Locate

Tips, legs, perturbations and body are relative concepts for a geometry model. For example, a T-shape model has three branches (Figure 7.33). Any two of them can be seen as the main body and the leftover section can be assumed as the tip. For instance, in Figure 7.33(a), branch B-C and B-D are selected as the body, and branch A-B is the tip. For the corresponding medial axes, segments l_1 and l_3 are the main MAT and l_2 is a branch. The other two body-tip definitions are shown in Figure 7.33(b) and 7.33(c) respectively.

Assuming only one branch segment is checked in one step, finding out the start and end vertices is a key issue for getting the radius function for the segment. The first step is the same as the branch searching algorithm–simplification. Fig-

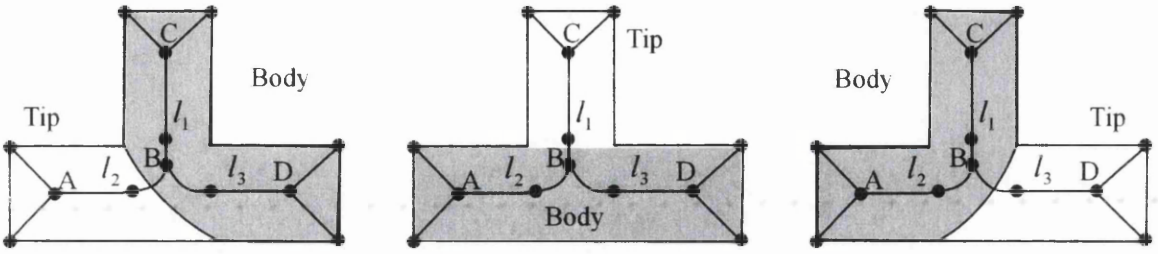

(a) (b) (c)

Figure 7.33: Geometry body selection and corresponding tip section

ure 7.34(a) shows the MAT result of the T-shape model. The first step removes all end branches as mentioned. The result is shown in Figure 7.34(b). Degrees need to be recalculated after the first step. In the second step, a vertex with degree 1 is selected. Say it is vertex A. The algorithm keeps searching vertices at the other side recursively until it finds a vertex with a degree more than 2 (vertex B in the figure). The path from A to B is the medial axes of the section we are looking for. The third step is to get the radius functions of this MAT section (Figure 7.34(c)). It is noted here that since the backward derivative method is used, the derivative of the first point can not be calculated.

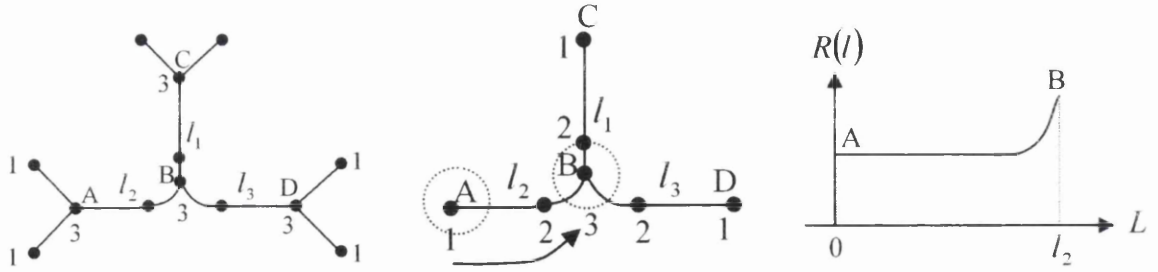

(a) (b) (c)

Figure 7.34: Geometry body selection and corresponding tip section

As an instance, Figure 7.35 shows the radius functions of section $A \rightarrow B$ and $C \rightarrow B$. Since the section width are the same from A to D, section $A \rightarrow B$ has uniform width except in a very short area close to point B. On the other hand, section $C \rightarrow B$ is narrower than section $A \rightarrow B \rightarrow D$, therefore, the width changing area of section $C \rightarrow B$ is longer than that of section $A \rightarrow B$ and $C \rightarrow B$ has larger width value changing range compared to $A \rightarrow B$. Please note that the section width of both $A \rightarrow B$ and $C \rightarrow B$ at the junction point, i.e. point B, are same (since there is only one radius at one point).

Because different shapes and sections have different regional width, section width can not be used as a criteria for the classification. The figures illustrate this clearly. For example, the maximum values of both radius functions are equal in this case (The maximum value achieved at point B in this case). So, there is no reasonable upper limit for shape classification. Also it is clear that there is no easy mark for choosing the lower limit.

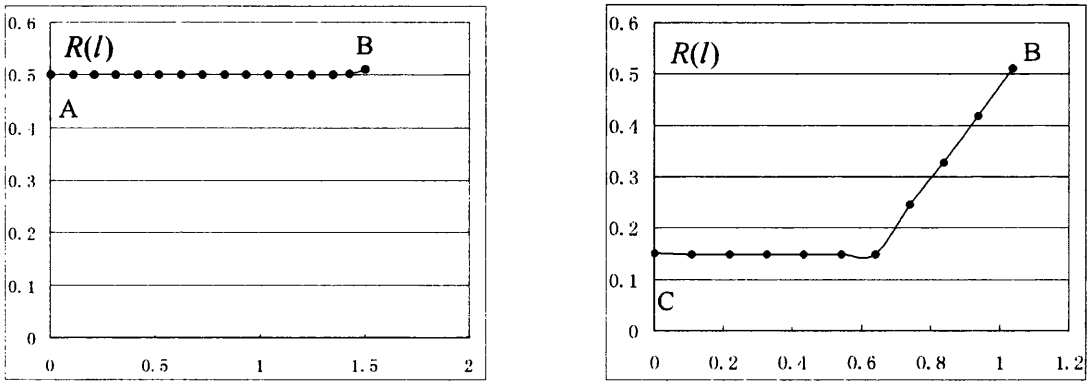

(a) Radius function of section $A \rightarrow B$

(b) Radius function of section $C \rightarrow B$

Figure 7.35: Radius functions for section $A \rightarrow B$ and $C \rightarrow B$

Looking at Figure 7.35 carefully, an interesting observation can be made that is, for big parts with smooth boundaries of a shape, the value of the regional width might change in a very wide range but the width changes slowly. For small sections, tips, section with rough boundaries and similar things, the regional width always changes quickly. This gives the motivation to use a differentiation of the radius function rather than the radius function itself.

Figure 7.36 shows the differentiation results of the radius function of section $A \rightarrow B$ and $C \rightarrow B$ respectively. In Figure 7.36(a), most part of the differentiation function equals zero (from 0 to about 1.3). This implies that the original function gives the same value in the area. In other words, since the section holds its width from A to some point quite close to B, the radius function of $A \rightarrow B$ gives the same radii in the range. The differentiation function goes up when reaching close to point B. This is due to the increasing radii in that region. It is clear that the maximum value of the differentiation function is less than 0.2.

The differentiation result for section $C \rightarrow B$ is shown in Figure 7.36(b). Compared to Figure 7.36, the differentiation function of $C \rightarrow B$ gives a much shorter

length where it equals zero (from 0 to about 0.7). At the same time, the shape of the differentiation function changes dramatically when approaching point B and the maximum value is close to 1.0.

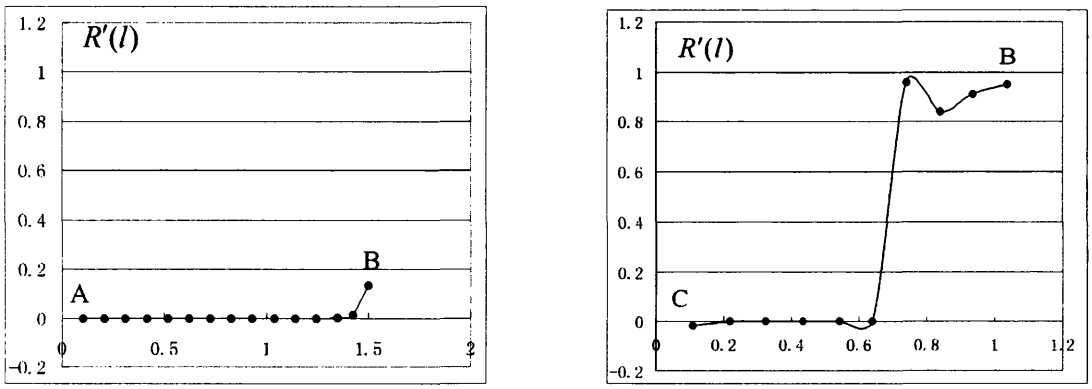

(a) Differentiation for section $A \rightarrow B$

(b) Differentiation for section $C \rightarrow B$

Figure 7.36: Differentiation of radius functions

This example shows that by using the differentiation results, section $A \rightarrow B$ and $C \rightarrow B$ can be separated easily. The rule is therefore that a section is defined as a branch if the maximum value of its radius function differentiation crosses a pre-defined limit. For instance, 0.5 is used in this case so that section $A \rightarrow B$ is a normal section and section $C \rightarrow B$ is a branch.

7.6.4 Algorithm Validation

To validate this algorithm, an arbitrary geometry is used (Figure 7.37). The MAT result is shown in Figure 7.38. All crucial vertices are marked from A to O individually. The MAT result is divided into 15 sections by these vertices, which are section $A \rightarrow B$, $C \rightarrow B$, ... , $M \rightarrow N$, $O \rightarrow N$.

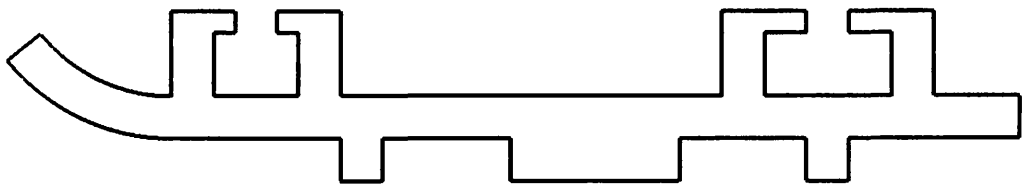

Figure 7.37: Shape for branch searching algorithm

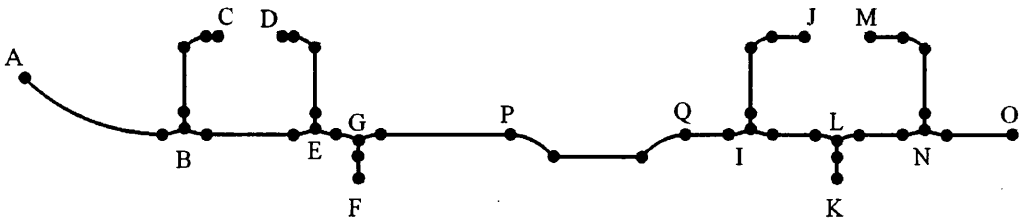

Figure 7.38: MAT and the segments in the result

Since not all the sections are required for implementing the algorithm, only section $A \rightarrow B$, $C \rightarrow B$, $F \rightarrow G$, $M \rightarrow N$, $O \rightarrow N$ and their radius functions and the radius function's differentiation are taken into consideration. The radius function and corresponding differentiation result are shown in Figure 7.39, 7.40, 7.41, 7.42 and 7.43 respectively. It is clear that comparing with the radius function, the differentiation of radius function gives more details about the shape changing information. Therefore, the differentiation results provide a better way for separating perturbations from normal part of the geometry.

For checking whether the algorithm can mark the main part of the geometry, the radius function and its differentiation of the main axis of the geometry are used. In this case, the main axis is $A \rightarrow B \rightarrow E \rightarrow G \rightarrow P \rightarrow Q \rightarrow I \rightarrow L \rightarrow N \rightarrow O$. Figure 7.44 and 7.45 illustrate the result of the radius function and its differentiation respectively. As clearly be shown in 7.45, $A \rightarrow B \rightarrow \cdots \rightarrow P$ and $Q \rightarrow \cdots \rightarrow O$ have low differentiation value. But in section $P \rightarrow Q$, the maximum and minimum value of the differentiation result cross the marking limits. This indicates a perturbation which can be easily found in Figure 7.37. These results show that the algorithm works properly for the main parts of the geometry as well.

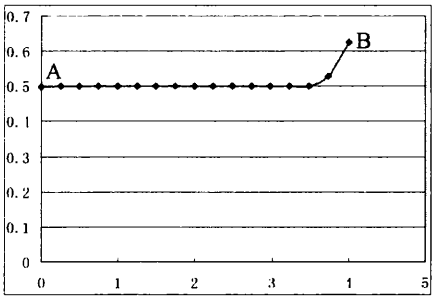

(a) Radius function of section $A \rightarrow B$

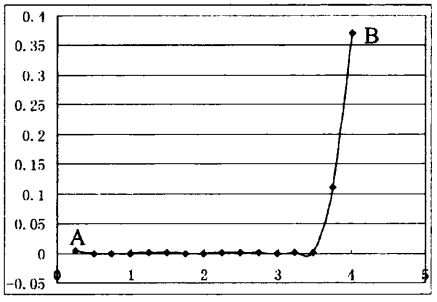

(b) The corresponding differentiation

Figure 7.39: Radius functions and its Differentiation for section $A \rightarrow B$

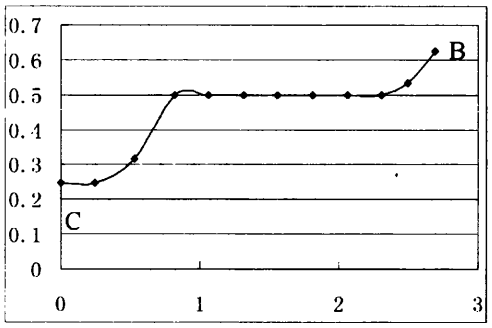

(a) Radius function of section $C \rightarrow B$

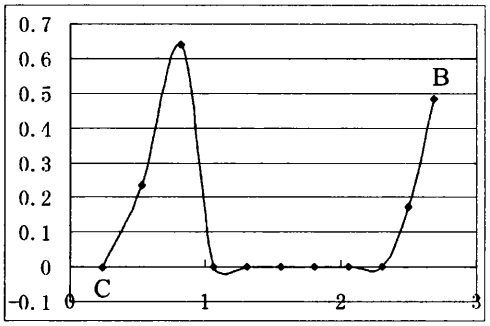

(b) The corresponding differentiation

Figure 7.40: Radius functions and its Differentiation for section $C \rightarrow B$

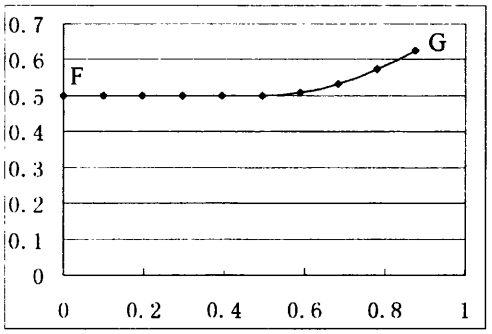

(a) Radius function of section $F \rightarrow G$

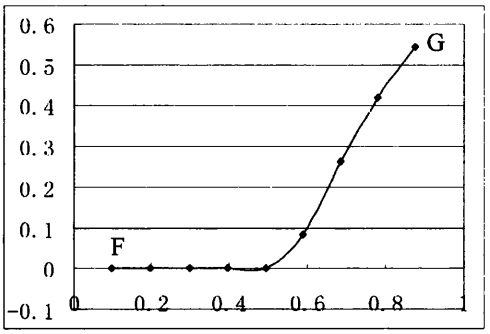

(b) The corresponding differentiation

Figure 7.41: Radius functions and its Differentiation for section $F \rightarrow G$

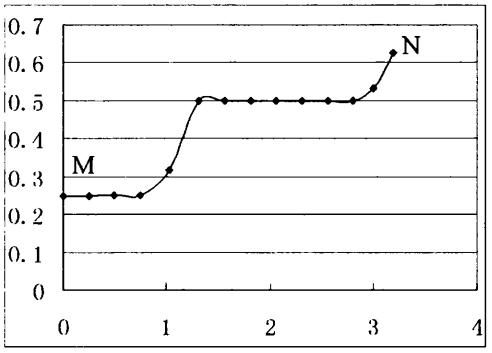

(a) Radius function of section $M \rightarrow N$

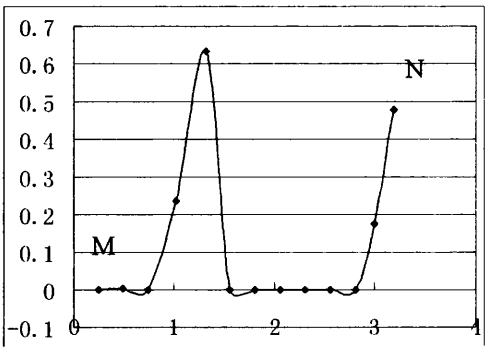

(b) The corresponding differentiation

Figure 7.42: Radius functions and its Differentiation for section $M \rightarrow N$

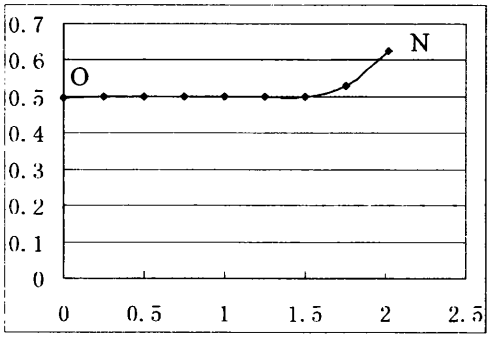

(a) Radius function of section $O \rightarrow N$

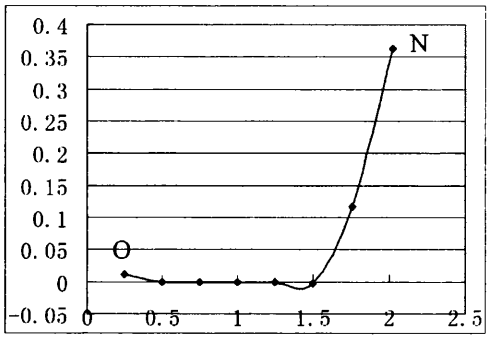

(b) The corresponding differentiation

Figure 7.43: Radius functions and its Differentiation for section $O \rightarrow N$

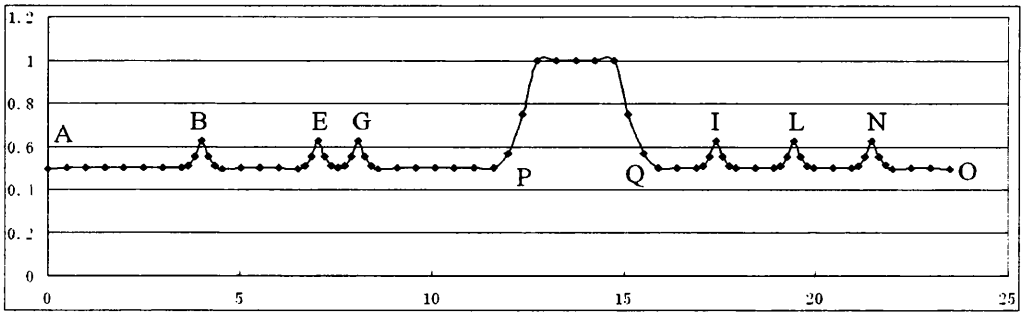

Figure 7.44: Radius function of all main axes

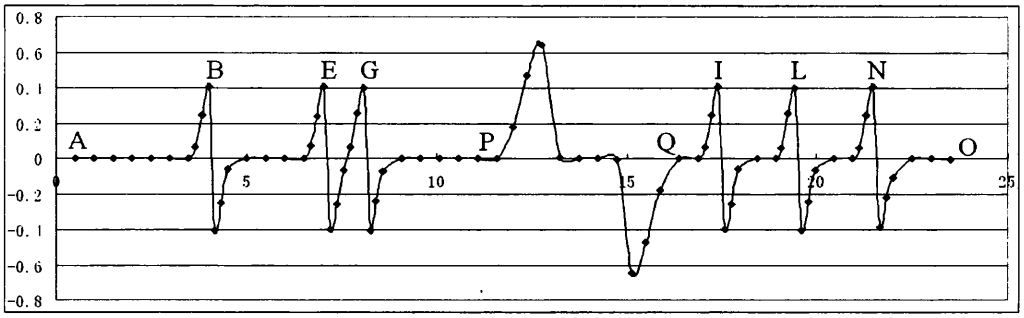

Figure 7.45: Differentiation of main axes radius functions

All the results show that the differentiation of the radius function is a better tool than radius function for separating the narrow/small sections or sections with rough boundaries from normal sections. It is also clear that a single number can be used as the mark of separating. In this case, 0.5 works pretty good with the algorithm.

7.6.5 The Flow Chart of the Algorithm

The procedures of the whole algorithm for searching boundary perturbations or small section of geometry shapes are shown in Figure 7.46.

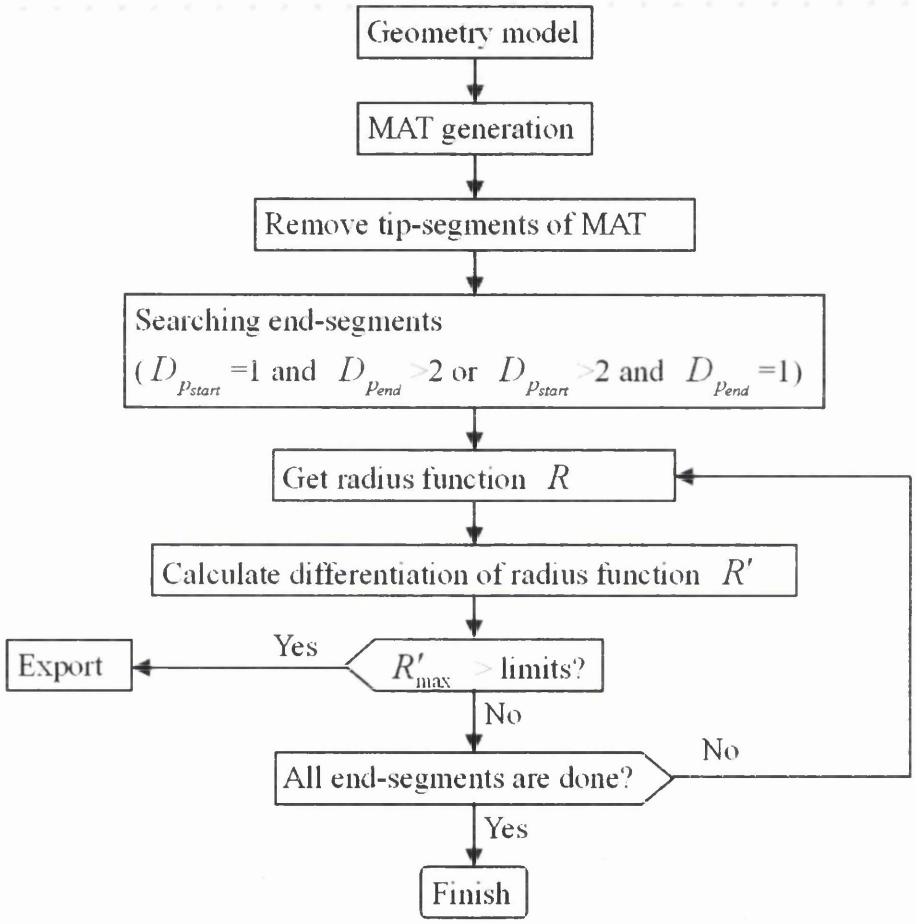

Figure 7.46: The flow chart of perturbation and small section searching algorithm

7.6.6 Summary

In this section, an algorithm for recognizing boundary perturbations and branch sections has been demonstrated. By using the medial axis transform technique, the radius function of each segment of the medial axes can be got. Then, a differentiation of the radius functions is calculated for separating the perturbations and branches from the normal/main part of the model. The validation results illustrated that the algorithm is versatile and robust for the separating work.

7.7 Regional Aspect Ratio

7.7.1 Definition and Properties of Aspect Ratio

For any geometry shape, length and width are the most basic and important geometric information. As mentioned earlier, medial axis transform can be used to calculate the width and length easily. Very often it is asked if the shape is 'fat' or 'thin'. A well-known shape factor known as *aspect ratio* is an useful expression to identify this feature.

An *Aspect ratio* is defined as the ratio of width to length of a shape. For simple geometry shapes, their lengths and widths are used for the calculation. For complicated shapes, the lengths and widths of the shapes' minimum enclosing rectangle (MER) can be used [16].

$$R_A = \frac{W}{L} \tag{7.11}$$

where W is the width of the shape, L is the length of the shape.

Armstrong *et al.* mentioned the *edge aspect ratio* which was given by Bridgett and Donaghy in 1997 and 1998 respectively [5]. The method calculates the ratio for each segment of MAT and is given by:

$$R_{EA} = \frac{r_{ave}}{l} \tag{7.12}$$

where R_{EA} is the *edge aspect ratio*, r_{ave} is the average circumcircles radius of MAT segment, l is the length of the segment. Note that since the circumcircles' radii are used instead of the regional width, R_{EA} in this equation equals $\frac{1}{2}R_A$.

An example for aspect ratio definition is shown in Figure 7.47, which shows a general 2D shape with its MAT. It is clear that the 2D shape has two segments. The main medial axes for these two segments are marked as A–B and C–D in the figure and the regional radii of circumcircles' are R1 and R2. Since the length A–B is longer than the length of C–D and radius R1 is less than radius R2, it is clear that aspect ratio for segment A–B is less than the ratio for segment C–D. It is thus seen that the aspect ratio is a good factor for analyzing shape features.

Although Eq. 7.11 and Eq. 7.12 can be used for analyzing shapes, these only calculate one ratio for each segment of the shape. Therefore, they suffer from

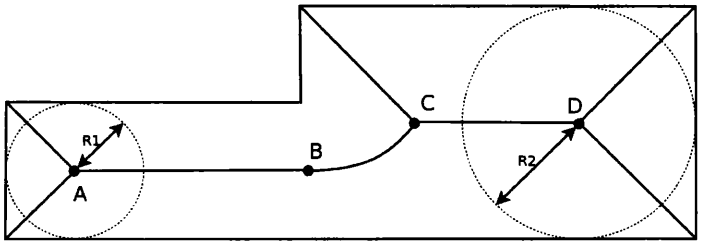

Figure 7.47: Circumcircles radii of MAT

two drawbacks. Firstly, the shape has to be partitioned properly before further calculations can be implement. The second disadvantage is that the aspect ratio reflects only the entire shape of each segment. A modified ratio is used in this research work to overcome these limitations.

7.7.2 Local Aspect Ratio and its Calculation

Although a region based aspect ratio calculation and analysis is sufficient for most applications, it does not work properly under certain circumstances, e.g. if the shape boundary contains a lot of small structures, such as recesses and bulges, or the shape is extremely difficult to be partitioned. A feature recognition algorithm, based on the traditional aspect ratio, fails to provide accurate solutions. Therefore, a local aspect ratio calculation method is introduced for geometry reasoning work. Similar to the original definition, the local aspect ratio is defined by lengths and widths as well. The only difference is that the lengths and widths are local sizes and are not segment based. An example for the definition is shown in Figure 7.48. As can be seen, instead of calculating aspect ratios for only two segments, the whole shape has been sub-divided into sub-regions of same length and aspect ratios are calculated for these divided sub-regions. For instance, the aspect ratio of a sub-region s is calculated by the local section width, R, and length L. The new definition is:

$$R_{A_l} = \frac{R_{ave_s}}{L_s} = \frac{\frac{\oint_{p1}^{p2} R(l)dl}{\oint_{p1}^{p2} dl}}{L_s} = \frac{\oint_{L_s} R(l)dl}{L_s^2} \tag{7.13}$$

For the discrete case, the equation is:

$$R_{A_l} = \frac{R_{ave_s}}{L_s} = \frac{\frac{\sum_{i=1}^{n} R_i}{n}}{\sum_{i=1}^{n} l_i} = \frac{1}{n} \cdot \frac{\sum_{i=1}^{n} R_i}{\sum_{i=1}^{n} l_i} \tag{7.14}$$

where R_{A_l} is local aspect ratio, R_{ave_s} is the average radius of section s, L_s is the length of section s, n is the number of sample points.

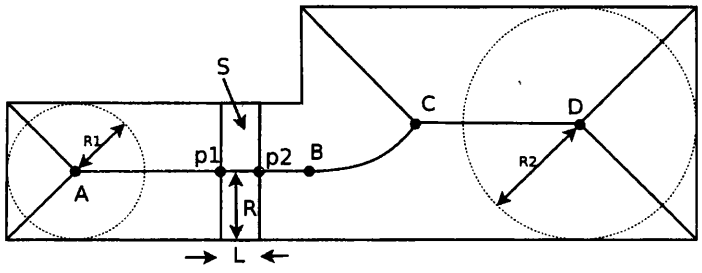

Figure 7.48: Local aspect ratio

Note that if the sub-section widths are uniform and equal to 1, Eq. 7.13 can be simplified to $R_{A_l} = R(l)$, which is the radius function of MAT. Therefore, the conclusion given in section 7.6 holds good in this case too.

7.7.3 Validation using a Case Study

The geometry shape shown in Figure 7.37 is used to check the applicability of the aspect ratio. The MAT result and sections are shown in Figure 7.38. Following the definition, the local aspect ratio along the main axes of the shape from left to right is shown in Figure 7.49. Finally, for checking the rate of variation, the differentiation of the aspect ratio function is calculated and the result is shown in Figure 7.50.

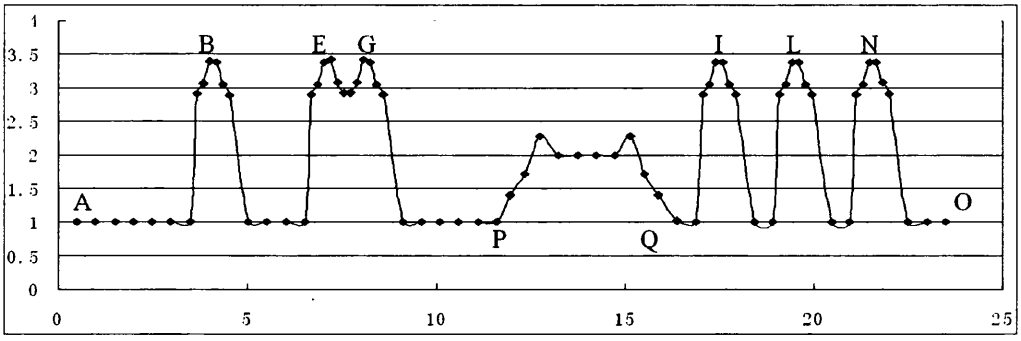

Figure 7.49: Local aspect ratio along the main axes of the shape

Compared with Figure 7.44 and 7.45 (the radius function and its differentiation along the main medial axes for the same shape), the aspect ratio function and

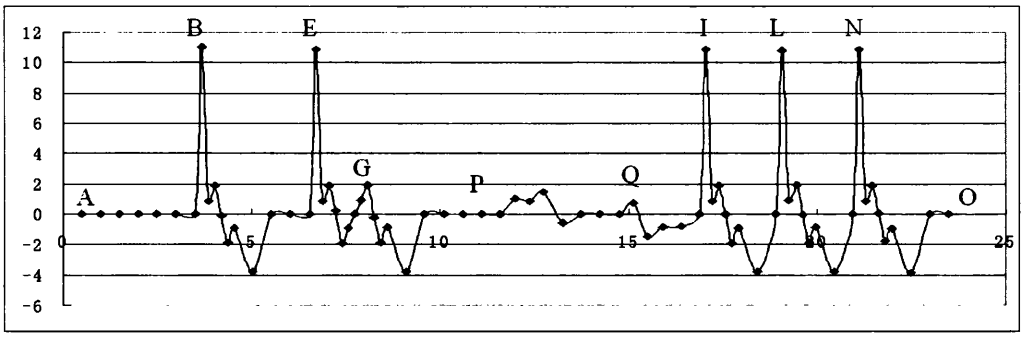

Figure 7.50: Differentiation of local aspect ratio

its differentiation are sensitive to the regional width variation. In regions such as corners or junctions, the aspect ratio function shows visible changes, e.g both aspect ratio function and its differentiation give very high values around points B, E, G, I, L and N as shown in Figure 7.49 and 7.50. These areas are junctions of the shape (Figure 7.37). It is thus seen that the differentiation shows a better performance than the original function for identifying shape features.

7.7.4 Conclusion

In this section, the definition and properties about aspect ratio were discussed. To avoid the disadvantages posed by the traditional method, the local aspect ratio was defined and the generating algorithms were discussed. By using a backward derivative method, the differentiation of the regional aspect ratio function was studied. Once more, the differentiation result shows a powerful capability for shape recognition. It is thus seen that the regional aspect ratio function and its differentiation are good tools for geometry reasoning.

7.8 Complexity estimation for Geometry Shapes

Complexity offers natural properties and useful information for any object. Usually, if an object is complex, it contains a lot of subordinate structures such as branches, corners, holes, tips, etc. While a simple object always has simple shapes with uniform lengths and widths and smooth boundaries.

7.8.1 Complexity Estimation using Circularity Measures

For two-dimensional geometry shapes, circles are the most simple object. Each circle has a uniform thickness and a smooth boundary. By contrast, a complex two-dimensional geometry object could have curvilinear boundaries, complex shapes, branches, holes and so on. Therefore, a group of shape features called *circularity measures* can be used to check the complexity of two-dimensional shapes.

Ratio of Perimeter Squared to Area

The most commonly used circularity measure is called the *perimeter squared to area* ratio [16]:

$$R_c = \frac{P^2}{A} \tag{7.15}$$

where R_c is the ratio of perimeter squared to area, P is perimeter of the shape, and A is the area of the shape.

For a circle, R_c takes a minimum value of 4π. For more complex shapes, the higher values of Eq. 7.15 will give the value. The ratio R_c roughly gives a quantification method for complexity estimation.

Five randomly selected geometry shapes are shown in Figure 7.51. The perimeter squared to area ratios for these shapes are calculated individually. According to the sizes labeled in the figure, the ratios are:

1. A circle.
   $R_c = \frac{(\pi D)^2}{\pi(\frac{D}{2})^2} = \frac{\pi^2 D^2}{\pi \frac{D^2}{4}} = 4\pi$

2. A rectangle with size 3×1.
   $R_c = \frac{((3+1)\times 2)^2}{3\times 1} = \frac{64}{3} \approx 21.33$

3. A cross shape with all boundary segment lengths eqauls 1.
   $R_c = \frac{(3\times 4)^2}{1\times 4+1} = \frac{144}{5} = 28.8$

4. A 3×3 square with a 1×1 square hole in it.
   $R_c = \frac{(12+4)^2}{9-1} = \frac{256}{8} = 32$

5. An arbitrary shape with sizes as marked in the figure.
   $R_c = \frac{112^2}{95} = \frac{12544}{95} \approx 132.04$

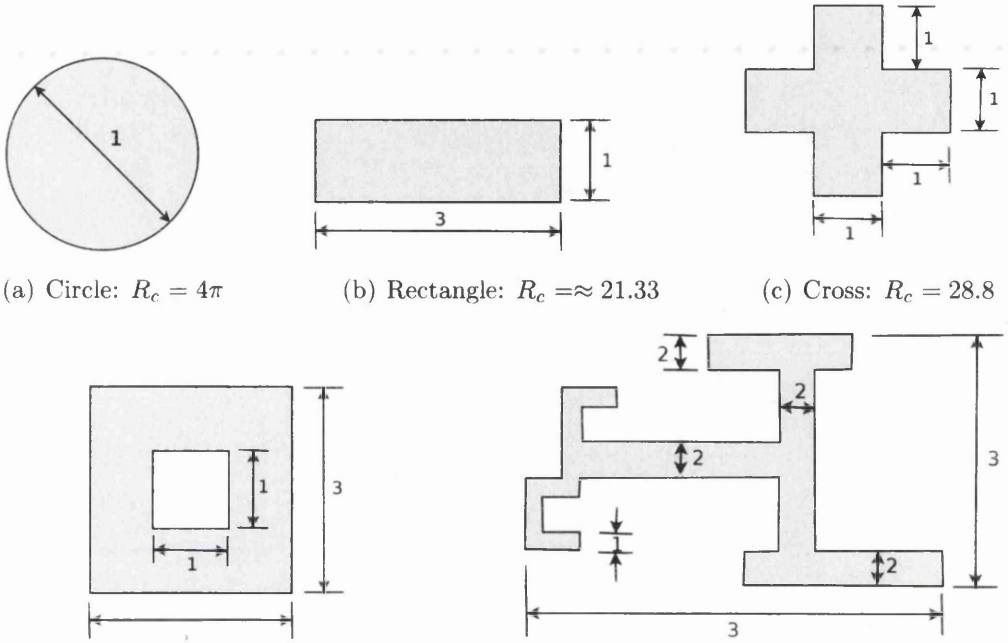

(a) Circle: $R_c = 4\pi$ (b) Rectangle: $R_c = \approx 21.33$ (c) Cross: $R_c = 28.8$

(d) Hollow square: $R_c = 32$ (e) Complex: $R_c \approx 132.04$

Figure 7.51: Examples for perimeter squared to area ratio

As mentioned earlier, a circle is the simplest shape and has the minimum ratio, i.e. 4π. It is trivial that rectangles are more complicated than circles, therefore, the perimeter squared to area ratio for the rectangles are larger than 4π. The ratio of the rectangle shown in Figure 7.51(b) is 21.33. Compared with the rectangle, the cross shown in Figure 7.51(c) has a more complex shape. It is clear that the ratio of the cross is greater than the ratio of the rectangle. Another two geometries with more complex shapes give more evidence for the algorithm. The values of the ratio are 32 and 132.04 for each shape as shown in Figure 7.51(d) and 7.51(e) individually. All the cases indicate that the *perimeter squared to area* ratio is a quite good quantitative factor for shape complexity estimation.

Boundary Energy

Another successful circularity measurement is called *boundary energy*. For any given two-dimensional shape with a perimeter P and for any point p on the bound-

ary with the curvature radius at point p equalling $r(p)$, the curvature function at a point p given by:

$$K(p) = \frac{1}{r(p)} \tag{7.16}$$

Therefore, the average energy per unit length of boundary is:

$$E = \frac{1}{P}\int_0^P |K(p)|^2 dp \tag{7.17}$$

It is easy to prove that for a fixed area, the circle has minimum boundary energy. The boundary energy of a circle with radius R is $E_O = (\frac{1}{R})^2$. It is known that the boundary energy can quantify the shape complexity better than the perimeter squared to area ratio [16].

In this section, two widely known shape factors for shape complexity estimation have been introduced and examples for the first method were given to illustrate its applicability. Since these methods use geometry boundaries and some other shape related geometric informations, the implementation of the methods can be a difficult work. Therefore, a new complexity estimation approach using MAT has been studied and is introduced in the next sub-section.

7.8.2 Complexity Estimation using MAT

New Design Factor for Complexity Estimation

As mentioned in Chapter 4, MAT provides the skeleton of geometry objects. The main medial axes show the main frames of the shapes. It is trivial that for long and thin sections, the total length of medial axes is approximately half of its perimeter. If medial axes lengths are used to substitute the perimeter of geometry shapes, Eq. 7.15 can be modified to:

$$R_{LA} = \frac{L^2}{A} \tag{7.18}$$

where R_{LA} is the medial axis length to area ratio, L is the total length of medial axes and A is the shape area.

Out of the two two-dimensional geometry shapes of same size, one containing sub-structures is more complex than the other one. e.g. from amongst a bar, an

'L' shape and a cross of similar size, we assume that the cross is the most complex shape as it contains more segments than the other two.

Minimum Enclosing Rectangle (MER) is introduced for complexity estimation. MER is a minimum rectangle box in which the corresponding shape can be held. Following this idea, for any two shapes with the same MER areas, the one with longer perimeter is more complex. Therefore, the area of the MER can be a good substitute for the shape area as calculating area of MER is much easier than that of the full corresponding geometry object. By using the area of MER, Eq. 7.18 can be modified as:

$$R_{LA_{MER}} = \frac{L^2}{A_{MER}} \tag{7.19}$$

where $R_{LA_{MER}}$ is the ratio, L is the total length of main medial axes and A_{MER} is the area of minimum enclosing rectangle.

For two geometries with the same MER areas and total medial axes lengths, the one with the thiner sections is given a higher complexity value. Therefore, section width information is needed. As mentioned in chapter 4, section width information is represented by the radius function of MAT. The average radius can be calculated by:

$$R_{ave} = \frac{\oint_L R(l)dl}{\oint_L dl} = \frac{\oint_L R(l)dl}{L} \tag{7.20}$$

Therefore, the final form of the new design factor is:

$$R_c = \frac{L^2}{A_{MER} \cdot R_{ave}} \tag{7.21}$$

where R_c is the ratio of complexity, L is the total length of main medial axes, A_{MER} is the MER area of the shape, $R(l)$ are MAT radius functions.

7.8.3 The Complexity Ratio Calculation

Calculation of MER Area

The main task for calculation of MER area comprises finding out the minimum and maximum x and y of the shape and then the area can be calculated by using:

$$A_{MER} = (x_{max} - x_{min}) \times (y_{max} - y_{min}) \tag{7.22}$$

If MAT is used for the calculation, the radii of the points where a minimum and maximum x and y are achieved also need to be taken into account. The corresponding formula will then become:

$$\begin{aligned} A_{MER} &= ((x_{max} + r_{x_{max}}) - (x_{min} - r_{x_{min}})) \times \\ &\quad ((y_{max} + r_{y_{max}}) - (y_{min} - r_{y_{min}})) \end{aligned} \tag{7.23}$$

Calculation of the Length of Main Medial Axes

The calculation of the total length of the main medial axes is undertaken by first finding out the main medial axes. The algorithm for achieving this has been explained in section 7.4. A simple calculation is then applied:

$$L = \oint_L dl \tag{7.24}$$

For the discrete case, it is:

$$L = \sum_{i=1}^{n} l_i \tag{7.25}$$

where L is the total length of the main medial axes, n is the number of sample points and l_i is the length of each axis segment between the sample points.

Calculation of Average Radius

For calculating the main medial axes average radius for a shape, the formula takes the form of:

$$R_{ave} = \frac{\oint_L R(l)dl}{L} \tag{7.26}$$

For discrete case, it is:

$$R_{ave} = \frac{\sum_{i=1}^{n} R_i}{n} \tag{7.27}$$

where R_{ave} is the average radius of MAT, R is the radius function of MAT, L is the medial axes, n is the number of sample points, R_i is the radius at sample point i.

The Process of the Algorithm

The flow chart for the whole process is shown in Figure 7.52.

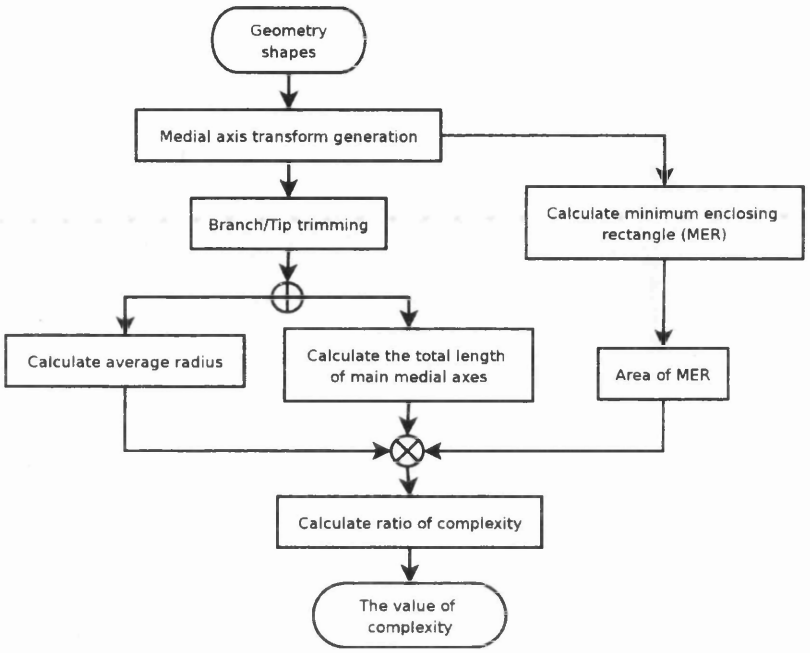

Figure 7.52: The flow chart of complexity estimation algorithm

7.8.4 Validation of the New Complexity Ratio

For validating the new complexity estimating factor and the algorithm, three simple geometries are used. The shape of the geometries are shown in Figure 7.53. The complexity ratio values of each geometry shape are discussed in the following paragraphs.

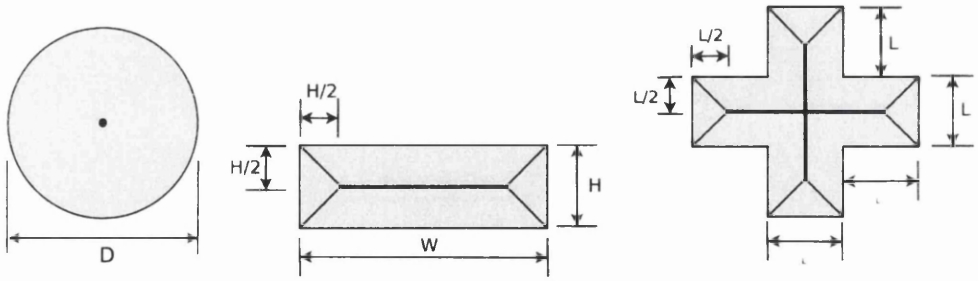

(a) Circle (b) Rectangle (c) Cross

Figure 7.53: Examples for new complexity ratio validation

1. The geometry of the first case is a circle (Figure 7.53(a)). It is clear that for the circle, $L = 0$, $A_{MER} = D \times D = D^2$ and $R_{ave} = \frac{D}{2}$. Therefore, $R_c = 0$.

2. The second geometry is a rectangle with width W and height H as shown in Figure 7.53(b). For this case, $L = W - \frac{H}{2} - \frac{H}{2} = W - H$, $A_{MER} = W \times H$ and $R_{ave} = \frac{H}{2}$. The complexity ratio is given by:

$$R_c = \frac{L^2}{A_{MER}.R_{ave}} = \frac{(W-H)^2}{W \times H \times \frac{H}{2}} = \frac{2(W-H)^2}{W.H^2}$$

For different rectangle, the ratio of complexity is determined by its width and length. The complexity ratio of four different size rectangles are shown in Table 7.8.

Table 7.8: Typical R_c value for rectangles with different aspect ratio

R_c	width	Height
0	1	1
4	3	1
6.4	5	1
19.2	10	1

3. The last case is a cross shape geometry with uniform widths and branch lengths (as shown in Figure 7.53(c)). It is clear that $L = 2 \times (3L - L) = 4L$, $A_{MER} = 3L \times 3L = 9L^2$ and $R_{ave} = \frac{L}{2}$. Therefore, the ratio of complexity R_c is given by:

$$R_c = \frac{L^2}{A_{MER}.R_{ave}} = \frac{(4l)^2}{9L^2.\frac{L}{2}} = \frac{16L^2}{\frac{9L^2}{2}} = \frac{32}{9} \approx 3.56$$

7.8.5 Summary

In this section, several widely used design factors for estimating complexity were described. A new design factor for complexity estimation was introduced. Finally, three cases were used to validate the new design factor and the validation results for these three cases were correct. It is thus seen that by using MAT, the new design factor provides a simple and efficient technique to estimate the complexity of geometry shapes.

7.9 Conclusion

In this chapter, seven different geometry reasoning topics were discussed. Several existing geometry reasoning based classification and quantification algorithms and factors were presented. At the same time, a new algorithms and design factors were introduced. The Medial axis transform was used in these algorithms to reduce the calculating complexity and provide robustness to newly developed techniques.

Using the algorithms presented in this chapter, the primary geometric information of geometry shapes can be known. The number of branches and/or sections can be calculated. The topology shape of shapes can be investigated and the number of holes in any shape can be found. Besides, small structures and perturbations on geometry boundaries can be identified automatically. These algorithms can also separate chunky and slim sections of shapes. Finally, the shape complexity of any geometry models can be estimated.

All approaches and algorithms mentioned in this chapter indicate that MAT is a good and powerful tool for geometry reasoning work. It can be used to automate algorithms, to simplify calculations and to classify and quantify geometry shape.

All the algorithms and results shown in this chapter will now be used for extrusion die classification and shape feature recognition which will be discussed in next chapter.

Chapter 8

Extrusion Die Classification based on Shape Features

Chapter Layout

A new die opening profile category and classification algorithm for extrusion dies have been introduced in this chapter. The first section shows a die classification which is widely used by designers, and a brand-new category for extrusion dies based on different criteria. In the second section, well-known design factors are introduced. A new classification algorithm and several new criteria have been also introduced in this section. The last section shows some classification cases using the new algorithm and criteria.

8.1 The Classification of Extrusion Dies

The Extrusion process can produce almost all desired shapes with easily extrudable alloys. To manufacture extrusion dies for different shape extrudate profiles, the manufacturing difficulty are various according to the complexity of the profile shapes. Therefore, degree of difficulty is a widely used design factor in extrusion industry for extrusion die design work. Owing to the complexity of the profile shapes, a single number – difficulty degree can not solve all the problems. Therefore, extrusion dies are always classified into different shape groups before any further design work can take place.

8.1.1 Shape Groups of Extrusion Dies

Section category	Section type	Examples
A	Simple bar	
B	Shaped bar	
C	Standard sections	
D	Simple solid sections	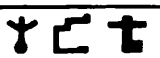
E	Semihollow sections	
F	Sections with abrupt section transitions and thin walls; wide sections	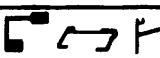
G	Sections with difficult tongues and very narrow inlets	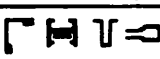
H	Tubes	
J	Simple hollow sections	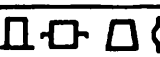
K	Difficult hollow sections; hollow sections with two or more cavities	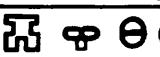
L	Tube sections with external projections	
M	Tube shapes with internal projections or K + L	
N	Large or wide hollow sections	

Figure 8.1: Classification of aluminum extruded sections according to the degree of difficulty [13]

Figure 8.1 shows a basic extrusion die classification according to the degree of difficulty of die section profiles. This classification provides a better representation for the degree of difficulty than solid/semi-hollow/hollow grouping technique.

On carefully observing this classification, it becomes evident that all groups are divided based on certain criteria which are:

The size of die section profiles This criteria separates large or wide section from a normal section

Presence of holes Based on the presence of close or semi-close structures, extrusion dies can be classified into solid, semi-hollow and hollow sections.

The complexity of section shapes Based on this criteria, extrusion dies can be divided into simple or complex sections. Dies for simple sections, such as bars, tubes, are easy to design and extrudate while very thin walls, long legs, small tips and tongues are usually found in complex sections.

The variation of section widths If a die section contains any thick and/or big parts, the design work assumes greater difficulty and demands more attention. Therefore, this kind of section is separated from the normal ones.

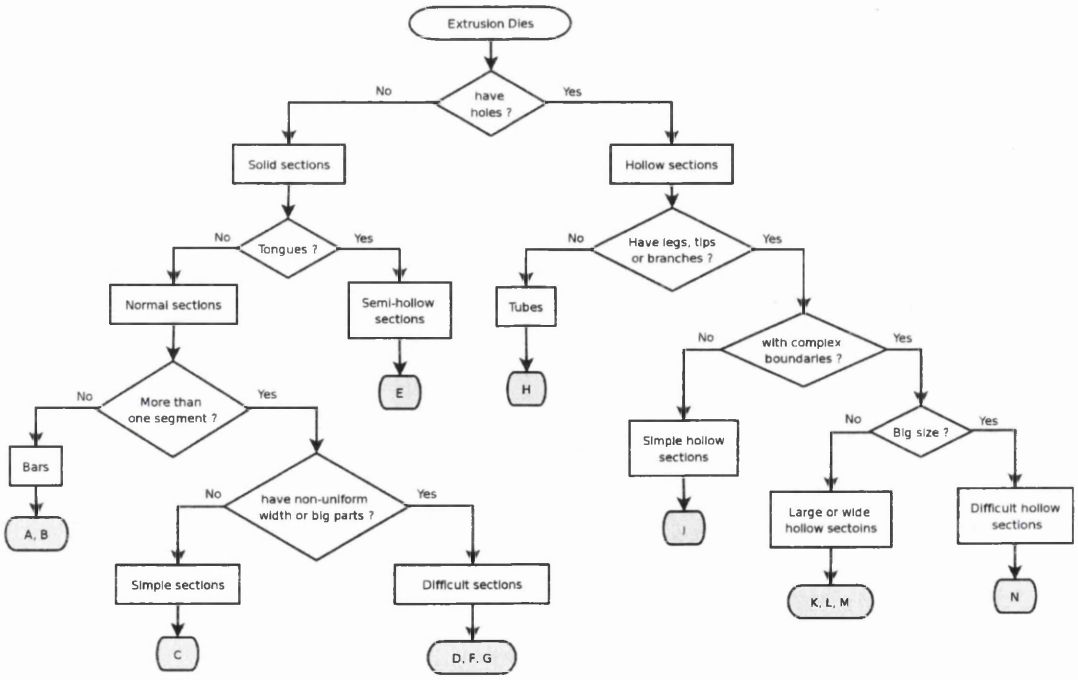

Figure 8.2: Flow chart of extrusion die classification

8.1.2 The Disadvantages of Current Die Classification

The whole classification process based on these classification criteria is shown in Figure 8.2. It can be noticed that not all sections types are separated properly. The problems are:

- For some section categories defined by Laue, the shapes are similar and the classification rules can not differentiate them. e.g. in category A and B, simple bars and shaped bars are alike. There is no visible difference between these two shapes from a geometry reasoning point of view.
- The number of steps which are required to obtain each section category are different. For example, checking holes and tongue shapes are the only two steps which are needed for testing semi-hollow sections. On the other hand, for any difficult solid sections, checking holes, tongues, shape complexity and section width are essential for the classification work.
- Different criteria are used for different section shapes. For example, *shape complexity* is a design criteria for solid sections, which separates bars, standard sections and simple solid sections (category A, B, C and D). But this criteria does not apply to semi-hollow sections since there is only one type, E – semi-hollow section.

These problems indicates that for different die opening profiles, the classification approach varies without any clear established procedure. Therefore, a set of new classification criteria have been proposed and a new classification process has been tested in the following section.

8.2 New Classification for Extrusion Dies

With an aim to overcome the drawbacks of the current approach and to provide a better classification result, a multi-level classifying approach is proposed and validated. The new approach uses only one classifying criteria at each step and applies the same step for all extrusion die sections. The details of each step are discussed in the following paragraphs.

8.2.1 Design Factors for New Classification

Size checking

For extrusion die design, if the size of a die section is relatively big as compared to the size of the die, the section belongs to a large/wide section group. Otherwise, it is a normal size section. Big sections are more difficult to design than for normal size sections. Therefore, the first design factor of the new classification is a size factor. Two possible values of the factor are shown in Table 8.2 respectively.

Table 8.1: New category 1 – size checking

Category C_s	Section type	Shape features
1	Normal size sections	section has normal size
2	Large or wide sections	Section has big size or extremely long.

Close structure checking

Different type of dies and die designs are required for normal solid sections, semi-hollow and hollow sections. For hollow section dies, mandrel, bridge, weld chamber etc. have to be taken into account. For semi-hollow dies, bearing length and recess designs have to be adjusted around the semi-hollow sections (also called as "tongue"). Therefore, classifying solid semi-hollow and hollow dies are very important for design work.

The second classification rule checks semi-hollow and hollow structure, that is tongues and holes, of the die opening profile. Based on the checking results, extrusion dies can be classified into three different groups as shown in Table 8.2.

Table 8.2: New category 2 – close structure checking

Category C_h	Section type	Shape features
1	Normal solid sections	There are no branches, legs, tips,
2	Semi-hollow sections	section contains tongues
3	Hollow sections	section has at least one hole

Complexity checking

It is clear that for complex sections, extrusion die design work needs greater effort. For example, for a bearing length design, the bearings should be reduced to 3/5 4/5 of the normal designs [27, 1] for tips and legs of the opening. So, if the die opening sections contain legs, tips, corners and etc., a correction for bearing lengths and recesses design is needed at these parts. Table 8.3 shows the third classification criteria, the shape complexity factor. The possible values and details are shown in the table.

Table 8.3: New category 3 – complexity checking

Category C_c	Section type	Shape features
1	Simple sections	section without branches, legs and tips
2	Complex sections	section with branches

Difficulty checking

If a die opening profile contains big parts, or the section width varies, the metal flow rate would be changed in these areas during the extrusion process. Due to this, a die with thick sections and varying section widths is difficult to design and therefore need to be separated from normal sections with uniform wall thickness. Therefore, the last classification criteria is difficulty checking. The section categories for this criteria are shown in Table 8.4.

Table 8.4: New category 4 – difficulty checking

Category C_d	Section type	Shape features
1	Uniform sections	section with nearly uniform wall thickness
2	Difficult sections	section with abrupt section transitions, very thin walls, big parts and etc.

summary

Four new die section categories have been introduced in this sub-section. Each category uses its own classifying criteria and it is clear that all the criteria are

independent from each other. Therefore, these classification rules can be used together to classify different die opening profiles. The whole classifying process is shown in the next sub-section.

8.2.2 The Process of New Classification Approach

Using the new classification criteria and results, the new classification approach is easy to implement. Due to the size of the chart, the flow chart for the new classification process has been split into two parts. These two parts are shown in Figure 8.3 and Figure 8.4 respectively. It is clear that four criteria are used to classify the die opening profiles and the new category has 24 different section types.

Compared with Figure 8.2, it is clear that all section categories are now listed at the bottom of the chart (grey round-corner boxes in the figure). This implies that there are same classifying steps for each category. In this case, there are four steps, which have been mentioned as level 1 to 4 classification rules in Table 8.1 to 8.4.

All types of die opening profiles can be classified by this new approach. e.g. For example, for a normal size rectangular bar section, which is marked as category A by Laue, it is clear that it does not have tongue structures and branches, and that it has an uniform wall thickness and normal size. Thus, the category of it is 1-1-1-1 according to the new categorisation rules. It is the first category type which is shown by a grey box at the left-bottom in Figure 8.3.

8.3 Geometry Reasoning based Design Factors for the New Extrusion Die Classification

8.3.1 Widely Used Factors for Extrusion Die Designs

In the past, the die designers introduced a few design factors for extrusion die classification. Some of them are listed in the following paragraphs.

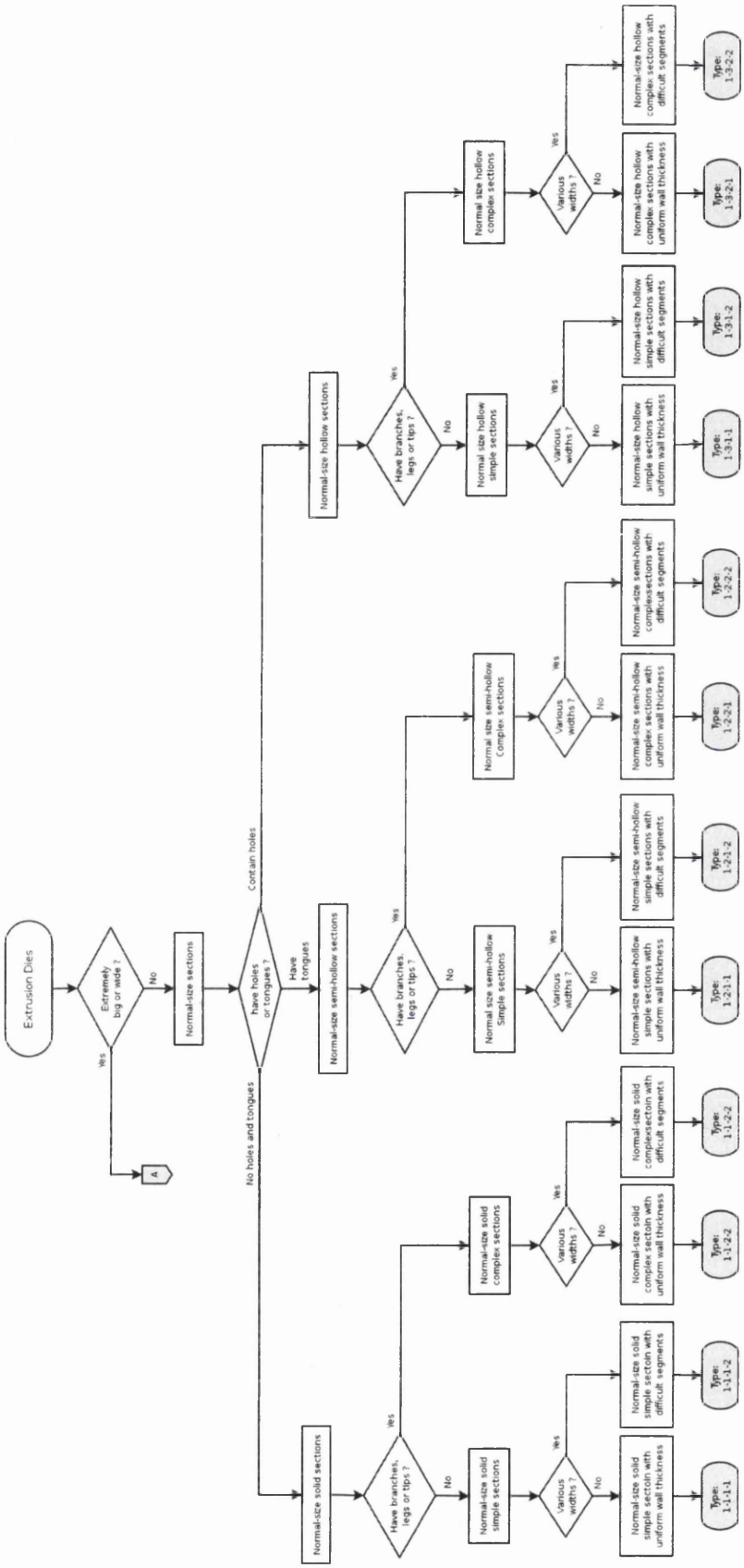

Figure 8.3: New section category for extrusion dies (Part I)

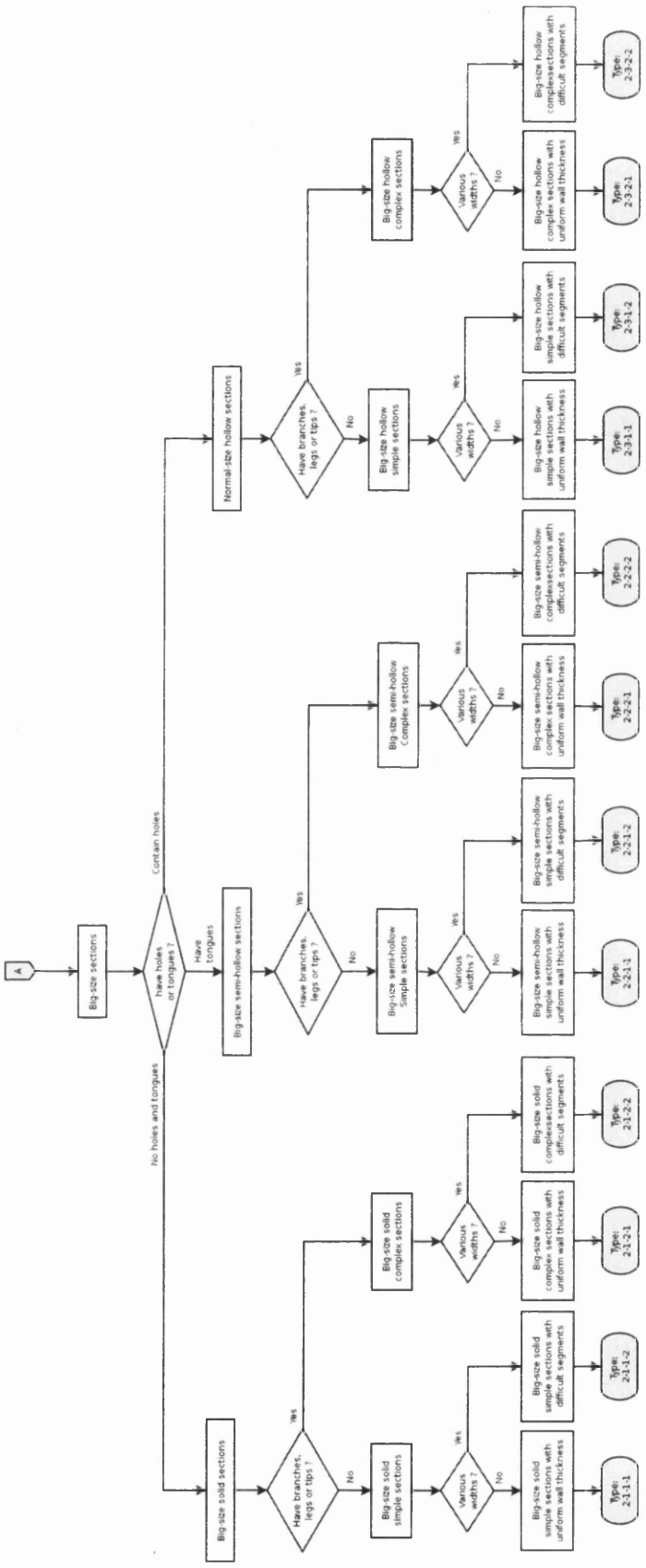

Figure 8.4: New section category for extrusion dies (Part II)

Circumscribing Circle Diameter

A very important and popular design factor is the diameter of the circumscribing circle (D is used in following sections). The circumscribing circle is the circle which can just hold the entire die opening profile. The larger the circumscribing circle, the bigger the press required [13].

Shape Factor

Another quite useful design factor is the *shape factor* which is used as a measure of the degree of difficulty in the U.K. and in the United States. The factor takes the form[13]:

$$Shapefactor = \frac{Peripheryofthesection}{Weightperunitlength} \tag{8.1}$$

Since we know that for any object which is made up of uniform material, the weight equals the volume of the object times the average density of the material, or using mathematical expression: $W = \rho.V$. For a cylindrical object, the volume can be calculated easily by the cross-section area and the length. The formula is: $V = A.L$ where A is the cross-section area of the object and L is the total length. By combining two formulae, the weight can be calculated by $W = \rho.A.L$ and weight per unit length is $W = \rho.A.1 = \rho.A$. Therefore, the equation for shape factor can be re-written as:

$$F_s = \frac{P}{\rho.A} \tag{8.2}$$

where F_s is the shape factor, P is the periphery of the section and A is the area of the section. It is obvious that for a given material, the density, ρ, is a constant, and it is also clear that for shape feature analysis, ρ does not contribute. So, the shape factor can be written as:

$$F_s = \frac{P}{A} \tag{8.3}$$

The final definition of the shape factor implies that it is one kind of *circularity measure* factors. Another quite commonly used *circularity measure* is [16]:

$$F_s = \frac{P^2}{A} \tag{8.4}$$

From all these equations, it is clear that the shape factor increases with the complexity of the section and the reduction of the wall thickness.

Form Factor

The form factor is a measure of the section and is expressed as [13]:

$$F_f = \frac{D}{w_{min}} \tag{8.5}$$

where F_f is form factor, D is the diameter of the circumscribing circle, w_{min} is the minimum wall thickness.

8.3.2 Design Factors for the New Classification Approach

As mentioned in the last section, the new approach uses four criteria for classifying die opening profiles. Four geometry reasoning based design factors have been chosen for the new approach and will be studied one by one in the following sub-sections.

Design Factor for Checking Size

The first classification criteria is the size of die opening profile (Table 8.1). For extrusion die design, the relative size of profiles are more relevant than the absolute sizes as mentioned earlier. Therefore, the circumcircle diameter to die diameter ratio is used as the criteria for the algorithms. The definition of this ratio is:

$$F_s = \frac{D_c}{D_{die}} \tag{8.6}$$

where F_s is the design factor for checking size , D_c is the circumcircle diameter of the shape, D_{die} is the diameter of the extrusion die.

Design Factor for Checking Close-structure

As mentioned in section 7.5, the holes counting algorithm base on MAT results is fast and efficient. It is a good criteria for checking close-structure process. i.e.:

$$F_h = N_e - N_n + 1 \tag{8.7}$$

where R_h is the hole check factor, N_e is the MAT edge number of the shape, N_n is the MAT node (vertices) number of the shape.

Design Factor for Checking Complexity

For checking complexity, there are two available design factors that can be used. The first one is the number of branches, as mentioned in Section 7.4, and the second is the perimeter to area and width ratio which has been introduced in section 7.8.

$$F_c = \frac{L^2}{A_{MER}.R_{ave}} \tag{8.8}$$

where R_c is the complexity design factor, L is the total length of main medial axes, A_{MER} is the area of minimum enclosing rectangle, R_{ave} is the average radius of MAT.

Design Factor for Checking Difficulty

If die sections contain big parts, various wall thickness, small structure etc., it is difficult to be produced. Therefore, a proper design factor has to be chosen for classifying and quantifying the difficulty of die manufacturing.

As mentioned in section 7.6, the differentiation of the radius function, $R'(l)$, is a very effective tool which can be used to identify thin segments, tips, recesses and bulges. Since the value of $R'(l)$ equals zero for smooth segments of MAT, non-zero values of the function indicate change in geometry boundaries. Therefore, the total changes can be calculated by:

$$F_d = \oint_L |R'(l)|dl \tag{8.9}$$

where R_d is the difficult factor, $R'(l)$ is the differentiation of radius functions.

For discrete models, the formula is:

$$F_d = \sum_{i=1}^{n} \left| \frac{\Delta R_i}{\Delta l_i} \right| \tag{8.10}$$

An arbitrary geometry object is used to demonstrate the calculation process. The shape and MAT result of the object is shown in Figure 8.5 and 8.6 respectively.

To check the algorithm, the radius functions along the main medial axes of the shape are used. The main medial axes of the shape are labeled as $A \rightarrow B \rightarrow$

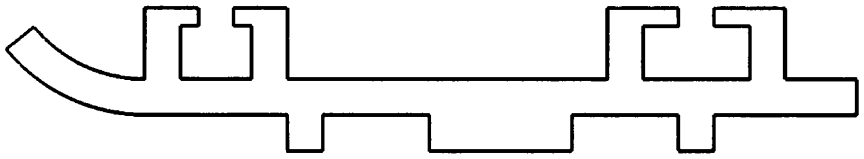

Figure 8.5: Difficult quantification example — the shape

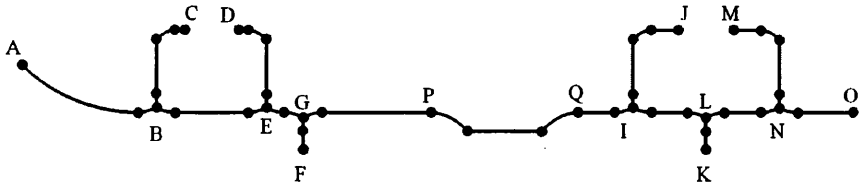

Figure 8.6: Difficult quantification example — the MAT

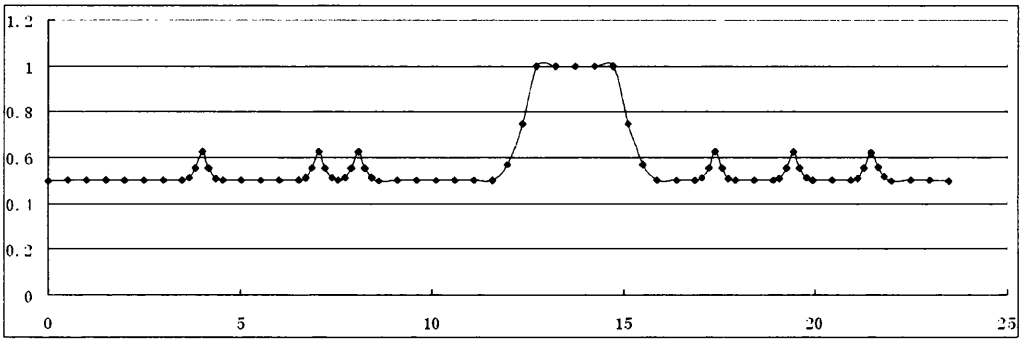

Figure 8.7: The radius function along the main medial axes of the shape

$E \rightarrow G \rightarrow P \rightarrow Q \rightarrow I \rightarrow L \rightarrow N \rightarrow O$ in Figure 8.6. The radius function is shown in Figure 8.7.

According to the radius function, its differentiation can be easily calculated. Figure 8.8 shows the differentiation of the radius function for the main medial axes. The calculation methods can be found in section 7.6.

Figure 8.9 shows the absolute result of the differential function. After this step, the difficulty factor can be calculated by Eq. 8.10. In this case, $F_d \approx 11.24$.

As different shapes has different sizes, a normalized difficulty factor should be used when comparison is needed between different shapes.

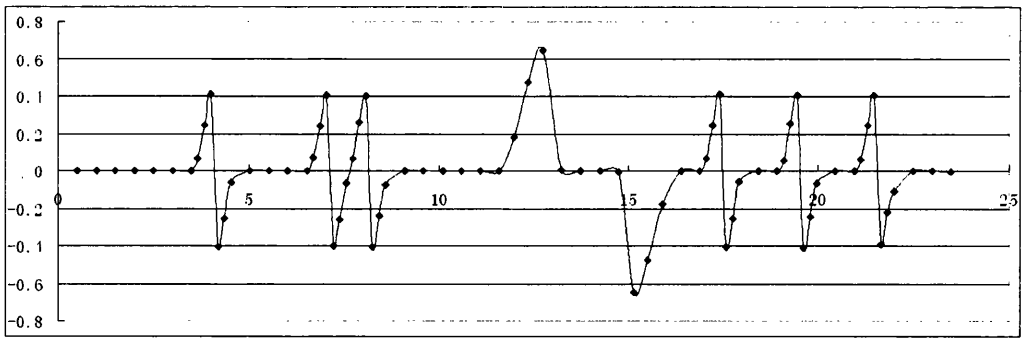

Figure 8.8: The differentiation of radius function

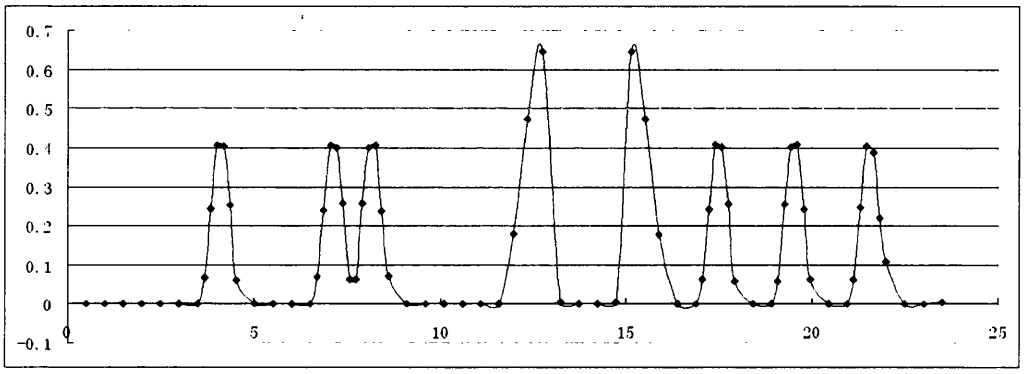

Figure 8.9: The absolute value of the differentiation function

8.4 Validation for the New Extrusion Die Classification

In this section, several randomly chosen die profiles are used for checking the new classification algorithms and criteria.

8.4.1 Case 1

The first case for the algorithm is a 'T' shape geometry object as shown in Figure 8.10(a). Figure 8.10(b) shows the MAT result of the shape.

Assuming the size of the shape is $5cm \times 5cm$, the thickness of all branches is

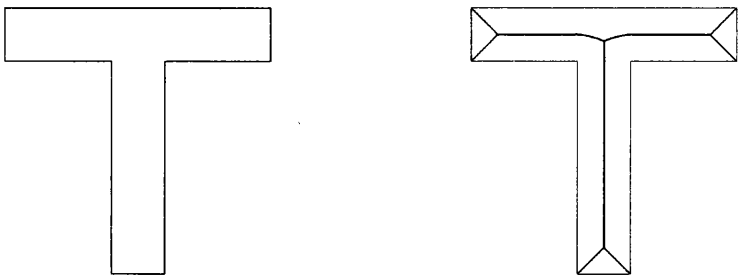

(a) Shape (b) MAT

Figure 8.10: Die profile shape and corresponding MAT result

equal to $2cm$, and 7"($\approx 17.78cm$) die is used. It is now easy to calculate:

$$\begin{aligned} F_s &= \frac{D_c}{D_{die}} = \frac{5\sqrt{2}}{17.18} = \frac{7.07}{17.78} \approx 0.398 \\ F_h &= 0 \\ F_c &= \frac{L^2}{A_{MER}.R_{ave}} \approx \frac{8^2}{25 \times 0.5} = 5.12 \\ F_d &\approx 0.459 \end{aligned}$$

Therefore, $C_s = 1$, $C_h = 1$, $C_c = 2$ and $C_d = 1$. It is type: 1-1-1-1. According to Laue's classification, it is a standard section or solid section (category C and D in Figure 8.1).

8.4.2 Case 2

The geometry shape used in this case is a round tube (Figure 8.11(a)). Its MAT result is shown in Figure 8.11(b).

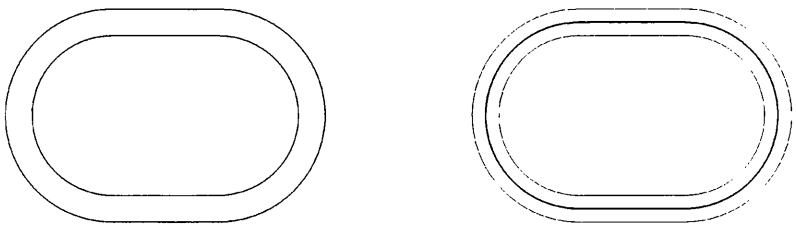

(a) Shape (b) MAT

Figure 8.11: Die profile shape and corresponding MAT result

Suppose the size of the shape is $10cm \times 7cm$, the wall thickness is $1cm$ and

7"($\approx 17.78cm$) die is used. It is easy to calculate:

$$\begin{aligned} F_s &= \frac{D_c}{D_{die}} = \frac{\sqrt{10^2+7^2}}{17.18} \approx \frac{12.2}{17.78} \approx 0.686 \\ F_h &= N_e - N_n + 1 = 4 - 4 + 1 = 1 \\ F_c &= \frac{L^2}{A_{MER} \cdot R_{ave}} = \frac{(6+6\pi)^2}{10 \times 7 \times 1} = \frac{617.47}{70} \approx 8.82 \\ F_d &= 0 \end{aligned}$$

Therefore, $C_s = 1$, $C_h = 2$, $C_c = 1$ and $C_d = 1$. It is type: 1-2-1-1. According to Laue's classification, it is a tube (category H in Figure 8.1).

8.4.3 Case 3

In this case, a realistic extrusion die profile is used to test the classification algorithm. The geometry shape is shown in Figure 8.12(a) [42]. The MAT result is shown in Figure 8.12(b).

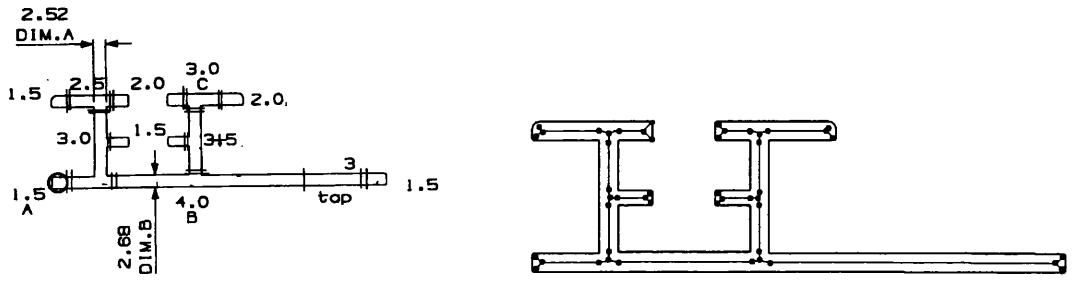

(a) Shape (b) MAT

Figure 8.12: Die profile shape and corresponding MAT result

Suppose the size of die is 7"($\approx 17.78cm$). According to the sizes marked in the figure, all factors can be calculated. The value of each factor is:

$$\begin{aligned} F_s &= \frac{D_c}{D_{die}} \approx \frac{\sqrt{7^2+2^2}}{17.18} \approx \frac{7.28}{17.78} \approx 0.409 \\ F_h &= N_e - N_n + 1 = 47 - 48 + 1 = 0 \\ F_c &= \frac{L^2}{A_{MER} \cdot R_{ave}} \approx \frac{14.6^2}{2 \times 7 \times 1.26} = \frac{213.16}{17.64} \approx 12.08 \\ F_d &\approx 0 \end{aligned}$$

Therefore, $C_s = 1$, $C_h = 1$, $C_c = 2$ and $C_d = 1$. It is type: 1-1-2-1. According to Laue's classification, it is a normal solid section (category D in Figure 8.1).

8.4.4 Summary

Three different die opening profiles are used to validate the new classification. The values of the four classification criteria are calculated for each of the profiles. The results show that all the three die opening profiles are classified into three die groups properly. It is also clear that the new categories for extrusion die design are properly chosen, and all the four new design factors are easy to use and can classify all kind of shapes quickly and correctly.

8.5 Conclusion

Die classification is an important process for extrusion die design. In the first section of this chapter, traditional classification criteria and typical section categories are introduced. Due to the drawbacks of the current category, a totally new category has been developed. For classifying dies into the new groups, a set of new criteria and algorithms are introduced and validated. By using geometry reasoning approaches with MAT, all extrusion dies can be classified into different categories accurately and efficiently.

Chapter 9

Conclusion and Future Work

9.1 Conclusion

In this thesis, a novel geometry based extrusion die design methodology has been presented. Combining methodologies allowing data reusability, empirical design formulae, geometric reasoning techniques and optimization methods, a new design approach has been proposed that can provide optimal die designs based on past successful designs.

The following sections draw out the conclusions from the research study.

9.1.1 Design knowledge Representation and Reusability

As mentioned earlier, the current extrusion die design practise depends heavily on designers' expertise, skills and intuitive knowledge. This poses difficulties for automating the extrusion die design and also takes into account past successful designs. A new design knowledge representation scheme has been introduced that can also account for the data reusability issue. The approach analyses die opening profiles and designs automatically and represent the knowledge in corresponding design spaces.

The design knowledge can be acquired from designers' designs, experiments data or FE simulation results. The normalisation procedure of design spaces improved

the reusability of past successful designs.

9.1.2 Bearing Length Prediction

As one of the most important design factor, a bearing length design is vital for designing extrusion dies. By combining empirical bearing length design formulae with the new design knowledge representation approach, a hybrid bearing length design methodology has been proposed and validated.

By reusing historical design data and deploying general purpose optimization methods, the proposed bearing length design formulae can be optimized and therefore, bearing length design for new extrusion dies can be estimated more efficiently and accurately.

9.1.3 Extrusion Die Layout Design

Like the bearing length, the die layout is another important design factor for extrusion dies. Current approaches for die layout design are based on trial-and-error methods employing basic rules and criteria. To the authors knowledge, a robust computer based extrusion die layout design approach has been proposed in this thesis for the first time.

Using maximum bearing length difference (BLD) as a criterion, this new approach investigates all possible locations and orientations of die openings and provides an optimal die layout design for single- and multi-hole extrusion dies. With properly defined constraints, both flat and radial layouts can be optimized.

9.1.4 Extrusion Die Classification

For extrusion die designing, die classification is an essential requirement. A properly defined classification can reduce and simplify the design work. To overcome the drawbacks and limitations posed by currently used categories, a new extrusion die classification technique has been proposed.

Several geometric reasoning algorithms have been proposed and validated in this

research work for classifying die opening profiles. Based on *medial axis transform* (MAT), these algorithms provide several ways to classify and quantify a die opening profile shape into appropriate shape groups.

9.1.5 The Comparison of Different Approaches

The primary features of different conventional and modern extrusion die design approaches are listed in Table 9.1 and their performance is compared to the proposed approach. It is clear that the proposed approach is more comprehensive, efficient faster, cost effective and flexible and offers features (such as knowledge representation) that other methods fail to provide.

Table 9.1: Advantage and disadvantage of die design approaches

Design approach	Trial-and-error	Empirical	FE simulation	The Proposed Approach
Speed	-	•	-	•
Design quality	•	-	o	o
Cost	-	•	•	•
Amenability	-	•	-	•
Easy-to-use	-	•	-	•
Flexibility	•	o	-	•
Design knowledge accumulation	-	-	-	•
Data reuse	o	-	-	•

(• good, o medium, – bad)

9.2 Future Work

The work presented in this thesis can be extended in the future in the following ways:

- All proposed algorithms could be implemented to provide a fully functional software for extrusion industries and achieve industrial standard validation.

- Proposed and new geometric reasoning algorithms can be further used to recognize shape features for evaluating local design effects.
- Other criteria, such as *average bearing length deviation*, can be used to quantify the quality of die layout design.
- More bearing length design formulae and/or other design formulae can be developed for the design work. More past design data needs be used for optimising
- At the moment, the acquired design knowledge is kept in common files using normal text format. A well designed design knowledge database can be extremely useful for maintaining and reusing data.

Bibliography

[1] Guy Evans Nick Miles and Alan Middletitch. Automatic bearing length assignment using the medial axis transform. In *Proceedings of the* 6^{th} *International Aluminum Extrusion Technology Seminar*, pages 59–65, Chicago, Illinois USA, May 14-17 1996.

[2] Guy Evans Nick Miles and Alan Middleditch. Bearing length assignment for extrusion dies, part i:background and current practice. Technical report, Centre for Geometric Modelling and Design, Tower A, Brunel University, Uxbridge, UB8 3PH, UK, 1996.

[3] Guy Evans Nick Miles and Alan Middleditch. Bearing length assignment for extrusion dies, part ii: Automation using the medial axis transformation. Technical report, Centre for Geometric Modelling and Design, Tower A, Brunel University, Uxbridge, UB8 3PH, UK, 1996.

[4] Guy Evans Nick Miles and Alan Middleditch. Bearing lengths for extrusion dies: raionale, current practice and requirements for automation. *Journal of Materials Processing Technology*, 72:162–176, 1997.

[5] Cecil G. Armstrong. Design applicatios of the medial axis transform. Technical report, Department of Mechanical and Manufacturing Engineering, The Queen's University, The Queen's University of Belfast, Ashby Bulding, Stranmillis Road, Belfast BT9 5AH, Northern Ireland, 2000. Final report for ROPA project.

[6] P. Y. Ang and C. G. Armstrong. Adaptive shape-sensitive meshing of the medial axis. *Engineering with Computers*, MS No.235 Vol 18 Part 3:253–264, 2002.

[7] C. G. Armstrong D. J. Sheehy and D. J. Robinson. Shape description by medial surface construction. *IEEE Transactions on Visualization and Computer Graphics*, 2:62–72, 1996.

[8] C. G. Armstrong T. S. Li and R. M. McKeag. Automatic partitioning of analysis models using the medial axis transform.

[9] C. G. Armstrong R. J. Donaghy and M. A. Price. Dimensional reduction of surface models for analysis. *Engineering with Computers*, 16, part 1:24–35, 2000.

[10] Cecil G. Armstrong Alan Casement and Alan Middleditch. Identification of thin sheets and slender bars in solid models. Technical report, Department of Mechanical and Manufacturing Engineering, The Queen's University, The Queen's University of Belfast, Ashby Bulding, Stranmillis Road, Belfast BT9 5AH, Northern Ireland, 2000. Paper listed in the final report.

[11] Cecil G. Armstrong Alan Casement and Alan Middleditch. Identifying blends and axisymmetric profiles in model reconstruction using the approximate medial axis. Technical report, Department of Mechanical and Manufacturing Engineering, The Queen's University, The Queen's University of Belfast, Ashby Bulding, Stranmillis Road, Belfast BT9 5AH, Northern Ireland, 2000. Paper listed in the final report.

[12] Cecil G. Armstrong Alan Casement and Alan Middleditch. Solid model reconstruction from scattered surface points. Technical report, Department of Mechanical and Manufacturing Engineering, The Queen's University, The Queen's University of Belfast, Ashby Bulding, Stranmillis Road, Belfast BT9 5AH, Northern Ireland, 2000. Paper listed in the final report.

[13] Kurt Laue and Helmut Stenger. *Extrusion.* American Society for Metals, 1981. Second printing, English translation, ISBN 0-87170-094-8.

[14] R. W. Lewis R. S. Ransing and Lin Chao. Understanding extrusion die design. Epsrc final report, EPSRC GR/R15382/01, University of Wales, Swansea, 2004.

[15] William T. Vetterling William H. Press, Saul A. Teukolsky and Brian P. Flannery. *Numerical Recipes in C++; The Art of Scientific Computing.* Cambridge University Press, second edition, 2003. ISBN: 0521750334.

[16] Kenneth R. Castleman. *Digital Image Processing.* Prentice Hall, Inc, 1996.

[17] Frank Harary. *Graph Theory.* Addison-Wesley Publishing Company, 1969. Professor of Mathematics, University of Michigan.

[18] Joeri Lof. *Developments in finite element simulations of aluminium extrusion.* PhD thesis, Universiteit Twente, 2000. ISBN 90-365 14789.

[19] T. Sheppard. *Extrusion of Aluminium Alloys.* Kluwer Academic Publishers, P.O.Box 17, 3300 AA Dordrecht, The Netherlands, 1999. ISBN 0 412 59070 0.

[20] Claude E. Pearson and Redvers N. Parkins. *The Extrusion of Metals.* Chapman and Hall Ltd, 37 Essex Street W. C. 2, second edition, 1960. First published 1944.

[21] The Aluminum Association Inc. http://www.aluminum.org/.

[22] The European Aluminium Association. http://www.aluminium.org/.

[23] Pradip K. Saha. *Aluminum Extrusion Technology.* ASM International, Materials Park, Ohio44073-0002, March 2000. ISBN 0-87170-644-X.

[24] P. Rodriguesz and A. Rodriguez. System to calculate chambers and feeds to obtain a minimum single bearing. In *Proceedings of the* 5^{th} *International Aluminum Extrusion Technology Seminar*, pages 283–290, Chicago, Illinois USA, May 19-22 1992.

[25] M. Thomma and J. Reissner. The use of a planning system to support the design of extrusion dies-rapid determination of bearing lengths. In *Proceedings of the* 6^{th} *International Aluminum Extrusion Technology Seminar*, pages 161–167, Chicago, Illinois USA, May 14-17 1996.

[26] Cliff Lotzenhiser. Die layout and design. In *Proceedings of the* 2^{nd} *International Aluminum Extrusion Technology Seminar*, pages 57–63, Chicago, Illinois USA, November 15-17 1977.

[27] Castle A, Flory R, and Gagg J. Die design and construction in europe. In *Proceedings of the* 4^{th} *International Aluminum Extrusion Technology Seminar*, volume 2, pages 25–34, Chicago, Illinois USA, May 11-14 1988.

[28] Clark O. Stockdale. The application of cad/cam to extrusion die design. In *Proceedings of the* 5^{th} *International Aluminum Extrusion Technology Seminar*, pages 391–394, Chicago, Illinois USA, May 19-22 1992.

[29] Jean-Pierre Hardouin. Bearing length calculation by control of metal flow pressure. In *Proceedings of the* 5^th *International Aluminium Extrusion Technology Seminar*, pages 502–509, Chicago, Illinois, U.S.A., May 19-22 1992.

[30] M. Y. Shridhara. Cad/cam systems for extrusion dies. In *Proceedings of the* 5^th *International Aluminium Extrusion Technology Seminar*, pages 395–398, Chicago, Illinois, U.S.A., May 19-22 1992.

[31] Boal B.V. F.J.A.M. van Houten K.E. Nilsen, P.T.G.Koenis and T.H.J. Vaneker. Developmet of a 3d die design tool for aluminum extrusion. In *Proceedings of the* 7^{th} *International Aluminum Extrusion Technology Seminar*, pages 245–250, Chicago, Illinois USA, May 16-19 2000.

[32] Alfred Raggenbass and Josef Reissner. Computer-based design of extrusion tool. In *Proceedings of the* 7^{th} *International Aluminum Extrusion Technology Seminar*, pages 187–194, Chicago, Illinois USA, May 16-19 2000.

[33] F.J.A.M. van Houten F. P. Lindeman and H.J.J. Kals. A 3d feature based computer support tool for the design of aluminum extrusion tool assemblies. In *Proceedings of the* 6^{th} *International Aluminum Extrusion Technology Seminar*, pages 37–58, Chicago, Illinois USA, May 14-17 1996.

[34] Kari Gundes John Herberg and Inge Skauvik. Application of numerical simulations in design of extrusion dies. In *Proceedings of the* 5^{th} *International Aluminum Extrusion Technology Seminar*, pages 275–281, Chicago, Illinois USA, May 19-22 1992.

[35] K. E. Nilsen H. G. Mooi, A. J. den Bakker and J. Huétink. Simulation of aluminium extrusion based on a finite element method (fem). In *Proceedings of the* 6^{th} *International Aluminum Extrusion Technology Seminar*, pages 67–73, Chicago, Illinois USA, May 14-17 1996.

[36] J. Huétink J. Lof, G. Klaseboer. Fem simulations of aluminum extrusion using an elasto-viscoplastic material model. In *Proceedings of the* 7^{th} *International Aluminum Extrusion Technology Seminar*, pages 157–168, Chicago, Illinois USA, May 16-19 2000.

[37] J. Lof and J. Huétink. Fem simulation of the material flow in the bearing area of the aluminum extrusion process. In *Proceedings of the 7th International Aluminum Extrusion Technology Seminar*, pages 211–222, Chicago, Illinois USA, May 16-19 2000.

[38] J. Lof and Y. Blokhuis. Fem simulations of the extrusion of complex thin-walled aluminium sections. *Materials Processing Technology*, 122:344–354, 2002.

[39] Xinquan Zhang and John Heathcock. Modeling of metal flow for bearing design. In *Proceedings of the 7th International Aluminum Extrusion Technology Seminar*, pages 169–176, Chicago, Illinois USA, May 16-19 2000.

[40] Soo-Young Kim Guen-An Lee, Dae-Young Kwak and Yong-Taek Im. Analysis and design of flat-die hot extrusion process 1. three-imensional finite element analysis. *International Journal of Mechanical Sciences*, 44:915–934, 2002.

[41] Geun-An Lee and Yong-Taek Im. Analysis and die design of flat-die hot extrusion process; 2 numerical design of bearing lengths. *International Journal of Mechanical Sciences*, 44:935–946, 2002.

[42] C. Harris Q. Li, C. Smith and M. R. Jolly. Finite element simulations and experimental studies on inhomogeneous metal flow in aluminium extrusions with tree-dimensional complex geometries. *Materials Science and Technology*, 18:1377–1381, 2002.

[43] C. Harris Q. Li, C. J. Smith and M. R. Jolly. Finite element investigations upon the influence of pocket die designs on metal flow in aluminium extrusion part i. effect of pocket angle and volume on metal flow. *Materials Processing Technology*, 135:189–196, 2003.

[44] C. Harris Q. Li, C. J. Smith and M. R. Jolly. Finite element modelling investigations upon the influence of pocket die designs on metal flow in aluminium extrusion part ii. effect of pocket geometry configurations on metal flow. *Materials Processing Technology*, 135:197–203, 2003.

[45] H. Blum and Harry. A transformation for extracting new descriptors of shape. *Models for the Perception of Speech and Visual Form*, pages 362–380, 1967.

[46] H. Blum and Harry. Biological shape and visual science. *Journal of Thoretical Biology*, 38:205–287, 1973.

[47] H. Blum and R. G. Nagel. Shape description using weighted symmetric axis features. *Pattern Recognition*, 10:167–180, 1978.

[48] M. Ramanathan and B. Gurumoorthy. Constructing medial axis transform of planar domains with curved boundaries. *Computer-Aided Design*, 35:619–632, 2002.

[49] C. G. Armstrong D. J. Sheehy and D. J. Robinson. Computing the medial surface of a solid from a domain delaunay triangulation. In *Proceedings of the* 3^{rd} *ACM symposium on Solid modeling and applications*, pages 201–212, Salt Lake City, Utah, USA, 1995.

[50] G. L. Dirichlet. Über die reduktion der positiven quadratischen formen mit drei unbestimmten ganzen zahlen. *J. Reine Angew. Math*, 1850.

[51] G. M. Voronoi. Nouvelles applications des paramètres continus à la théorie des formes quadratiques. deuxième mémoire: Recherches sur les parallélloèdres primitifs. *J. Reine Angew. Math.*, 134:198–287, 1908.

[52] G. F. Voronoi. Deuxième mémoire: recherches sur les parallèloedres primitifs. *J. Reine Angew. Math.*, 136:67–181, 1909.

[53] Mathworld. http://mathworld.wolfram.com/.

[54] M. I. Shamos and D. Hoey. Closest-point problems. In *Proceeding of* 16^{th} *Annu. IEEE Sympos. Found. Comput. Sci.*, pages 151–162, 1975.

[55] J. L. Bentley and T. A. Ottmann. Algorithms for reporting and counting geometric intersections. *IEEE Trans. Comput.*, C-28(9):643–647, September 1979.

[56] S. J. Fortune. A sweepline algorithm for voronoi diagrams. *Algorithmica*, 2:153–174, 1987.

[57] Thomas Henricus Jozef Vaneker. *The Development of an Integrated Design Tool for Aluminum Extrusion Dies; The use of the Medial Axis Transformation in Die Design.* PhD thesis, Universiteit Twente, 2001. ISBN 90-365-1672-2.

[58] Tamal K. Dey and Wulue Zhao. Approximate medial axis as a voronoi subcomplex. *Computer Aided Design*, 36:195–202, 2004.

[59] John Keyser Tim Culver and Dinesh Manocha. Exact computation of the medial axis of a polyhedron. *Computer Aided Geometric Design*, 21:65–98, 2004.

[60] A. Csabai and P. Xirouchakis. On the meidal surface approximations of extrusions. *Engineering with Computers*, 20:65–74, 2004.

[61] Sunghee Choi Nina Amenta and Ravi Krishna Kolluri. The power crust, unions of balls, and the medial axis transform. *Computational Geometry*, 19:127–153, 2001.

[62] D. Milne A. G. Casement, C. G. Armstrong and D. Robinson. Dimensional addition of beam models. In B. H. V. Topping, editor, *Developments in Engineering Computational Technology*, pages 57–62, Edinburgh, Scotland, 2000.

[63] Helen L. Lockett and Marin D. Guenov. Graph-based feature recognition for injection moulding based on a mid - surface approach. *Computer - Aided Design*, 37:251–262, 2005.

[64] Cecilia Di Ruberto. Recognition of shapes by attributed skeletal graphs. *Pattern Recognition*, 37:21–31, 2004.

[65] Michela Mortara and Michela Spagnuolo. Similarity measures for blending polygonal shapes. *Computer & Graphics*, 25:13–27, 2001.

[66] M.P. Sood R.S. Ransing W.K.S. Pao, C. Lin and R.W. Lewis. Medial axis based interpolation tool-kit for an approximate estimation of casting temperature. In Bonet J. et al., editor, *Proceedings* 10^{th} *Annual Conference of the Association for Computational Mechanics in Engineering (ACME)*, pages 89–92, University of Wales Swansea, UK, 14-17, April 2002.

[67] R.W. Lewis W.K.S. Pao, R.S. Ransing and C. Lin. A medial-axes-based interpolation method for solidifcation simulation. *Finite Elements in Analysis and Design*, 40:577–593, 2004.

[68] C. Lin M.P. Sood R.S. Ransing, W.K.S. Pao and R.W. Lewis. An enhanced interpolation algorithm using medial axis and its application to hotspot prediction in a mould-casting assembly. *International Journal of Cast Metals Research*, 18(1):1–12, February 2005.

[69] R.S. Ransing C. Lin and R.W. Lewis. Optimal bearing length design for extrusion dies using medial axis transform. In Bonet J. et al., editor, *Proceedings* 11^{th} *Annual Conference of the Association for Computational Mechanics in Engineering (ACME)*, pages 25–28, University of Strathclyde, 24-25, April 2003.

[70] Chris Devadas and Olaf Celliers. Metal flow during the extrusion process. In *Proceedings of the* 5^th *International Aluminium Extrusion Technology Seminar*, pages 359–368, Chicago, Illinois, U.S.A., May 19-22 1992.

[71] O. Reiso M. Leftsa and V. Johnson. Flow of the billet surface in aluminium extrusion. In *Proceedings of the* 5^th *International Aluminium Extrusion Technology Seminar*, pages 502–509, Chicago, Illinois, U.S.A., May 19-22 1992.

[72] Bas Jan Emile van Rens. *Finite Element Simulation of the Aluminum Extrusion Process; Shape prediction for complex profiles.* PhD thesis, Universiteit Eindhoven, 1999. ISBN 90-386-2731-9.

[73] Mark Jolly. Understanding extrusion die design. Epsrc final report, EPSRC GR/R15382/01, Birmingham University, 2004.

[74] Robert Sedgewick. *Algorithms.* Addison-Wesley Publishing Company, Inc., second edition edition, 1989. ISBN 0-201-06673-4.

[75] Joseph O'Rourke. *Computational Geometry In C.* Combridge University Press, 1993. ISBN 0-521-44592-2 (paperback).

[76] P.P. Das J. Mukherjee, M. Aswatha Kumar and B.N. Chatterji. Use of medial axis trasforms for computing normals at boundary points. *Pttern Recognition Letters*, 23:1649–1656, 2002.

[77] Steven W. Smith. *The Scientist and Engineer's Guide to Digital Signal Processing.* Second edition edition, 1999. ISBN 0-9660176-6-8.

[78] Alan S. Willsky Alan V. Oppenheim and S. Hamid Nawab. *Signals & Systems.* Pretice-Hall Internationa, Inc., second edition edition, 1997. ISBN 7-302-03058-8.

[79] Dick Clements Phil Dyke John Searl Clyn James, David Burley and Jerry Wright. *Modern Engineering Mathematics.* Second edition edition, 1999. ISBN 0-201-87761-9.

[80] Marc van Kreveld Mark de Berg, Otfried Schwarzkopf and Mark Overmars. *Computational Geometry: Algorithms and Applications.* Springer-Verlag, second edition, 2000. ISBN: 3-540-65620-0.

[81] Eric Foster-Johnson. *Graphical Applications with Tcl& Tk.* M& T Books, second edition edition, 1997. ISBN 1-55851-569-0.

[82] John K. Ousterhout. Scripting: Higher level programming for the 21^{st} century. *IEEE Computer*, March 1998.

[83] Bjarne Stroustrup. *The C++ Programming Language.* Addison–Wesley, third edition edition, 1997. ISBN 0-201-88954-4.